Technical Report Documentation Page

1. Report No.	2. Government Accession No.	3. Recipient's Catalog No.
FHWA/TX-90/452-3F		

4. Title and Subtitle	5. Report Date
Permanent Deformation Potential in Asphalt Concrete Overlays over Portland Cement Concrete Pavements	November 1988
	6. Performing Organization Code
7. Author(s)	8. Performing Organization Report No.
Mahmoud Ameri-Gaznon and D.N. Little	Research Report 452-3F
9. Performing Organization Name and Address Texas State Department of Highways and Public Transportation, Transportation Planning Division P.O. Box 5051 Austin, Texas 78763	10. Work Unit No. (TRAIS) 11. Contract or Grant No. Study No. 2-8-86-452
12. Sponsoring Agency Name and Address Texas Transportation Institute The Texas A&M University System College Station, Texas 77843	13. Type of Report and Period Covered September 1986 Final- November 1988 14. Sponsoring Agency Code

15. Supplementary Notes
Research performed in cooperation with DOT, FHWA.
Research Study Title: Design and Performance of ACP Overlays in Concrete.

16. Abstract

Rutting potential in asphalt concrete pavements (ACP) over both flexible (granular), and rigid (PCC) pavements is investigated.

A detailed analysis of the influence of ACP mixture stiffness, stiffness ratios between the ACP surface and the supporting base, ACP layer thicknesses, surface shear, realistic tire contact stresses, and degree of interlayer bonding is presented. The result of the analysis is presented in terms of octahedral shear stress contours. Over 250 plots of octahedral shear stress contours for a wide variety of structural conditions are presented in Appendix C.

The triaxial shear strength test and the octahedral shear strength calculated from the parameters of ϕ' and C' derived from the triaxial test are used, in concert with the maximum octanedral shear stress within a selected pavement structure and for selected conditions of interlayer bonding and surface shear, to develop a ratio of induced octahedral shear stress to octahedral shear strength. This ratio is used to evaluate deformation potential for a wide variety of mixtures under a wide variety of conditions.

More traditional creep testing and cyclic permanent deformation testing are also presented and the modified ILLIPAVE finite element computer model is used to predict permanent deformatio in these mixtures under specified pavement structural, climatic, and traffic conditions.

Four ACP overlays over PCC bases were evaluated and the data were used as a link between the field and theory to develop a first approximation of critical octahedral shear stress ratios.

A long-term creep test, performed at a higher level of stress than is normally used in the more traditional creep test, is presented as a potential laboratory test procedure to differentiate among the permanent deformation potentials of asphalt concrete mixtures. The combination of high stress level and long-term loading (eight hours) may be necessary to adequately differentiate among mixtures as to rutting potential. This technique, together with triaxial testing (octahedral stress ratio approach), is presented as the preferred analysis technique.

17. Key Words	18. Distribution Statement
Asphalt, Asphalt paving, mixtures, cracking, rutting, permanent deformation, octahedral shear stress, triaxial shear testing, Mohr-Coulomb theory	No restrictions. This document is available to the public through the National Technical Information Service, 5285 Port Royal Road, Springfield, Virginia 22161

19. Security Classif. (of this report)	20. Security Classif. (of this page)	21. No. of Pages	22. Price
Unclassified	Unclassified	219	

Form DOT F 1700.7 (8-72) Reproduction of completed page authorized

PERMANENT DEFORMATION POTENTIAL IN ASPHALT CONCRETE OVERLAY OVER PORTLAND CEMENT CONCRETE PAVEMENTS

by

Mahmoud Ameri-Gaznon

and

Dallas N. Little
Research Engineer

Research Report 452-3F
Research Study 2-8-86-452

Sponsored by:

Texas State Department of Highways and Public Transportation

In cooperation with

U.S. Department of Transportation, Federal Highway Administration

November 1988

Texas Transportation Institute
Texas A&M University System
College Station, Texas

METRIC CONVERSION FACTORS

Approximate Conversions to Metric Measures

Symbol	When You Know	Multiply by	To Find	Symbol
	LENGTH			
in	inches	*2.5	centimeters	cm
ft	feet	30	centimeters	cm
yd	yards	0.9	meters	m
mi	miles	1.6	kilometers	km
	AREA			
in^2	square inches	6.5	square centimeters	cm^2
ft^2	square feet	0.09	square meters	m^2
yd^2	square yards	0.8	square meters	m^2
mi^2	square miles	2.6	square kilometers	km^2
	acres	0.4	hectares	ha
	MASS (weight)			
oz	ounces	28	grams	g
lb	pounds	0.45	kilograms	kg
	short tons (2000 lb)	0.9	tonnes	t
	VOLUME			
tsp	teaspoons	5	milliliters	ml
Tbsp	tablespoons	15	milliliters	ml
fl oz	fluid ounces	30	milliliters	ml
c	cups	0.24	liters	l
pt	pints	0.47	liters	l
qt	quarts	0.95	liters	l
gal	gallons	3.8	liters	l
ft^3	cubic feet	0.03	cubic meters	m^3
yd^3	cubic yards	0.76	cubic meters	m^3
	TEMPERATURE (exact)			
°F	Fahrenheit temperature	5/9 (after subtracting 32)	Celsius temperature	°C

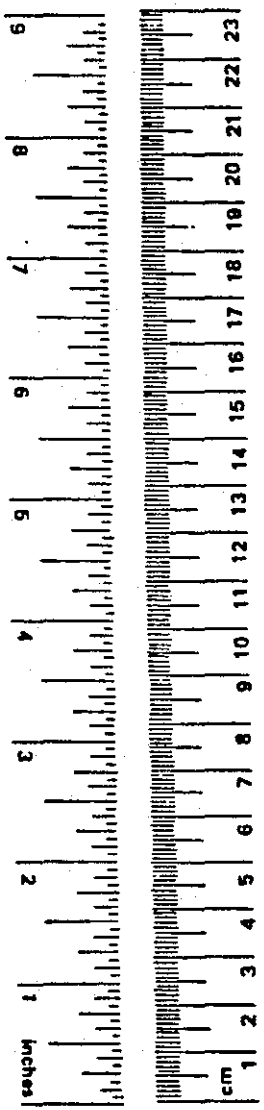

Approximate Conversions from Metric Measures

Symbol	When You Know	Multiply by	To Find	Symbol
	LENGTH			
mm	millimeters	0.04	inches	in
cm	centimeters	0.4	inches	in
m	meters	3.3	feet	ft
m	meters	1.1	yards	yd
km	kilometers	0.6	miles	mi
	AREA			
cm^2	square centimeters	0.16	square inches	in^2
m^2	square meters	1.2	square yards	yd^2
km^2	square kilometers	0.4	square miles	mi^2
ha	hectares (10,000 m^2)	2.5	acres	
	MASS (weight)			
g	grams	0.035	ounces	oz
kg	kilograms	2.2	pounds	lb
t	tonnes (1000 kg)	1.1	short tons	
	VOLUME			
ml	milliliters	0.03	fluid ounces	fl oz
l	liters	2.1	pints	pt
l	liters	1.06	quarts	qt
l	liters	0.26	gallons	gal
m^3	cubic meters	35	cubic feet	ft^3
m^3	cubic meters	1.3	cubic yards	yd^3
	TEMPERATURE (exact)			
°C	Celsius temperature	9/5 (then add 32)	Fahrenheit temperature	°F

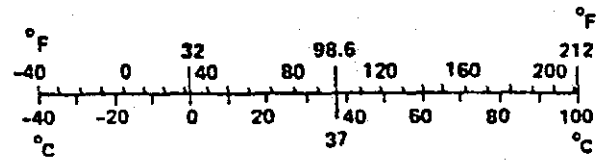

*1 in = 2.54 (exactly). For other exact conversions and more detailed tables, see NBS Misc. Publ. 286, Units of Weights and Measures, Price $2.25, SD Catalog No. C13.10:286.

IMPLEMENTATION STATEMENT

Octahedral shear stress is a realistic criterion by which to evaluate the deformation potential of asphalt concrete overlays over rigid (PCC) bases. The value is a scalar quantity which represents the nine stresses which fully define the stress condition of any point within the pavement. The modified finite element program ILLIPAVE provides the ability to model pavement structures and to account for the effects of interface bonding and surface shear which influence the octahedral stress distribution within the asphalt concrete overlay as much or more than do the material properties of the overlay.

The triaxial shear strength test, performed at confining pressures ranging from 0 to 20 psi, can be used to develop a Mohr-Coulomb failure envelop and hence, to identify the magnitude of the strength parameters of C and ϕ. Based on these strength parameters and the actual stress condition induced in a selected pavement, an octahedral shear strength under the actual stress conditions within the pavement can be defined. The ratio of the induced octahedral shear stress to the failure octahedral stress under these stress conditions provides a measure of the safety factor of the mixture against permanent deformation.

The octahedral stress ratio (OSR) should be used as a tool by which to evaluate the potential of asphalt concrete mixtures to deform or rut under traffic. This report provides the methodology by which to utilize this tool.

This report, in Appendix C (provided under separate cover due to its volume), presents octahedral shear stress contours for 256 different conditions of pavement structure, interlayer bonding, surface shear, stiffness ratios of the base to the surface course, and type of supporting base. These contours can be effectively used to evaluate the potential of rutting in asphalt concrete overlays over both flexible, granular, and rigid, PCC, bases as a function of overlay thickness, overlay stiffness, condition of interface bonding, and condition of surface shearing stresses and contact pressure.

Tables 9.3 through 9.11 of this report present the OSR's calculated for a wide variety of asphalt concrete mixtures placed over various structural categories of both rigid and flexible bases. The trends

presented in these stables can be used to identify the significance of various mixture variables on rutting potential based on the OSR concept.

DISCLAIMER

The contents of this report reflect the view of the authors who are responsible for the opinions, findings, and conclusions presented herein. The contents do not necessarily reflect the official views or policies of the Federal Highway Administration. This report does not constitute a standard, specification, or regulation.

There is no invention or discovery conceived or first actually reduced to practice in the course of or under this contract, including, any art, method, process, machine, manufacture, design or composition of matter, or any new and useful improvement thereof, or any variety of plant which is or may be patentable under the patent laws of the United States of America or any foreign country.

SUMMARY

Pavement deformation in asphalt concrete pavements (ACP) placed over rigid (PCC) bases and flexible or granular bases have been analyzed by a number of semi-empirical and theoretical procedures. The empirical procedures do not consider the distribution of stresses within the ACP nor do they (normally) attempt to relate material characterization methodology to the stress conditions within the pavement. However, these procedures do have the advantage of being based on a large database relating pavement performance to engineering properties of ACP mixtures.

This study employs the concepts of octahedral stress as well as the widely-used creep and cyclic loading deformation testing for the evaluation of permanent deformation potential.

Octahedral stress theory was selected as it is directly related to energy concepts (i.e., strain energy of distortion) which may be applied independent of the type of failure criterion selected. Since octahedral stress theory is a logical means by which to examine the ductile deformation which often occurs in asphalt concrete pavement layers, its application to performance potential evaluation is a rational approach.

Octahedral shear stress contours were plotted for various pavement geometries subjected to various loading conditions and material layer stiffness ratios. The influence of both rigid (PCC) and flexible (granular) base support for the ACP surface was evaluated. The contact stress applied to the pavement surface was based on the predictions of the Teilking finite element tire model which accounts for the effect of the rigidity of the tire carcass and the development of surface shearing stresses. The octahedral shear stress contours were developed using a modified version of the ILLIPAVE finite element computer model. Over 360 cases were assessed for various combinations of ACP thicknesses, stiffness ratios, degree of interface bonding, surface shear, and base support conditions.

Asphalt concrete mixtures of various types were evaluated by triaxial shear strength testing. The concepts of Mohr-Coulomb failure theory were used to evaluate mixture stability in overlay conditions. The mixture stability and its applicability to a certain pavement structural category was evaluated based on the octahedral shear stress ratio (OSR), which is

the ratio of induced octahedral shear stress to the octahedral shear strength under the stress conditions produced for a specific pavement condition. Thus, the OSR approach offers a site-specific and material-specific solution.

Critical values of OSR were verified based on four in situ pavements where ACP was placed on PCC (continuously reinforced pavements). Thus, the validity of the approach was verified based on its sound theoretical foundation, ability to logically rank various mixtures and verification from in situ pavements.

More traditional static creep and cyclic load permanent deformation testing were used together with a modified finite element computer model, ILLIPAVE, to predict deformation potential of a variety of mixtures. The more traditional approach was generally less sensitive in its ability to differentiate among the permanent deformation potentials of various asphalt concrete mixtures.

TABLE OF CONTENTS

LISTS OF TABLES

LIST OF FIGURES

LIST OF FIGURES
(continued)

LIST OF FIGURES
(continued)

LIST OF FIGURES
(continued)

LIST OF FIGURES
(continued)

CHAPTER I

INTRODUCTION

General

Due to the rapid increase in traffic volume and the magnitude of loading on today's highways, more maintenance than ever before is required merely to preserve the original load-carrying capability of the pavement. For pavements subjected to moderate and heavy traffic, the most prevalent treatment is to overlay the pavement with asphalt concrete (1). The application of a properly-designed overlay can provide the most cost effective approach to correct defective areas or to increase the load-carrying capacity of the pavement. These overlays may be categorized as either flexible (asphalt concrete - ACP) or rigid (portland cement concrete - PCC).

A flexible or asphaltic overlay is made up of hot-mix asphalt concrete, while a rigid overlay may consist of plain, simply reinforced or continuously-reinforced concrete. These overlays are normally used to (2):

1. Strengthen existing pavements,
2. Reduce maintenance costs and increase pavement life,
3. Provide a smooth ride to improve service to motorists, and/or
4. Improve pavement surface skid resistance.

Background

Among the more common rehabilitation alternatives for deteriorated concrete pavement is an asphalt concrete overlay on top of the old portland cement concrete (PCC) surface. At the present time (1988), the asphalt overlay provides the most cost-effective method of rehabilitating existing pavements.

When old portland cement concrete (PCC) pavements are deteriorated to the point that they need major rehabilitation, the structural capacity is usually rejuvenated through the application of an overlay of either asphalt or portland cement concrete.

The present design of asphalt overlays is based largely on experience, expressed in the form of correlations between traffic, materials and thickness. Various methods have been proposed to determine the thickness of the overlay. These methods include arbitrary selection of thickness, empirically-based design procedures to correct structural design deficiencies, and the utilization of deflection measurements combined with principles of flexural fatigue cracking in the asphalt concrete pavement (ACP) (3,4,5). In more recent years, overlay design procedures have been developed utilizing reflection cracking analysis in combination with deflection measurements on the old pavements (2,6,7,8). Despite the fact that these proposed design procedures exist, asphalt concrete overlays (ACP) still continue to exhibit a high degree of distress only a few years after being placed in service (9), indicating that the basic mechanisms of the failure modes may not yet be well understood. To fully understand the cause(s) of failure in an ACP overlay, it is important to accurately characterize the development of any distress, and the stress and/or strain conditions that are causing the distress to occur (9).

A review of the current knowledge of the performance of asphalt concrete overlays on PCC pavements reveals that the ACP may experience one or a combination of four modes of failure:

1. Rutting,
2. Blow-ups,
3. Punchouts, and
4. Reflective cracking.

The rutting problem, which is associated with an alteration in the arrangement of aggregate particles within the asphalt mixture comprising the asphalt concrete overlay, is due to:

1. Viscous flow of the asphalt binder in the mineral aggregate voids,
2. Shearing displacements of aggregate coated with a thin film of asphalt binder, and/or,
3. Densification of the mixture due to a decrease in the air void content.

Blow-ups are caused by excessive movements of the PCC slab underlying the overlay. They occur at the joints of the concrete pavement which are

subjected to compressive stresses. Compressive stresses are believed to be induced by thermal movement in the slab enhanced by the change in surface coloring from white-gray to black upon resurfacing and, in some cases, trapped water at the PCC base and the asphalt concrete overlay interface coupled with intrusion of incompressible material at the joints (3).

The reflective cracking problem can be attributed to a combination of factors which include:

1. Change in PCC slab support due to pumping at joints,
2. Bending and shearing action at the joints due to traffic action,
3. Excessive thermal movement of the ACP overlay and/or the PCC base, and/or,
4. Debonding.

When closely-spaced transverse cracks in PCC pavement are linked by longitudinal cracks to form a block, and the block separates from the pavement, the block is called a punchout. Although not exclusive to continuously-reinforced concrete pavements (CRCP), punchouts seem to occur more frequently in CRCP than in jointed pavements. Punchouts are considered by many to be the most severe structural problem associated with CRCP.

Punchouts are invariably associated with either short transverse crack spacings (less than two feet) or with Y-cracks. Short crack spacings and Y-cracks are not always the forerunners of punchouts, and in some cases, they never become associated with punchout failure. However, they are viewed as potential sites of future punchout problems. Treatments such as undersealing with asphalt or cement grout, improvement of drainage, and crack sealing are common but of unknown effectiveness.

Punchouts in CRCP pavements overlaid with ACP are discussed in companion report 2452-2. This report summarizes the performance evaluation (based on punchouts) in eleven CRCP pavements in Texas.

Although blow-ups, reflection cracking, and punchouts are major concerns of distress in ACP overlays over PCC pavements, this report specifically addresses the problem of permanent deformation.

Problem Statement

Asphalt concrete overlays (ACP) placed on portland cement concrete (PCC) have, in many applications throughout the State of Texas, shown continuous development of distress only a few years after being placed in service. Rapid shear failure of the ACP in the first or the second year of service indicates that the state of stress induced by the wheel loads may be more critical than that assumed in the current design procedures.

Current asphalt mixture design, and many pavement design procedures, do not consider the role of external (loading and structural conditions) and internal (mixture) variables that alter the mechanical response of the overlay to the applied loadings. They do not provide a direct relationship between distress mechanisms and mixture properties. Furthermore, the relationships that are presently available are based on empirical data from test results such as Marshall and Hveem stabilities, and relationships among these test properties and performance criteria. These mixture design procedures are an art and may not be well-suited by themselves for satisfying all structural situations. These standard mixture designs include no mechanistic relationships to consider the internal ability of a mixture to resist permanent deformation. In order for this to be achieved, it is necessary to replace the test properties used to evaluate deformation potential with fundamental engineering properties which account for basic engineering behavior of these asphalt concrete materials under a specific and identifiable stress state.

A mixture design should provide guidelines to indicate when a mixture, though adequate for certain applications, may not be suitable for a specific installation in a particular situation.

Fatigue cracking is not of concern in ACP overlays over PCC pavements due to the absence of tensile strain at bottom of the overlay, which is supported by the stiff PCC layer below. It is the permanent deformation that has occasionally caused problems in the early portion of the life of ACP overlays on rigid pavements.

Purpose and Scope

The primary objective of this research was to investigate the shearing failure (rutting) in asphalt concrete overlays placed on concrete pavements and to identify the parameters that influence the initiation and

promotion of shear failure in these overlays during their early lives. This research also suggests a relationship between hot-mix asphalt concrete mixture variables and pavement structural parameters which can be used to identify the proper mixture for selected conditions using a mechanistic approach. This, in turn, allows a relatively simple and quick quantitative evaluation of overlay responses (stresses, strains, deflections) as the pavement layer geometry, material characteristics and/or loading conditions change.

As part of these objectives, this research assesses the state of stress developed within the hot-mix asphalt concrete (ACP) overlay when placed over a PCC (rigid) base as well as over a stress-sensitive aggregate base material.

The variables which influence permanent deformation were divided into two groups: external and internal. The external variables include pavement geometry (layer thickness combinations), load and contact tire pressure magnitudes, surface shear stresses, and interlayer bonding conditions. The internal variables are mixture parameters such as air void content, asphalt content, VMA, gradation, type of aggregate, type and quantity of mineral filler, and modifier addition.

CHAPTER II

REPORT ORGANIZATION

This report is organized into twelve chapters and four appendices.

Chapter I is an introduction to the problem with a concise discussion of the background information relative to the major distress mechanisms in ACP overlays over PCC pavements and over granular bases.

Chapter III discusses the research approach to the evaluation of the primary distress mode addressed in this report - permanent deformation in the ACP overlay. In order to develop a satisfactory research approach, it was first necessary to select the most applicable failure criteria available, identify a realistic laboratory testing procedure compatible with the failure or evaluation criteria, and identify analytical models which can effectively determine the pavement stress conditions which must be duplicated in laboratory testing and evaluated in predictive modeling.

Chapter IV presents an evaluation of potential laboratory testing procedures which have promise for use in predicting permanent deformation potential of ACP overlays. Particular attention is given in this chapter to triaxial shear strength testing and the use of the Mohr-Coulomb shear strength failure law.

Chapter V discusses the analytical computer models that were used and modified to predict stress conditions within the ACP overlays for which deformation potential was evaluated over a wide variety of environmental and structural conditions. These analytical models include the modified finite element program ILLIPAVE and a mechano-lattice model developed at Texas A&M University by Yandell (10).

Chapter VI explains the structural and material variables considered in the analyses of stresses in ACP overlays over PCC and granular bases. The variables considered in these analyses are: ACP thickness, ACP stiffness, base stiffness, base thickness, surface shear, and level of interface bonding. The octahedral shear stress was selected as the parameter most applicable to the appropriate failure or evaluation criteria selected for this analysis.

Chapter VII and VIII, respectively, discuss the results of the stress analyses for ACP overlays over granular bases, and ACP overlays

over PCC bases. These results are used in Chapter IX for evaluation of various mixture types as ACP overlays.

Chapter IX discusses the results of ACP mixture stability analyses based on the triaxial shear test. The methodology selected for running the triaxial test to mimic field conditions is discussed in Chapter IV.

Chapter X discusses the results of permanent deformation analyses using the repeated load permanent deformation test and the static creep test. Various mixtures and mixture variables are considered including aggregate gradation, aggregate type, inclusion of a polymer modifier and asphalt grade. These analyses are indicative of long-term resistance to deformation and are compared to the results of triaxial (octahedral shear stress) analyses of Chapters VII-X.

Chapter XI discusses the results of supporting studies that address similar problems of permanent deformation in ACP. These studies are discussed as a close coordination exists among all HP&R studies addressing the problem of deformation potential. Through field studies of rutting in ACP overlays over PCC bases, an empirical link was established between the analytical and laboratory testing results of Chapters VIII, IX, and X, and field performance.

Finally, Chapter XII presents conclusions and recommendations based on the analyses and tests discussed in Chapters I through XI.

This report includes four appendices. Appendix A is a more detailed discussion of the failure criteria considered in the analysis of permanent deformation potential. Appendix B is a discussion of sample preparation and testing techniques. Appendix C is a complete listing of the octahedral shear stress contours developed from the modified ILLIPAVE computer model. Due to the large number of contour charts (264), these plots are provided in Appendix C as a separate volume. Appendix D presents the results of static creep, cyclic permanent deformation, and resilient modulus versus temperature testing on the mixtures evaluated in this study.

This report is supplemented by two companion reports. The first companion report, 2452-1, is entitled "Use of Climatic Data for the Prediction of Permanent Deformation in Flexible Pavements." This report explains the development of the regression model which predicts temperature gradients within the ACP based on location of the pavement within the

State of Texas, depth within the ACP, and the time of year. This model was incorporated in the modified ILLIPAVE computer model for deformation evaluation as discussed in this report.

The second companion report, 2452-2, is entitled "Evaluation of Punchout Performance in CRCP Pavements in Texas." This report summarizes the results of a field survey of eleven, continuously-reinforced concrete pavements located throughout Texas. The report evaluates the performance of ACP overlays in preventing the occurrence of punchouts in these pavements.

CHAPTER III

RESEARCH APPROACH

General

The first step in any "rational" or mechanistic analysis is to select the proper failure criteria pertinent to the materials in use under the environmental conditions that govern and are associated with the distress modes to be evaluated. Next, the best analytical model available must be selected. This model must include material parameters which characterize the fundamental behavior of the ACP and are compatible with the failure criterion or criteria selected. Following the results of such an analysis, comparisons of the predicted output parameters and the field performance must be made. The degree of discrepancy between these parameters will then result in the determination of the extent of modifications required to the model and/or input parameters. Moreover, the validity of the results obtained from any particular model are controlled by the underlying assumptions. The method is "exact" if and only if the assumptions on which it is based are correct.

Development of a mechanistic design or analysis procedure in general includes the following steps:

1. Identification of significant input parameters. These parameters represent material characteristics, and it is essential to perform appropriate laboratory tests to obtain these parameters.
2. Selection of a suitable structural model for calculating critical responses (strains, stresses, deflections).
3. Satisfactory comparisons between predictions from the solution scheme, which the structural model provides, and the performance characteristics of the material in situ (verification).

Failure Criteria

The response of a pavement structure, and hence its failure, depends on the materials used, whose response, in turn, depends on the type and history of the applied loading. Accordingly, a suitable failure criteria

must account for the influence of using different materials, the influence of different loading conditions, as well as the influence of other factors that affect the stress distribution within the pavement (such as type of base, interfacial bonding, etc.). Once the appropriate failure mechanism under assumed service conditions is determined, a parameter such as stress, strain, or energy may be chosen as a critical or limiting parameter used to evaluate the performance potential of the pavement structure.

A suitable test procedure must be adapted to determine the parameter deemed as critical to performance. However, a theory that works for ductile failure may not work for brittle fracture. Therefore, a single theory may not always apply to a given material, because the material may behave in a ductile fashion under some conditions (hot and warm climate) and in a brittle fashion under others (cold and freezing climate). Not only must the proper failure mode be defined, but also the various stress states likely to be produced within the pavement system must be considered. Because of the possibility of a virtually unlimited number of stress states, not only is it undesirable, but it is also unacceptable to test at every state of stress. In general we are limited, because of practical considerations, to test only a few specimens in order to obtain material properties. Thus, selection of the critical failure criterion is essential as this criterion defines how the material will fail in the selected distress mode and under the stress states expected to occur in the pavement system. This allows the presumption that the critical value of the parameter selected is achieved without regard to the stress state.

Situations exist in which permanent deformation in ACP occurs rapidly under only a few load applications (9). The failure of asphalt concrete under only a few loadings is due to lack of stability in the mixture and thus to the inability of the mixture to resist induced shear stress from wheel load applications and/or improper mixture design.

It is possible for an asphalt concrete mixture to posses high tensile strength but lack sufficient internal friction. On the other hand, a good level of internal friction at higher temperatures does not insure resistance to deformation when the confining pressure within the pavement layer is quite low. In the latter case, the cohesive strength is the major contributor to shear strength.

Several theories are available for predicting failure of various types of materials. However, none of the theories agree with test data for all types of materials and combinations of loading. From the classic theories of failure, this research study considers octahedral shear stress to be the most appropriate criterion by which to study the rapid shear failure of ACP overlays resulting in permanent deformation early in life. In this study, octahedral shear stress at failure for the ACP mixture will be defined by the Mohr-Coulomb failure envelope.

A review of the classic failure theories considered in this research is presented as Appendix A of this report.

Mohr-Coulomb Failure Theory

The application of the Mohr-Coulomb failure criterion is well documented in its application to soil mechanics. This criterion states that the failure of an isotropic material, either by fracture or by the onset of yielding will occur when (in a three-dimensional state of stress) a Mohr's circle (having diameter $(\sigma_1 - \sigma_3)/2$ where $\sigma_1 > \sigma_2 > \sigma_3$) touches a failure envelope. This criterion may be used to predict the effect of a given state of stress at a point. The motivation is that the region enclosed by Mohr's circle for any possible state of stress not causing failure must be a region safe from failure. According to this criterion the shear strength increases with increased normal stress on the failure plane. Experimental evidence demonstrates that the envelope, which is tangent to all the failure circles and bonds the safe region, is usually slightly curved concave downward. A simple way to approximate the envelope is to draw a straight line tangent to at least two Mohr's circles.

Thus a Mohr-Coulomb failure envelope is defined by the Mohr-Coulomb equation:

$$\tau = c + \sigma_f \tan \phi \qquad (3.1)$$

where: τ = shear strength, psi,
σ_f = normal stress at failure, psi, and
ϕ = angle of internal friction, degree.

In order to define the C and ϕ terms, (cohesion and angle of internal friction, respectively) at least two triaxial tests must be performed, an unconfined compression test and one confined compression test with confining pressure (σ_3) that best simulates the field condition. Ideally, it is preferred to conduct triaxial tests at several values of confining pressure. However, a minimum of two tests is required to determine the angle of internal friction, ϕ, and the cohesion, C. The values of these parameters (ϕ and C) could simply be determined as shown in Figure 3.1. This procedure is sensitive to the stress condition developed within the asphalt concrete, and the stress state can be defined adequately and relatively simply by the major and the minor principal stresses. With this method the critically important conditions of the tire pressure and interlayer bonding can be simply and accurately evaluated (11).

Figure 3.2 is a graphic representation of a Mohr-Coulomb failure envelope. This is a simple and direct method of evaluating stability of ACP overlays and their potential to resist rapid deformation. For a particular mixture, conditions causing failure under any vertical principal (compressive) stress from the wheel load can be calculated from the geometry of the failure envelope. The equation representing the relationship between major and minor principle stresses at failure is as follows:

$$\sigma_1 = \sigma_3 \left[\frac{1+\sin\phi}{1-\sin\phi} \right] + 2C \left[\frac{1+\sin\phi}{1-\sin\phi} \right]^{\frac{1}{2}} \qquad (3.2)$$

where: σ_1, σ_3 = major and minor principal stresses,
ϕ = angle of internal friction, and
C = cohesion.

Equation (3.2) demonstrates that the maximum vertical stress that can be supported by any given material is influenced directly by lateral support, σ_3, cohesion, C, and angle of internal friction, ϕ.

Octahedral Shear Stress Theory

The octahedral shear stress parameter offers a scalar parameter which defines the influence of nine stresses at a specific point. This technique offers a method that is more directly quantifiable. Octahedral shear stress in a general form is defined as:

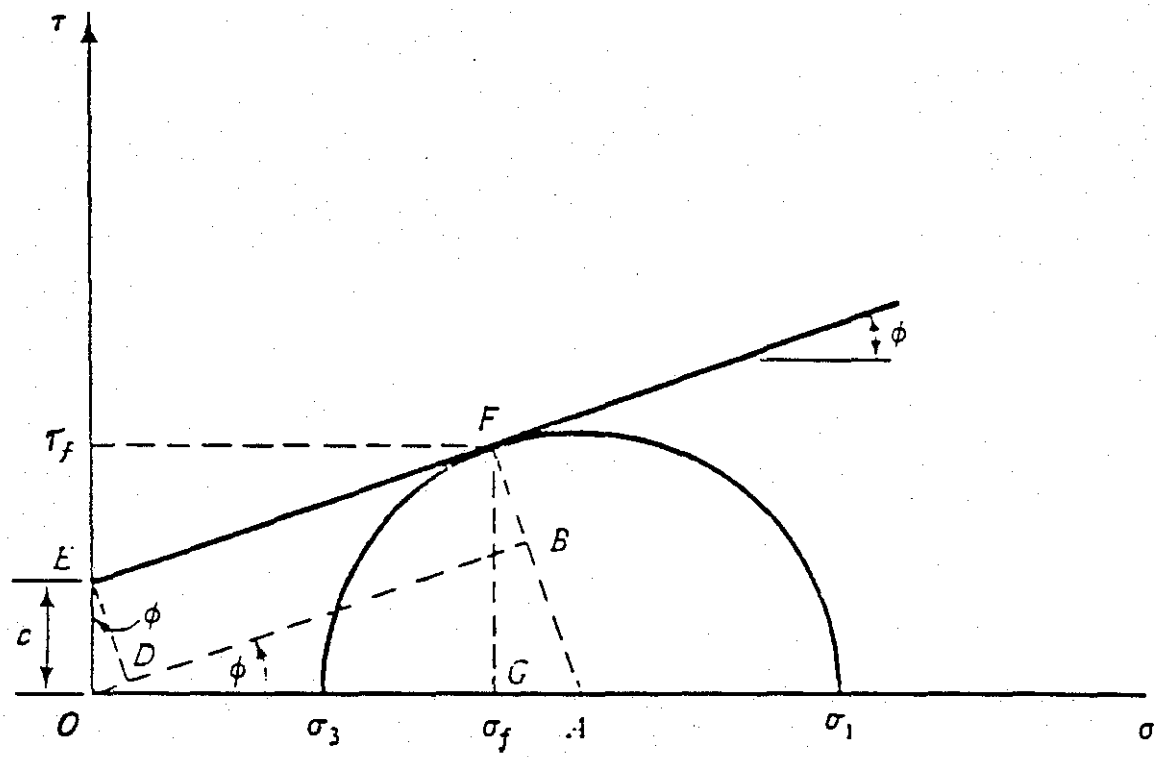

Figure 3.1. Schematic representation of Mohr-Coulomb failure envelope for determination of C and ϕ parameters.

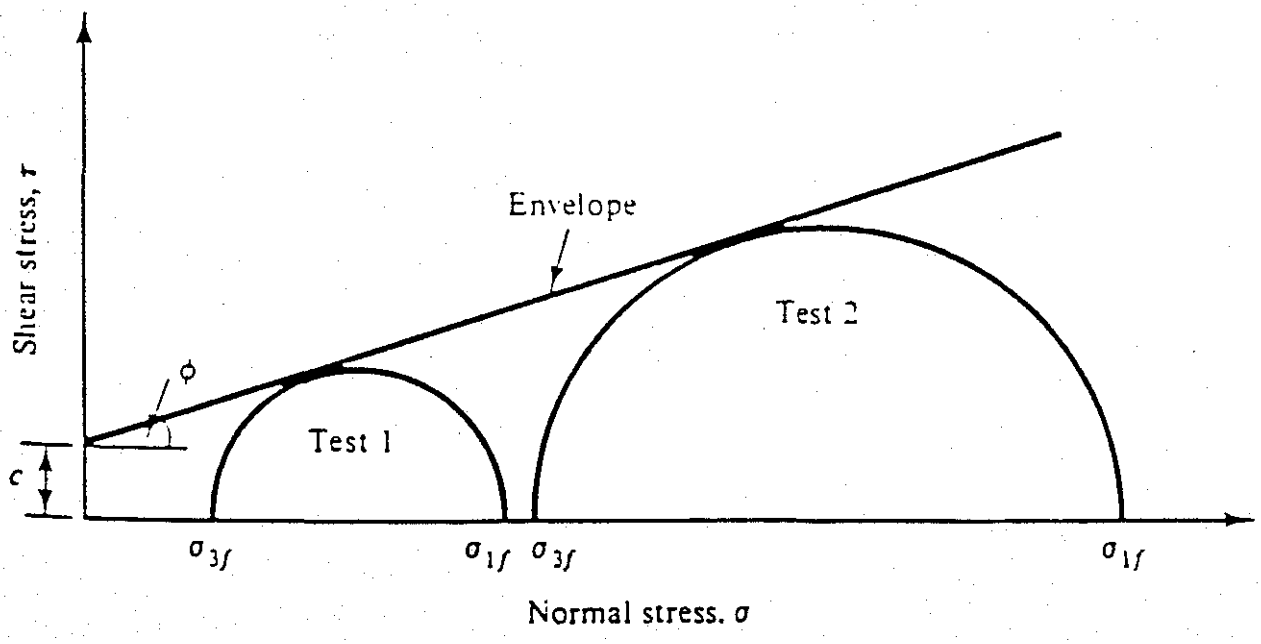

Figure 3.2. Parameters of Mohr-Coulomb model where σ_{3f} is the major principal stress at failure.

$$\tau_{oct} = 1/3\ [(\sigma_x - \sigma_y)^2 + (\sigma_y - \sigma_z)^2 + (\sigma_z - \sigma_x)^2 + (\tau_{xy}^2 + \tau_{yz}^2 + \tau_{zx}^2)]^{1/2} \quad (3.3)$$

where: σ_x, σ_y, σ_z = normal stresses in x, y and z directions,
τ_{xy}, τ_{yz}, τ_{zx} = shearing stresses on xy, yz and zx planes, and
τ_{oct} = fundamental stress invariant.

The above expression, in terms of principal stresses on a plane where shearing stresses are zero, will reduce to:

$$\tau_{oct} = \frac{1}{3}\sqrt{(\sigma_1 - \sigma_2)^2 + (\sigma_2 - \sigma_3)^2 + (\sigma_1 - \sigma_3)^2} \quad (3.4)$$

where: σ_1 = major principal stress,
σ_2 = intermediate principal stress, and
σ_3 = minor principal stress.

Equation (3.2) can also be transformed to calculate the octahedral shear stress for any condition in an overlay structure:

$$\tau_{oct} = 0.942 \left[\frac{\sigma_3 \sin\phi}{1-\sin\phi} + C \left(\frac{1 + \sin\phi}{1 - \sin\phi} \right)^{\frac{1}{2}} \right] \quad (3.5)$$

According to this theory, inelastic action at any point in the material under any combination of stress begins when the maximum octahedral shear stress $(\tau_{oct})_{max}$ becomes equal to 0.471 σ_f. This criterion makes it possible to apply the strain energy of distortion criterion of failure, by dealing with stresses rather than dealing with energy directly. Thus, failure occurs when $\tau_{oct} = 0.471\ (\sigma_1 - \sigma_3)$.

Although the two theories (Octahedral Shear Stress and Mohr-Coulomb) are completely different, a study of Mohr-Coulomb failure theory indicates (9) that at failure the octahedral shear stress is exactly equal to 0.471 times deviator stress on the sample at failure. The ratio of actual octahedral shear stress in the pavement to the octahedral shear stress predicted by theory can be used to indicate how close to failure the overlay may be. The closer this value is to unity, the more likely it is that rutting will develop at an accelerated rate.

Although the value of τ_{oct} may not be the maximum shear stress on any plane through a point in the paving mixture, it has the significance of being used to define the onset of yielding in a general state of stress.

Study of Stress

The total stress condition in the mixture has a profound influence on its performance; therefore, the state of stress which causes the failure in a material must be accurately characterized. The response to loads on an asphalt concrete overlay, depends not only on the type of material from which it is made, but also on environmental conditions.

Traditional analysis of a pavement structure assumes that the maximum stresses occur under the centerline of the wheel load or at the bottom of the asphaltic concrete layer. It is also conventional laboratory practice to use a single vertical compressive principle stress to characterize the failure mechanism occurring in a pavement structure. However, rapid failure due to plastic deformation or yielding, which causes a permanent undesirable change in shape, is due to significant shearing action developed within the ACP overlay.

Study of octahedral shear stress theory and stress analysis of overlays placed on a number of different pavement structures has revealed that the maximum octahedral shear stress does not always occur under the centerline, nor does it always occur at the bottom of the asphalt layer. This indicates the need for a new approach to investigate the stress state in a pavement structure and to avoid traditional analysis when investigating new concepts or when examining a specific distress type.

Octahedral shear stress theory is considered in this study as an acceptable indicator of whether inelastic conditions or permanent deformation develops in an ACP overlay material. With this theory, it is possible to provide a single numerical parameter that describes the total stress state in the material, and also accurately relate this to the onset of inelastic deformation (9).

Estimating Deformation Potential

This research uses octahedral shear stress as the criterion by which to evaluate deformation potential in ACP overlays over PCC and granular bases for a variety of structural and environmental conditions. The

triaxial shear strength test is used, together with the octahedral shear stress theory, to evaluate the potential for various ACP mixtures to resist shear failure leading to permanent deformation.

In addition to triaxial shear strength testing, repeated load permanent deformation testing and static compressive creep testing are used to evaluate accumulated permanent deformation potential for various ACP mixtures under a variety of structural and environmental conditions. Two computer models were used to predict the performance of the mixtures tested. These models were the ILLIPAVE finite element model and the mechano-lattice model.

CHAPTER IV

EVALUATION OF LABORATORY TEST PROCEDURES

Currently available hot mixture design procedures are based on empirical methods which predict the ability of a mixture to perform based on mixture volumetric relationships and stability. The Marshall (12) and Hveem (13) test methods were devised to measure stability. These methods are empirical in nature and are not conducive to performance prediction when the material is used in a pavement layer, but can only be used as acceptance/rejection criteria. On the other hand, a rational or mechanistically-based analysis of asphalt paving mixtures can provide solutions to certain distress problems in ACP overlays that may never be found on the basis of empirical tests.

Vertical stress is often applied in a compressive mode to cylindrical asphalt concrete samples in a test intended to mimic the consolidation and permanent deformation that occurs under tire contact stresses in the field. Yet, the responses to these stresses may not accurately reflect the deformation occurring within the actual asphalt overlay. As the level of loading increases or decreases, the material experiences continuous changes in its physical characteristics. At any instant during the change in the load, the material is different than it was at some previous instant. In other words, the moduli or parameters that define the stiffness of the material experience continuous changes as the loading is changed. For instance, at low vertical stress levels, the compressive stress is proportional to the deformation and presents the proper relationship for gradual accumulation of rutting over a period of time. At higher stress levels, the relationship may no longer maintain the same constitutive relationship between stress and strain and, in turn, with the mechanism related to failure in the pavement. Moreover, this test may not provide an accurate relationship with any modes of deformation that develop rapidly. This is because the stress and strain magnitude for a given material at a given point in a pavement structure is a direct function of the triaxial stress state. Therefore, use of this test (axially-loaded compressive creep test) does not completely model the state of stress that causes yielding of the overlay in its early life.

Essentially, uniaxial, unconfined testing can be divided into two categories: (1) monotonic loading resulting in shear failure (unconfined compressive strength testing); and (2) constant stress application creep testing. The creep test has been used more extensively to mimic the condition induced in ACP pavements subjected to wheel loads. However, both tests suffer from the limitation of being subjected to a uniaxial, and hence, unrealistic stress state.

Argument for a Multi-Parametric Test

Figure 4.1 presents a hypothetical situation illustrating the shortcomings of a one parameter test, such as unconfined compressive strength, to measure the stability of bituminous paving mixtures. In this illustration, three different mixtures are compared with values of cohesion, C, and angle of internal friction, ϕ, of $C_1\phi_1$, $C_2\phi_2$, and $C_3\phi_3$, respectively (11). Figure 4.1a indicates that the unconfined compressive strength, Oa, is exactly the same for each of the different mixtures represented by Mohr-Coulomb envelopes zu, yv and xw. For an unconfined compressive strength test, the amount of lateral support provided is zero; whereas, in the field, lateral support is mobilized by the pavement adjacent to the loaded area. This lateral support could approximate the unconfined compressive strengths of the mix. The triaxial stability under service conditions is represented by the complete Mohr-Coulomb failure envelopes zu, yu, and xw. If traffic loads exert a vertical pressure of magnitude equal to a level between c and d in Figure 4.1a, then only the bituminous mixture represented by Mohr envelop xw would be stable in the field and the other two would be unstable. An unconfined compression test could not distinguish among these bituminous mixtures since it would give exactly the same stability rating, Oa, to all three of these different mixtures.

On the other extreme, Figure 4.1b represents the reverse of the situation illustrated in Figure 4.1a. The unconfined compressive strength of the three bituminous mixtures with failure envelopes Ir, mq, and np are indicated by Oe, Of and Og, respectively. If the unconfined compressive strength is the measure of lateral support provided by the pavement adjacent to the loaded area, Figure 4.1b demonstrates that these three bituminous mixtures are all capable of developing exactly the same resistance, Oh, to the applied vertical loads under the conditions that

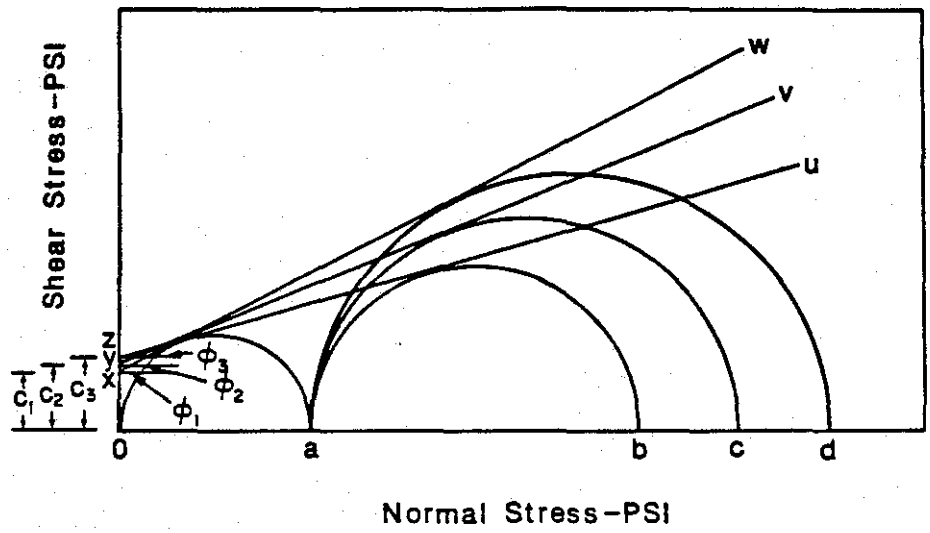

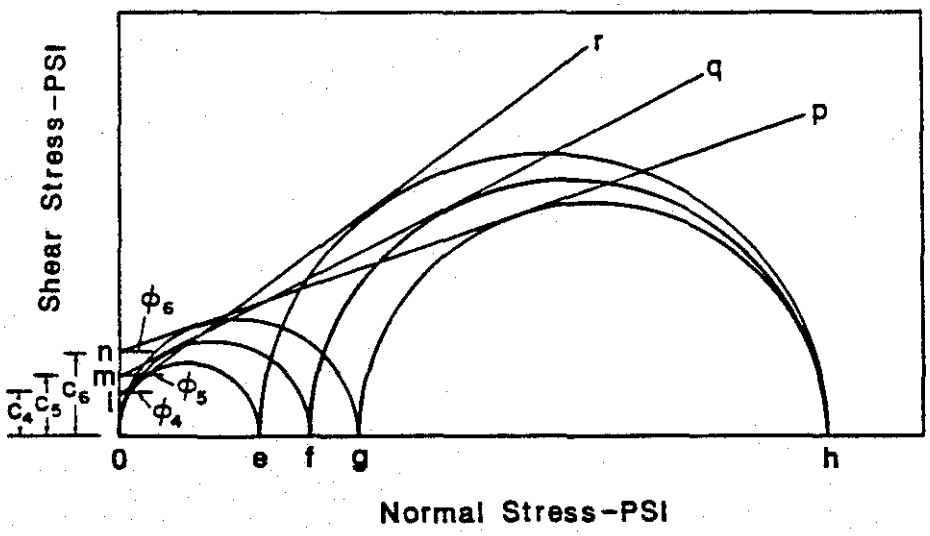

Figure 4.1. Evaluation of asphalt concrete mixture with Mohr-Coulomb failure envelope.

exists in the field. Nevertheless, if the stability of these three mixtures were evaluated solely by the unconfined compression test, the widely different stabilities, Oe, Of, and Og, would be inferred.

The above discussion demonstrates that the one parameter test method used to measure stability of a paving mixture may or may not be influenced by changes in the composition of the bituminous mixtures and may lead to erroneous conclusions. Furthermore, a one-parameter test such as unconfined compression does not account for the triaxial support of the surrounding material.

It is generally agreed that the triaxial test is the most appropriate test by which to characterize the shear resistance and hence rutting resistance of particulate material such as asphalt mixtures. Triaxially-derived strength of the asphalt concrete mixture forms the basis for a "rational" method of evaluating rutting potential and also, more appropriately models the state of stress which exists in the overlay.

The triaxial test measures two fundamental characteristics of bituminous paving mixtures: cohesion, C, and angle of internal friction, ϕ. The magnitudes measured of these parameters depend upon the temperature and the loading rate at which the testing is performed. Typically, nominal high pavement temperatures are in the 120°F to 140°F range. For traffic moving at 55 MPH, the time that a typical tire contact surface spends in contact with a point on the road surface is less than 50 milliseconds. Insofar as moving vehicles are concerned, bituminous pavements are subjected to loads of very short duration, and the viscous resistance developed by the bituminous mixture must be quite high. Therefore, reasonably high loading rates for the laboratory testing of bituminous mixtures to measure stability are justified. However, many pavements on highways and city streets are subjected to breaking and acceleration stresses that have more severe effects on pavement performance and must be considered when employing a load rate. The results of indirect tension testing performed on asphalt mixtures (14) indicate that, at a temperature of 77°F and a stroke rate of two inches per minute, the tensile strength is typically in the 120 psi range. At the same temperature, but at a slower loading rate, the tensile strength is reduced to about one-third its value at a 2-inch per minute stroke rate. This reduction in tensile strength is also true for the mixtures tested at

higher temperatures and the same loading rate. Moreover, if the load rate is increased to a dynamic rate (greater than 2 inches/minute), the strength at a high temperature will substantially increase.

Goetz, et al. (15) have obtained triaxial test data which indicate that the magnitude of the angle of internal friction is not affected by the rate of strain but that the value of cohesion, C, increases steadily as the rate of strain increases. The results of their findings are presented in Figure 4.2.

A 2-inch per minute stroke rate is still relatively slow (16) and does not account for the dynamic effect of the wheel when rapid shear failure is suspected. Also, the 77°F test temperature is quite low and would substantially increase the mixture strength. A combination of stroke rate and temperature that more realistically approximates and simulates the conditions in the field is a stroke rate of 4-inch per minute at 104°F. However, the stroke rate of 4-inches per minute is believed to be more damaging (in terms of permanent deformation) than the dynamic rate representing 55 mph. Further research and field investigation in this area is needed to provide average values and the range of values possible for these variables. Nevertheless, at the present time, the proposed temperature and load rate is more appropriate to develop Mohr-Coulomb failure envelope than the triaxial testing procedure which is conventionally used to characterize stabilized mixes.

Uniaxial Creep and Repeated Load Deformation Testing

Repeated load permanent deformation testing will be discussed in more detail in Chapter X with respect to the ILLIPAVE and mechano-lattice performance models. The authors have selected the Tseng and Lytton (17) 3-parameter power law for description of permanent deformation under cycles of loading. Constants used in this model are generated from a nonlinear regression process. The model has the following form:

$$\epsilon_a = \epsilon_o \cdot \text{EXP} - \left(\frac{\rho}{N}\right)^{\beta} \qquad (4.1)$$

where: ϵ_a = permanent strain,

N = load cycles, and

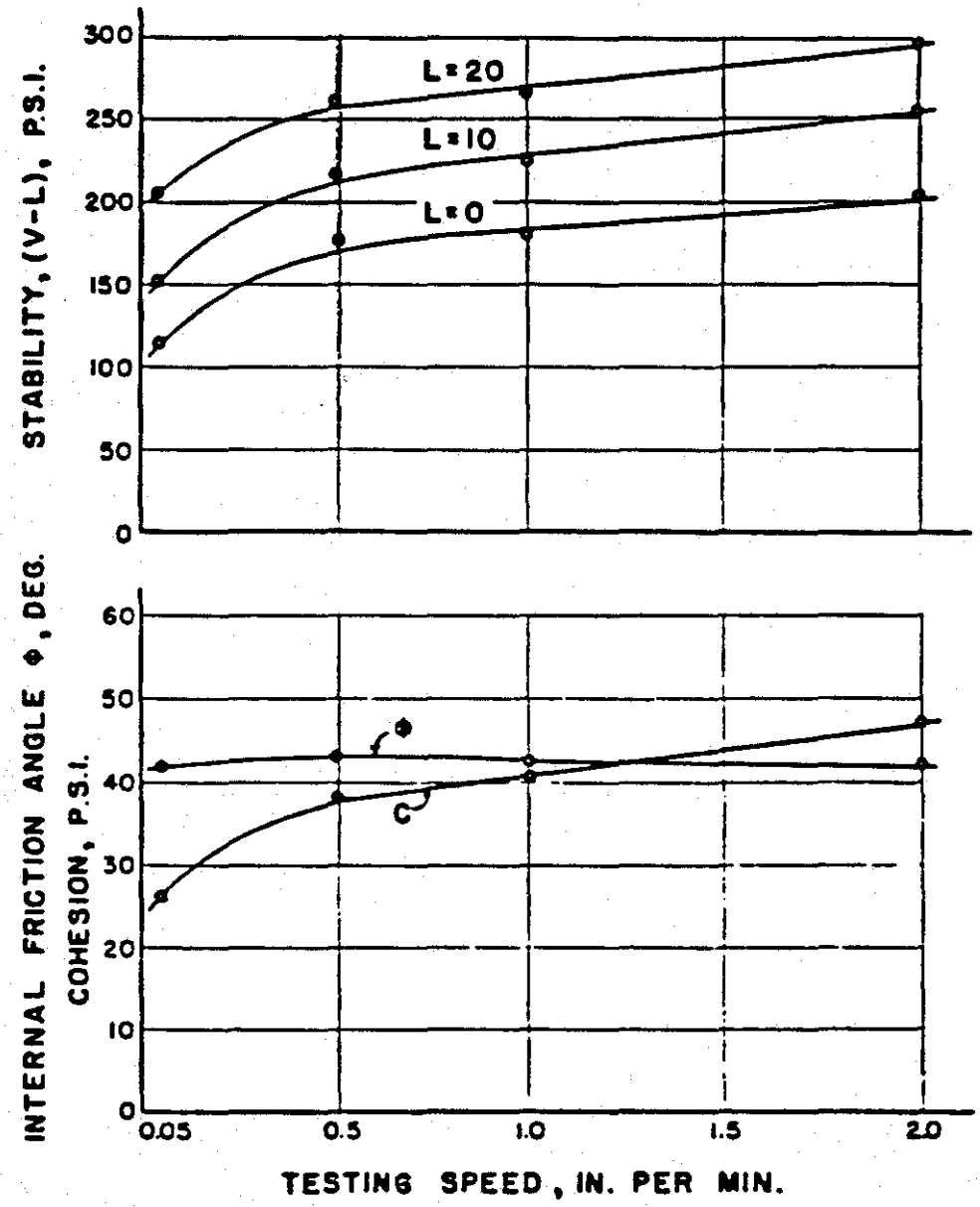

Figure 4.2. Test properties vs. testing speed for asphalt paving mixtures (after Reference 15).

ϵ_o, β, ρ = regression constants.

The Tseng-Lytton model provides a better fit for the permanent deformation data and justification for the form of the equation based on activation energy concepts. Although this relationship provides a powerful tool for permanent deformation data analysis, it requires repeated load testing rather than static creep testing. The three parameters in the Tseng-Lytton model are highly interdependent and are determined by nonlinear regression techniques. These constants are treated as pseudo material properties.

The Tseng-Lytton model, together with input data from cyclic load permanent deformation testing, will be used in the modified ILLIPAVE computer model to evaluate various asphalt concrete mixtures under various structural conditions. These results will be compared to those employing the octahedral shear stress analysis and triaxial shear strength testing.

Static, uniaxial creep testing is another test to be considered by which to evaluate deformation potential. The most popular way to expediently analyze static, uniaxial creep testing is by means of the Shell equation of predictive rutting. This well-established, straightforward relationship states:

$$h = H \cdot c_m \cdot Z \cdot \frac{\sigma_{tire}}{S_{mix}} \qquad (4.2)$$

where: h = rut depth in inches,
C_m = correction factor used in transforming from static loads in the laboratory to dynamic field loads,
Z = stress distribution factor,
σ_{tire} = tire constant pressure in psi, and
σ_{mix} = stiffness of the mixture as measured from the creep test.

Mahboub and Little (18) have pointed out substantial limitations in the Shell relationship. Concisely stated, these limitations are:

1. The assumed Hookian constitutive relationship as established by the relationship between σ_{tire} and h based on the pseudo-elastic parameter, σ_{mix}.

2. The correction factor, C_m, which works to correct laboratory data to match field observations but in an illogical manner as explained by Mahboub and Little.
3. The assumption of linearity between stress and permanent strain in the Shell Hookian relationship which has been shown by Mahboub and Little to be nonlinear.

Mahboub and Little developed a modified form of the Shell equation which accounts for the viscous and visco-plastic components of mixture stiffness which lead to permanent deformation and which account for the effects of nonlinearity.

The modified Shell equation thus reads:

$$h = H \left(\frac{Z\sigma_{tire}}{\sigma_{lab}} \right)^{1.61} \epsilon_{vp}(t) \qquad (4.3)$$

where:
- h = calculated rut depth in inches,
- H = asphalt concrete thickness in inches,
- Z = vertical stress distribution from layered elastic solutions,
- σ_{tire} = average tire contact pressure in psi,
- σ_{lab} = stress level in psi at which the creep test was conducted, and
- $\epsilon_{vp}(t)$ = viscoplastic strain in the creep test measured in units of in./in.

This relationship can be used with uniaxial, compressive, static creep data to predict relative rutting potential among various asphalt concrete mixtures.

When the potential of repeated load deformation (uniaxial), static uniaxial creep testing, and triaxial shear testing to predict permanent deformation is compared, triaxial testing over a range of confining pressures emerges as the most fundamentally sound procedure. This is especially true when the triaxial testing is coupled with failure criteria based on strain energy or the closely-allied octahedral shear stress concept. This procedure will be developed subsequently.

CHAPTER V

COMPUTER MODELS AND OVERLAY STRUCTURE

The ILLIPAVE Model

Many computer programs have been developed to model pavement structures. These programs can be generally divided into elastic-layered programs and finite element programs. Most pavement materials exhibit nonlinear stress-strain behavior. A finite element method can be adopted to handle this nonlinearity. A program based on the finite element method incorporating nonlinear material properties was developed by Duncan et al. (19). This program was improved to include a failure model for granular and subgrade soils based on the Mohr-Coulomb failure theory (20) and was renamed ILLIPAVE. The program predicts the response of flexible pavements to load, and the results have been compared with field test data with favorable results (21). The modified version of ILLIPAVE models a pavement three-dimensionally by using a two-dimensional halfspace of a finite solid of revolution.

Modified ILLIPAVE has the ability to incorporate linear and nonlinear characterization of materials, to interface relationships between the pavement layers, and to predict rut depth, slope variance, fatigue cracking, and present serviceability index with time (22). The ILLIPAVE mechanistic design concepts and procedures have been validated for 9,000 pound traditional highway wheel loading for conventional flexible pavements, for full-depth asphalt concrete pavements, and for flexible pavements containing lime-stabilized layers. It has also been validated for low-volume F-4 aircraft loading on flexible pavements containing cement and lime-stabilized layers (23). Modified ILLIPAVE was further modified to incorporate a technique developed in this study to account for seasonal temperature variations for different locations within the State of Texas. Four typical climatic zones in Texas, each containing four seasonal temperature distributions in the asphalt layer, were developed. Maps of average monthly high temperatures, as shown in Figure 5.1, were used to help in defining the regions. Another important factor incorporated into the program is the traffic distribution in combination with

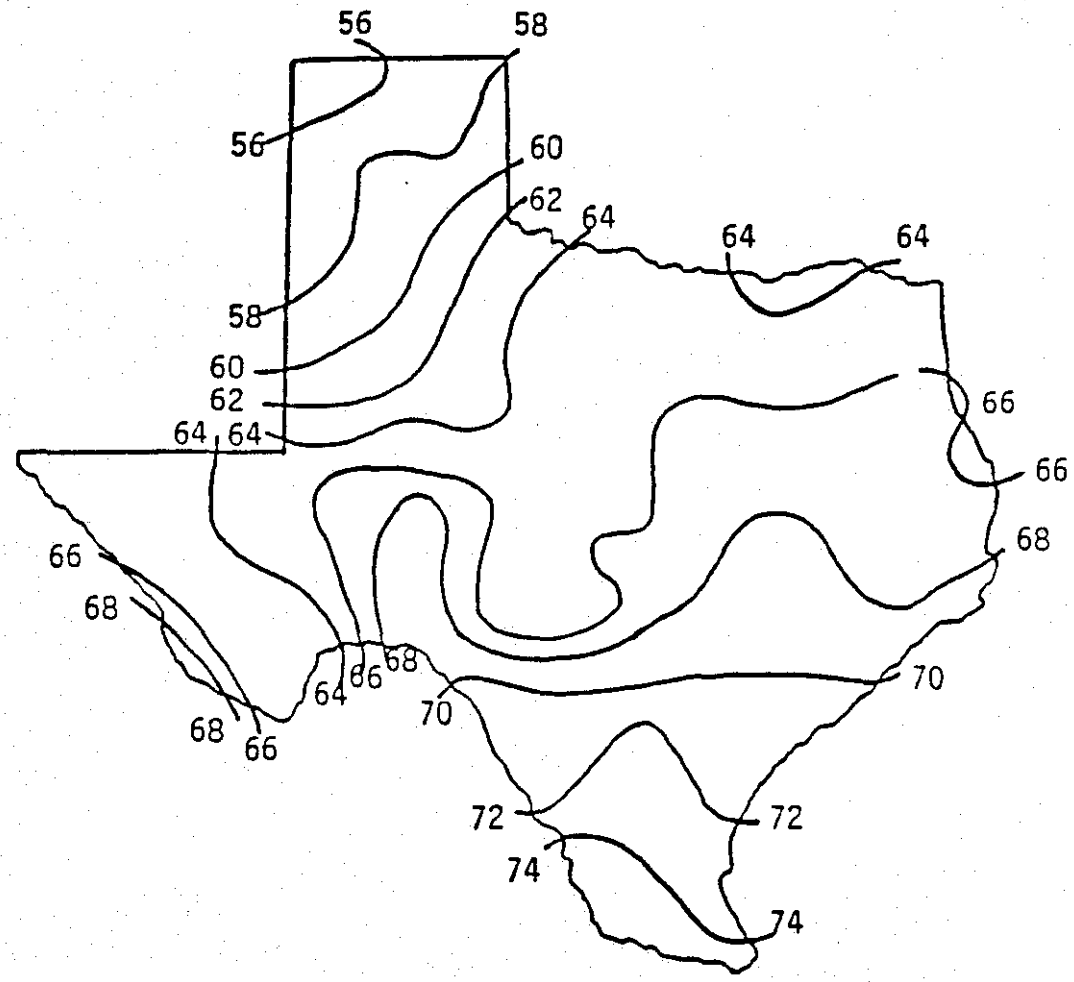

Figure 5.1. Texas weather data, mean annual air temperature in degrees Fahrenheit (after Reference 18).

temperature and climatic variation. A distribution function was developed (22) that considers the combined effect of traffic and temperature within the time frame (history) that both temperature and traffic occupy. Thus, the modified ILLIPAVE computer model used in this study has the ability to evaluate pavement rutting and slope variance for a specific traffic and temperature history.

Permanent Deformation Model

As discussed in Chapter IV, permanent deformation in a pavement layer under repeated loading has been modeled in various ways. However, most investigators have agreed that the permanent deformation characteristics of a paving mixture can be approximated by a constitutive power-law relationship.

In the mechano-lattice model, Yandell (24,25) estimated the rut depth at the surface of the pavement using a linear relationship of log ϵ_p versus log N. However, there are certain limitations which have affected the program's efficiency, and the program needs extensive modification to reduce iteration steps, computation time, and variable convergence, especially for the problem of ACP overlays over rigid, stiff bases such as PCC bases.

The VESYS model for permanent deformation (26) uses the simple power-law to characterize rutting as a strain hardening process. The equation is of the form:

$$\epsilon_{vp} = at^b \tag{5.1}$$

where: ϵ_{vp} = viscoplastic strain,
t = time, and
a, b = regression constants.

Many other investigators (27,28) have also suggested power law constitutive equations of a similar nature with incorporation of additional stress dependent terms to address permanent deformation characteristics of asphalt concrete mixtures.

However, this research study will concentrate on using the ILLIPAVE computer program which has been modified to incorporate a model that was developed as part of an extensive research study at Texas A&M University

(TTI) to predict permanent deformation of asphalt concrete overlays on concrete pavements (22). In this method, the prediction of rutting is based on characterization of permanent deformation in terms of three parameters, ρ, β, ϵ, representing material characteristics. These parameters are derived from the results of creep and recovery or repeated load triaxial laboratory testing at different temperatures. The curve used by the program to describe the relationship among these three parameters is represented by the form:

$$\epsilon_a = \epsilon_0 e^{-(\rho/N)^\beta} \tag{5.2}$$

where: ϵ_a = permanent strain,
N = number of cycles,
ρ, β, ϵ = material properties obtained from nonlinear regression equation.

Equation (5.2) was derived from activation energy concepts and provides an excellent fit to the permanent deformation data (18). The physical meaning of Equation (5.2) can be explained by the graph in Figure 5.2. The parameter ρ is the rate of accumulated permanent strain; a larger number indicates a smaller accumulation of permanent strain. The exponent β permits the curve to take on a variety of shapes. All of the curves pass through a common point where $N = \rho$ and $\epsilon_a/\epsilon_o = 1/e$ (where $e = 2.718$). The multiplier ϵ_o is a weighing factor; a larger number indicates larger accumulated permanent strain. The values of ϵ_o, β, and ρ are different for each sample depending on the type of the materials and their physical properties, stress state, and conditions such as temperature during testing.

These three parameters can be obtained from the SAS NLIN program (29) simply by incorporating the plastic (nonrecoverable) strain, measured from the repeated load permanent deformation test, as a function of the number of loading cycles or time of loading at various cycles or time increments through various cyclic testing. This relationship provides a least-square estimate of the parameters of a nonlinear model. However, another accurate and simple method to calculate these parameters has been developed (30). By taking the derivative of Equation (5.2) and manipulating the results, the result becomes the equation of a straight line:

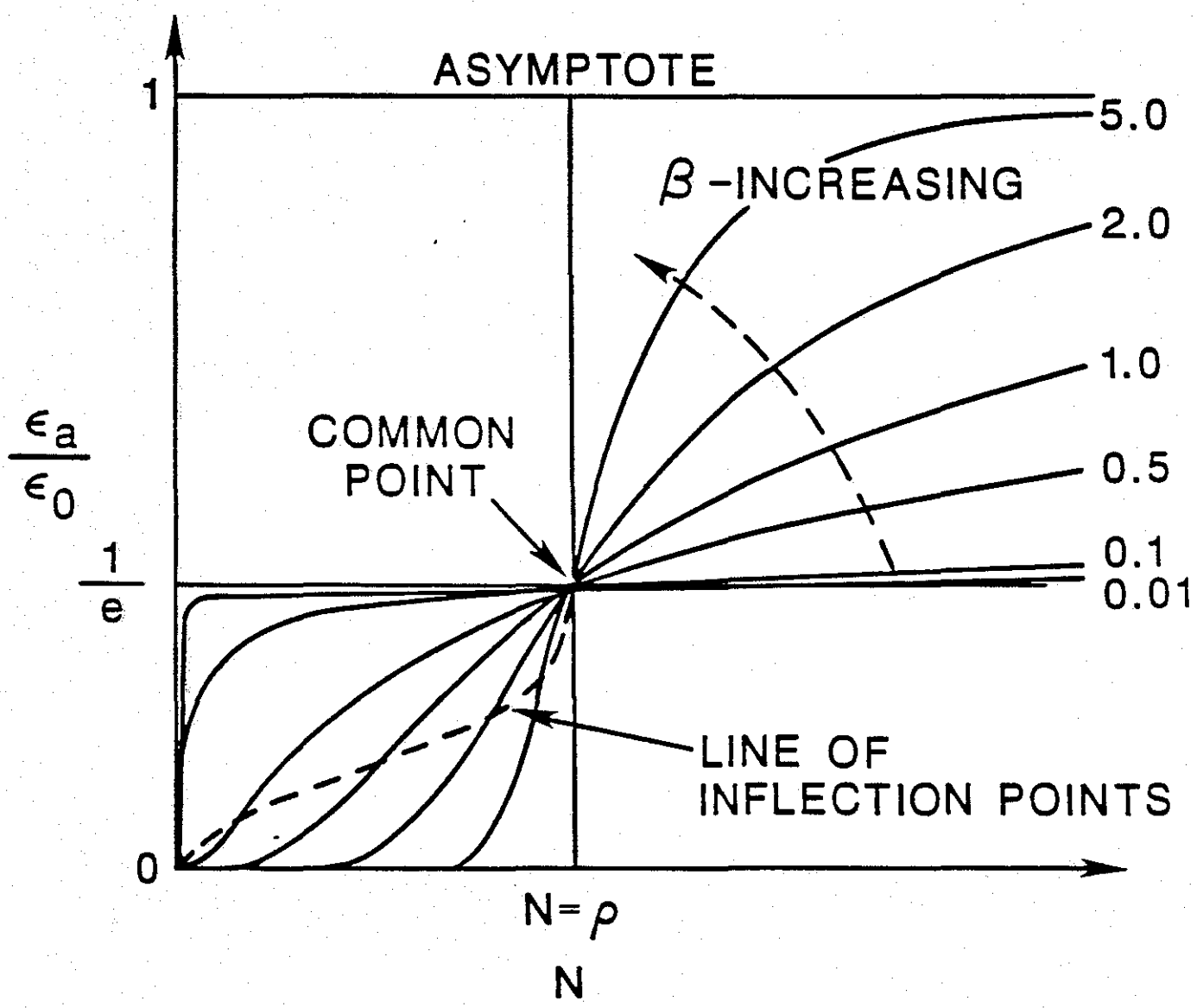

Figure 5.2. Shape of three-parameter equation used in permanent deformation characterization (after Reference 66).

$$\log [\Delta(\ln \epsilon_a)/\Delta(\ln N)] = \log (\beta\rho)^{\beta} - \beta \log N \qquad (5.3)$$

Beta, β, is the slope of the line given by Equation (5.3). Once β and ρ are obtained, ϵ_o can be computed from Equation (5.2) by averaging the values of permanent strains against the number of load cycles. Although the procedure can be performed by hand calculations, a FORTRAN computer program has been developed to facilitate the necessary calculations and to obtain the desired parameters.

The modified ILLIPAVE computer program was used extensively for this analysis as well as analyses of stress and development of octahedral shear stress contours within the overlay surface layer. The rectangular halfspace was divided into a set of rectangular elements connected at their nodal points. A uniform contact pressure of 100 psi at the pavement surface was used with and without the presence of surface shear.

Horizontal Surface Shear

Surface shear is developed when an inflated tire is deflected against the pavement surface as well as by rolling resistance between tire and the pavement surface. Restrained tangential motion due to vertical deflection of the tire generates tangential stress, as shown in Figure 5.3, for both a standing and a rolling tire. A finite element tire model was developed at Texas A&M University (TTI) to investigate tire-pavement interaction during vehicle maneuvering. For this program, neither the contact pressure distribution nor the contact area are known a priori (30). The mathematical model developed by Tielking and Schapery was used to calculate the pressure distribution and deformation of the tire deflected against the pavement surface. This model not only includes a nonuniform vertical distribution (Figure 5.4) of the load and pressure, but also the horizontal shear stress distribution at the surface (Figure 5.5). The magnitude of horizontal loads is usually dependent on the coefficient of friction between the tire and the pavement, which will vary with pavement and tire conditions. It is also a function of tire construction and structure. For instance, the transverse pavement force developed by a radial tire is about one-half the peak transverse force developed by a bias-ply tire (30). Therefore, variation of horizontal shear force is dependent upon the tire print geometry.

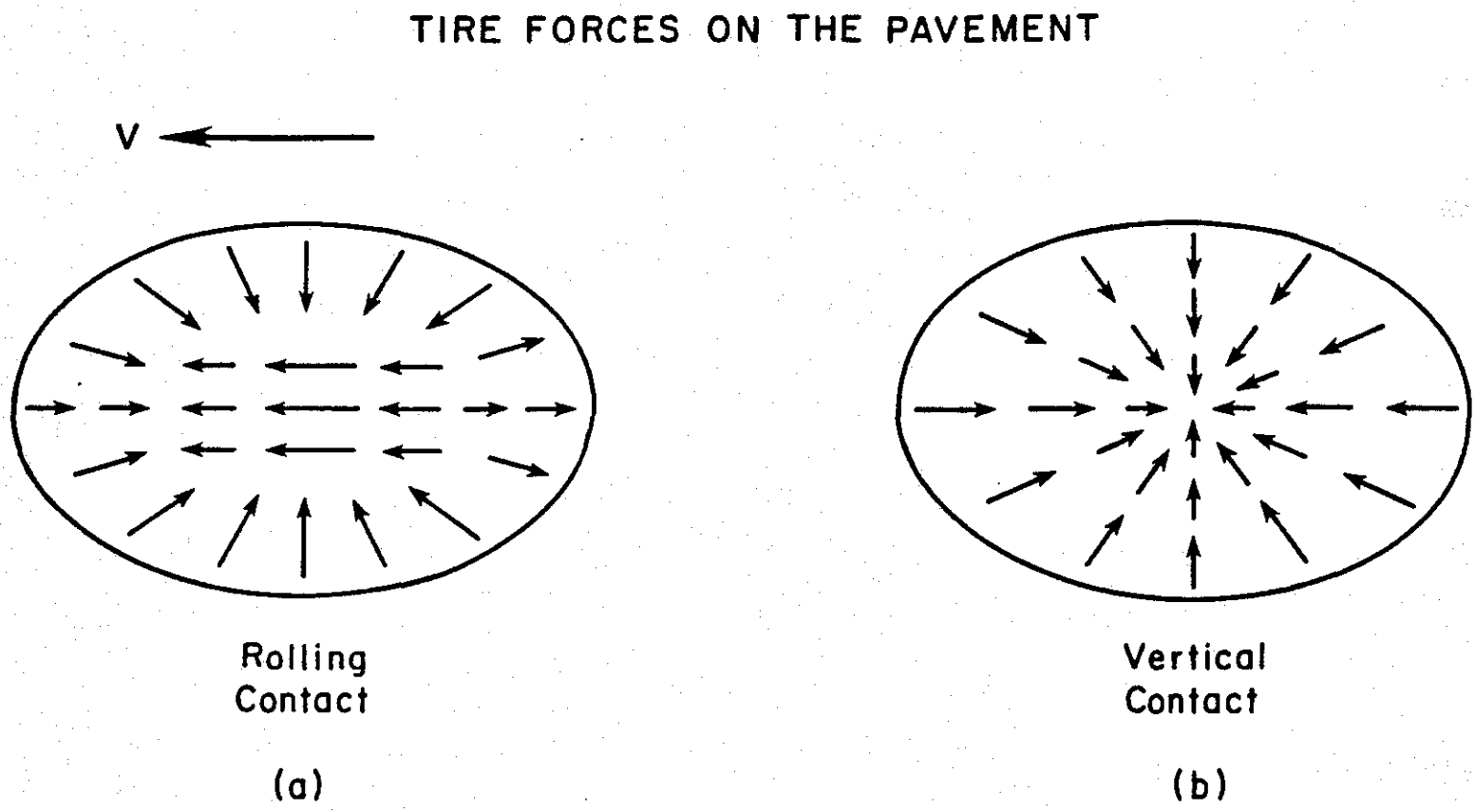

Figure 5.3. Distribution of tire shear forces under a standing tire (vertical) contact and under a rolling tire (after Reference 21).

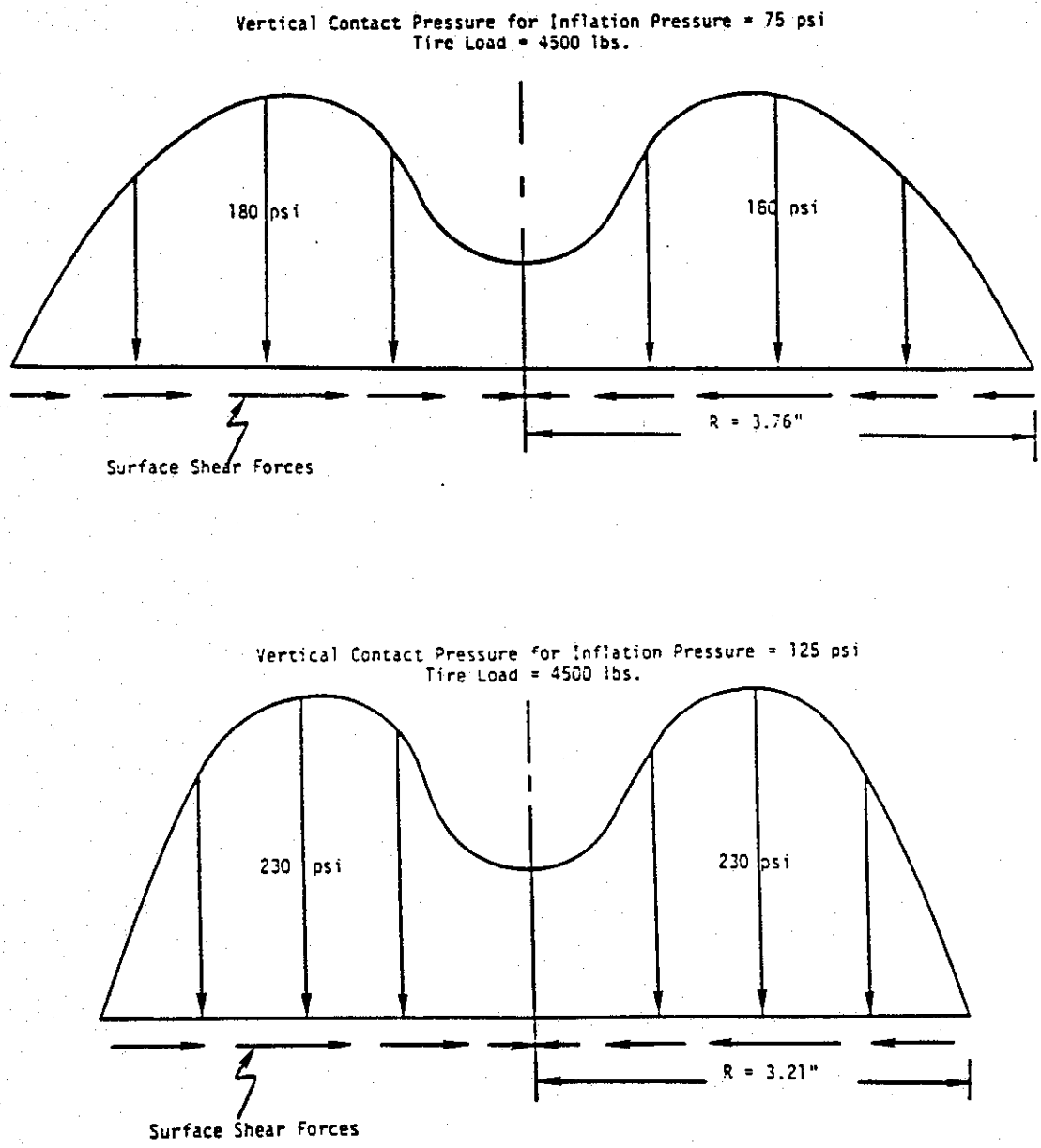

Figure 5.4. Nonlinear vertical tire pressure distribution with lateral surface forces as developed using finite element model by Tielking (after Reference 21).

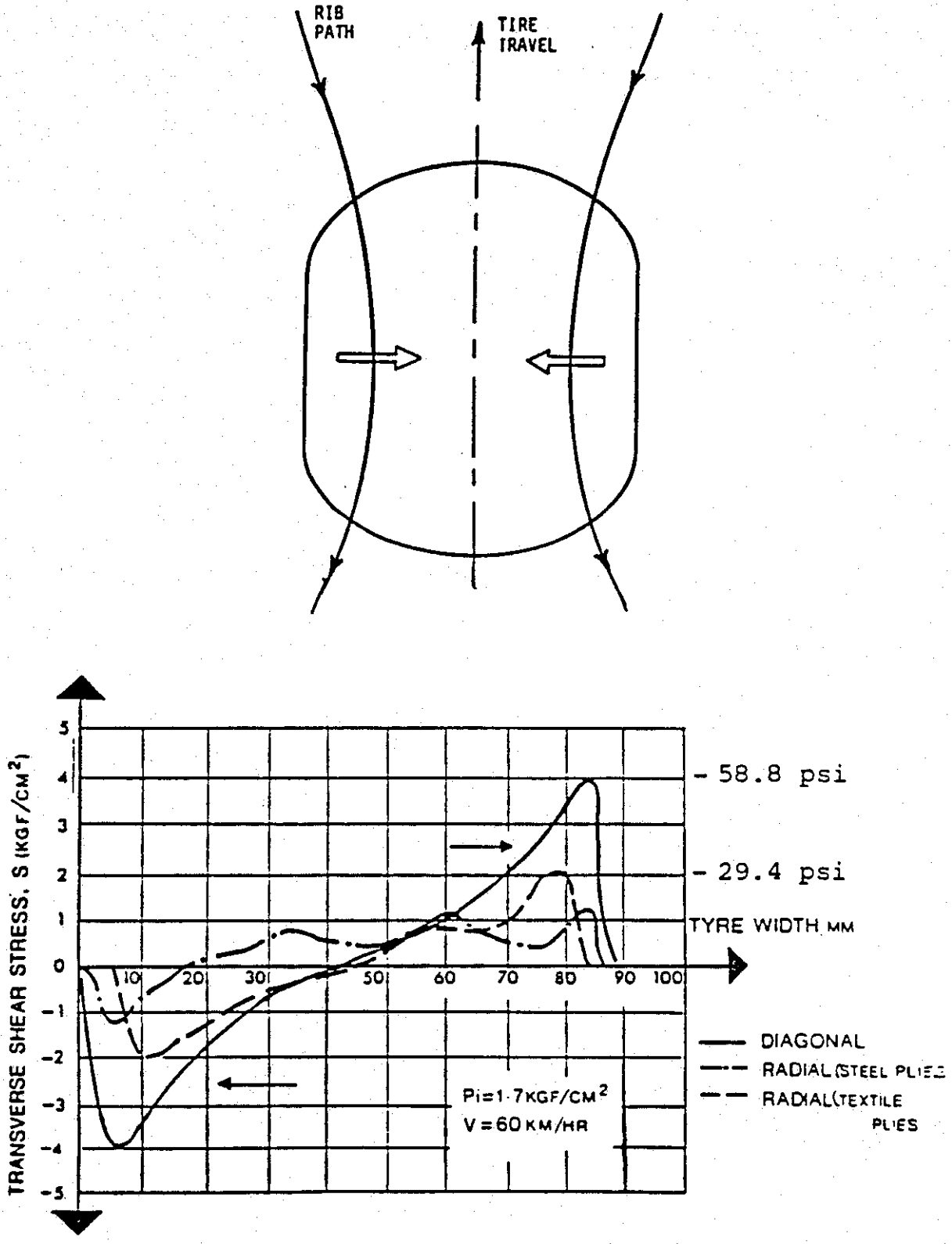

Figure 5.5. Transverse shear stress distribution across the footprint of radial and bias-ply (diagonal) tires during free-rolling (after Reference 21).

In this investigation horizontal shear pressures were modeled as a function of a sine curve with a maximum lateral pressure of 50 psi. This distribution and maximum value of pressure were selected to be a reasonable representation of lateral pressure distribution (21). A separate computer program was developed to transform the calculated horizontal surface shear forces from an elliptical tire print, assumed by the Tielking tire model, to equivalent horizontal surface shear forces on a circular tire print used by the modified ILLIPAVE computer program. These forces were then resolved and applied to the nodal points within the contact area of the loaded rectangular mesh developed for overlay stress analyses.

Temperature and Traffic Models

The mechanical response of asphalt concrete overlay mixtures is greatly influenced by the external variables of temperature and traffic. Climate and traffic are the two main external factors in the accumulation of rutting for asphalt concrete overlays. Under the same climate, different traffic patterns with the same traffic volume (ADT) could result in different rut depths for an identical asphalt pavement. Therefore, it is important to find the relationship between traffic distribution and temperature distribution. Although traffic and temperature are two different variables, i.e., the temperature distribution in the asphalt concrete layers varies with different geographical locations and with thicknesses of the layers, and traffic distributions vary with the types of roadways; they can be linked by the time frame (history) that both occupy.

Texas occupies at least four distinct climatic regions. The map of average high temperatures during the month of July (31) (Figure 5.6) was used to divide the state into these four distinct regions (Figure 5.7). In this study, thirty years of climatic data (from 1955 to 1984) was obtained from the National Data Center in Asheville, North Carolina. Based on this extensive volume of the weather data, a regression model was developed (22), which predicts air temperature at any locality within the state of Texas at any time during the year. This model then translates the air temperature into pavement temperature profiles which are expressed as a function of depth for any type of overlay structure.

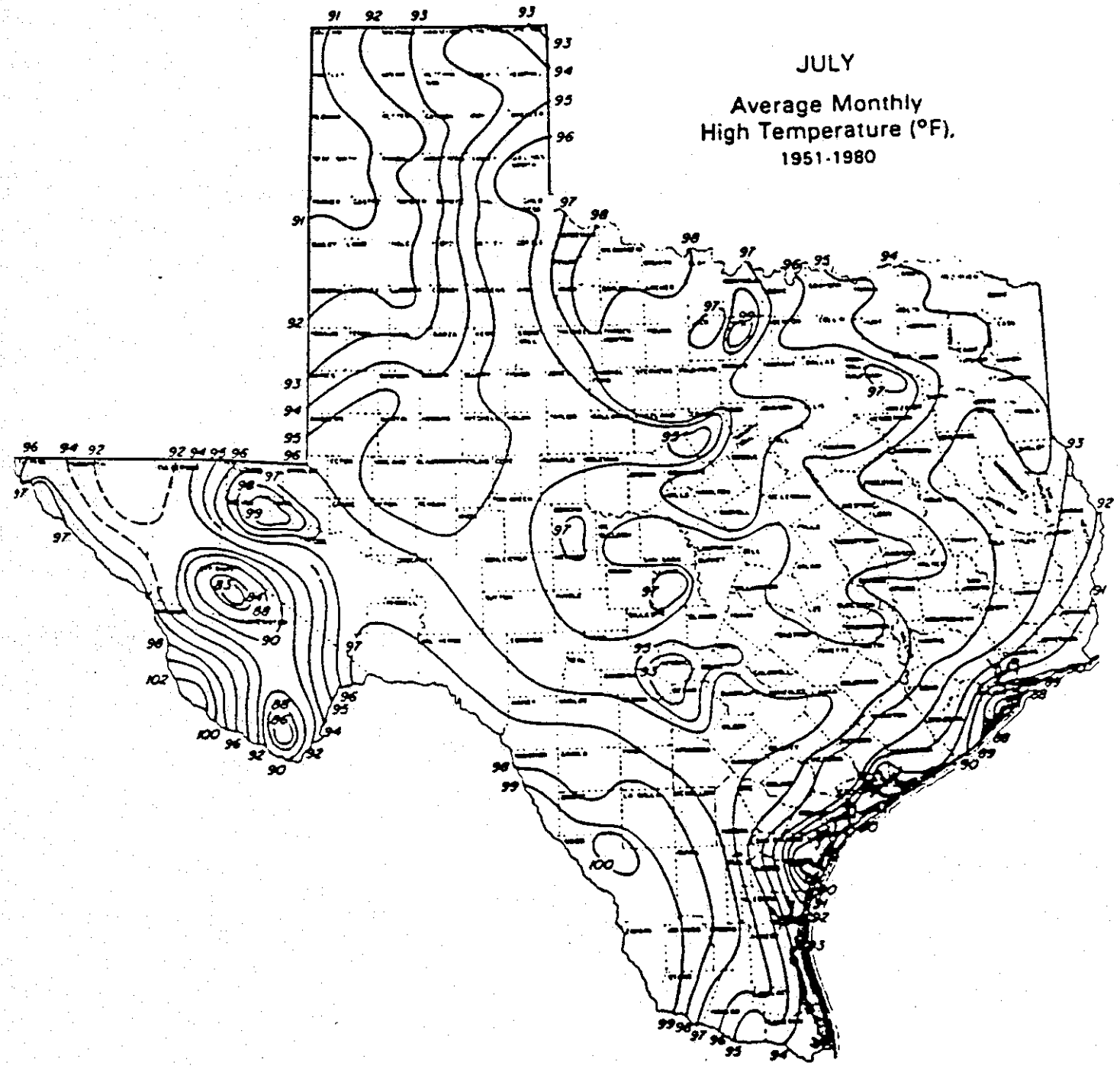

Figure 5.6. Average monthly high temperature of July (after Reference 22).

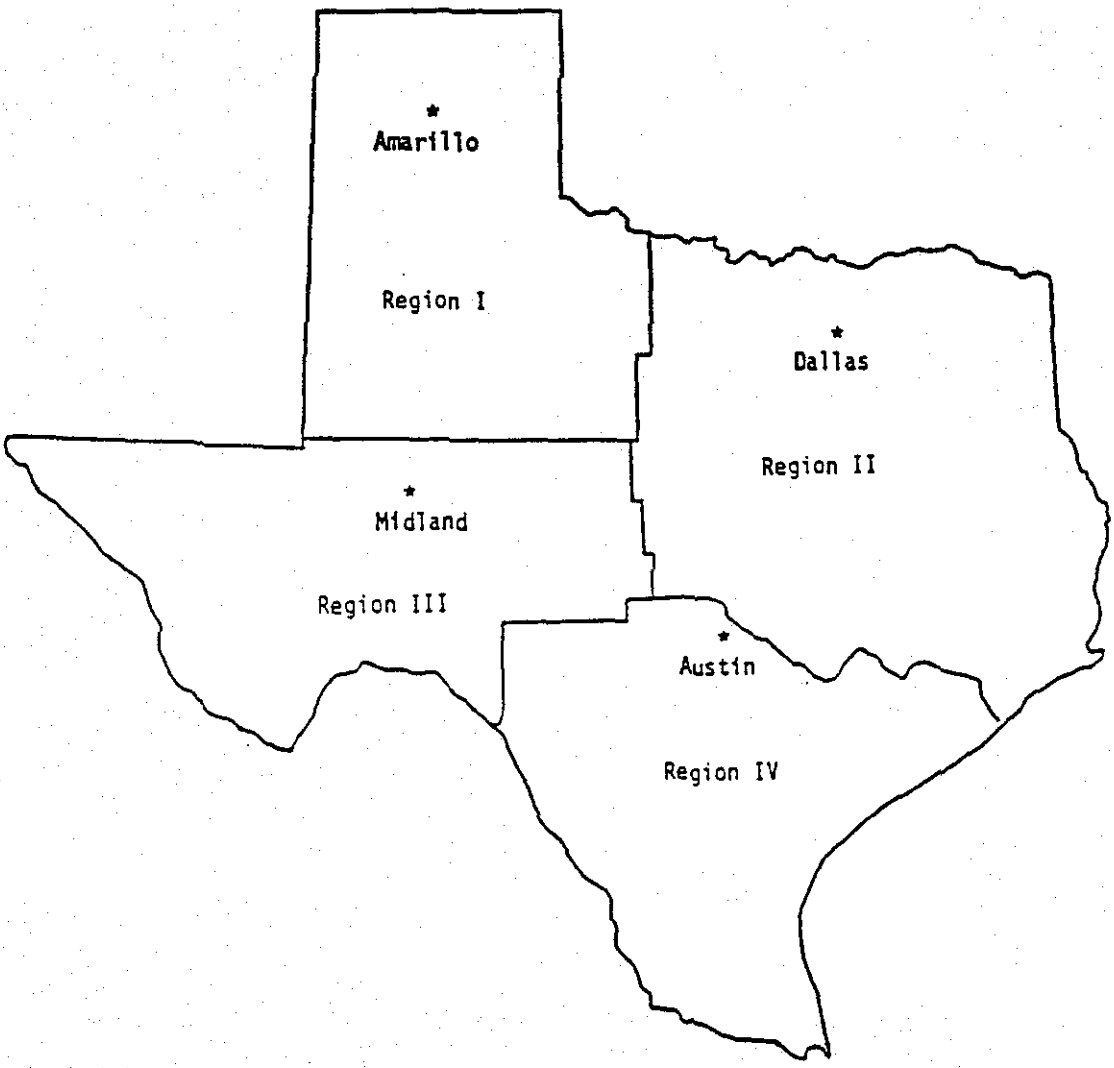

Figure 5.7. Temperature regions within Texas (after Reference 22).

The model considers the 180 hottest days of an average year within the 30 years of the weather data studied. In developing the average monthly temperature distribution with depth, the following assumptions were made (22):

1. Permanent deformation occurs daily over the time interval from 0730 to 1730 hours,
2. Permanent deformation occurs only in the period from April to October, inclusive, and
3. Permanent deformation can be ignored at temperatures below 50°F.

The temperature model is divided into two important periods: one representing the daytime; another representing the nighttime. The R^2 values for the regression models for asphalt-concrete overlays varying from 2 to 5 inches are all above 0.98. The general forms of the models are:

$$T = a_o + a_1 x + a_2 y + a_3 z + a_4 yz + a_5 x^2 + y^2 + a_7 y^2 z + a_8 y^3 \qquad (5.4)$$

where: T = temperature of the center of each sub-layer,
x = period of year (x=1, 2, 3, ... 36),
y = hours of the day (y>7 or y<19),
z = sublayer (z = 1, 2, 3,... n), and
$a's$ = regression constants, and

$$T = b_o + b_1 x + b_2 y + b_3 z + b_4 x^2 + b_5 y^2 + b_6 y^3 + b_7 y^4 \qquad (5.5)$$

where: T = temperature at the center of each sub-layer,
x = period of year (x=1, 2, 3, ..., 36),
y = hours of the night (y<7 or y<19),
z = sublayer (z=1, 2, 3, ..., n), and
$b's$ = regression constants.

Companion report 2452-1 (22) describes the development of these regression models in detail. When used in conjunction with appropriate traffic models and incorporated into ILLIPAVE, these regression models provide comprehensive rutting predictions. The effect of traffic is accounted for by a stepwise integration of traffic and temperature over

the range of the common time variable in the rutting model. A procedure outlined by Li et al. (22) is presented in Figures 5.8 and provides the necessary steps to superimpose these two independent (temperature and traffic) variables.

The traffic distribution function is developed by recording traffic data, and plotting a relative frequency histogram over certain time intervals of an assumed traffic density function. If a continuous curve defines the distribution, the relative frequency histogram becomes the traffic density function (22). The relationship between temperature and traffic density was found by relating the temperature distribution at the top of the asphalt concrete sublayer and the traffic density function as follows:

1. According to the temperature at the center of the overlay sublayer, six temperature profiles were obtained (Table 5.1a).
2. The mean temperature at the center of each sublayer for each temperature range was calculated by mean analysis, and then the frequency of each temperature range was calculated by frequency analysis.
3. The same temperature ranges (Table 5.1a) were used to superimpose the whole traffic volume into the six temperature profiles according to the time history that both temperature and traffic occupy.

The ILLIPAVE computer program has been modified to accommodate these models. Modified ILLIPAVE is now capable of predicting rut-depth while accounting for specific temperature and traffic frequency histograms according to the procedures and the methods outlined.

Variables Considered in the Octahedral Shear Stress Analysis Utilizing the Modified ILLIPAVE Computer Model

As discussed in Chapter III and Appendix A, the octahedral shear stress is perhaps the failure criterion most applicable to the evaluation of deformation potential in the asphalt concrete overlay. The distribution of octahedral shear stresses within the ACP overlay and evaluation of material properties which determine the success or failure of a

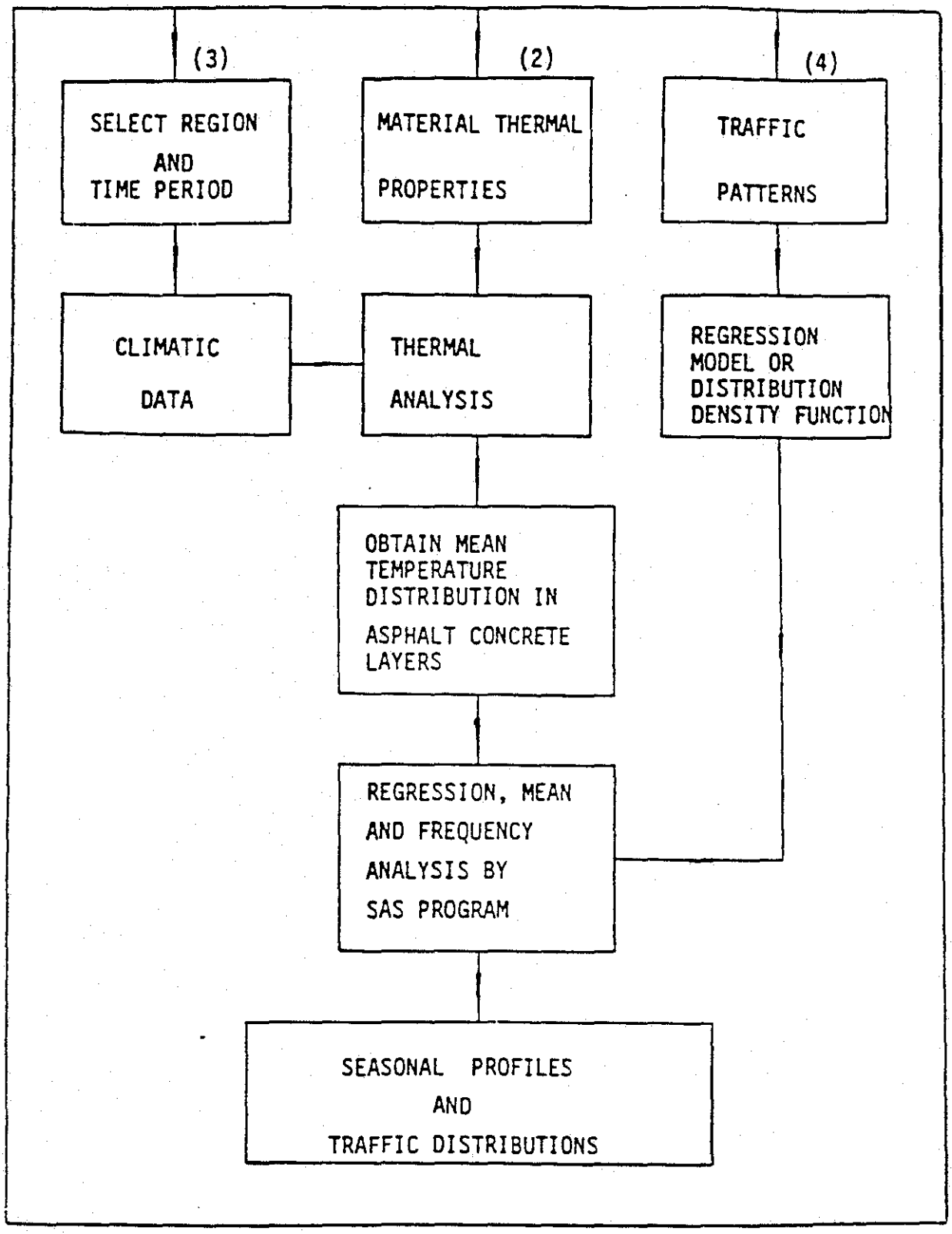

Figure 5.8. Schematic outline procedure for considering the effects of temperature and traffic on deformation (after Reference 22).

pavement layer cannot be assessed without consideration of the pavement structure.

The eight pavement structures discussed below represent the pavement types considered in the development and analysis of octahedral shear stress distributions. The performance evaluation of asphalt concrete overlay mixtures are based upon their mechanical response within these pavement structures.

The structural categories and representative pavement cross-sections are:

1. Thin overlay rigid base: 2 inches asphalt concrete, 8 inches PCCP ($E_c = 3 \times 10^6$ psi), clay subgrade ($E_{subgrade} = 7500$ psi).
2. Intermediate overlay rigid base: 4 inches asphalt concrete, 8 inches PCCP ($E_c = 3 \times 10^6$ psi), clay subgrade ($E_{subgrade} = 7500$ psi).
3. Semi-Thick overlay rigid base: 6 inches asphalt concrete, 8 inches PCCP ($E_c = 3 \times 10^6$ psi), clay subgrade ($E_{subgrade} = 7500$ psi).
4. Thick overlay rigid base: 8 inches asphalt concrete, 8 inches PCCP ($E_c = 3 \times 10^6$ psi), clay subgrade ($E_{subgrade} = 7500$ psi).
5. Thin overlay flexible base: 2 inches asphalt concrete, 8 inches granular base ($E_r = k\theta^n$), clay subgrade ($E_{subgrade} = 7500$ psi).
6. Intermediate overlay flexible base: 4 inches asphalt concrete, 8 inches granular base ($E_r = k\theta^n$), clay subgrade ($E_{subgrade} = 7500$ psi).
7. Semi-thick overlay flexible base: 6 inches asphalt concrete, 8 inches granular base ($E_r = k\theta^n$), clay subgrade ($E_{subgrade} = 7500$ psi).
8. Thick overlay flexible base: 8 inches asphalt concrete, 8 inches granular base ($E_r = k\theta^n$), clay subgrade ($E_{subgrade} = 7500$ psi).

Considering these structural categories and pavement cross sections, the influence of the following factors on the distribution of octahedral shear stress was investigated:

1. Total interface bonding,
2. Partial interface bonding,
3. Zero interface bonding,

4. Total interface bonding with presence of surface shear,
5. Zero interface bonding with presence of surface shear and
6. Stiffness of the overlay.

In the above pavement structures, the resilient modulus of granular base materials is modeled as:

$$(E_r = k\theta^n) \tag{5.6}$$

where: E_r = resilient modulus in psi,
θ = sum of the three principal stresses in psi and
k, n = constant determined from testing.

From the 1986 AASHTO Guide for Design of Pavement Structures (32), midrange values of K = 6000 and n = 0.6 were selected for these analyses as these are representative of high-quality granular base material.

The Mechano-Lattice Model

The mechano-lattice technique offers a unique method of modeling multilayered pavement systems. In this model, approximately 4000 mechano-lattice units are connected at their frictionless joints to simulate the asphalts, base, and subbase structure of the pavements. A 9000 pound wheel load is simulated to roll in one direction. The asphalt-base and base-subgrade interfaces have provisions for slip which depend on the interface friction parameter. Thus, interface bonding may be varied from a free slip condition to full frictional development.

Figure 5.9 is a longitudinal section of the simulated mechano-lattice pavement through the load. The units on the extreme left hand side shown by broken lines represent the initial conditions before a particular wheel pass. Elastic theory is used for predicting the shape of each unit as it arrives at the simulating region from the residual, no load condition well forward of the "present" load. The consequent change in unit shape will cause the elements to change in length, and therefore, change their element load also. Similar things happen when the "wall" of units move another place closer to the load. Thus, as the sequential movement of the wall of units from left to right - toward, under, and away from the load - takes place, the load-deflection history of each element is followed mathematically. This is done by calculating changes in length

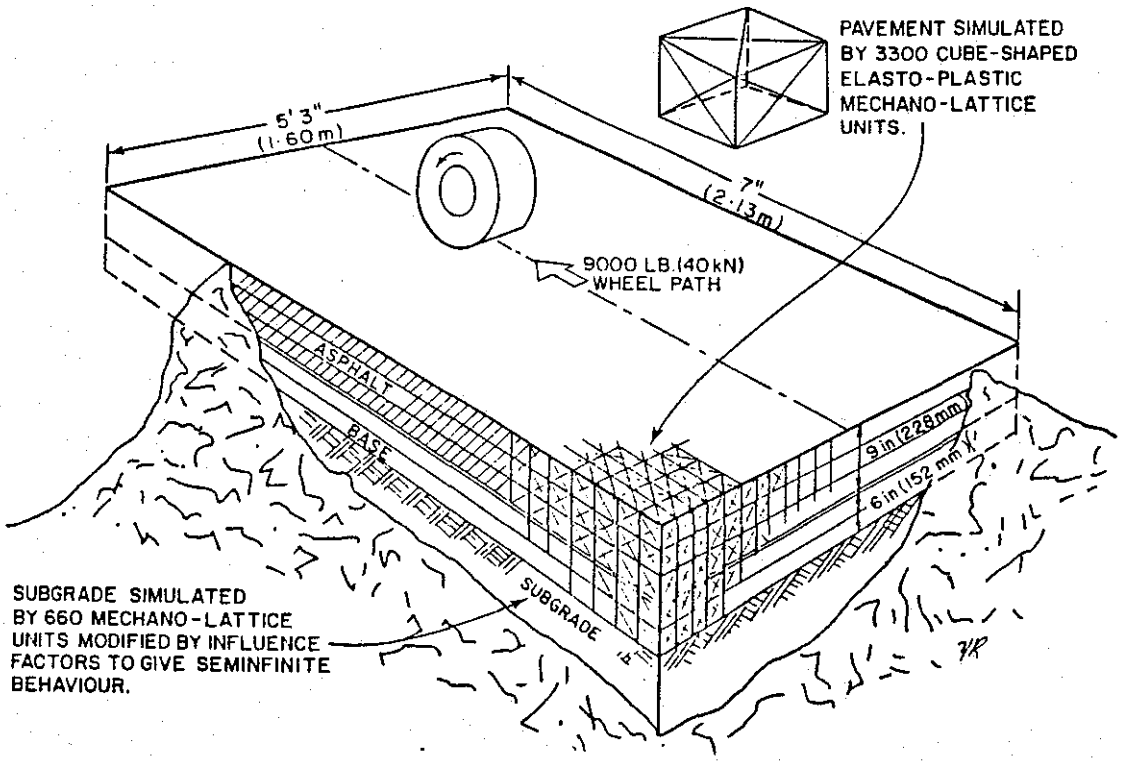

Figure 5.9. Representation of mechano-lattice model (after Reference 24).

and changes in load with the aid of the stiffness factors. A permanent inventory of element loads is kept "up-to-date." The computer program performs a similar, though more complex task after each cycle of element length-load calculations in which the forces at each joint emanating from their attached elements are resolved into vertical, longitudinal, and lateral components. The joint is then moved in a damped manner in the direction of the unbalanced forces. The calculation damping factor is proportional to the largest force that is instantaneously out of balance at any free joint. The process is continued until all out of balance forces on free joints become insignificant. For this problem, between 1500 and 2000 computation cycles are needed. After convergence and after stresses have been calculated, the wall of units on the right of Figure 5.9 (in the residual condition) is used as initial conditions for the next simulated wheel pass and the above process is repeated.

The mechano-lattice computer model is an extremely powerful tool and was tried extensively in this study. However, Professor Yandell, developer of the model, was unable to achieve successful convergence (all out of balance forces on free joints become insignificant) of the elements when the rigid PCC base was modeled into the system. Initial attempts required over 4,000 iterations before convergence was achieved. After much alteration of the model, convergence was achieved in approximately 2,500 iterations. However, each time a pavement structural parameter was changed in the analysis, it was not possible to achieve convergence without time-consuming and expensive program alterations. Consequently, the mechano-lattice model was not used, in favor of the modified ILLIPAVE model which could be more easily altered to incorporate the traffic and temperature models and could be more efficiently run.

Modified Shell Deformation Model

As discussed in Chapter IV, Evaluation of Laboratory Test Procedures, the modified Shell equation developed by Mahboub and Little (18) offers an expedient method by which to evaluate deformation potential. Because of the simplicity and expediency of the approach, this analysis was used in this study to supplement the Mohr-Coulomb shear strength analysis and repeated load (cyclic) permanent deformation testing analyzed by the modified ILLIPAVE computer model.

The procedure for using the modified Shell equation is introduced in Chapter IV and is explained in detail in Reference 18. Concisely stated, this procedure utilizes the static, compressive, uniaxial creep test, and a recovery test to define plastic, nonrecoverable strain as a function of time of loading. Nonlinearity of the constitutive model is accounted for as explained by Mahboub and Little (18).

CHAPTER VI

COMPARATIVE ANALYSIS AND OCTAHEDRAL SHEAR STRESS ANALYSES

Background

When a pavement structure is subjected to the compressive action of a wheel load, a certain amount of deformation is produced. The load does work during its application due to the deformation of the loaded region. The quantity of strain energy of distortion may therefore be used as a basis for determining the limiting energy at which failure occurs. However, a companion relationship to the strain energy of distortion, namely octahedral shear stress, is used in this study since this procedure deals with stress which is a more familiar term to most civil engineers. Deformation in ACP overlays over PCC pavements results from either consolidation of under-compacted mixtures or plastic flow of instable mixtures or both. Regardless of which mode results in deformations, shear failure is associated with the deformation. Therefore, shear stress evaluation is a logical approach by which to evaluate permanent deformation potential.

Comparison of Stresses in Overlay for Two Pavement Types

This section of the report presents a brief comparison of an overlay placed on a PCC base with an overlay placed on a flexible base. In the subsequent sections of this report a detailed analysis of the ACP overlay performance on both pavement types will be discussed.

For this analysis (octahedral shear stress), a 9000-lb. circular wheel load was used to represent the design axle load - an 18,000-lb. equivalent single axle load (ESAL) with a tire pressure of 100 psi. A recent survey study of tire pressure (33) in the state of Texas has shown that most trucks operate at a tire pressure of 98 psi or higher. Therefore, 100 psi is considered to be a typical representation of tire pressure in Texas. As discussed in Chapter V, the Tielking tire model modification was applied to determine the contact pressure and shearing stresses to be used in the modified ILLIPAVE consistent with the 100 psi inflation pressure.

The eight pavement structures presented in Figures 6.1 and 6.2 were selected for comparative evaluation. For both pavement types (flexible base and PCC base) the influence of all variables previously listed were considered.

A series of charts were developed which show the variation of octahedral shear stress as a function of overlay thickness, interface bonding, stiffness and horizontal surface shear for ACP overlays placed both on portland cement concrete bases and flexible bases. A complete set of graphs are presented in Appendix C, and Figures 6.3 through 6.10 present a summary of the results. In addition to the octahedral shear stress distribution, a typical distribution of vertical compressive stresses with depth for conventional and full-depth pavements are presented in Figure 6.11.

Most pavement design and analysis methodologies (3, 34) assume that the vertical stress is a maximum directly under the wheel load at the surface, and that the horizontal radial stress is a maximum at the bottom of the surface layer directly under the applied load. This approach overlooks any differences between the overlays placed on PCC or stiff (rigid) and/or flexible base structures. This research study has examined the distribution of octahedral shear stress in the overlay placed on both the PCC base and the flexible bases and has concluded that substantial differences exist between the stress state developed within the overlay of the two pavement types. This clearly indicates that shearing stresses have a more logical relationship with rutting especially when the rutting problem occurs in the early life of the overlay structure or is due to plastic flow of a low air void mixture.

Unlike the vertical compressive stress which is practically independent of overlay thickness (9), Figures 6.3 through 6.10 clearly show that the state of stress in the overlay varies substantially with variation in the overlay thickness. Moreover, the stress states for overlays placed on a PCC base are quite different when compared with stress states in overlays placed on flexible bases.

These figures further show that, when an overlay is placed on a granular base, the value of the maximum octahedral shear stress decreases with an increase in the overlay thickness. The reverse is true for an

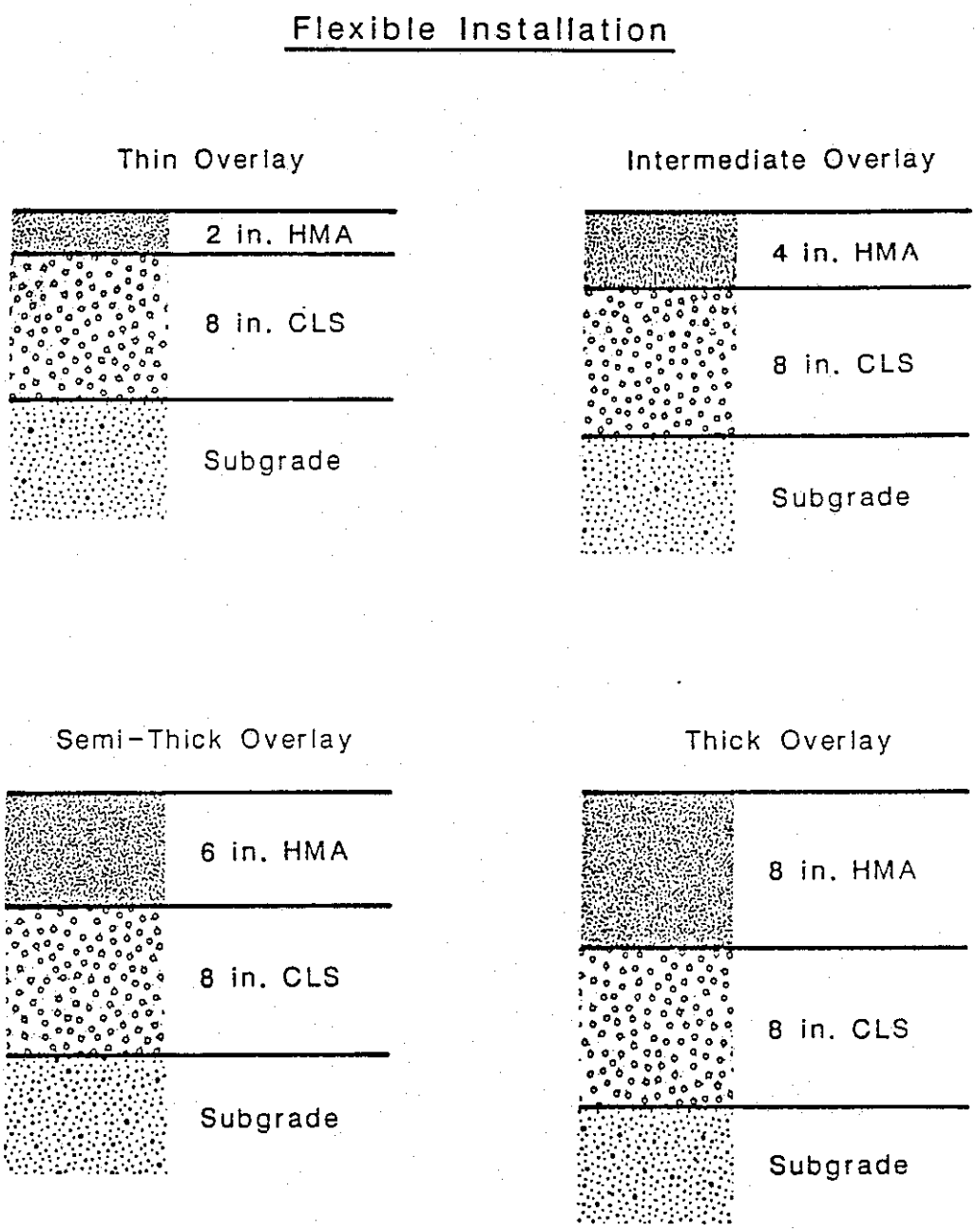

Figure 6.1. Installation of pavement structures and overlay thicknesses evaluated on flexible bases.

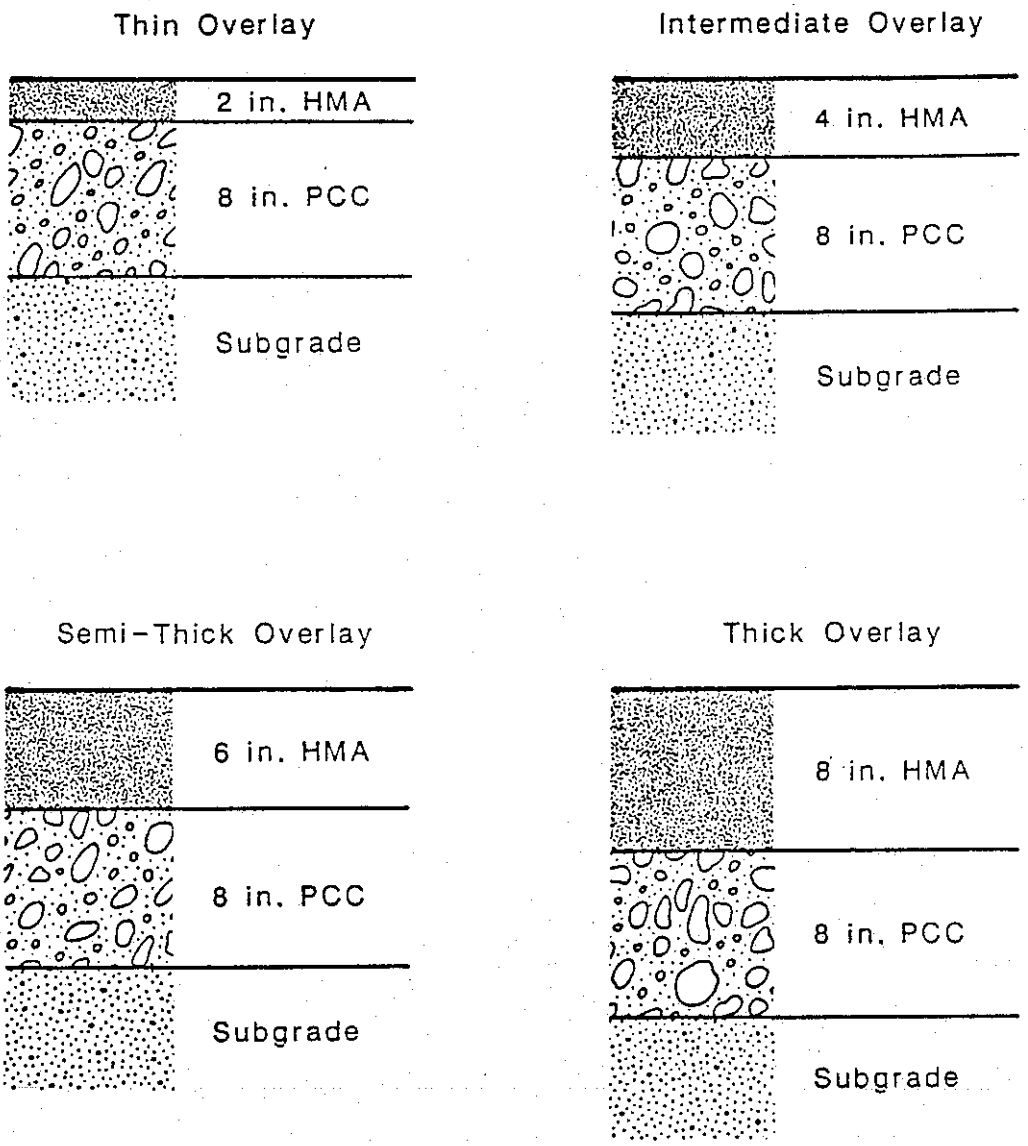

Figure 6.2. Installation of pavement structures and overlay thicknesses evaluated on rigid bases.

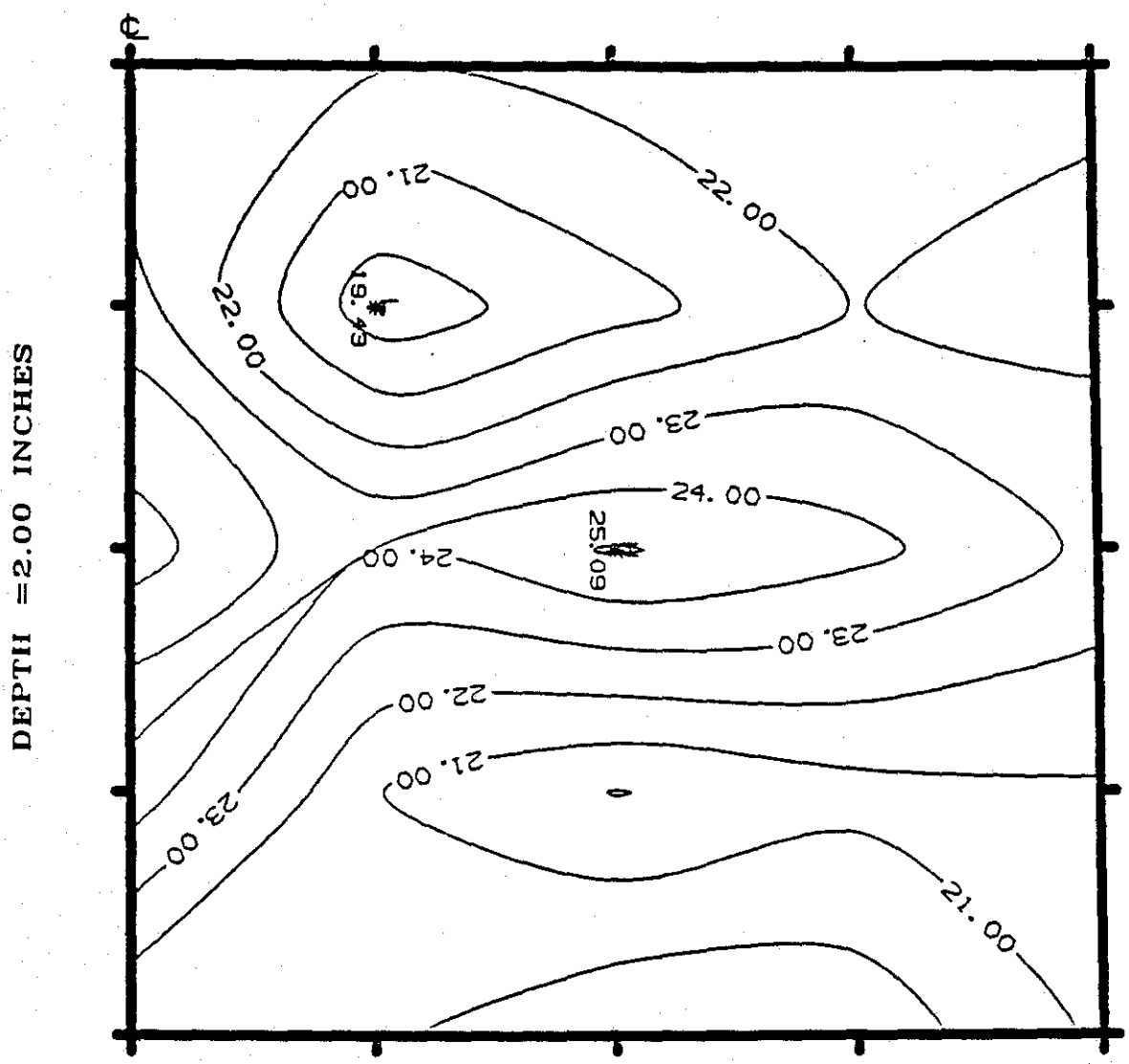

Figure 6.3. Contours of octahedral shear stress (psi) distribution for 2-inch overlay on rigid base pavement (M_R of ACP = 100,000 psi, full interlayer bond and no surface shear).

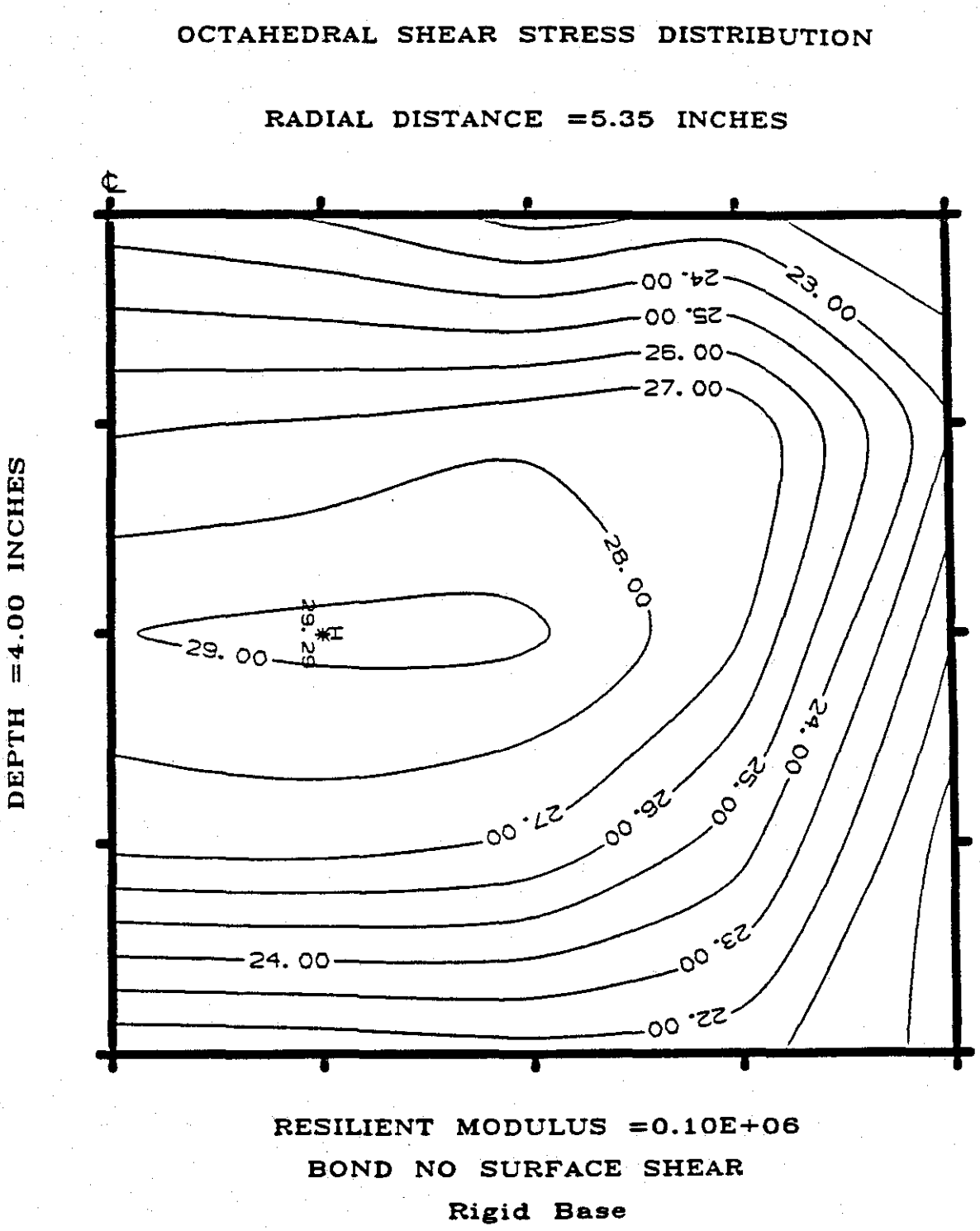

Figure 6.4. Contours of octahedral shear stress (psi) distribution for 4-inch overlay on rigid base pavement (M_R of ACP = 100,000 psi, full interlayer bond and no surface shear).

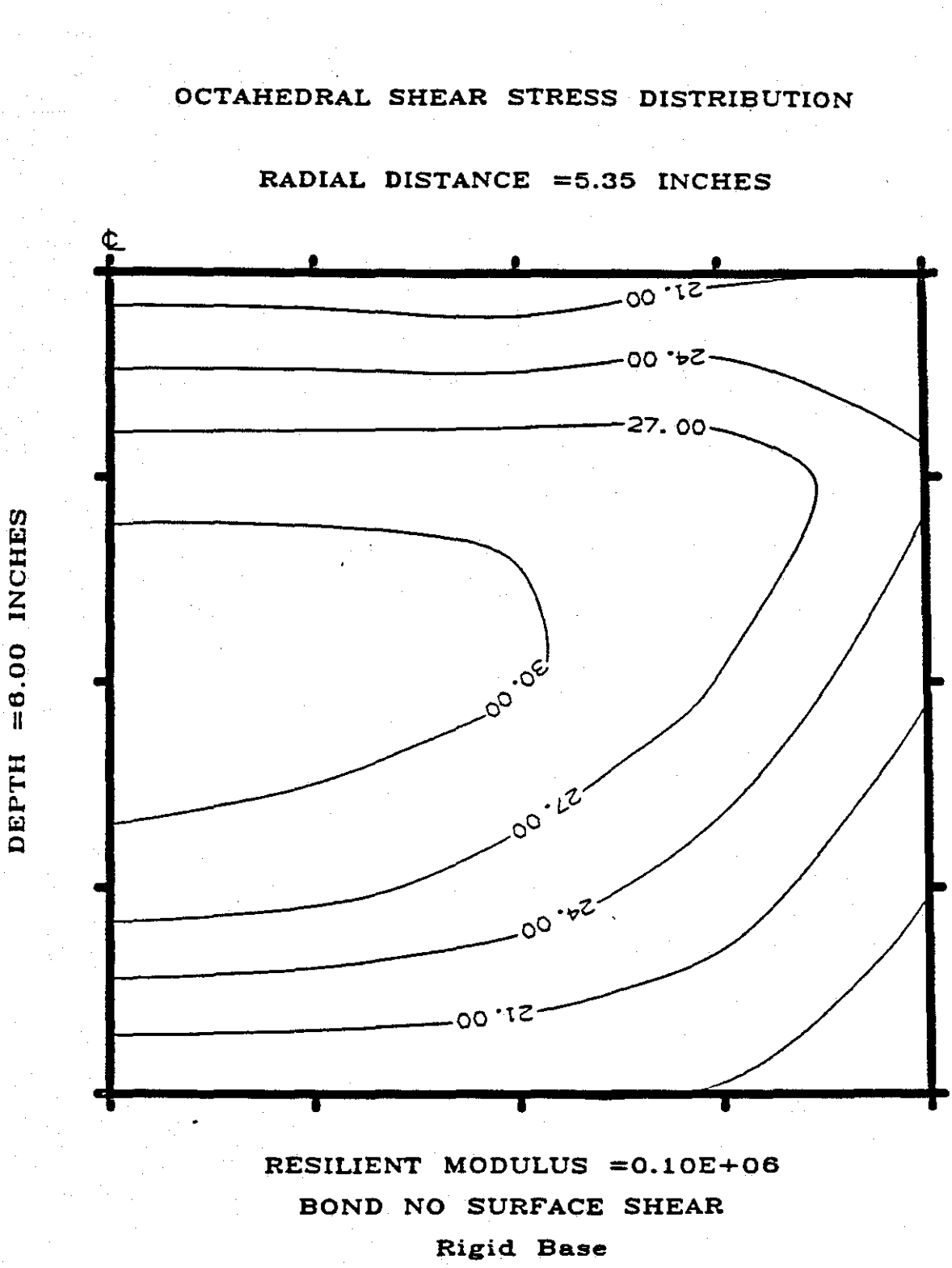

Figure 6.5. Contours of octahedral shear stress (psi) distribution for 6-inch overlay on rigid base pavement (M_R of ACP = 100,000 psi, full interlayer bond and no surface shear.

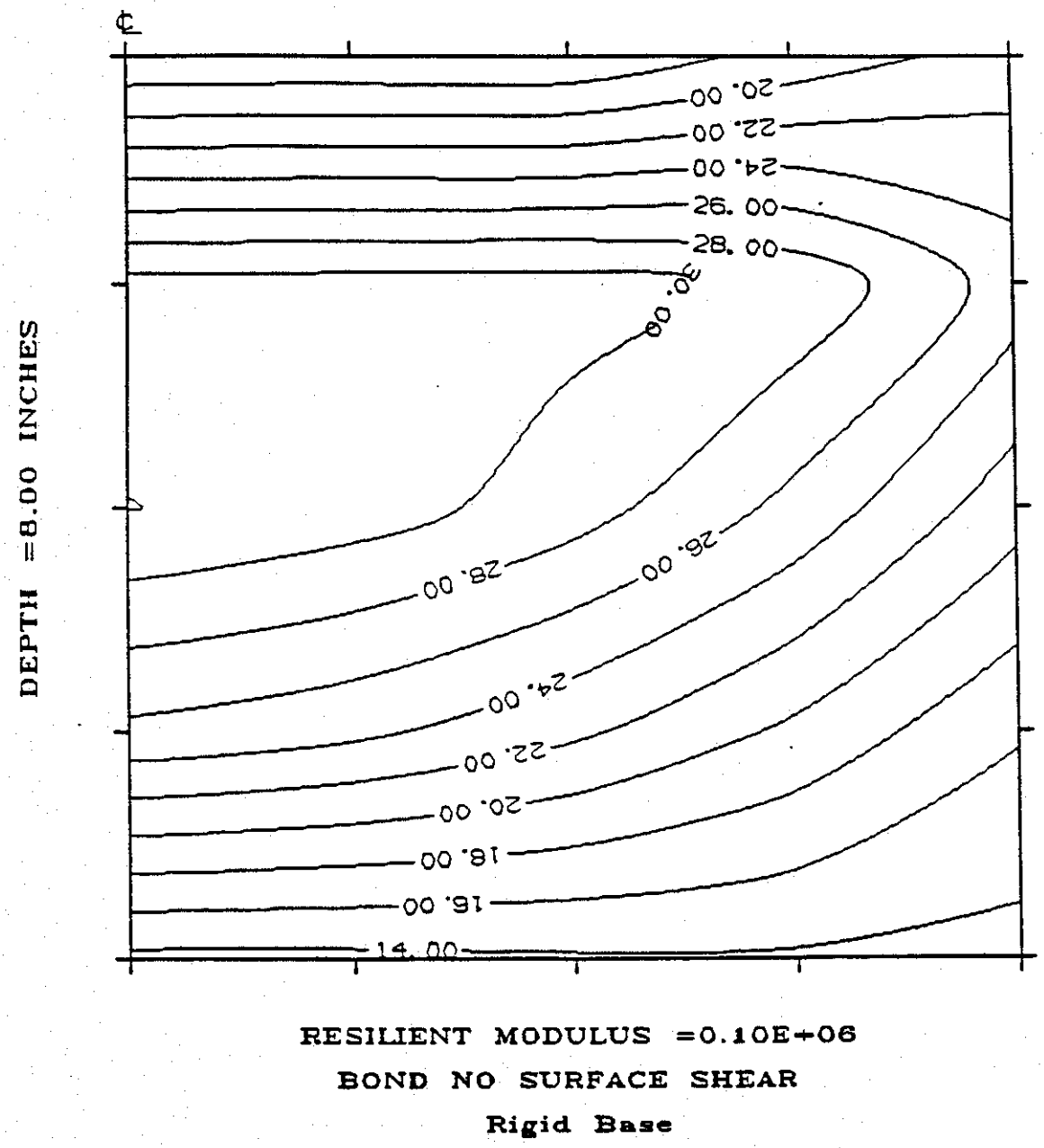

Figure 6.6. Contours of octahedral shear stress (psi) distribution for 8-inch overlay on rigid base pavement (M_R of ACP = 100,000 psi, full interlayer bond and no surface shear.

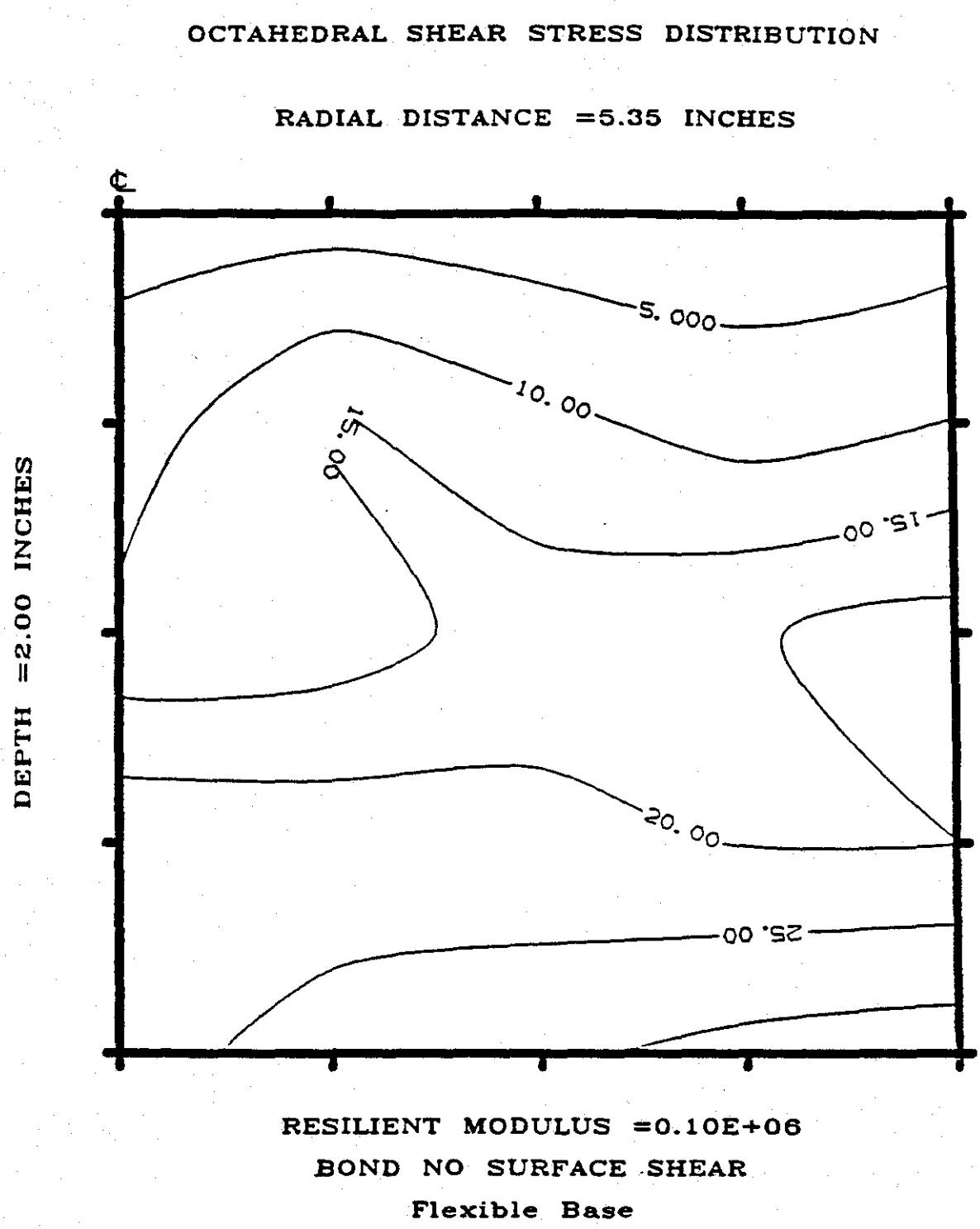

Figure 6.7. Contours of octahedral shear stress (psi) distribution for 2-inch overlay on flexible base pavement (M_R of ACP = 100,000 psi, full interlayer bond and no surface shear.

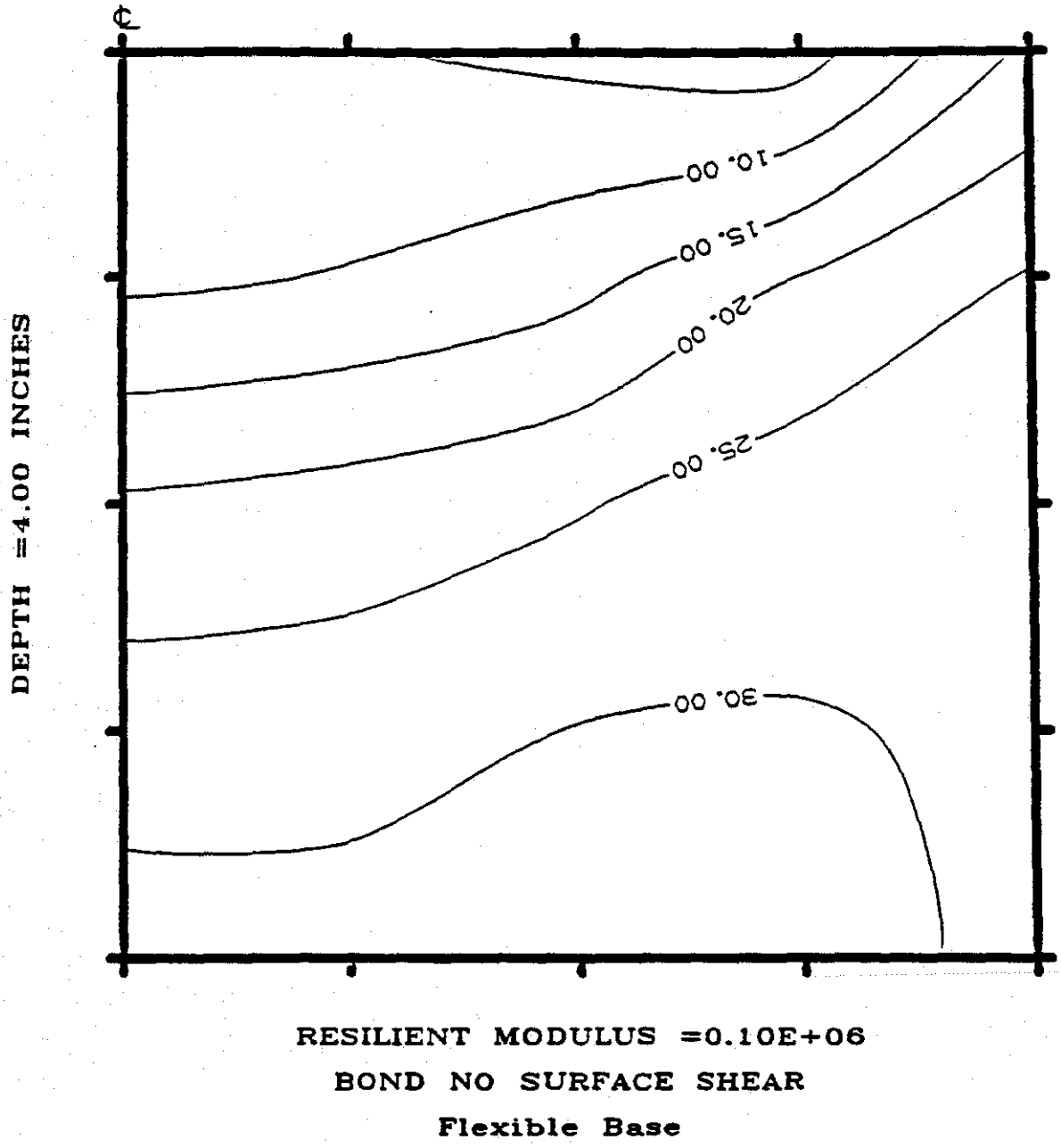

Figure 6.8. Contours of octahedral shear stress (psi) distribution for 4-inch overlay on flexible base pavement (M_R of ACP = 100,000 psi, full interlayer bond and no surface shear.

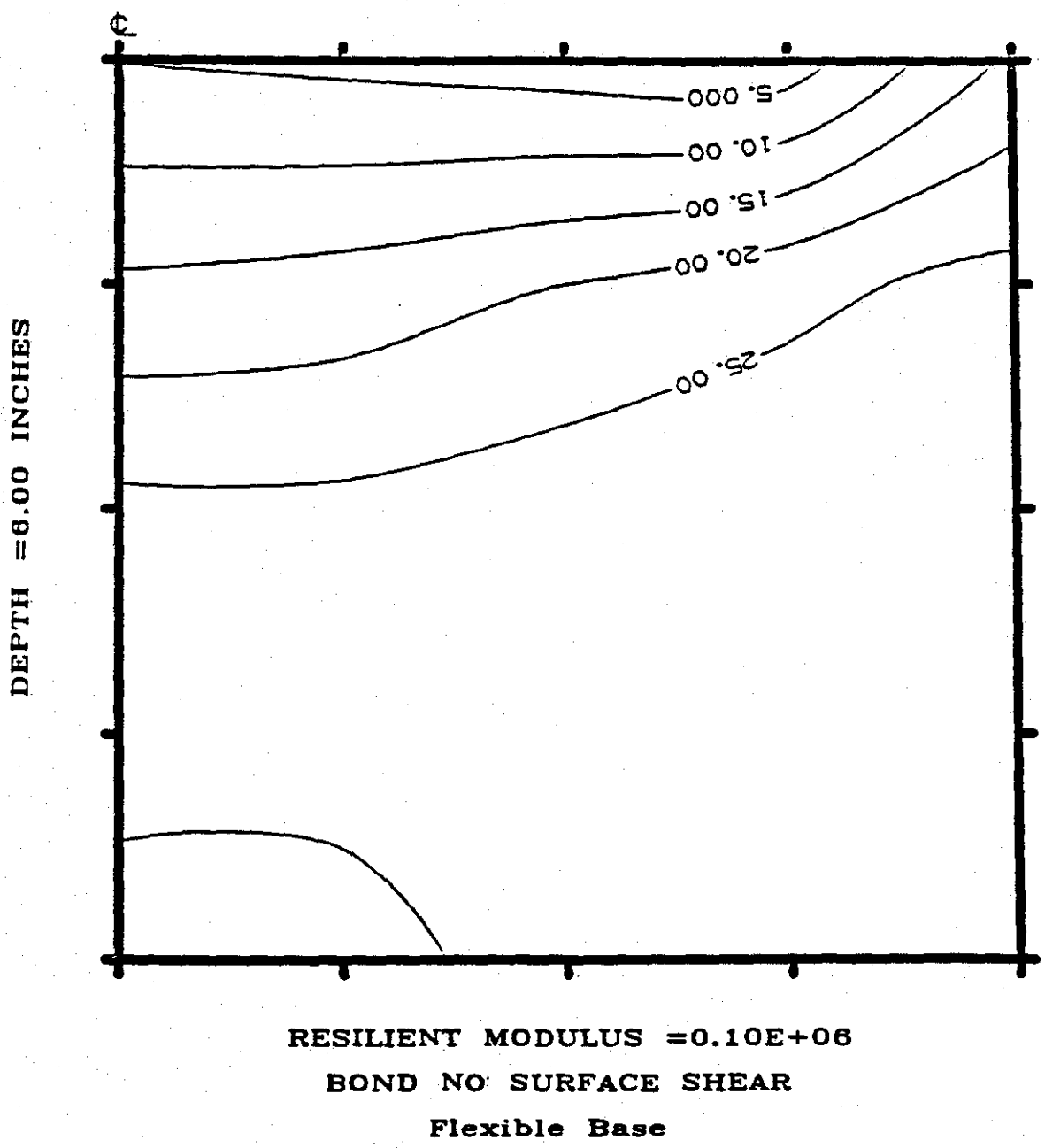

Figure 6.9. Contours of octahedral shear stress (psi) distribution for 6-inch overlay on flexible base pavement (M_R of ACP = 100,000 psi, full interlayer bond and no surface shear.

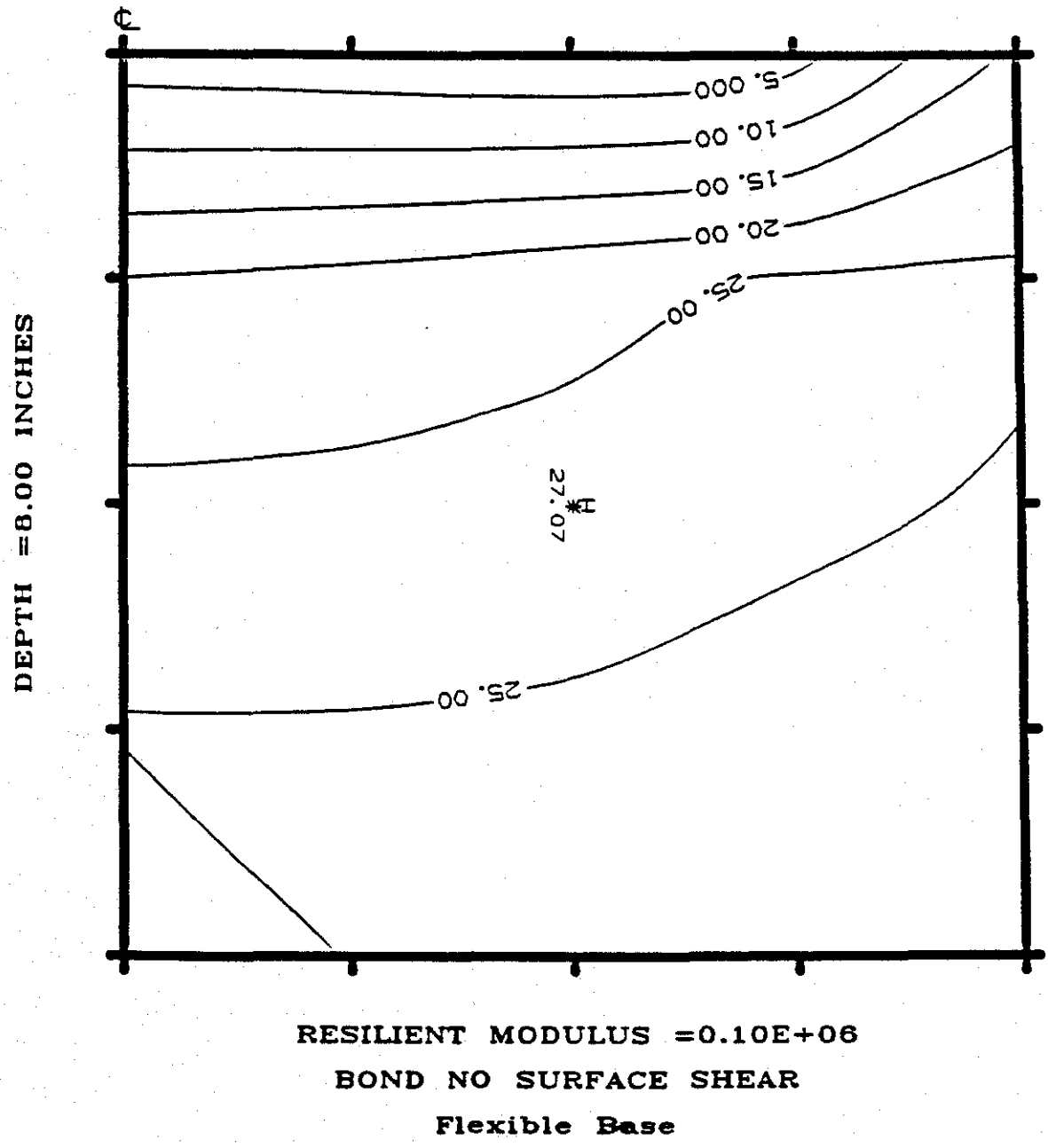

Figure 6.10. Contours of octahedral shear stress (psi) distribution for 8-inch overlay on flexible base pavement (M_R of ACP = 100,000 psi, full interlayer bond and no surface shear.

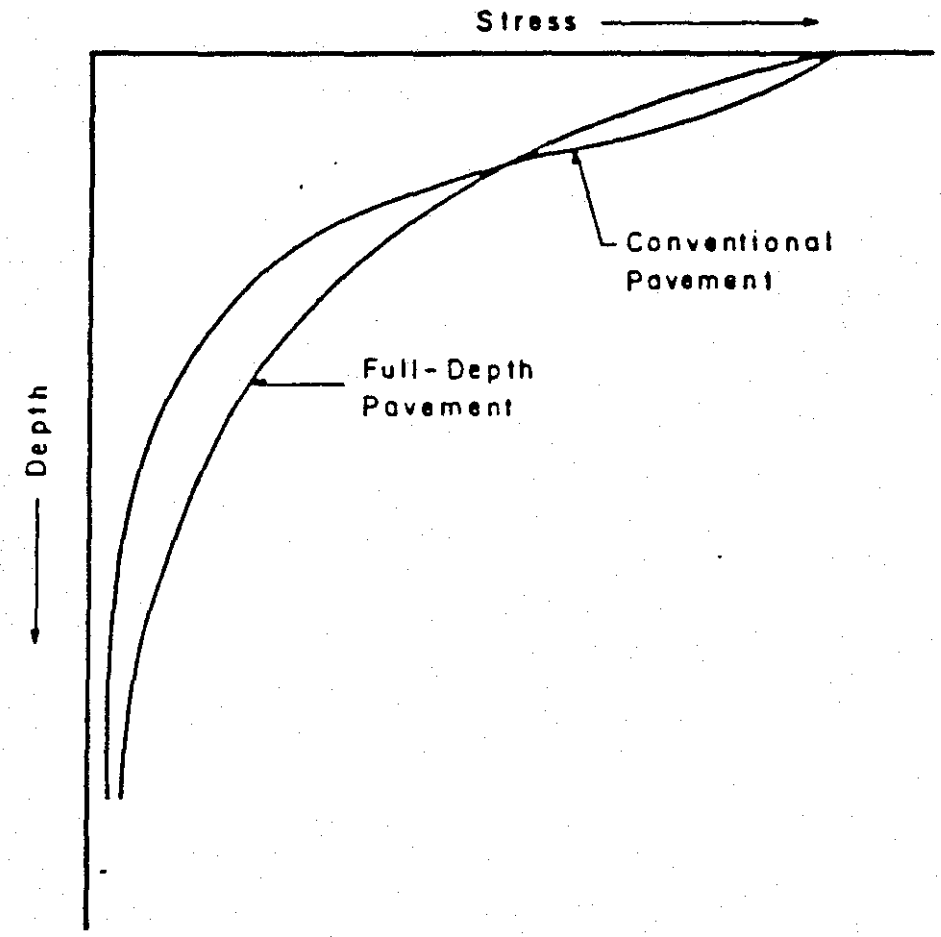

Figure 6.11. Typical vertical stress distribution in asphalt concrete pavements (after Reference 62).

overlay on PCC base, i.e., the value of maximum octahedral shear stress increases with an increase in the overlay thickness.

Comparison of the maximum octahedral shear stress values for the two pavement types (PCC and flexible bases) reveals that:

1. When a complete interface bond exists between the overlay and the base layer, and when the overlay stiffness is relatively high, i.e., 500,000 psi, the magnitude of the maximum octahedral shear stress will be significantly higher in the flexible base overlay.
2. When a complete interface bond exists between the overlay and the base layer, and when the overlay stiffness is relatively low, i.e., 100,000 psi, there will be no apparent difference in the octahedral shear stress magnitude for the two pavements.
3. Regardless of the bonding condition, the inherent flexibility of the flexible pavement produces higher tensile stresses than are developed through pavement bending action. The combined effects of the normal and the flexural stresses lead to a significantly larger octahedral shear stress in the flexible base overlay.
4. Rigidity of the original PCC surface prevents development of any significant bending stress in the ACP overlay due to pavement bending action.

Figure 6.12 illustrates the distribution of horizontal tensile strain for the two pavement types. It can be seen that the distribution of tensile strain in overlays on rigid bases is significantly different than that of overlays on flexible bases. A substantial level of radial tensile strain exists in the overlay on rigid pavement, but it does not occur at the location usually expected in conventional pavement design procedures (9).

Although not completely structural, there are some other noted differences that can produce structural difference between the two pavements (9). These factors cannot be directly modeled in an analytical procedure, but, nevertheless, must be considered in a full analysis of all factors influencing ACP deformation. These factors include:

1. In a flexible structure, two similar materials (ACP over ACP) are placed in direct contact producing a homogeneous mass, while

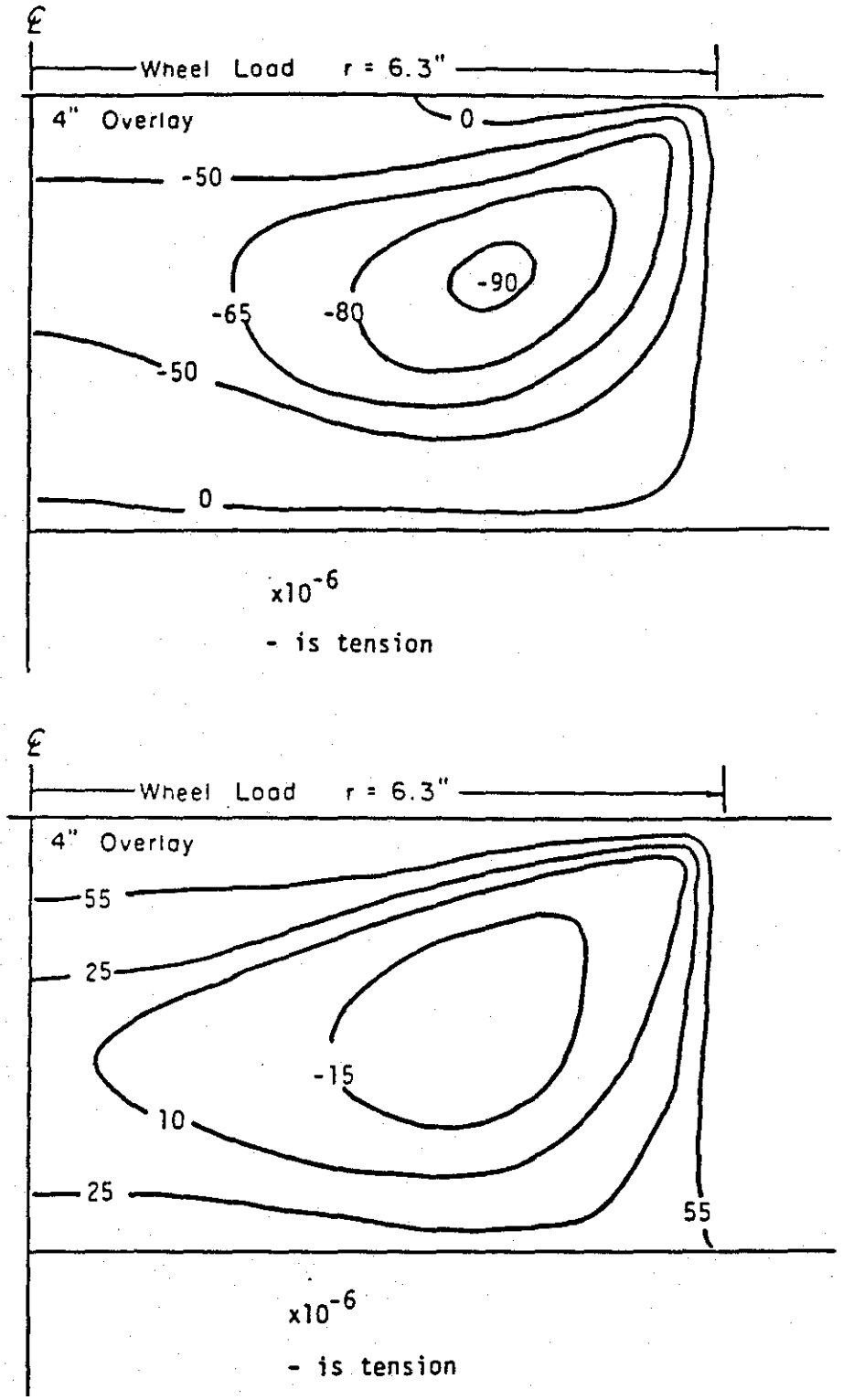

Figure 6.12. Distribution of radial strains under a standard wheel load for a 4-inch ACP overlay over: a) rigid base, b) flexible base (after Reference 9).

in a rigid pavement installation, two dissimilar materials, producing an nonhomogeneous body, are in direct contact. This dissimilarity of materials, and consequent dissimilarity in material properties such as coefficient of thermal contraction, could easily lead to debonding, or at least, reduction of the level of interface bonding.

2. Differences in performance related to discontinuities in the original surface, i.e., joints or D-cracks in the rigid pavement versus thermal cracks in flexible pavement.
3. Differences in moisture conditions in the rigid pavement compared with those in the flexible pavement.
4. Construction differences.

All of the above factors have the potential to reduce interface bonding potential.

Inflation Pressure and Contact Pressure

If the bending effect of the tire wall is considered, the peak contact pressure between the tire and pavement could be approximately equal to twice the inflation pressure of the tire. For low pressure tires, contact pressure under the tire wall will be greater than the center of the tire. For high pressure tires the reverse may be true.

The interfacial pressure between a free rolling tire and the pavement is highly nonuniform (30). This nonuniformity is due to bending stiffness in the tire structure. In the absence of bending stiffness (e.g., an inner tube) the contact pressure is uniform and equal to the inflation pressure. Results of the tire studies (30) have indicated that the contact pressure distribution is significantly influenced by either changing the tire load or tire pressure, and the two effects are not interchangeable. Figures 6.13 and 6.14 illustrate the effect of inflation pressure and tire load on contact pressure. Figure 6.13 shows the effect of increasing the inflation pressure while keeping the tire load fixed at 4500 lbs. The contact pressure distributions here are calculated on one-half of the tire meridian passing through the center of the footprint. The effect of increasing the tire load while keeping the inflation pressure fixed at 100 psi is shown in Figure 6.14.

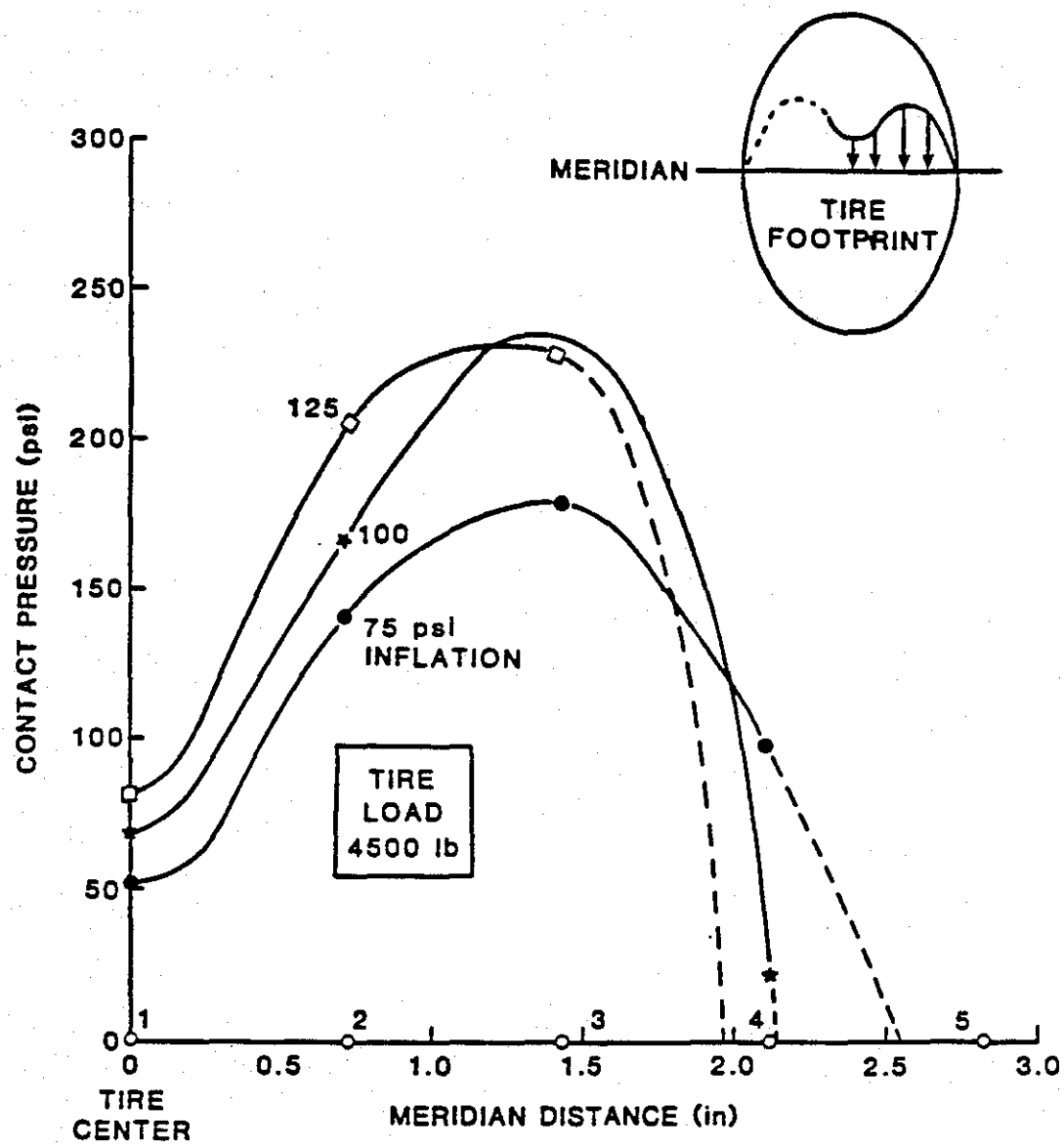

Figure 6.13. Effect of inflation pressure on contact pressure for a 10.00-20 truck tire with a 4,500 pound load.

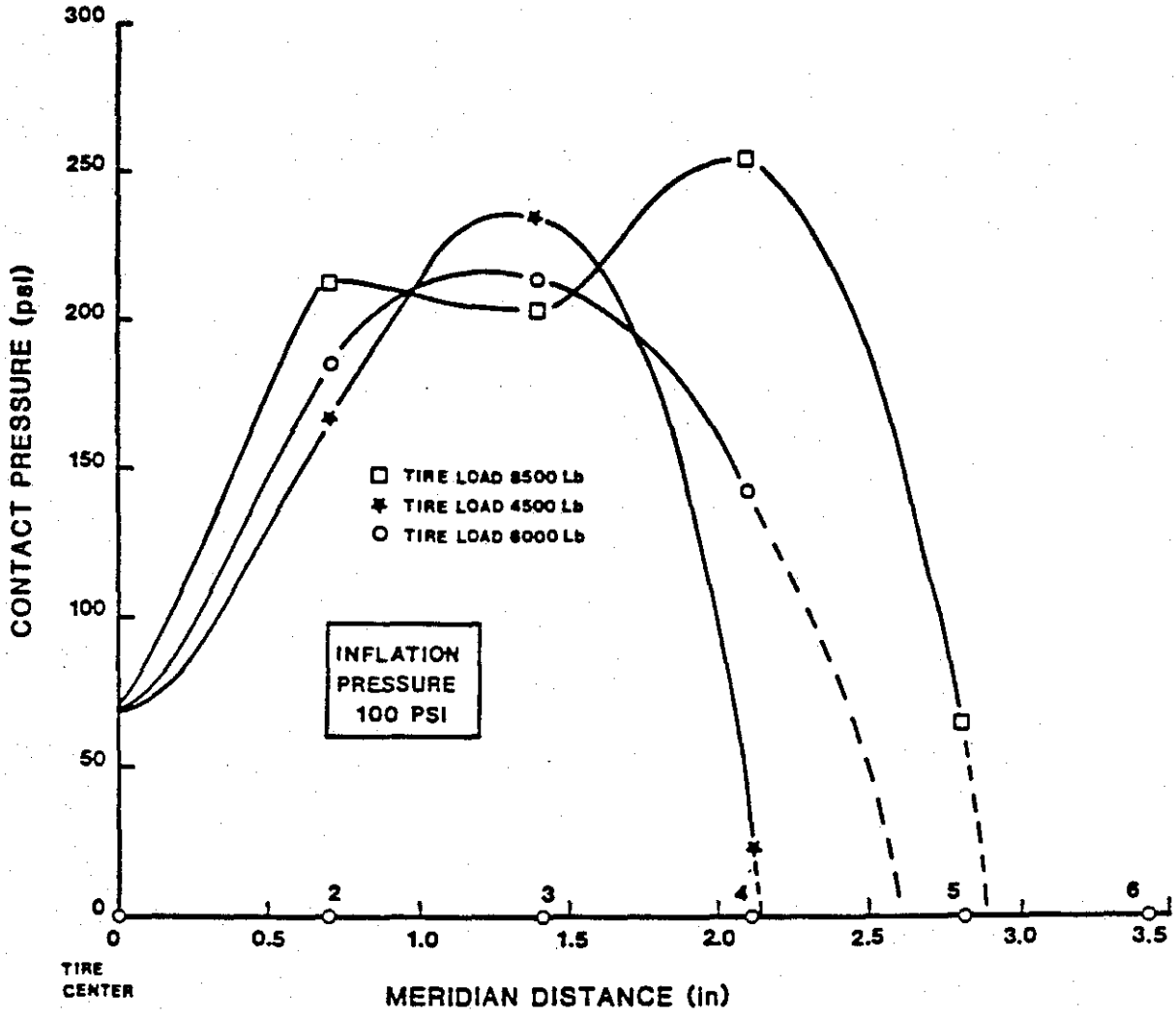

Figure 6.14. Effect of tire load on contact pressure calculated for a 10.00 truck tire with 100 psi inflation pressure.

The effect of high tire pressure is pronounced in the upper layers of the pavement whereas an increase in total load increases the vertical stress for all depths. Use of higher tire inflation pressures causes a high tensile strain at the bottom of the surface layer in a flexible pavement structure (35).

Further investigation of tire-pavement interaction (36) reveals that an increase in tire pressure produces an increase in the tensile strain ranging from 20 to 30 percent for a 1-inch thick ACP surface to a tensile strain increase of about 10 percent for the 4-inch thick ACP surface.

Overall high tire pressures necessitate high quality materials only in the upper layers of the pavement, since the total pavement depth will not be affected by increased tire pressure. On the other hand, for a constant tire pressure, increases in total load will increase the vertical stress for all depths (3). Figure 6.15 shows the predicted rut depth resulting when a 125 psi inflation pressure is larger than that from 75 psi inflation pressure for all surface thicknesses. It has also been found (21) that predicted rut depth is lower for the locations with lower seasonal temperatures regardless of the tire pressure and that the thicker surfaces are more sensitive to increase in seasonal temperature than the thinner ones.

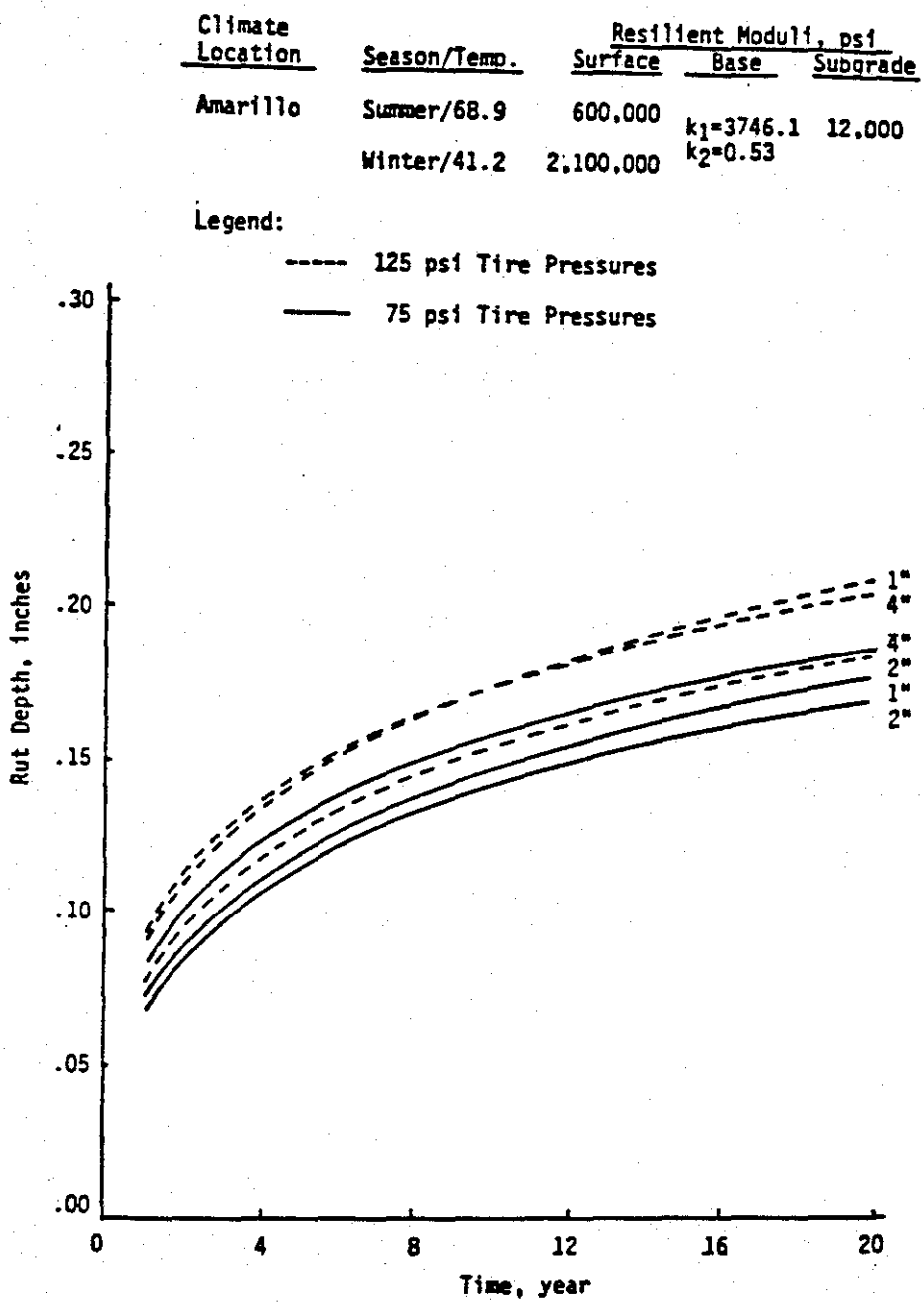

Figure 6.15. Predicted rutting for Amarillo, Texas (after Reference 21).

CHAPTER VII

OCTAHEDRAL SHEAR STRESS ANALYSIS OF AN ACP OVERLAY ON A GRANULAR BASE

General

This section of the report examines the influence of thickness of the asphalt concrete overlay in combination with other influential factors such as interfacial bonding, stiffness, and surface shear in development of maximum octahedral shear stress with respect to rutting.

Although the maximum octahedral shear stress magnitude developed under any loading condition is important in the assessment of an overlay performance potential, determination of the critical overlay thickness as well as the material quality level is possible only via the octahedral shear stress ratio. This is true because stability of the paving mixtures is greatly influenced by the triaxial stress field induced by the load application. The shear resistance increases with increased octahedral normal stress on the failure plane. Consequently, a paving mixture will exhibit a higher stability under a complete and/or partial compressive stress field than it will exhibit under a complete and/or partial tensile triaxial state of stress. Therefore, the discernment of the critical overlay thickness for a particular mixture based on the maximum octahedral shear stress theory can only be determined when the stress field condition at which the maximum octahedral shear stress is developed is known. This is because the material stability (as described by octahedral shear strength) must be determined at this state of stress.

For the remainder of this chapter and the next, the hypotheses are that the subgrade and the base course material will not fail under the shear stresses imposed by the applied loads, and the maximum octahedral shear stress is an indicator of the most critical overlay condition. These assumptions will enable the authors to evaluate the influence of the other critical parameters that are not related to the mixture strength properties but strictly to the overlay geometry, loading conditions, boundary conditions, and mixture stiffness to sublayer stiffness ratios.

It is emphasized that the critical overlay thickness is a function of the loadings and the overlay boundary conditions as well as the cohesive

and frictional components of the ACP material and must be determined via the octahedral shear stress ratio and not by the octahedral shear stress only. In Chapter IX, this ratio is calculated and discussed for selected asphalt-aggregate mixtures and various overlay loading and boundary conditions.

Thickness Effect

Overlay thickness has a profound influence on the development of the maximum octahedral shear stress. As the overlay thickness increases, the location of the maximum octahedral shear stress gradually shifts to the mid-depth portion of the overlay, away from the wheel load centerline.

Figures 7.1 through 7.9 show the variation of the maximum octahedral shear stress as a function of the overlay thickness, interface bonding, and the overlay stiffness. These figures clearly show that there is a subtle interaction among these variables (interface bonding, stiffness, and the overlay thickness).

The interaction among these three variables does not allow independent evaluation of the effect of thickness differences on the performance potential of the overlay. However, as the overlay gets thicker (Figures 7.1 through 7.4) the magnitude of the maximum developed octahedral shear stress in the ACP overlay becomes lower.

Although an increase in overlay thickness decreases the magnitude of the maximum octahedral shear stress, the variation in the maximum octahedral shear stress value is dependent upon both the degree of interface bonding between the overlay and underlying base layer as well as the overlay stiffness. If the bond at the interface between the overlay and the base layer is reduced (Figure 7.1), the magnitude of the maximum induced octahedral shear stress in a 2-inch overlay is two to three times larger than in an 8-inch thick overlay. This applies to overlays with stiffness values of 400,000 psi and 500,000 psi.

Figure 7.2 depicts the same interface bonding condition shown in Figure 7.1 for an overlay subjected to the combined action of the horizontal surface shear and vertical wheel load. The magnitude of the maximum octahedral shear stress increases rapidly for a 2-inch thick overlay and reaches a value two times larger than that which is found when the vertical load is applied without the horizontal surface shear. Figure 7.2

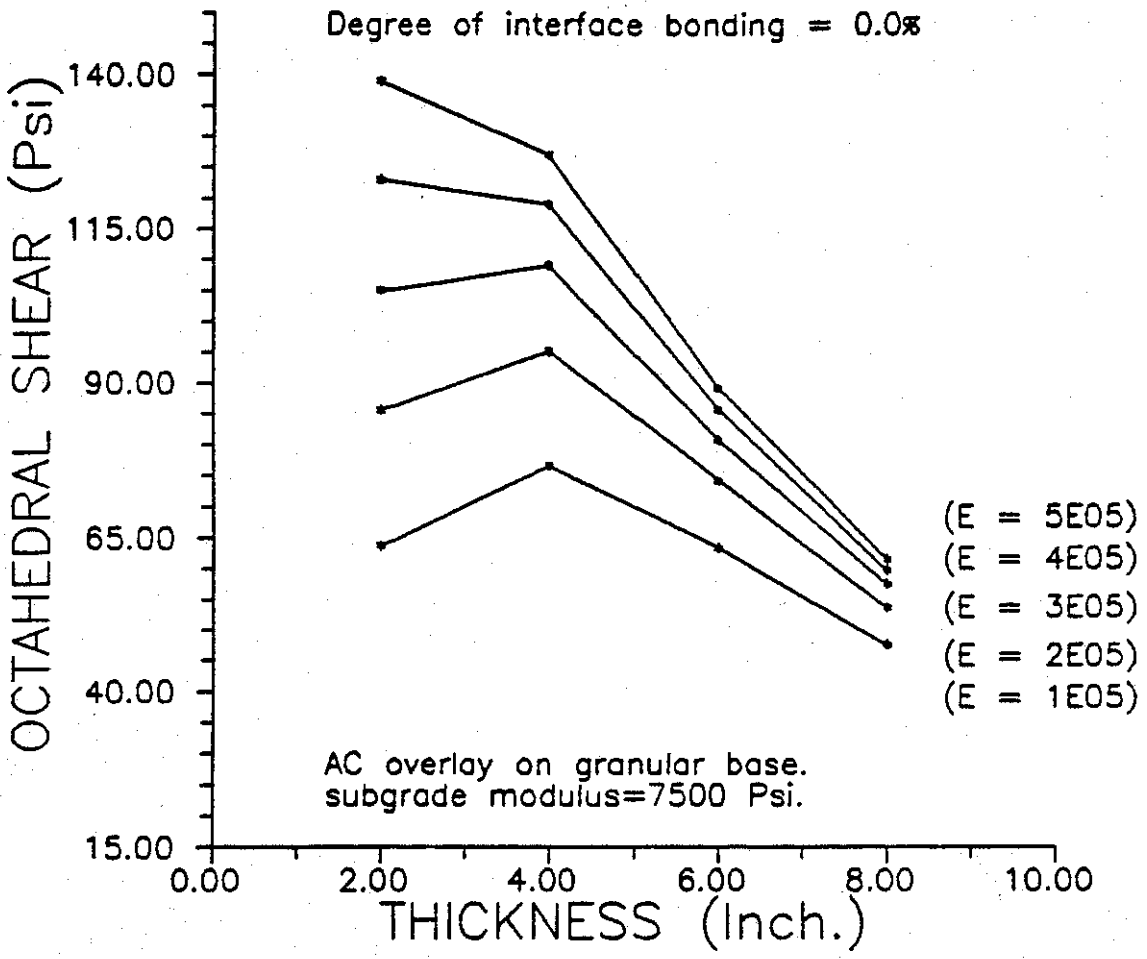

Figure 7.1. Variation of maximum octahedral shear stress in ACP (granular base) with overlay thickness without surface shear (no interface bonding).

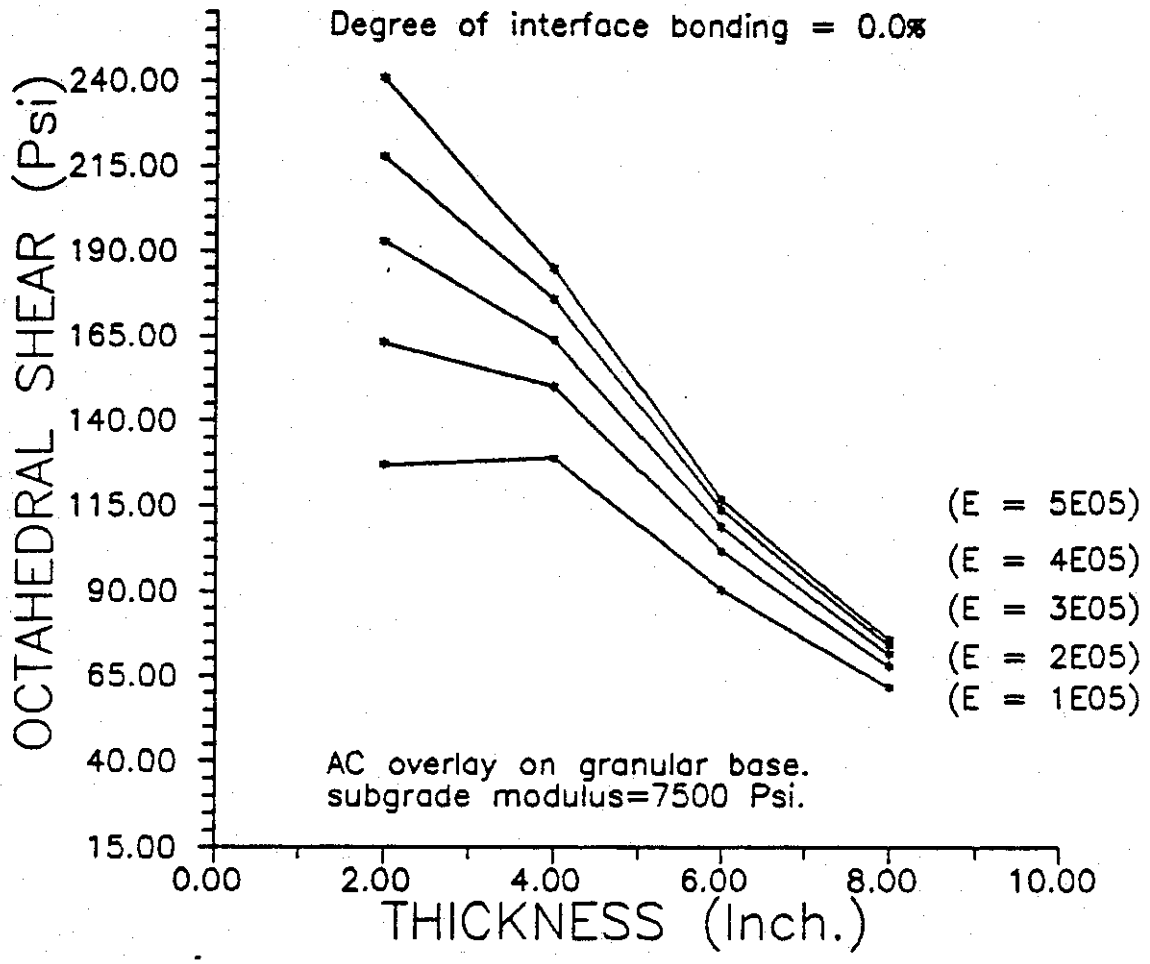

Figure 7.2. Variation of maximum octahedral shear stress in ACP (granular base) with overlay thickness with surface shear (no interface bonding).

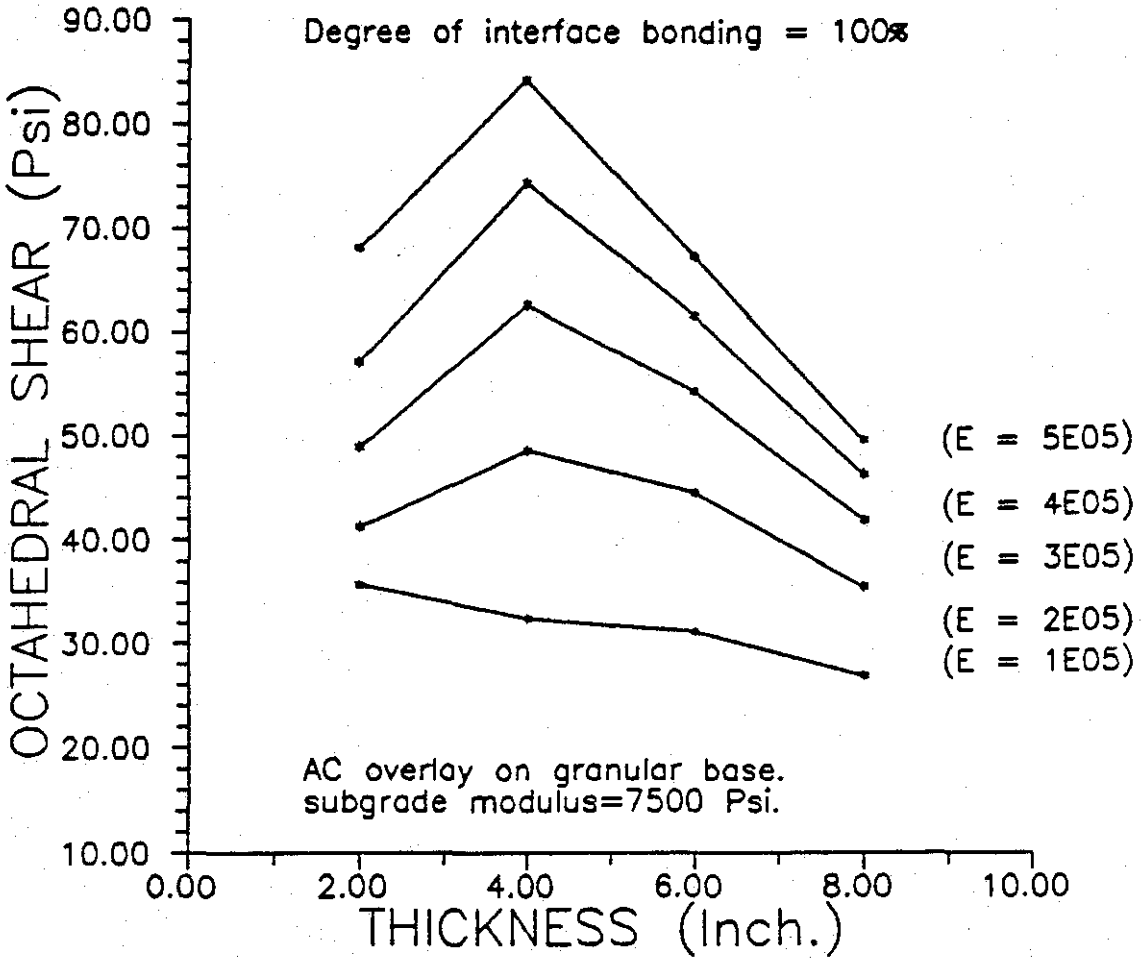

Figure 7.3. Variation of maximum octahedral shear stress in ACP (granular base) with overlay thickness without surface shear (full interface bonding).

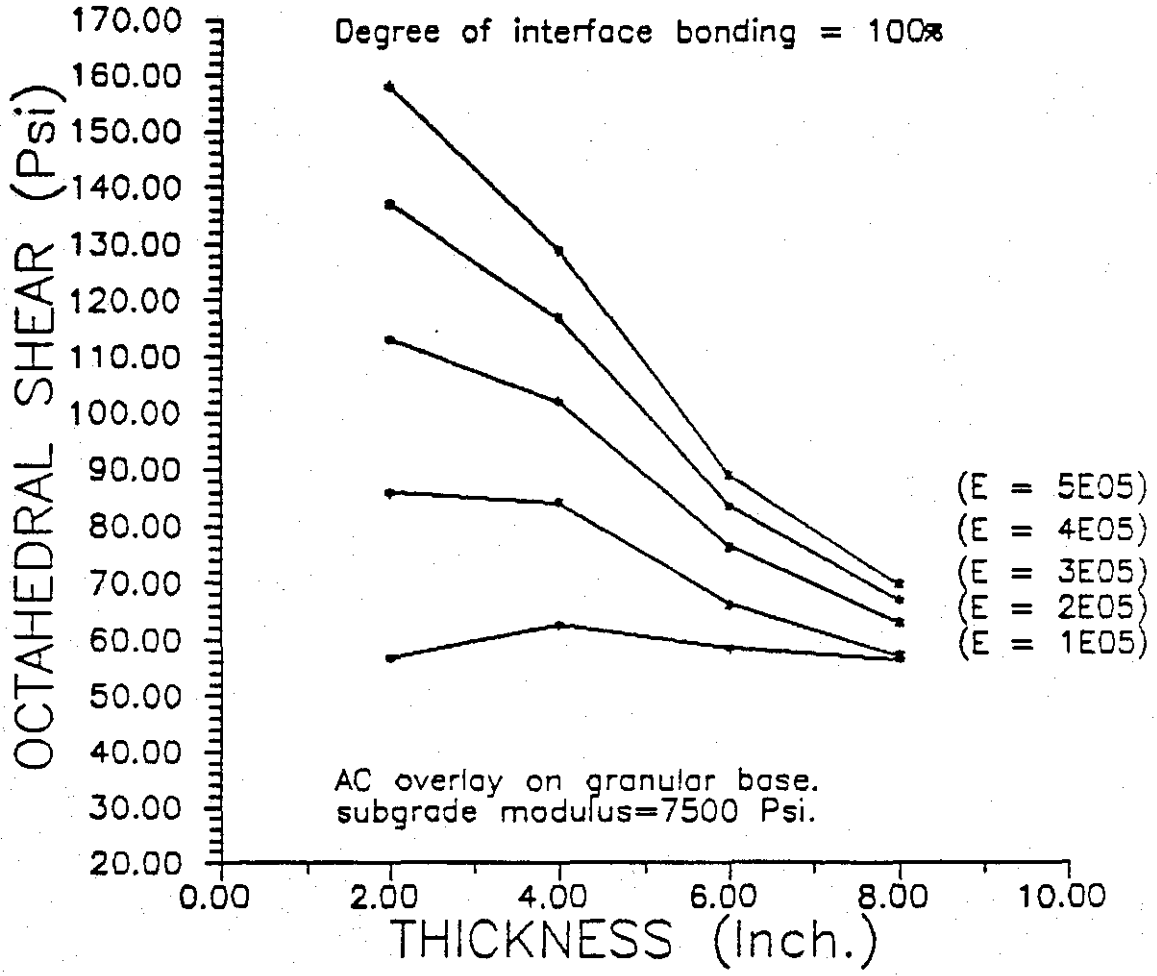

Figure 7.4. Variation of maximum octahedral shear stress in ACP (granular base) with overlay thickness with surface shear (full interface bonding).

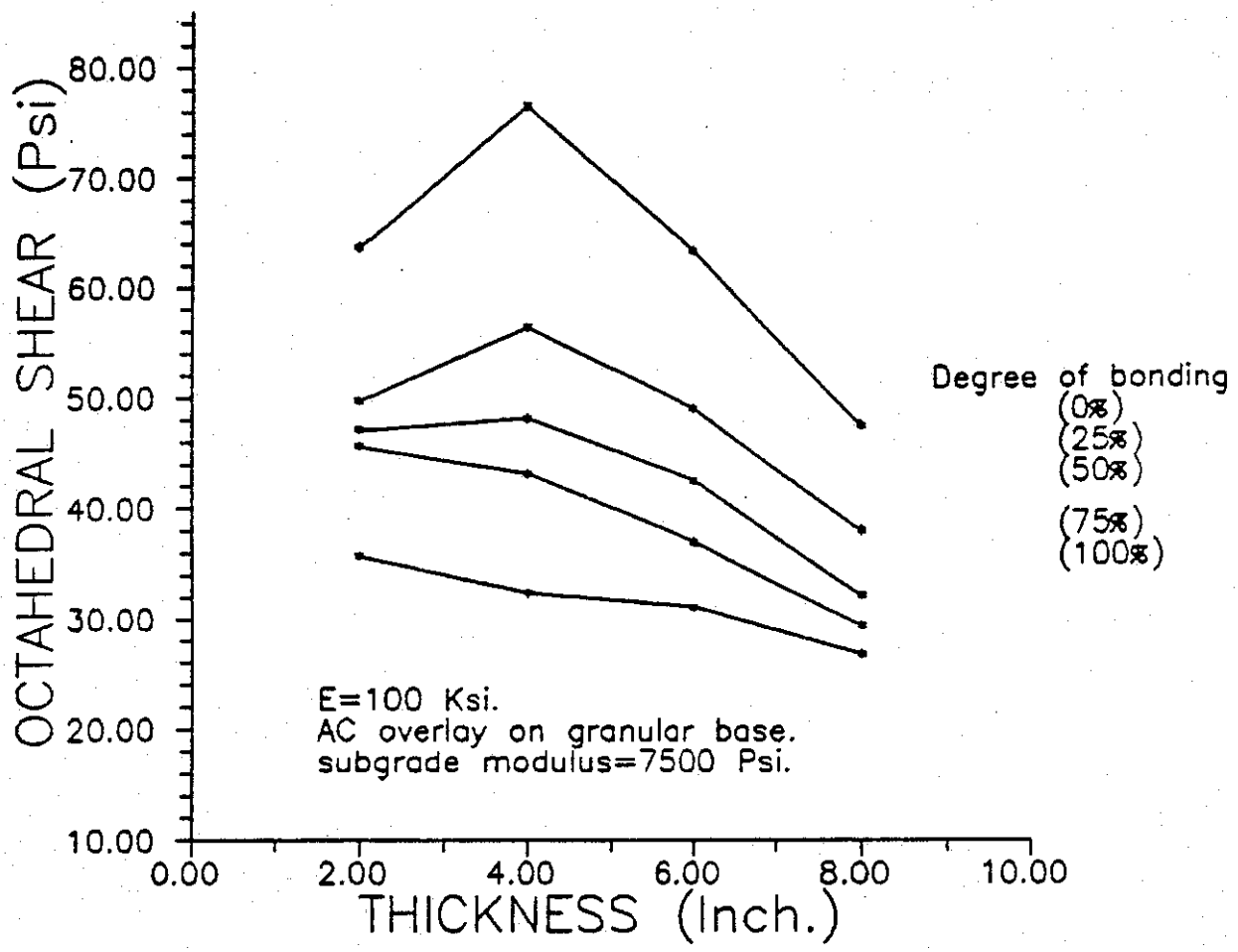

Figure 7.5. Variation of maximum octahedral shear stress in ACP (granular base) with overlay thickness for various interface bonding levels (E = 100 ksi).

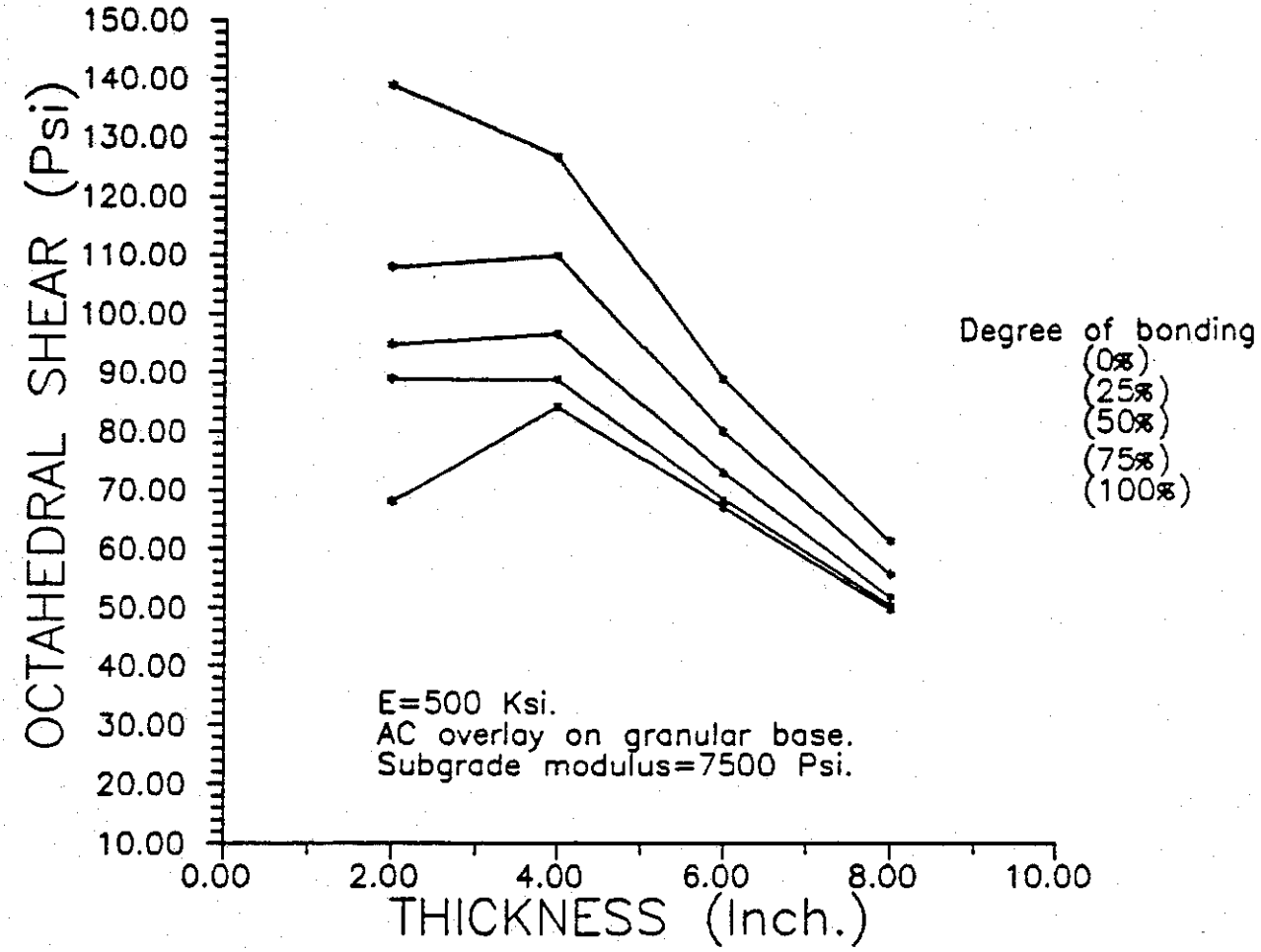

Figure 7.6. Variation of maximum octahedral shear stress in ACP (granular base) with overlay thickness for various interface bonding levels (E = 500 ksi).

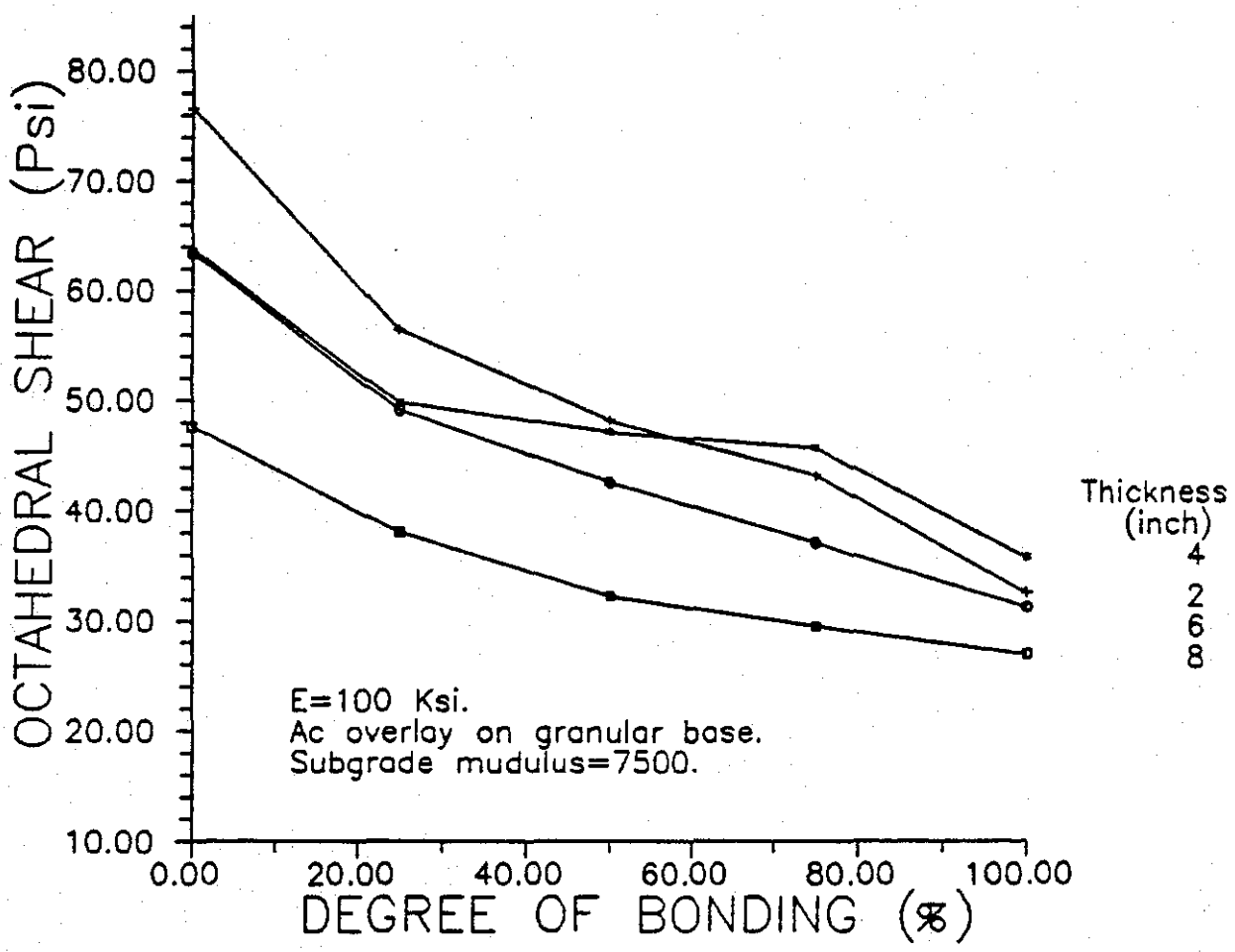

Figure 7.7. Variation of maximum octahedral shear stress in ACP (granular base) as a function of interface bonding (E = 100 ksi).

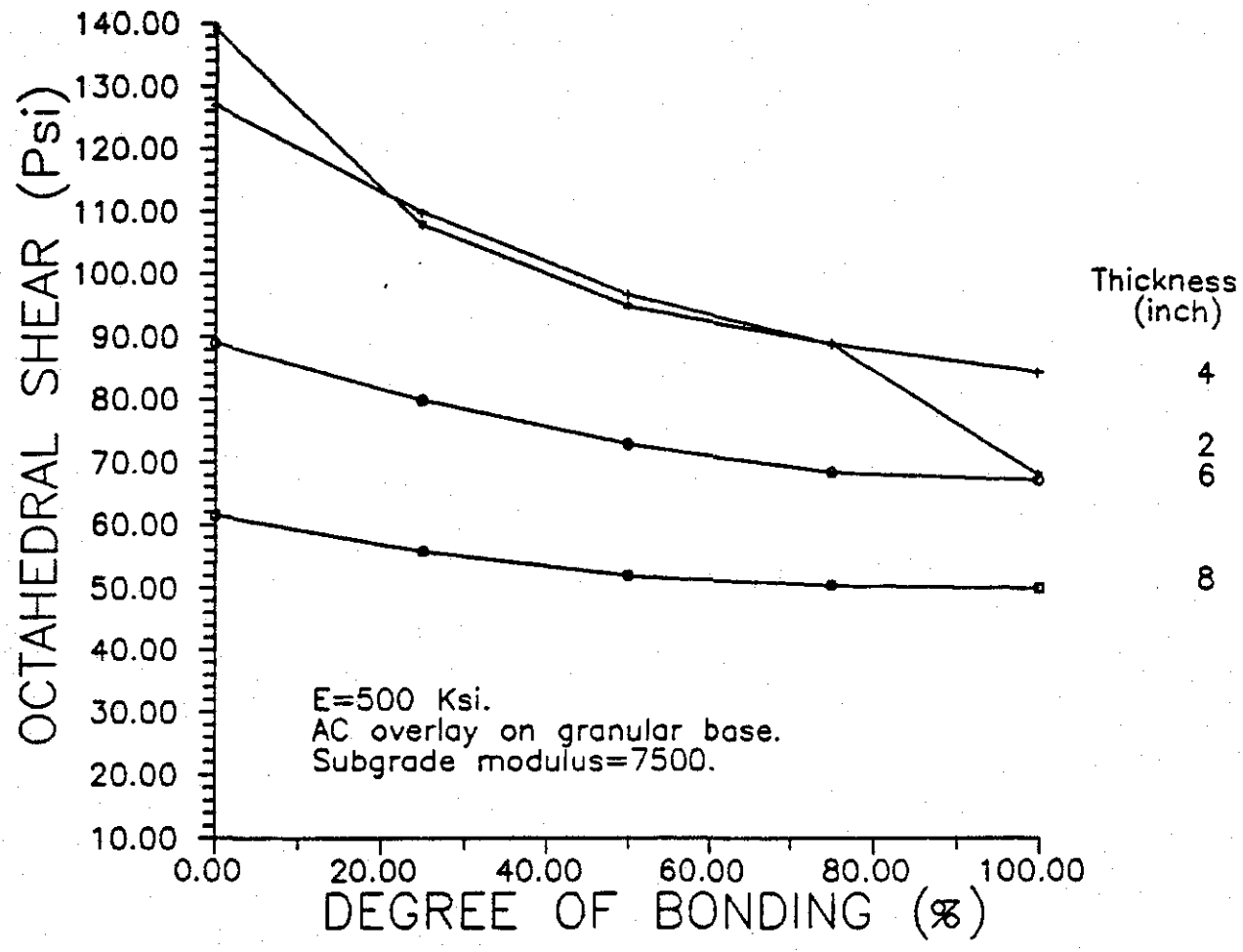

Figure 7.8. Variation of maximum octahedral shear stress in ACP (granular base) as a function of interface bonding (E = 500 ksi).

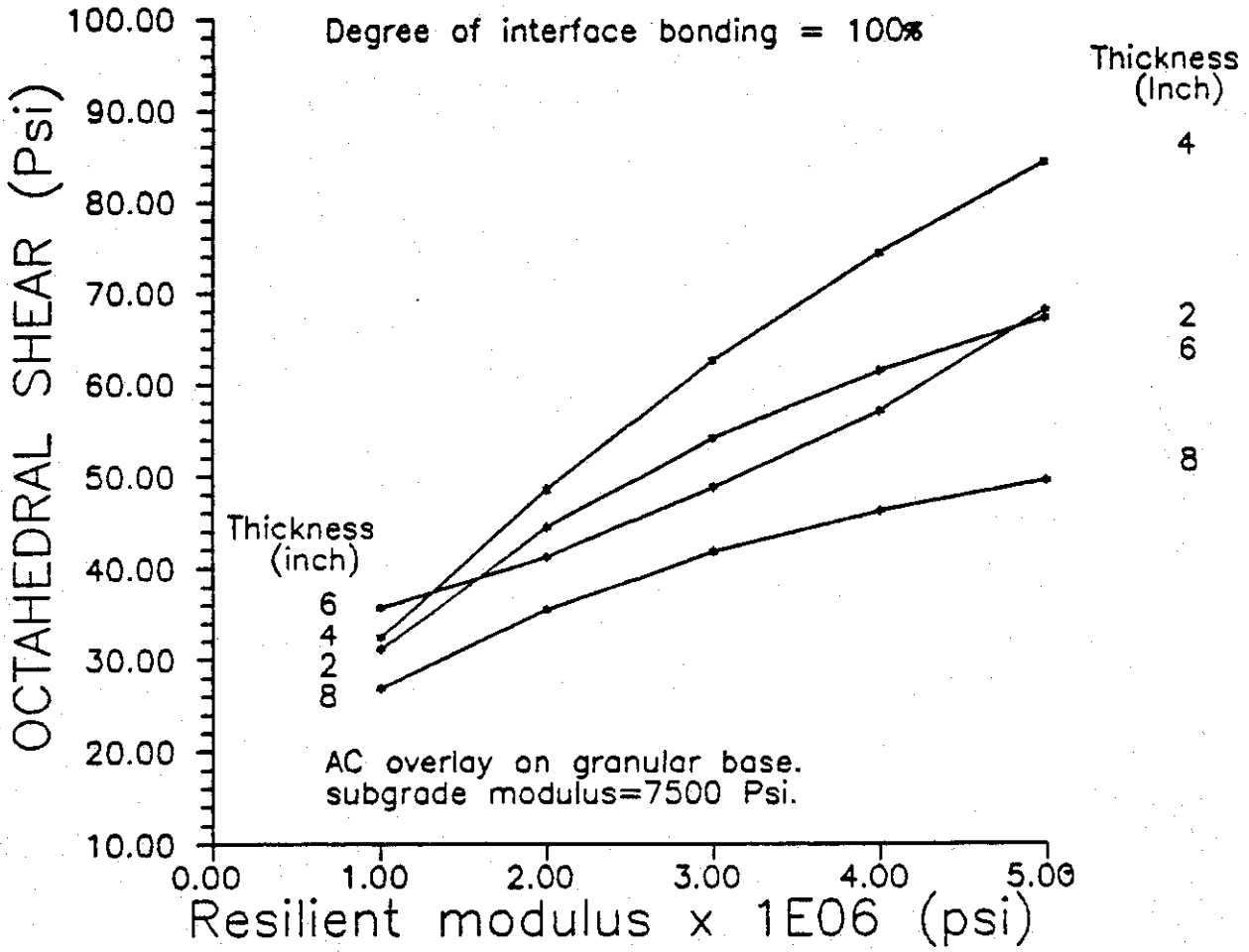

Figure 7.9. Variation of maximum octahedral shear stress in ACP (granular base) with overlay stiffness.

further demonstrates that, regardless of the overlay stiffness, the value of the maximum octahedral shear stress in a 2-inch overlay is two to three times larger than that found in an 8-inch thick overlay. Moreover, the influence of the horizontal surface force is less pronounced in the thicker overlays than it is in the thinner ones.

Thus, the benefits accrued by the thicker overlay are twofold:

1. More energy (traffic) can be accommodated,
2. Thicker overlays reduce the level of energy which is imparted to the pavement.

The interaction between the overlay thickness and the interface bonding is more noticeable in Figures 7.3 and 7.4, where variation in the maximum octahedral shear stress value is plotted as a function of the overlay thickness. In these figures it is assumed that there exists a well-integrated bond at the interface between the overlay and the underlying base layer. These figures demonstrate that for such a condition, the potential for a rapid shear failure is most likely in a 4-inch thick overlay, and the critical shear stress value progressively increases with an increase in the overlay stiffness. When the horizontal surface shear is applied together with the vertical load (Figure 7.4), the magnitude of the critical octahedral shear stress is increased substantially for all thicknesses of the overlay.

It is interesting to note that (Figures 7.2 and 7.4) when the horizontal surface force is applied together with the vertical load, and when the stiffness of the overlay is above 200,000 psi, the 2-inch thick overlay is always the most critical case. However, with a perfect bond at the interface, when the overlay stiffness is 100,000 psi, the 4-inch overlay becomes the most critical case. Furthermore, the stress condition developed in the overlay system under this loading and overlay condition produces the same maximum octahedral shear stress magnitude whether the 2-inch or 8-inch overlay is employed.

If the effect of the horizontal surface force is neglected and the vertical load is applied without surface shear (Figures 7.5 and 7.6), an increase in the degree of bonding significantly reduces the magnitude of the maximum octahedral shear stress in the overlay. For all overlay thicknesses employed, when the overlay stiffness is increased to 500,000 psi, the influence of interface bonding is more noticeable in the thinner

overlays than it is in the thicker ones. This indicates that thicker overlays are less dependent on the degree of bonding and can more effectively resist shear deformation.

Horizontal surface force in general produces substantially larger stresses in the pavement when applied in combination with vertical load. Nevertheless, an increase in the overlay thickness substantially reduces the damaging effects of the shear stresses (37).

For further analysis of the overlay thickness and its influence on pavement life the TFPS (Texas Flexible Pavement System) (38) computer program was utilized to predict the service lifespan of the overlaid pavement structure. If a highway were constructed with 1-inch, 2-inch, 3-inch, and 4-inch overlay, respectively, underlain by 7 inches of base and 8 inches of subbase material, and conforming to the AASHO Road Test material and construction specification (39), the TFPS analysis showed that for every one inch of increase in the overlay thickness, the lifespan of the structure increased 100 percent.

Bonding Effect

The degree of interfacial bonding greatly influences the state of stress within the overlay. Interfacial bonding can be singled out as the most significant factor that substantially affects overlay performance.

In the case of free slippage, the overlay acts independently of the rest of the pavement system. This allows excessive movement at the bottom of the overlay relative to the top where the wheel load is in contact with the pavement. This outward movement, in turn, reduces the confining pressure on the asphalt-aggregate mixture at the interface, which results in a smaller secondary principal stress (σ_3), and, therefore, a larger octahedral shear stress in the asphalt overlay. Loss of bond allows development of horizontal tensile stresses at the interface due to the bending action of the pavement which substantially increases the shear stress in the surface layer.

Loss of bond also alters the distribution of the octahedral shear stress. As the resistance to slip decreases, the magnitude of maximum octahedral shear stress increases rapidly and moves to the bottom of the surface layer.

Figures 7.7 and 7.8 represent the variation of the maximum octahedral shear stress as a function of the degree of interface bonding for overlays having stiffness values of 100,000 psi and 500,000 psi, respectively. These figures show that, in a situation where there is complete loss of bond, thinner overlays have considerably higher potential for premature failure (early rutting). At 100,000 psi stiffness value, a 4-inch thick overlay is the most critical thickness and at 500,000 psi stiffness value, a 2-inch thick overlay is the most critical thickness. However, with an increase in the degree of bonding (Figures 7.5 and 7.6) the reverse is true. That is, when the surface has a 100,000 psi stiffness, the potential to develop excessive rutting is more likely for a 2-inch thick overlay, and at a 500,000 psi stiffness of the surface asphalt layer, the critical thickness is a 4-inch thick overlay. At 25 to 75 percent bonding levels, the wheel load application will essentially produce the same maximum octahedral shear stress magnitude in both 2-inch and 4-inch thick overlays regardless of mixture stiffness.

With regard to interface bonding in flexible pavement rehabilitation, it is possible for the new overlay to soften the original surface of the flexible base during the placement and produce a relatively good bond. However, the assumption of developing a well-integrated interface bonding has been challenged (40), especially when there exists a substantial time lag between laying one layer and the next. Therefore, with reference to Figures 7.1 through 7.6, it can be concluded that the stress that activates rapid shear failure in an overlay over flexible base is more pronounced in thin layers of overlay, of up to about 4-inches in thickness. For overlays thicker than 5 inches, the influence of interfacial bonding is significantly reduced.

In a FAA sponsored study (41) it was determined that if a small amount of slippage is allowed, the bottom of the asphalt overlay undergoes tension whereas the top of the original asphalt surface is in compression. These different stress conditions, which result from slippage, cause points in the pavement near each other (but on different sides of the interface) to distort in different directions. This further weakens the bond between the asphalt layers, allowing more slippage, which leads to a higher octahedral shear stress in the asphalt overlay.

Stiffness Effect

In previous sections, the interaction of variables was discussed. In order to study the stiffness effect independently from overlay thickness, and thus to be able to investigate development of octahedral shear stress as a function of stiffness, the moduli of the 2-inch, 4-inch, 6-inch, and 8-inch asphalt overlays were varied from 100,000 psi to 500,000 psi, for several structural conditions. Figures 7.1 through 7.9 illustrate these effects.

Increasing overlay stiffness increases the shear stress magnitude within the overlay for all thicknesses. This is clearly shown in Figure 7.9. Figures 7.1 through 7.4 also show the effect of varying both the overlay thickness and the modulus for perfect bond and slip conditions. In both cases, altering overlay stiffness causes rapid changes in the state of stress in 2-inch and 4-inch overlays when surface shear is applied. These situations are shown in Figures 7.2 and 7.4. Figures 7.5 and 7.6, however, show that with increased stiffness, shear stress increases for all levels of bonding. Figure 7.6 further indicates that at a stiffness value of 500,000 psi, the degree of bonding has less effect on the resistance of the overlay to shear deformation when the surface thickness is equal to the base thickness.

Overall, the effect of increasing the overlay modulus while holding the base modulus constant ($E_1/E_2 > 1$), causes the tensile bending strain at the bottom of the overlay to increase. This would subsequently increase the shear stress in the overlay. The effect of stiffness on pavement life performance has also shown that, at all values of overlay moduli between $1/2 \leq E_1/E_2 \leq 5$, strains at the bottom of the overlay control the pavement life (41).

Effect of Horizontal Surface Shear

Pavements are usually designed only for static vertical loads, but horizontal loads also act on the top pavement surface. Horizontal loads are usually applied to the pavement surface when automobiles stop, turn, accelerate or decelerate. In fact, these horizonal loads are present simply as the result of tire deformation in a static condition. In this study, the horizontal forces were determined based on a finite element tire model developed at Texas A&M University, Texas Transportation

Institute (TTI). Appendix C includes contours of octahedral shear stress distribution for several pavement structures with and without horizontal surface shear for different overlay conditions. Figures 7.1 through 7.4 show the variation of maximum octahedral shear stress with and without surface shear, as a function of overlay thickness. The modulus of each asphalt layer was varied along with the interface conditions. The addition of the horizontal surface force generates a very large shear stress within the surface layer. This is two times as large as typical shear stresses that are generated by vertical wheel load without surface shear. Comparison of Figures 7.2 and 7.4 for the top overlay surface with and without interlayer slippage show that full adhesion reduces the magnitude of critical shear stress by 50 percent for thin thicknesses of overlay. However, when the overlay surface thickness approaches the base thickness (i.e., $h_1/h_2 = 1$), the effect of the horizontal surface shear in the development of critical maximum octahedral shear stress is significantly reduced and interlayer bonding is not as important.

Increasing the overlay stiffness when horizontal surface shear is applied increases the magnitude of maximum octahedral shear stress at both top and bottom surfaces of the overlay as shown in the stress contours in Appendix C. As can be seen from these graphs, the state of stress is significantly altered when a vertical load is applied in combination with the horizontal surface force. Octahedral shear stress is large at the top under the wheel load and is a maximum at the bottom of the overlay away from center of the wheel load. For a thin overlay, stresses at the top, along the edge of the contact area, were reduced in magnitude around the edge of the tire away from center line of the wheel load when a good bond existed; the magnitude was less for less stiff overlays, and progressively increased with an increase in overlay stiffness. However, in both slippage and complete bond cases, the maximum octahedral shear stress occurs at the bottom of the overlay, away from the load centerline.

If thin overlays are not properly bonded to the surface below, the overlay moves, and in the presence of horizontal surface shear this movement reduces the confining pressure and, in turn, creates tensile stresses of high magnitude which not only will lead to a very large octahedral shear stress magnitude, but also tensile strains of high magnitude.

Overall, horizontal tangential loads cause a large octahedral shear stress within the overlay surface layer. If slippage has occurred, the horizontal load must be completely withstood by the top, slipped layer. This leads to crescent cracks in slipped overlays (40,41).

When horizontal loading is present, regardless of the bonding condition, the shear stress developed in thicker overlays is substantially less than that which is produced in the thinner layers, and the effect of overlay stiffness is significantly reduced. This condition is shown in Figures 7.2 and 7.4.

CHAPTER VIII

OCTAHEDRAL SHEAR STRESS ANALYSES OF AN ACP OVERLAY ON A RIGID BASE

General

The purpose of any overlay design procedure is to determine the required additional thickness needed to provide a serviceable pavement over a given period of time. The degree to which the overlay provides a serviceable pavement surface during the selected design period is a primary measure of the success of the overlay design procedure (42). Therefore, a satisfactory design method will consider all the factors that influence overlay response to the surface wheel load.

As a result of adding an overlay to an existing pavement, the state of stress experienced by the base and subgrade layers changes. However, the state of stress developed within the asphalt overlay itself is highly dependent on the type of original surface layer being overlaid. If the original surface is portland cement concrete (PCC), the existing surface may have a rigidity as high as four to ten times larger than the ACP overlay. Subsequently, the neutral axes in the pavement structure may shift and approach the asphalt-base interface or in some cases may fall below the interface, resulting in excessive compressive stress within the top overlay.

This investigation studies the effect of variables that significantly influence overlay performance when the overlay is placed on a PCC base and also their impact on the load-carrying capability of an overlay structure.

Thickness Effect

In the previous chapter, the effect of overlay thickness was discussed for pavements where the supporting layer is comprised of granular materials.

When the asphalt concrete overlay is supported by a stiff portland cement concrete (PCC) layer, a different stress condition is developed in the overlay as shown in the octahedral shear stress contours presented in Appendix C for both rigid and flexible base overlay structures.

The octahedral shear stress varies considerably with the thickness of the overlay, as shown in Figures 8.1 through 8.10, for a complete interfacial bonding condition. These figures show that as the overlay becomes thicker, the maximum value of octahedral shear stress increases and moves under the centerline of the wheel load at the mid-depth portion of the overlay.

It is worth noting that, if the bottom of the overlay was examined, only low stress levels would be reported, whereas the critical shear is developed in the middle of the mixture.

The importance of the overlay thickness cannot be assessed without consideration of interfacial bonding. Figures 8.1 through 8.10 show the variation of the maximum octahedral shear stress as a function of the overlay thickness, interface bonding, and the overlay stiffness. Figure 8.1 shows that when the bond at the interface between the overlay and the base layer is lost, the maximum octahedral shear stress produced in an 8-inch thick overlay is significantly less than that which is developed in thinner overlays. This figure further demonstrates that the maximum octahedral shear stress is higher in 4-inch and 6-inch overlays than it is in a 2-inch thick overlay. This is true for all values of overlay stiffness. For this interface bonding condition however, the 4-inch overlay is always the most critical thickness regardless of the overlay stiffness level.

Figure 8.3, on the other hand, displays a condition of perfect bond at the interface between the overlay and the base layer. This figure shows that thinner overlays develop less octahedral shear stress which translates to a lower potential for rapid development of shear failure. This might be the reason why extremely thin overlays typically do not show rutting as the main failure distress when placed on portland cement concrete (PCC) base (9). However, when the bond is lost, a 4-inch overlay is seen to be more critical than the 2-inch, 6-inch, and 8-inch thick overlays. Figure 8.1 depicts this situation for overlays of different modulus values. This figure clearly demonstrates that a mixture that performs satisfactorily at other thicknesses may not perform as well at a thickness of 4 inches. Overlay thickness is also interrelated with overlay stiffness in terms of influence on the shear stress distribution. This interaction makes it difficult to evaluate the role of thickness

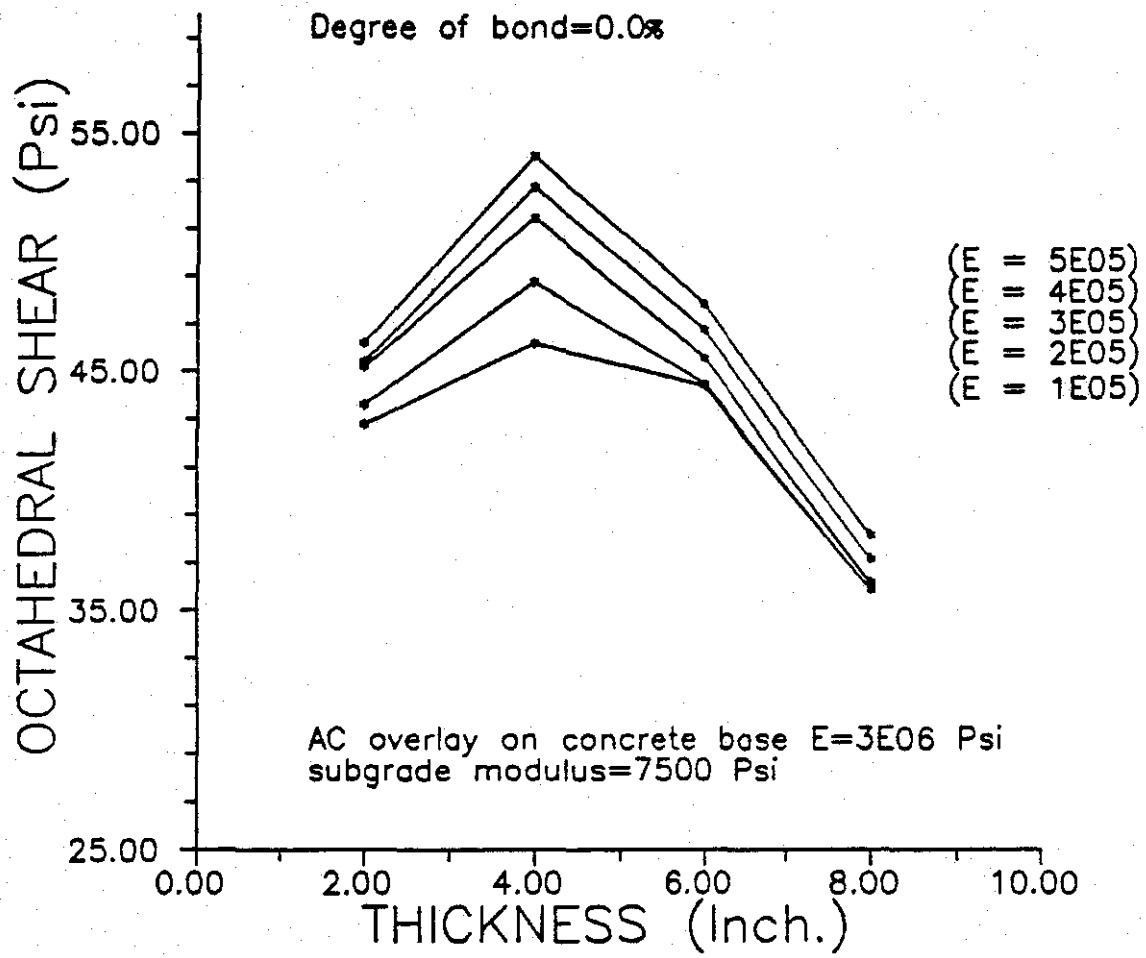

Figure 8.1. Variation of maximum octahedral shear stress in ACP (PCC base) with overlay thickness without surface shear (no interface bonding).

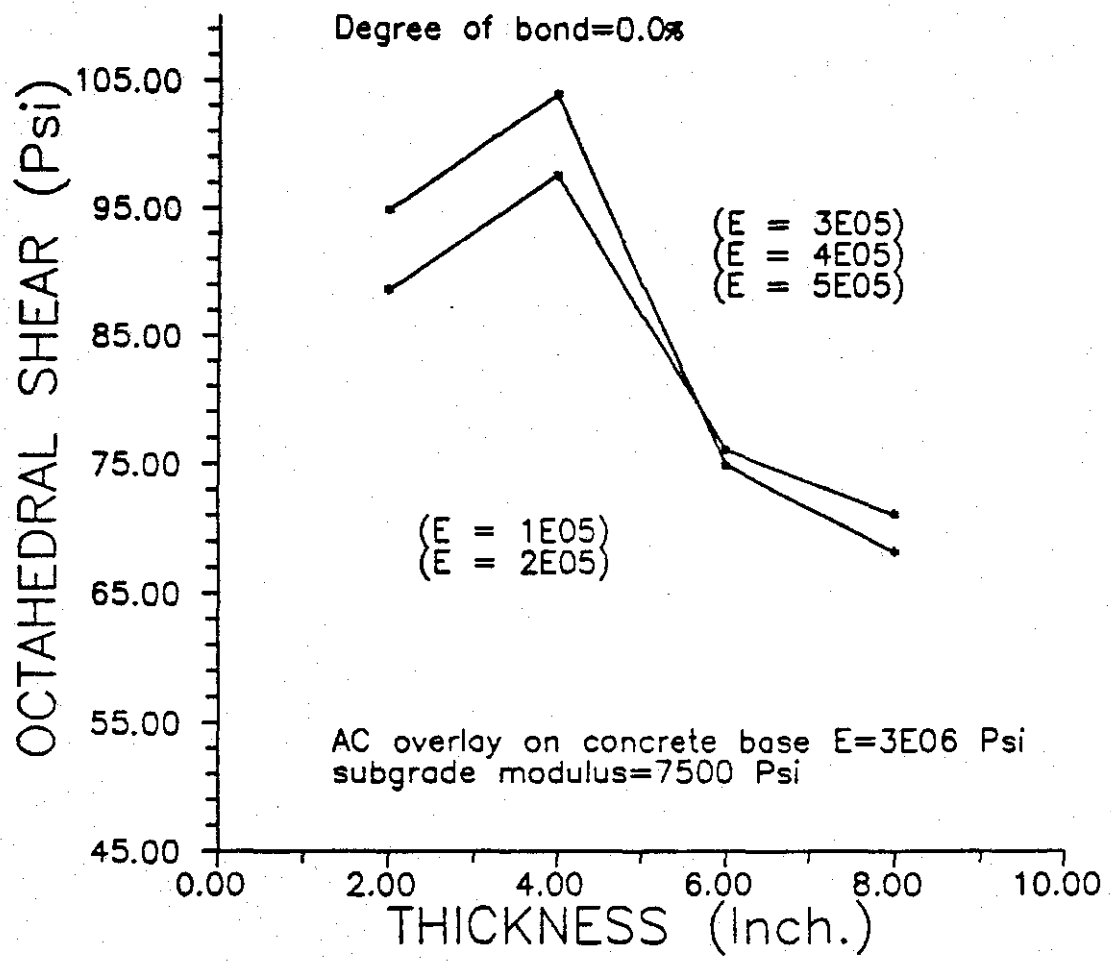

Figure 8.2. Variation of maximum octahedral shear stress in ACP (PCC base) with overlay thickness with surface shear (no interface bonding).

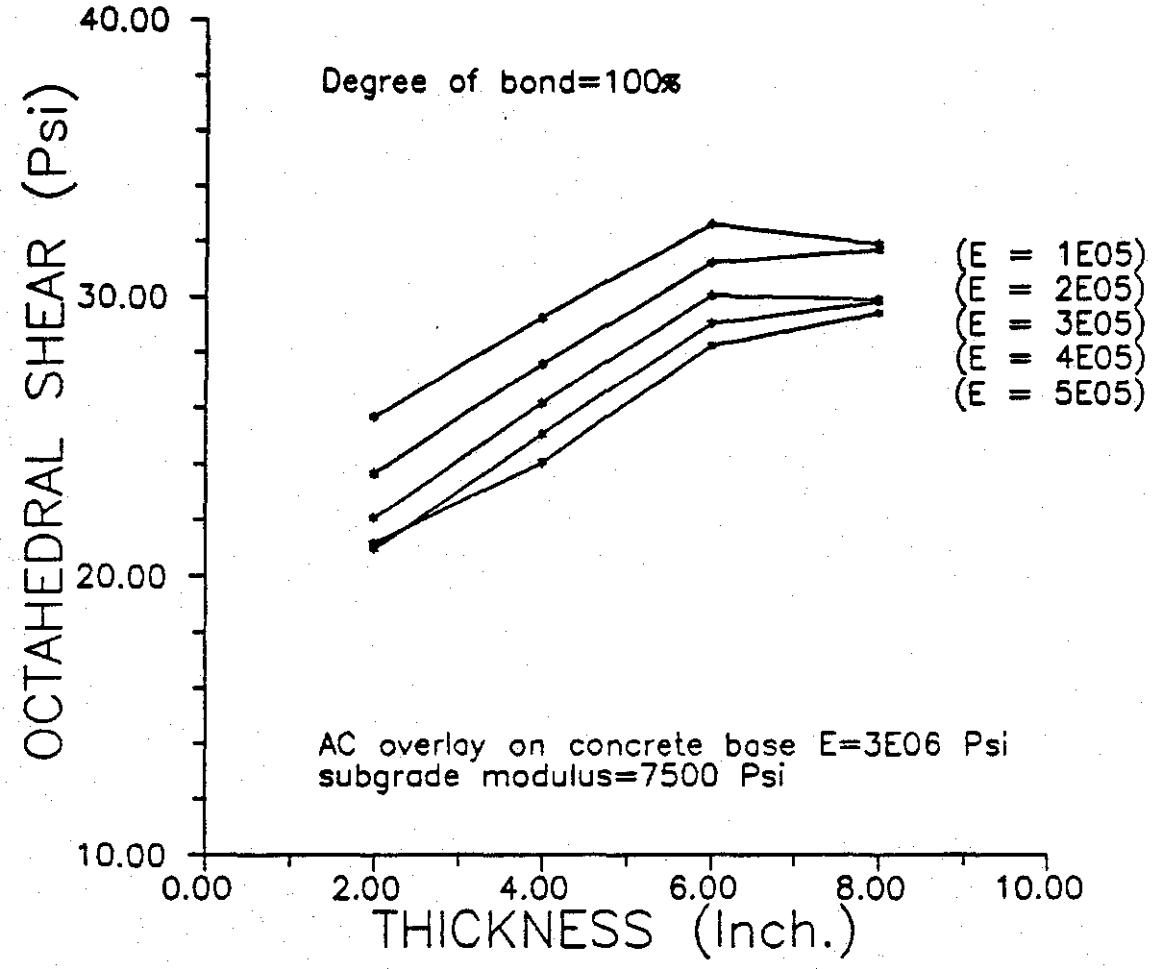

Figure 8.3. Variation of maximum octahedral shear stress in ACP (PCC base) with overlay thickness without surface shear (full interface bonding).

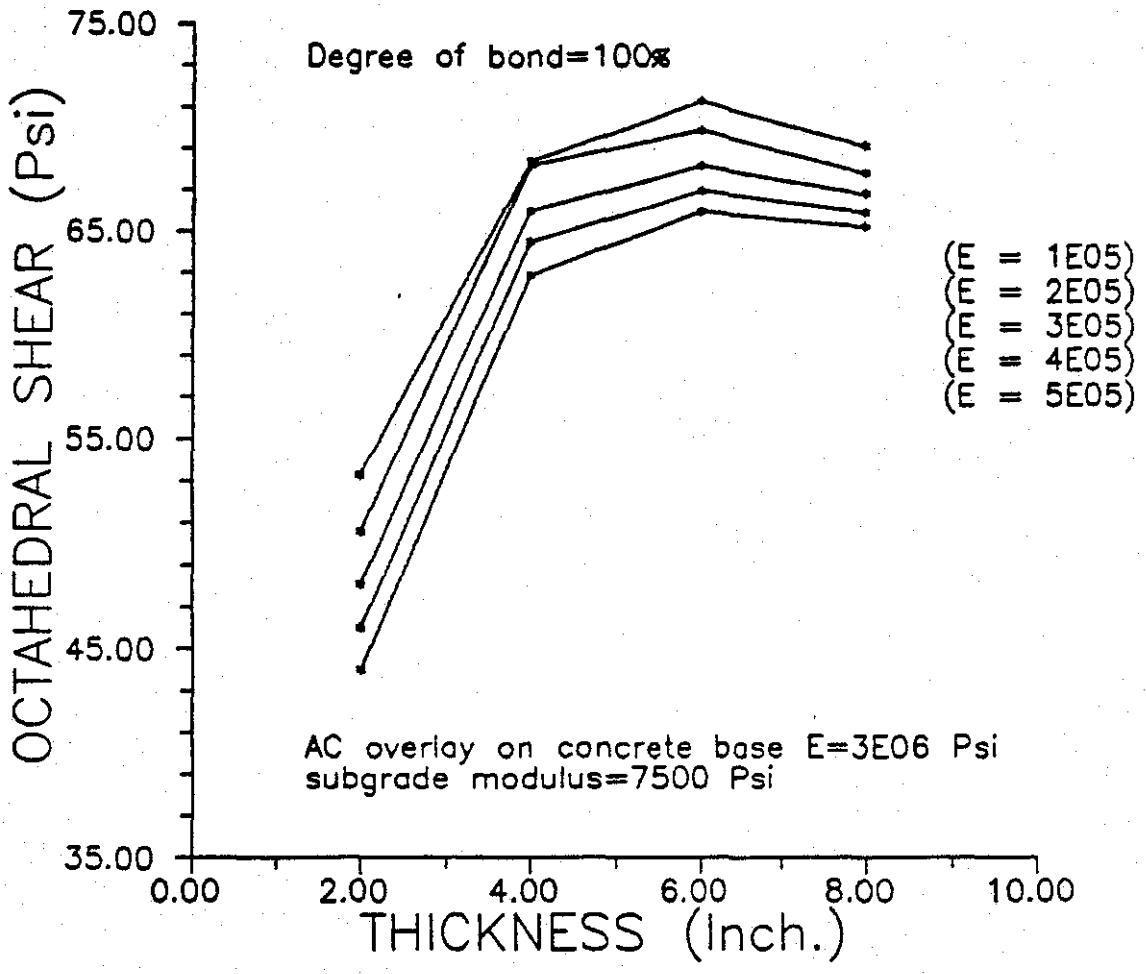

Figure 8.4. Variation of maximum octahedral shear stress in ACP (PCC base) with overlay thickness with surface shear (full interface bonding).

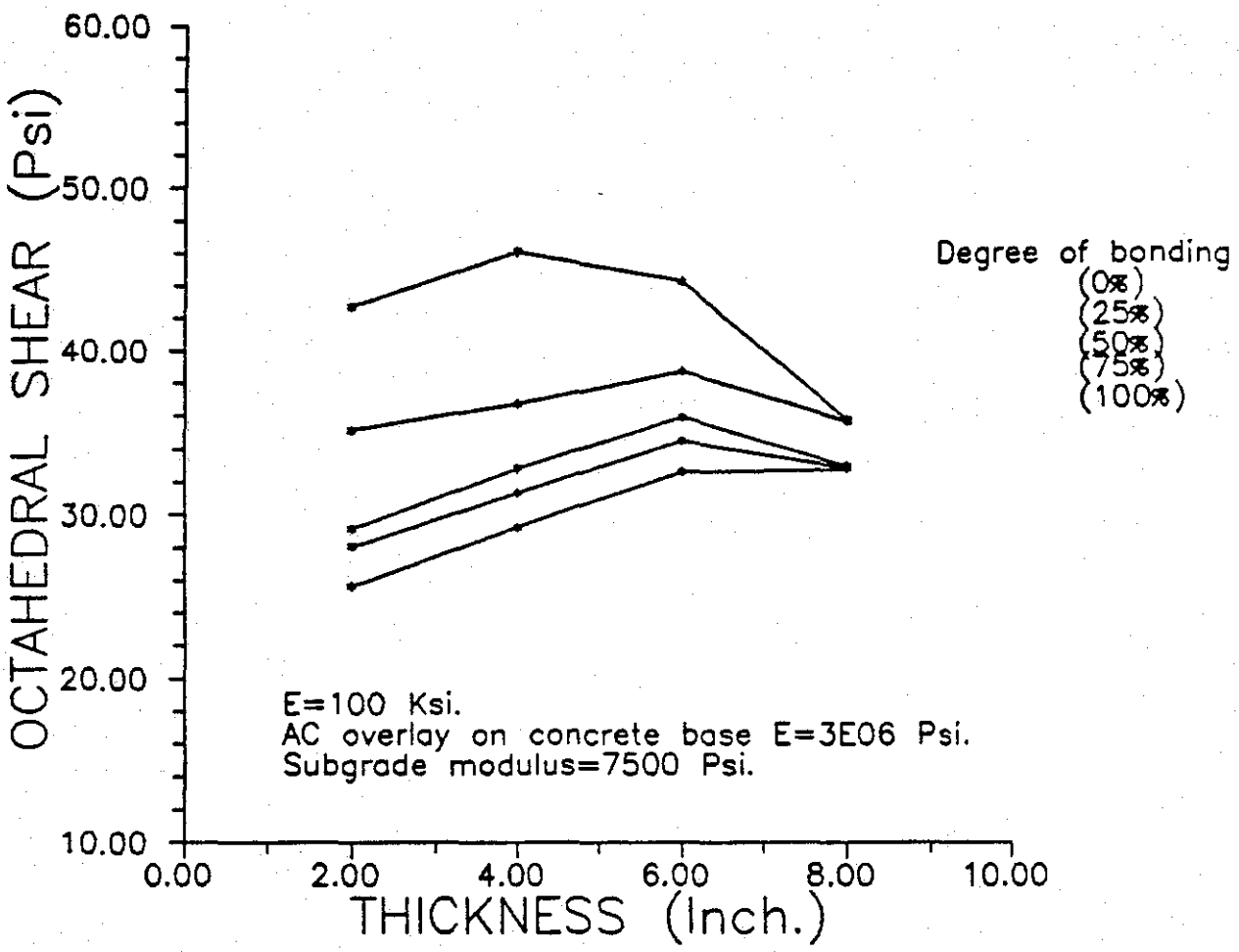

Figure 8.5. Variation of maximum octahedral shear stress in ACP (PCC base) with overlay thickness for various interface bonding levels (E = 100 ksi).

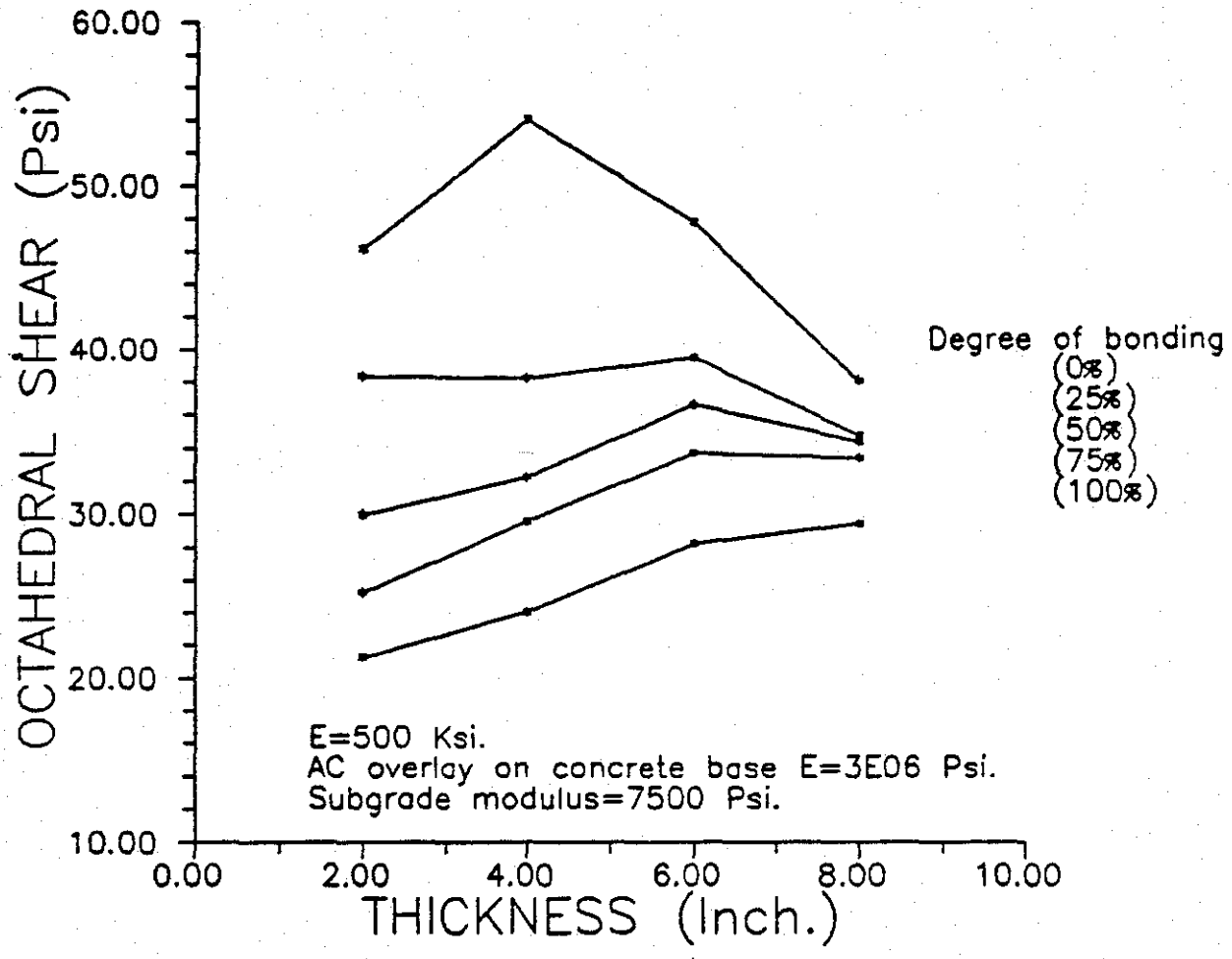

Figure 8.6. Variation of maximum octahedral shear stress in ACP (PCC base) with overlay thickness for various interface bonding levels (E = 500 ksi).

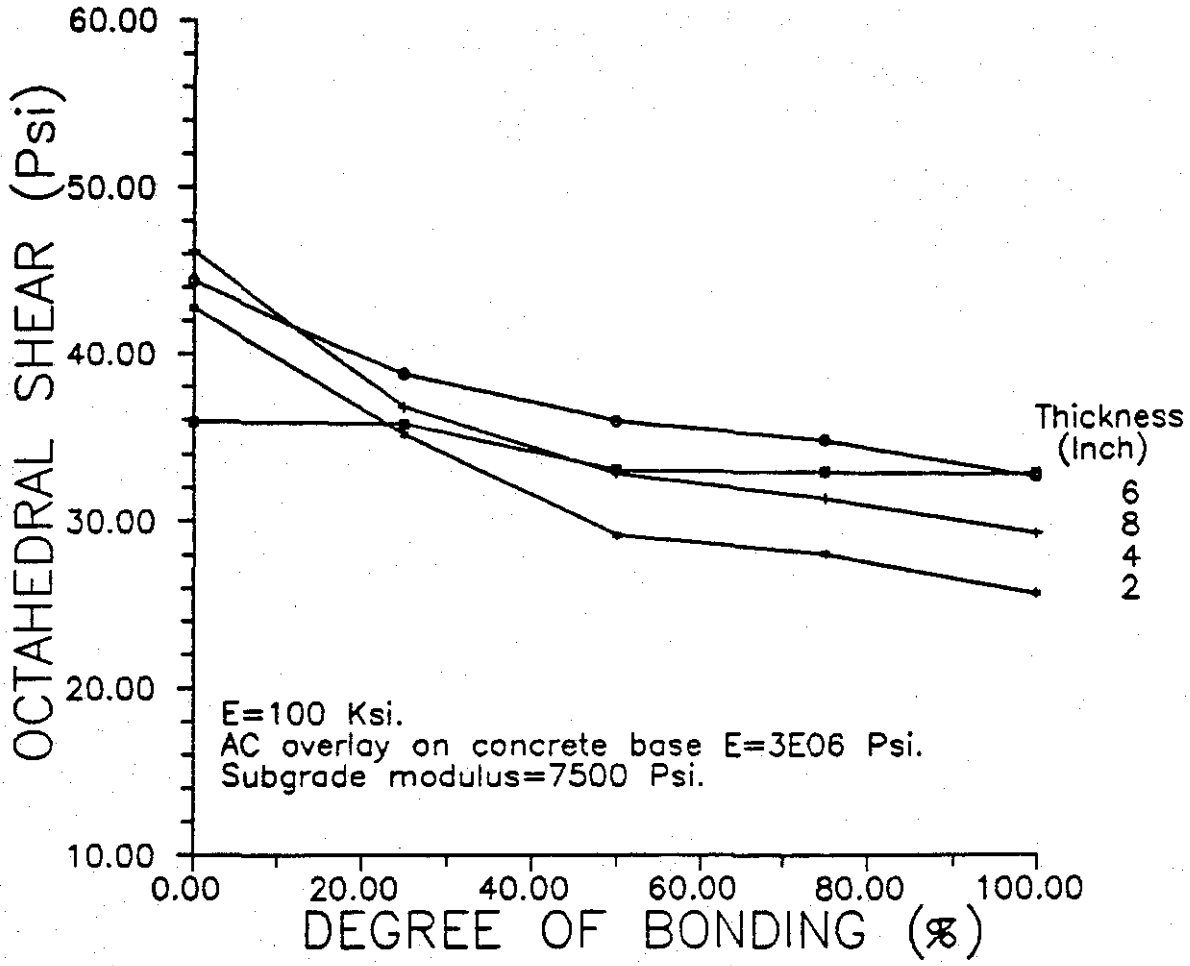

Figure 8.7. Variation of maximum octahedral shear stress in ACP (PCC base) as a function of interface bonding (E = 100 ksi).

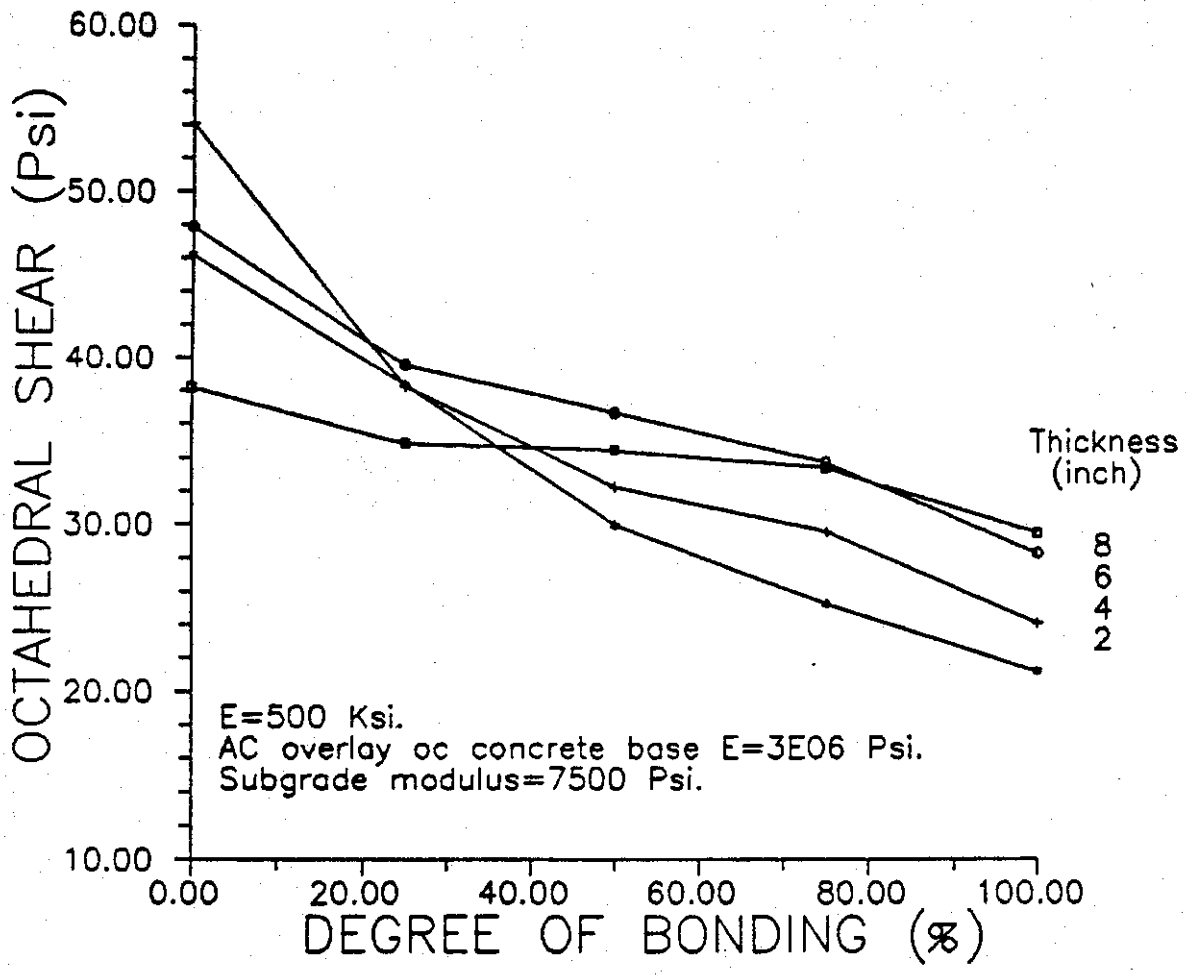

Figure 8.8. Variation of maximum octahedral shear stress in ACP (PCC base) as a function of interface bonding (E = 500 ksi).

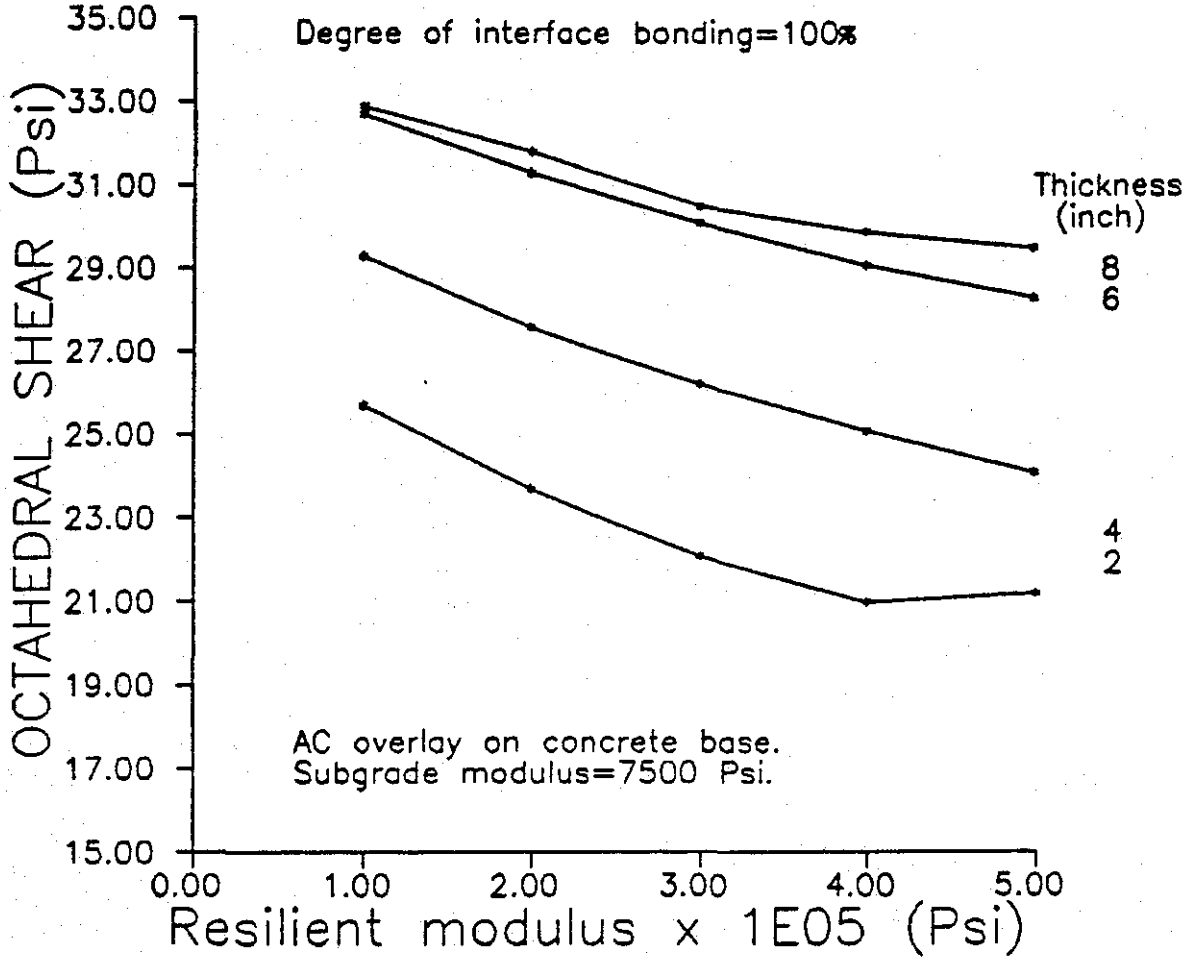

Figure 8.9. Variation of maximum octahedral shear stress in ACP (PCC base) with overlay stiffness.

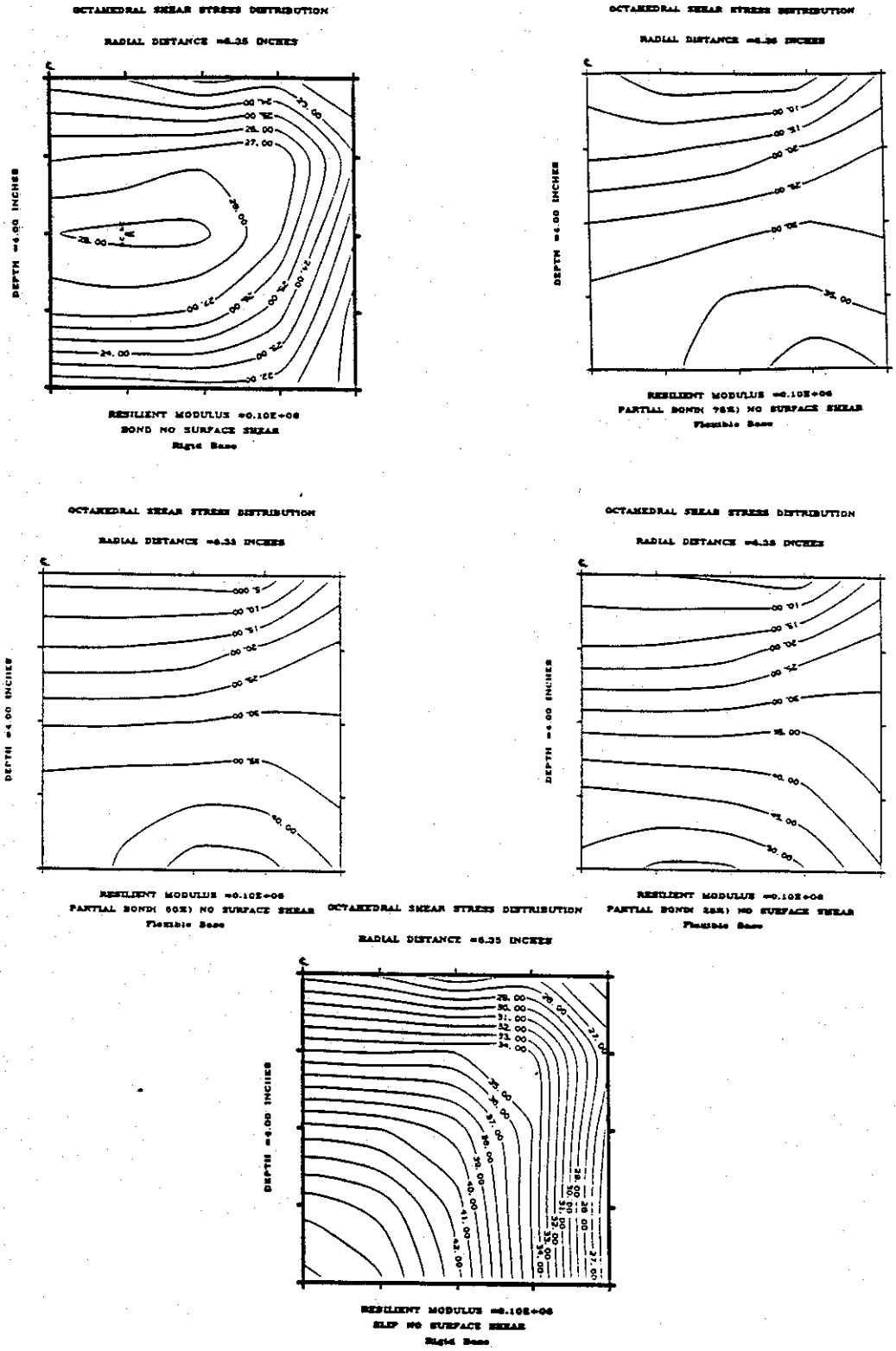

Figure 8.10. Contours of octahedral shear stresses in ACP (pcc base) with various levels of interface bonding.

differences independently. Figure 8.3 shows that at a stiffness value of about 100,000 psi the critical thickness is 6 inches; however, as the ratio of the overlay stiffness to the base stiffness (E_1/E_2) increases, the thicker overlays are more critical. The increase in octahedral shear stress at lower levels of overlay stiffness indicates a greater sensitivity of octahedral shear stress distribution to temperature changes in the surface layer than to overlay thickness.

Overall, it can be concluded that, when interlayer bond is lost, 4-inch ACP overlays represent the critical thickness (see Figure 8.1). However, the effective contribution of the thickness to pavement performance is less significant when interface bonding is good and the overlay is stiff.

Bonding Effect

The importance of interfacial bonding when an overlay structure is subjected to vertical and horizontal surface loads was discussed in Chapter VI for ACP overlays on granular bases. When two different types of material, such as hot-mix asphalt overlay and the portland cement concrete are in direct contact, the potential for development and maintenance of a good bond is questionable. For this type of installation, debonding is more likely if moisture intrudes into the system and/or tack coats are not applied properly. In addition, the thermal characteristics of the two different materials in rigid pavement installation interact to promote debonding, especially when combined with the action of freeze-thaw cycling. Thus, an overlay of rigid pavement has the least potential for the full bonding condition.

When the bond is lost, the magnitude of octahedral shear stress increases rapidly in a 4-inch overlay. Also the maximum octahedral shear stress induced in the slip condition is two times larger than that of a complete bond condition for all overlay thicknesses.

Figure 8.1 illustrates the slip condition and Figures 8.7 and 8.8 show the variation of octahedral shear stress as a function of interfacial bonding. From these figures it can be noted that, when the bond is lost, the potential for premature failure is greatest for a 4-inch thick asphalt concrete overlay. Moreover, Figures 8.5 through 8.8 show that an increase in the degree of bonding shifts the critical thickness to about the 6-inch

thick overlay at lower levels of overlay stiffness and the critical thickness increases with an increase in the stiffness value. This indicates that the degree of interfacial bonding almost invariably controls the geometric properties of the overlay, and subsequently, the performance characteristics of the overlay in response to surface loads.

Figure 8.10 illustrates the distribution of octahedral shear stress as the bond decreases for a 4-inch thick overlay. This figure shows that the location of the maximum octahedral shear stress shifts to the bottom of the surface layer as a direct result of the loss of restraint at the bottom of the surface layer. This figure also shows variation in the stress state as the degree of bonding is decreased. Under this stress condition, the stress levels are far more critical than when a complete bond exists.

Figures 8.5 and 8.6 also show variation in octahedral shear stress as a function of overlay thickness and degree of interfacial bonding for overlays with moduli of 100,000 psi and 500,000 psi, respectively. Figure 8.5 shows that if the overlay stiffness is equal to 100,000 psi, and when the overlay thickness is equal to the base thickness (i.e., $h_1/h_2 = 1$), partial interface bonding does not contribute to the overlay bearing strength. However, when the overlay is relatively stiff (Figure 8.6), the thickness contribution to the bearing capacity of the overlay is highly dependent upon the bonding characteristics at the interface. Lack of good bonding at the interface will drastically reduce the shearing resistance of the overlay to the surface loads.

Crescent cracks on the pavement surface in the direction of the wheel thrust, are caused by the lack of a good bond between the overlay and the base layer beneath. Reflective cracks are also the result of debonding. These cracks occur most frequently in asphalt overlays on portland cement concrete where bonding has deteriorated. Repeated wheel load action, exceeding the load-carrying capacity of the overlay structure, will cause these cracks to extend over the entire section of the pavement when the bond is lost (34).

It is important to note that the localized spalling of the pavement, which is most frequently encountered in areas of heavy traffic, is due to deterioration of the bond and the total loss of restraint at the bottom of the overlay. Loss of bond allows lateral and longitudinal movement of the

surface layer in an opposite direction to the wheel thrust and consequently results in spalling.

In the installation of overlays on rigid pavements, therefore, care must be exercised to properly clean the original rigid surface layer and apply a tack coat correctly to achieve adequate bonding.

Effect of Stiffness

In order to effectively evaluate the influence of overlay stiffness and to exclude the effect of other variables, the moduli of 2-inch, 4-inch, 6-inch, and 8-inch asphalt overlays were varied from 100,000 psi to 500,000 psi for overlays placed on a portland cement concrete (PCC) base. These changes are shown in Figures 8.1 through 8.9.

Figures 7.1 and 8.1 illustrate the stiffness effect, when movement is allowed at the bottom of the surface layer. In this case, an increase in stiffness increases the magnitude of shear stress in 2-inch and 4-inch overlays regardless of the type of support (rigid or flexible). In a rigid overlay installation with poor bonding condition, variation in the overlay stiffness does not significantly alter the magnitude of the maximum octahedral shear stress induced in an 8-inch overlay. Moreover, for the same bonding condition, an increase in thickness from 6 inches to 8 inches, substantially reduces the value of induced shear stress, as shown in Figure 8.1.

When the interface bond is good, an increasingly stiff overlay results in a lower magnitude of the maximum shear stress for all overlay thicknesses, as shown in Figure 8.3. Figure 8.5 also shows that when the overlay is less stiff, and when the thickness of the overlay is equal to the thickness of the base, the effect of partial interfacial bonding is not significant.

Development of maximum octahedral shear stress in a 2-inch thick overlay was further analyzed for a complete bond condition where the overlay modulus was increased to 550,000 psi and 600,000 psi, respectively. In both cases, it was found that excessive stiffness does not contribute to the overlay's performance and the maximum produced octahedral shear stress magnitude will not be lower than that which is reported for a 2-inch overlay with a stiffness of 400,000 psi.

Effect of Horizontal Surface Shear

Figure 8.2 illustrates the variation of octahedral shear stress as a function of overlay thickness, when surface shear acts together with the vertical load on a slip pavement condition. Figure 8.4 depicts the same situation for a complete bond condition. It is apparent from both figures that the addition of horizontal surface shear doubles the magnitude of maximum octahedral shear stress induced in the overlay for both slip and bond conditions. At a given point in a pavement structure, this loading condition leads to a different stress situation which is far more critical than that which has been assumed in conventional pavement design procedures. The possibility of failure becomes unacceptably large. This would indicate that the horizontal loads are the most important determinant of the magnitude of critical shear stress in the overlay structure.

In the slip condition, increasing the overlay stiffness when horizontal force is applied increases the magnitude of shear stress in a 2-inch, 4-inch, and 8-inch thick overlays, but the effect of increasing stiffness in the presence of surface shear is less significant in a 6-inch overlay (Figure 8.2). However, in the presence of a complete bond, increasing overlay stiffness decreases the magnitude of shear stress for all thicknesses in spite of horizontal shear forces at the surface (Figure 8.4).

For a complete bond condition, when horizontal force is applied in combination with a vertical load, and if the stiffness of the overlay is much less than that of the base layer, a 6-inch thick overlay has a higher potential for rutting (and the stresses that activate this permanent deformation are higher) than a 2-inch, 4-inch, or 8-inch thick overlays as shown in Figure 8.4.

CHAPTER IX

STABILITY ANALYSIS USING OCTAHEDRAL STRESS THEORY

Background

In asphalt paving mixtures, aggregate usually comprise between 90 to 95 percent of the weight and between 80 to 85 percent of the volume of the mixture. Moreover, the aggregate is primarily responsible for the load-supporting capacity of the asphalt mixtures. To properly design an asphalt paving mixture for a specific application, consideration must be given to a number of desirable mix properties such as:

1. Stability,
2. Durability,
3. Flexibility,
4. Skid resistance, and
5. Workability.

In studying permanent deformation (rutting), stability is the primary factor that determines the load-carrying capacity of a paving mixture. However, extremely high stability is often obtained at the expense of accepting less durability and vice versa. Figure 9.1 shows a schematic relationship between stability and durability. Making a stiff mixture results in smaller strains under the applied loads (45), but it does not insure resistance to shear failure. Thus, subsequent consideration must be given to insure that both the shearing resistance and the flexibility of a mixture is adequate to sustain surface loads for any specific design application.

Stability is the ability of a paving mixture to resist deformation under high tire pressures and/or a large number of load applications. Stability in general is a function of the following:

1. Interparticle friction of aggregates,
2. Cohesion of the asphalt, and,
3. Resistance to displacement due to mass viscosity effects.

These factors are further illustrated in Figure 9.2.

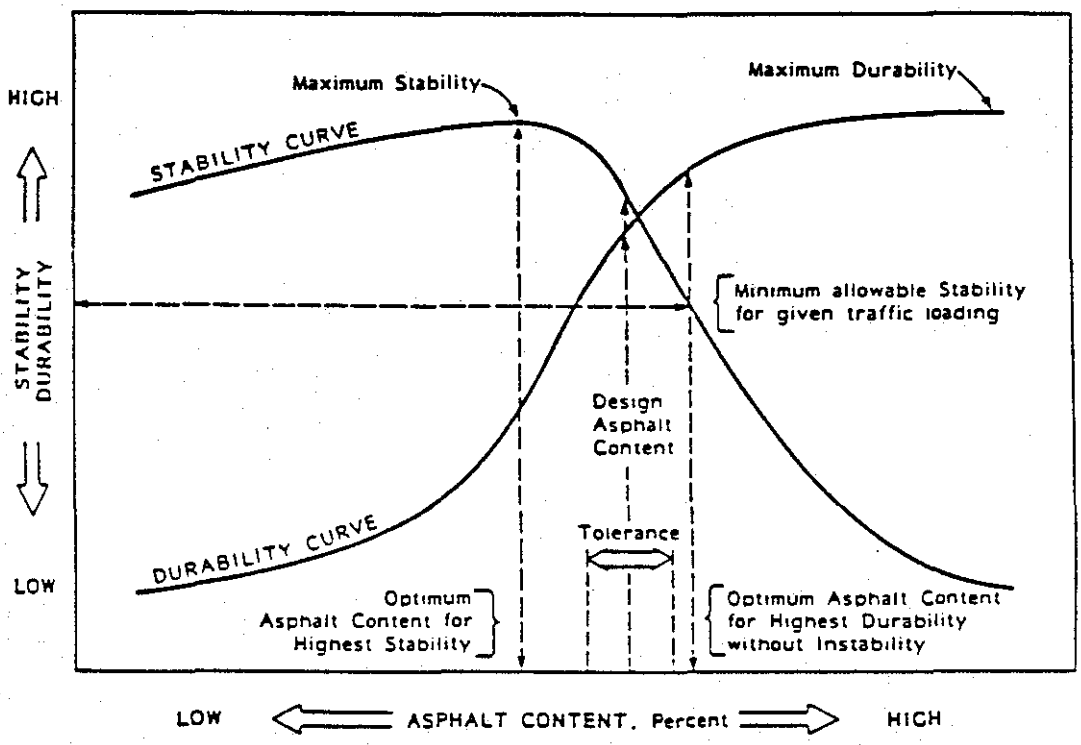

Figure 9.1. The trade-off between stability and durability (after Reference 63).

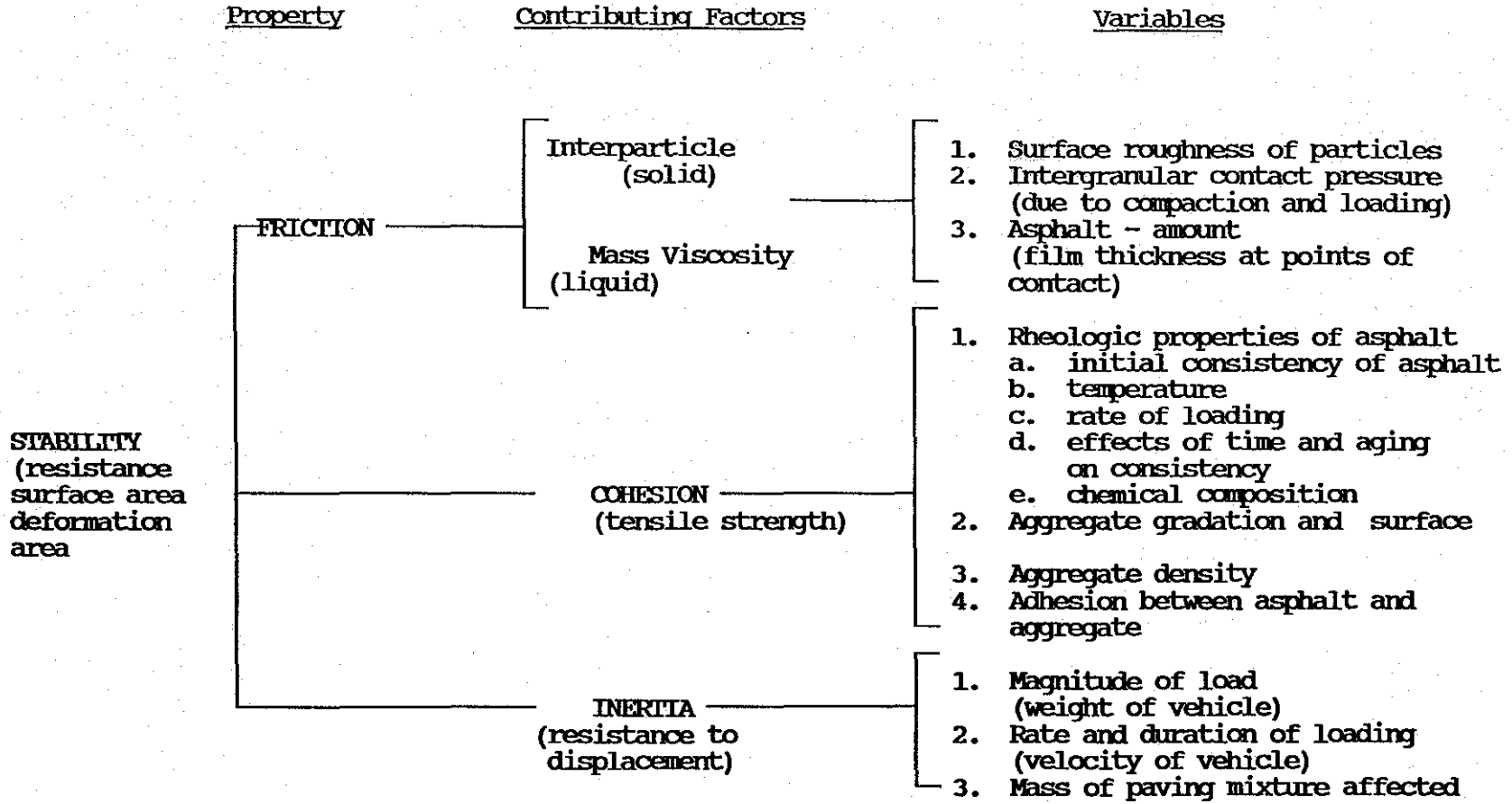

Figure 9.2 Analysis of stability of asphalt paving mixtures (after Reference 44).

Interparticle friction is primarily a function of the surface roughness of aggregates and intergranular contact pressure. This is not significantly influenced by load rate and/or temperature change. However, the amount of asphalt influences interparticle friction due to an increase in the asphalt film thickness at the contact points between aggregate particles.

The resistance to sliding offered by asphalt is a function of the rheologic properties of the asphalt, which, in turn, vary with temperature, load rate, and aging as well as with initial consistency of the asphalt binder.

Resistance to displacement, depends on the magnitude and number of traffic load applications. Asphalt paving mixtures that are subjected to moving loads exhibit greater stability than those under static or slowly applied loading. This is due to the inertia or resistance to displacement developed in the mixture, together with the mass of the pavement affected (44).

With regard to stability, three principal conditions must be considered (11). These are:

1. Stability under stationary wheel loads,
2. Stability under the wheel loads of vehicles moving at a relatively high and reasonably uniform rate of speed, and
3. Stability under the breaking and accelerating stresses of traffic.

Since asphalt paving mixtures may be subjected to various combinations of these loading conditions, it is necessary to determine the most critical condition. Moreover, any bituminous paving mixture should be designed to provide adequate stability in order to resist critical loads at any time during its useful life.

The Mohr-Coulomb failure envelope provides a fundamental basis to measure the strength of bituminous mixtures. For any specified value of lateral support, the strength according to the Mohr-Coulomb concept can be evaluated as octahedral shear strength at failure. In this study, an effort has been made to utilize Mohr-Coulomb shear failure theory to evaluate the stability (resistance to deformation) of asphalt concrete paving mixtures to wheel loads moving at a relatively high rate of speed (approximately 55 miles per hour).

Octahedral Shear Strength Application

On the basis of the geometry of Mohr-Coulomb failure envelope (Figure 3.1), the maximum vertical stress that can be supported by a paving mixture is given by the following equation:

$$\sigma_1 = \sigma_3 \frac{1 + \sin\phi}{1 - \sin\phi} + 2C \left[\frac{1 + \sin\phi}{1 - \sin\phi} \right]^{\frac{1}{2}} \quad (9.1)$$

where: σ_1 = vertical stress, psi,
σ_3 = lateral stress, psi,
ϕ = angle of internal friction, degree, and
C = cohesion, psi.

This relationship can be transformed to obtain octahedral shear strength in terms of fundamental material properties, ϕ, C, and σ_3, as follows:

$$\tau_{oct} = 0.942 \left(\left[\frac{\sigma_3 \sin\phi}{1 - \sin\phi} \right] + C \left[\frac{1 + \sin\phi}{1 - \sin\phi} \right]^{\frac{1}{2}} \right) \quad (9.2)$$

where: τ_{oct} = fundamental stress invariant
ϕ, C = angle of internal friction and cohesion.

Figure 9.3 is obtained when the value of octahedral shear strength (τ_{oct}) from Equation (9.2) is plotted for different degrees of lateral support (σ_3), and for various magnitudes of C and ϕ. Each stability curve in Figure 9.3 indicates that only those materials with combinations of C and ϕ values that lie on, or to the right of, the curve in Figure 9.3 have adequate shear strength (τ_{oct}). This plot assumes that the lateral support mobilized in the pavement adjacent to the loaded area is equal to the lateral support (σ_3) specified for that stability curve.

Equations (9.1) and (9.2) can be used to determine practical values of τ_{oct} if the lateral support, σ_3, provided by the pavement surrounding the loaded area can be determined. The values of cohesion, C, and the angle of internal friction, ϕ, for any bituminous mixture can be measured by the triaxial test.

One approximation of the magnitude of lateral support, σ_3, is that it is a function of the strength of the pavement immediately adjacent to and surrounding the contact area (11). Several researchers (45,46) have

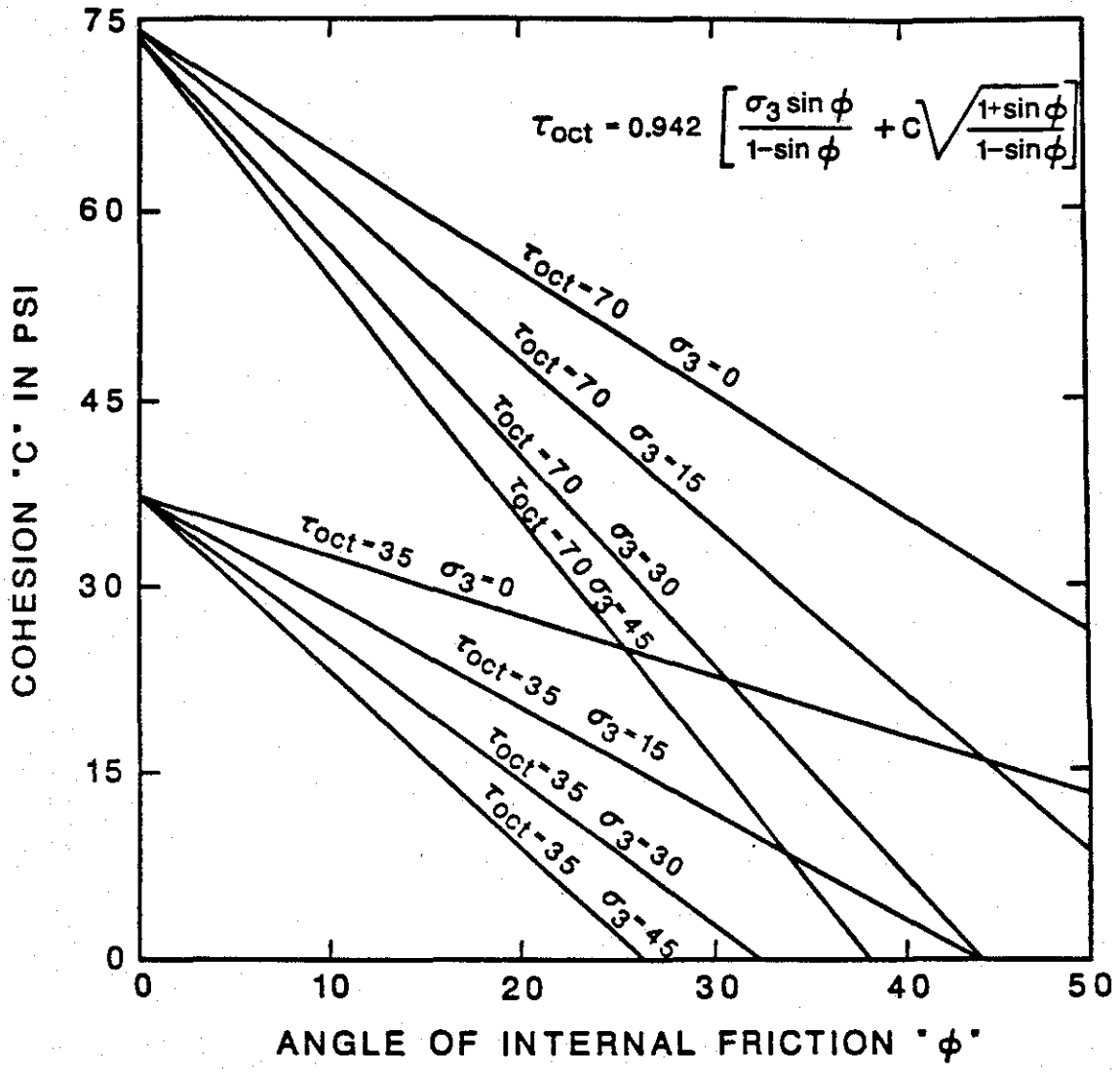

Figure 9.3. Octahedral shear strength for different degrees of lateral support (modified from Reference 11).

suggested that the unconfined compressive strength of the bituminous paving mixture can be taken as a conservative measure of the lateral support provided by the pavement immediately adjacent to the loaded area. That is:

$$\sigma_3 = 2C \left(\frac{1 + \sin\phi}{1 - \sin\phi} \right)^{\frac{1}{2}} \tag{9.3}$$

Upon substitution of this relation ship for σ_3 in Equation (9.2), Equation (9.4) is obtained.

$$\tau_{OCT} = 0.942C \left[\left(\frac{1 + \sin\phi}{1 - \sin\phi} \right) \left(\frac{1 + \sin\phi}{1 - \sin\phi} \right)^{\frac{1}{2}} \right] \tag{9.4}$$

Equation (9.4) is the stability equation for a bituminous mixture when it is assumed that the maximum lateral support, σ_3, provided by the pavement surrounding the loaded area is equal to the unconfined compressive strength of the mixture. Figure 9.4 is a plot of Equation (9.4) for various values of ϕ and C where lateral support (σ_3) is equal to the unconfined compressive strength of the paving mixture.

Influence of the Frictional Resistance and Interface Bonding

McLeod's approximate solution (46) is the only one (40) which takes into consideration the influence of the frictional resistance between the tire and the pavement as well as the influence of the frictional resistance between pavement layers. The stability solution given in Equation (9.5) is based on the following assumptions:

1. Vertical load is uniformly distributed in both vertical and horizontal directions,
2. Rectangular contact area of the tire, and
3. Frictional resistance between tire and surface as well as interface bonding is proportional to the vertical load.

The following expression results from equilibrium at the critical state:

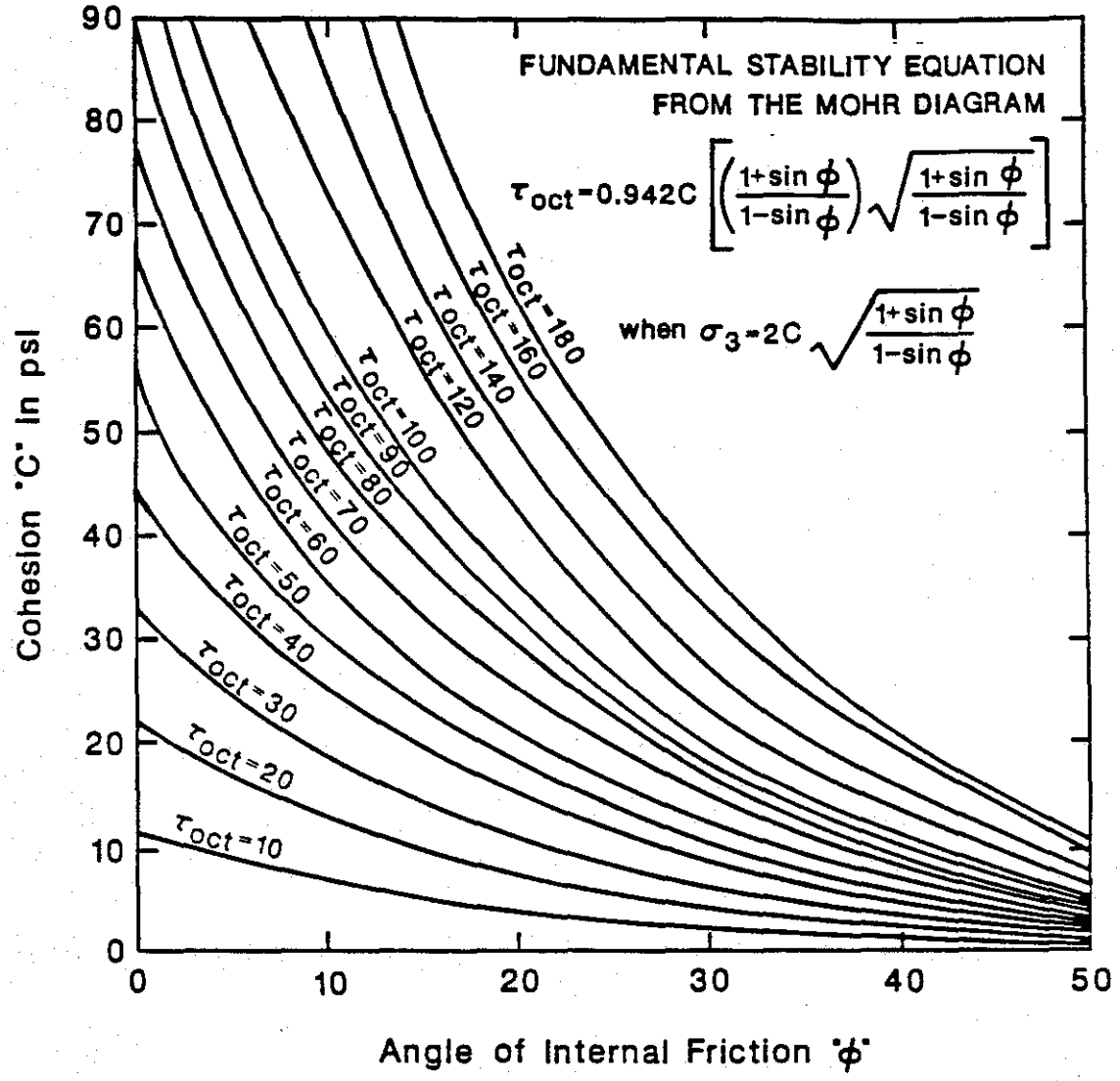

Figure 9.4. Octahedral shear strength as a function of ϕ and C when lateral support is equal to the unconfined compressive strength (modified from Reference 11).

$$\sigma = 2C \left[\frac{K_p^{\frac{1}{2}} (2K \ell/w \tan\phi + J) + \ell/w + 1/K_p^{\frac{1}{2}}}{1/K_p + \ell/t(f-g)} \right] \qquad (9.5)$$

where:
- σ = bearing capacity of the asphaltic layer (vertical stress),
- C, ϕ = as previously defined,
- K, J = coefficients expressing the influence of the vertical pressure outside the loaded area (K=J=1 is conservative),
- K_p = $\left(\frac{1 + \sin\phi}{1 - \sin\phi} \right)^{\frac{1}{2}}$
- t = thickness of the surface layer,
- ℓ, w = length and the width of the load area,
- f = coefficient of friction between tire and the pavement, and
- g = coefficient of friction at the surface and the base interface.

In the situations where longitudinal cracks exist, the contribution to the bearing capacity by the pavement adjacent to the loaded area should be omitted by equating the following expression in Equation (9.5) to zero (40):

$$[(2 \ell k/w \; K_p^{\frac{1}{2}} \tan\phi + \ell/w] \qquad (9.6)$$

Equation (9.5) neglects the tensile strength contribution to the asphalt bearing capacity provided by the rear wall due to the possible presence of transverse hair cracks in the surface of the pavement. The wall effect is defined as the effect of one of the four sides of the prism (with a rectangular base) that forms the tire model.

The typical values of the parameters in Equation (9.5) are:

1. ℓ/w approximately equal to unity, although higher ratios can be used,
2. Coefficient of friction, f, between tire and the surface ranges from 0.30 to 0.8 depending on the type of road and tire condition. However, 0.8 is typical for emergency breaking situations.

3. The value of the coefficient of interface friction, g, is significantly dependent on the asphalt overlay temperature and the magnitude of vertical pressure, as well as the tack coat rate. No specific value, or range of values are reported in the literature (to the authors' knowledge) regarding this variable. However, the maximum value that g can attain is equal to unity.

Examination of the stability Equation (9.5) indicates that when the frictional resistance between the pavement and tire is equal to the maximum frictional resistance between the pavement surface and the pavement base (Figures 9.5 through 9.8), pavement thickness has no influence on the stability which is developed by the pavement when subjected to severe breaking or accelerating stresses. Moreover, when the frictional resistance between pavement and tire is less than the maximum friction resistance between the pavement surface and the pavement base, an increase in pavement thickness leads to a decrease in the stability developed by the pavement under breaking stresses (46). Consequently, influence of overlay thickness on stability is a function of the (f-g) value.

When (f-g) = 0, overlay thickness has no influence on pavement stability as shown in Figures 9.5 through 9.8. Also, it should be noted from Figures 9.9 through 9.11, that when the values of the coefficient of friction, f, and the frictional property at the interface, g, are equal, the prime contributor to the shearing strength of the asphalt mixture is the cohesive component of the mixture.

The following items should be noted from Figures 9.5 through 9.11:

1. When there is no frictional resistance at the interface between the surface layer and the base layer, an increase in surface thickness will increase the bearing strength of the pavement.
2. When frictional resistance at the interface between the surface layer and the base layer is equal to the frictional resistance to sliding between the tire and the surface, increasing surface thickness will not contribute to the bearing resistance of the pavement. In this case, the main contributor to the pavement bearing capacity is the cohesive strength of the mixture.
3. The contribution to the pavement bearing strength provided by

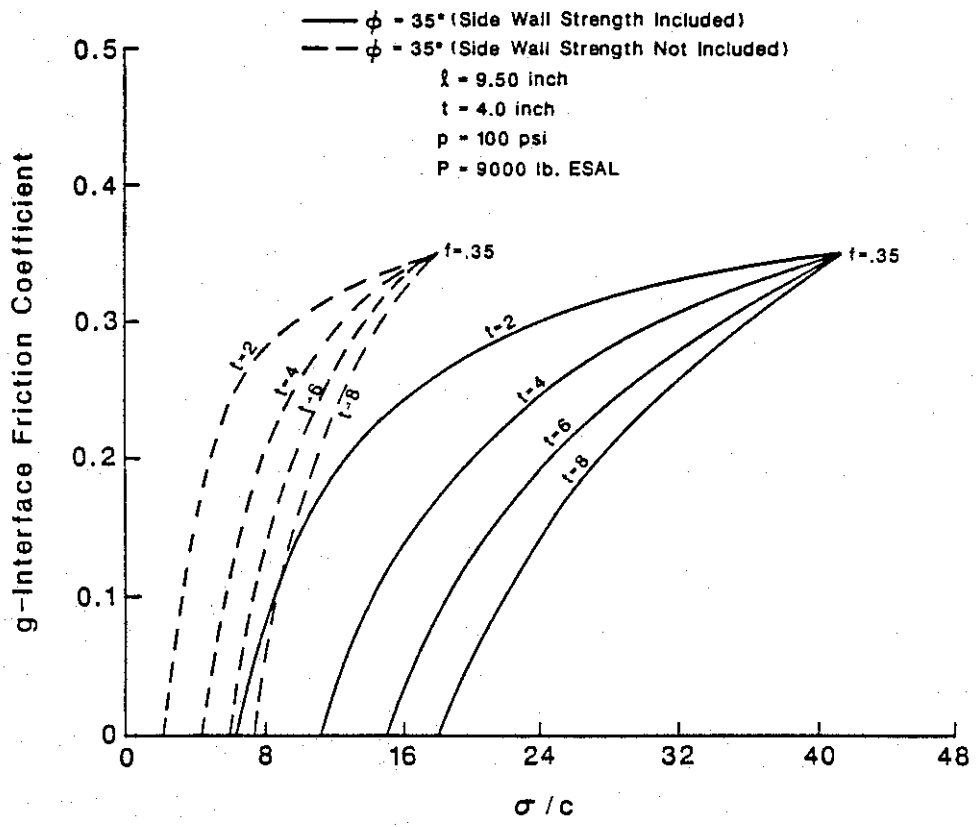

Figure 9.5. Bearing strength as a function of interface bonding for constant friction (ϕ = 35°, F = 0.35).

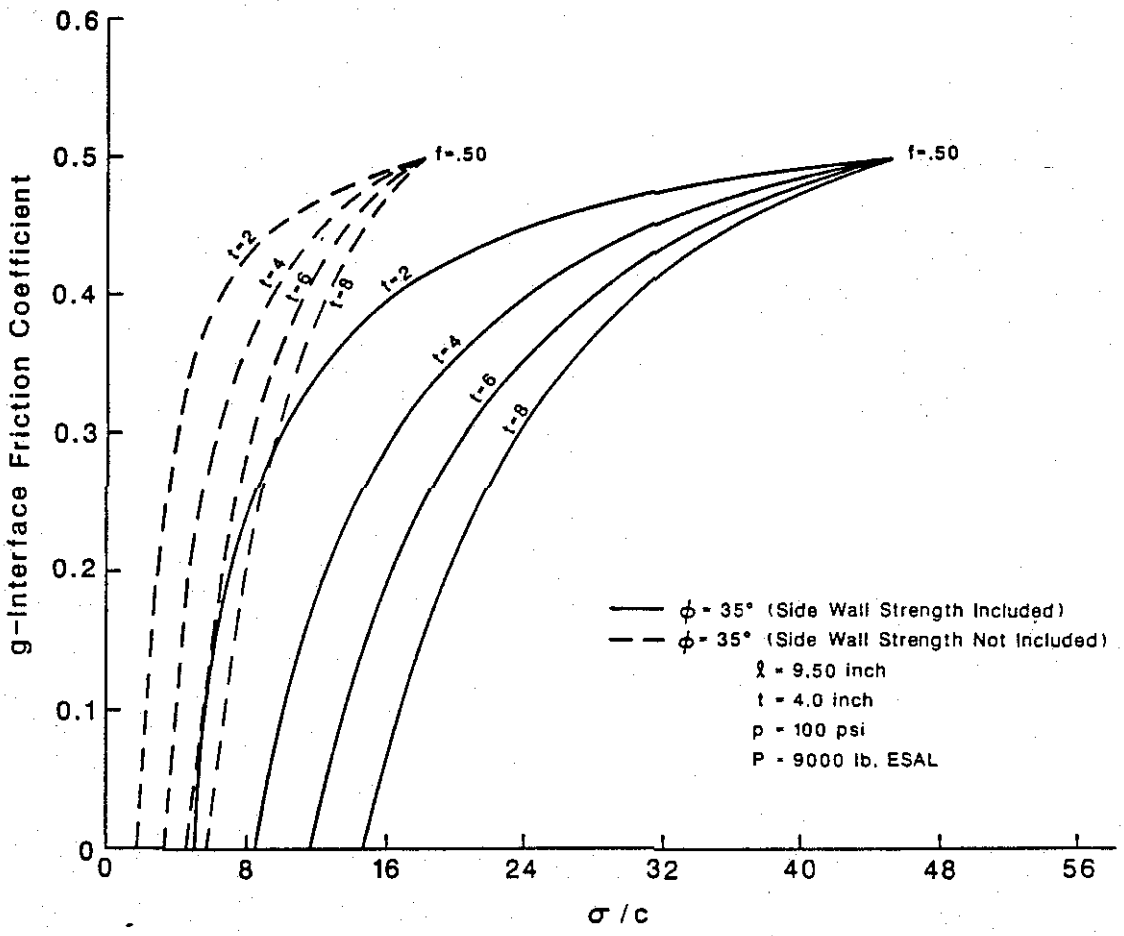

Figure 9.6. Bearing strength as a function of interface bonding for constant friction (ϕ = 35°, F = 0.50).

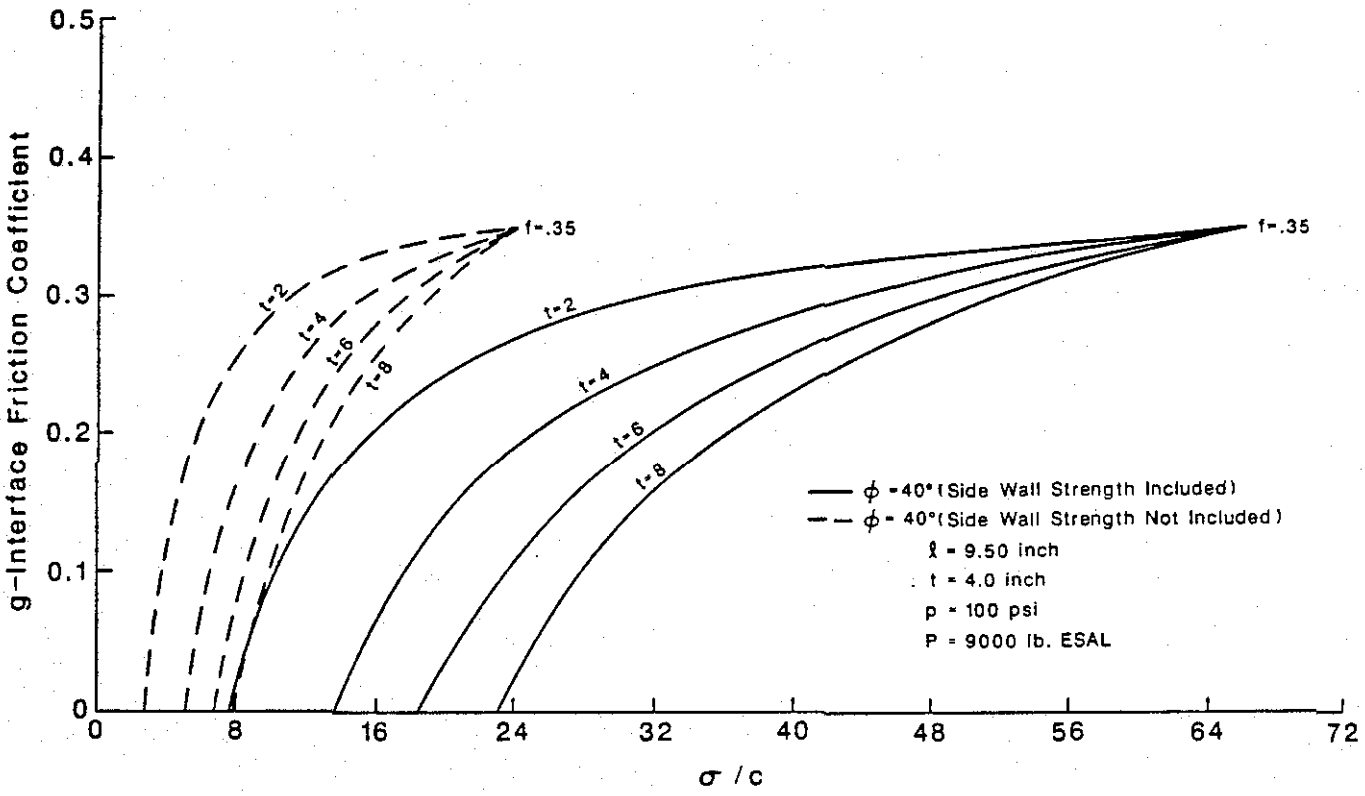

Figure 9.7. Bearing strength as a function of interface bonding for constant friction (ϕ = 40°, F = 0.35).

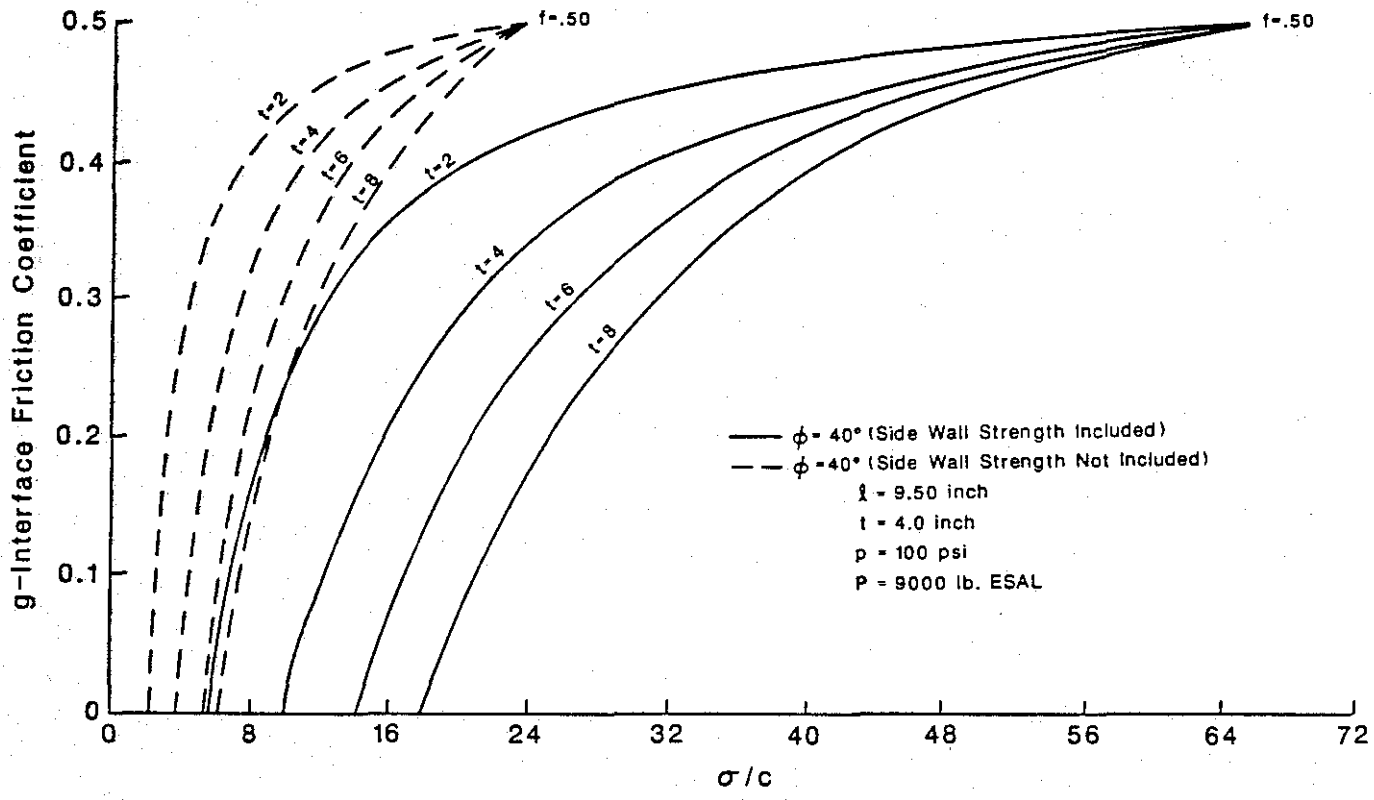

Figure 9.8. Bearing strength as a function of interface bonding for constant friction (ϕ = 40°, F = 0.50).

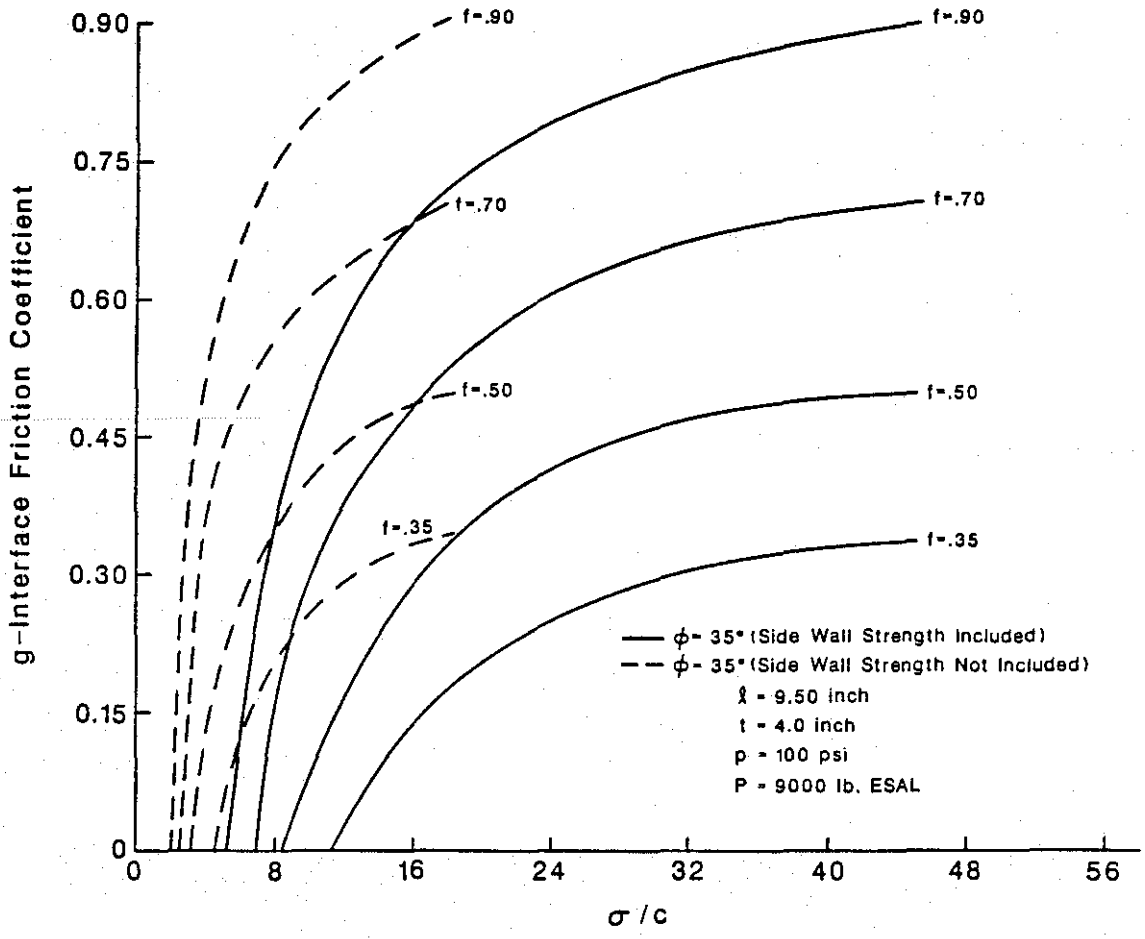

Figure 9.9. Bearing strength as a function of interface bonding for various levels of surface friction (ϕ = 35°, F = 0.35 - 0.90).

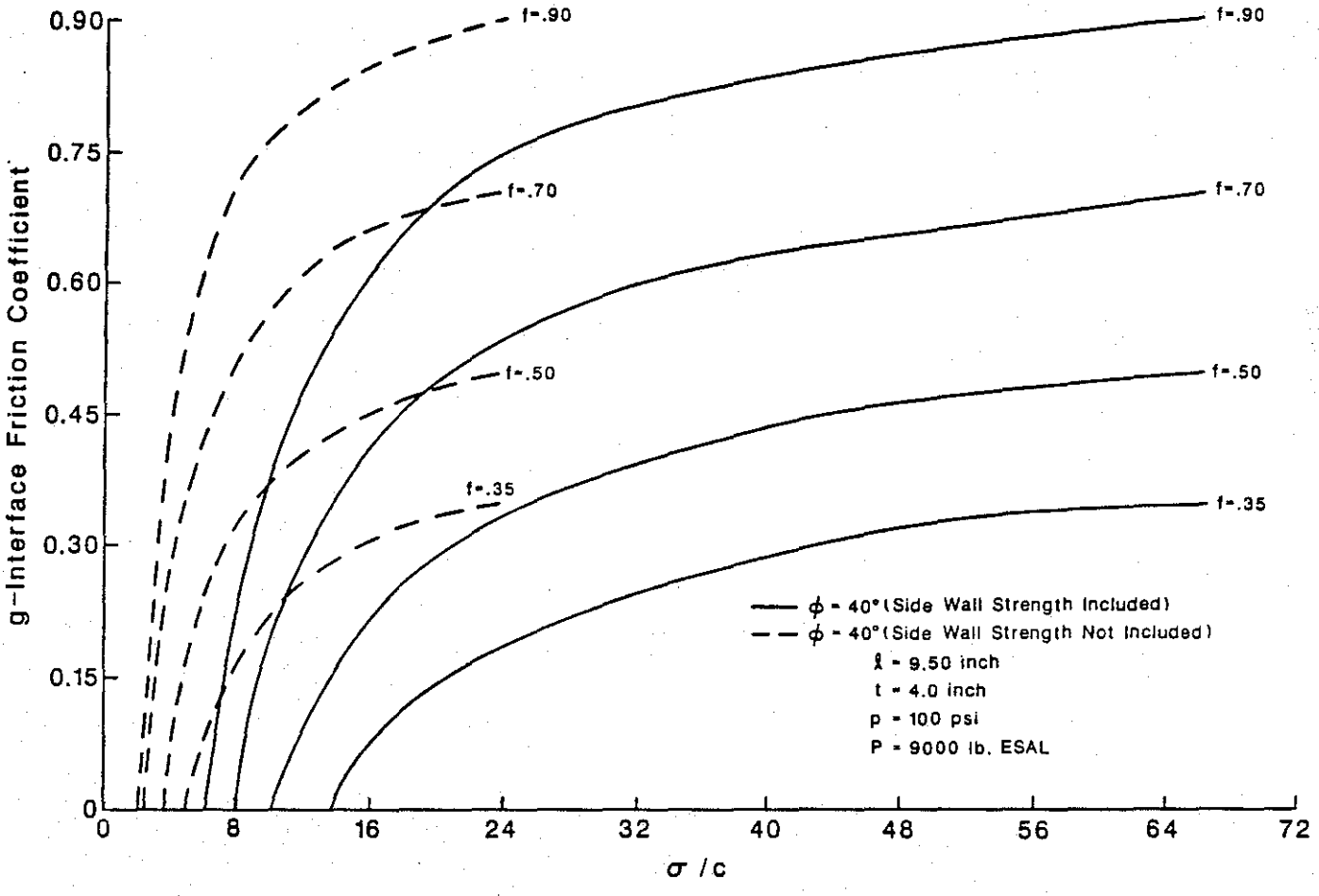

Figure 9.10. Bearing strength as a function of interface bonding for various levels of surface friction (ϕ = 40°, F = 0.35 - 0.90).

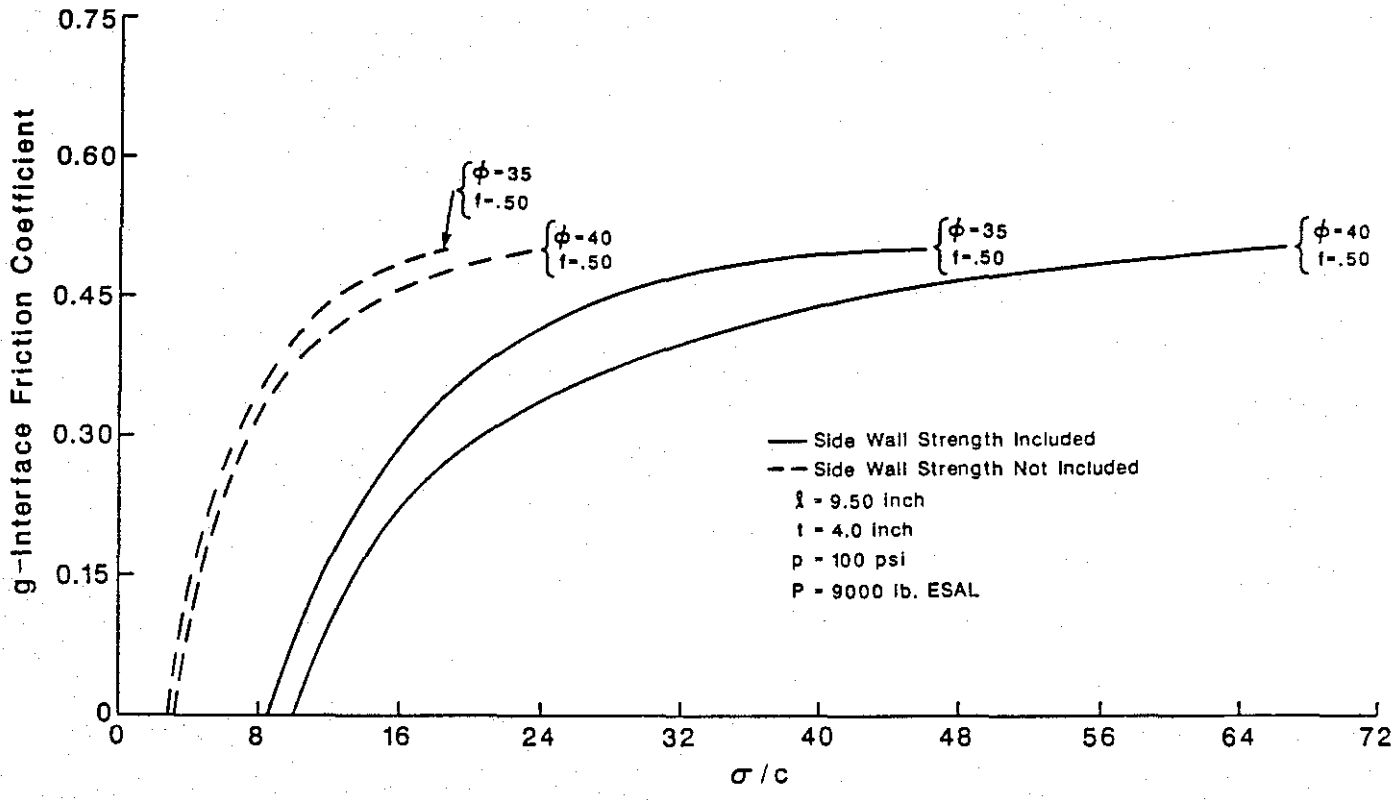

Figure 9.11. Bearing strength for different values of mixture internal friction and overlay surface friction.

the side walls of the tire, immediately surrounding the loaded area, is more than half the layer-bearing strength.

4. When acceleration or deceleration produce strong frictional resistance to sliding at the tire-pavement interface, the bearing capacity of the pavement is greatly reduced.

The most critical condition in a pavement bearing capacity analysis is when high frictional resistance exists at the top between the tire and the pavement surface and when there is little or no frictional resistance at the interface between the surface layer and the base layer. Therefore, in any bearing capacity analysis for moving traffic, one must include the horizontal surface force in the analysis, and consider the combined effects of horizontal and vertical stresses. However, static loads are also critical for design because of the creep within the ACP.

Equations 9.4 and 9.5 are based on the assumption that the lateral support (τ_3) provided by the pavement immediately adjacent and surrounding the loaded area is equal to the unconfined compressive strength of the mixture expressed by Equation 9.3. A more fundamental approach, which considers the pavement material's strength in situ and thereby avoids controversy, concerns the lateral support estimate (assumption) which is developed and presented in the following section. This method takes into consideration pavement boundary conditions as well as the loading conditions.

Determination of Octahedral Shear Stress Ratio

For a particular paving mixture, the Mohr-Coulomb failure envelope can be developed from triaxial test results. In these triaxial tests, a cylindrical specimen of asphalt is subjected to a set of confining pressures and is loaded to failure. The principal stress difference (deviator stress) is equal to the axial load applied to the specimen divided by the cross-sectional area of the specimen. The major principal stress is equal to the deviator stress plus the chamber pressure, and the minor principal stress in the specimen is equal to the chamber pressure.

The concept of the Mohr-Coulomb failure theory can be broadened and expressed in terms of critical octahedral shear stress values. For any Mohr's circle tangent to the Mohr-Coulomb failure envelope, octahedral shear stress at failure is equal to 0.47 times the deviator stress. The

With the appropriate computer analysis, the critical stress state at any point in the pavement structure under a given wheel load can be computed. The corresponding critical normal and shear stresses on the octahedral plane will depict the complete stress state and can simply be expressed in terms of stress invariants as follows:

$$\tau_{oct} = 1/3\ I_1 \tag{9.7}$$

$$\tau_{oct} = 1/3\ (2I_1^2 - 6I_2)^{1/2} \tag{9.8}$$

where:

$$I_1 = \sigma_x + \sigma_y + \sigma_z \tag{9.9}$$

$$I_2 = \sigma_x\ \sigma_y + \sigma_y\ \sigma_z + \sigma_z\ \sigma_x - (\tau_{xy}^2 + \tau_{yz}^2 + \tau_{zx}^2) \tag{9.10}$$

Quantities I_1 and I_2 are known as stress invariants because they are independent of how coordinate axes are oriented at a given state of stress. The advantage of expressing octahedral normal and shear stresses in terms of invariants is that these expressions do not require computation of principal stresses in order to determine normal and shear stresses on the octahedral plane.

Once the coordinates of the critical stress point in a given pavement structure are known, the octahedral shear strength of the asphaltic layer can be characterized by a law similar to Mohr's strength law, i.e.:

$$\tau_{oct} = C' + \sigma_{oct} \tan \phi' \tag{9.11}$$

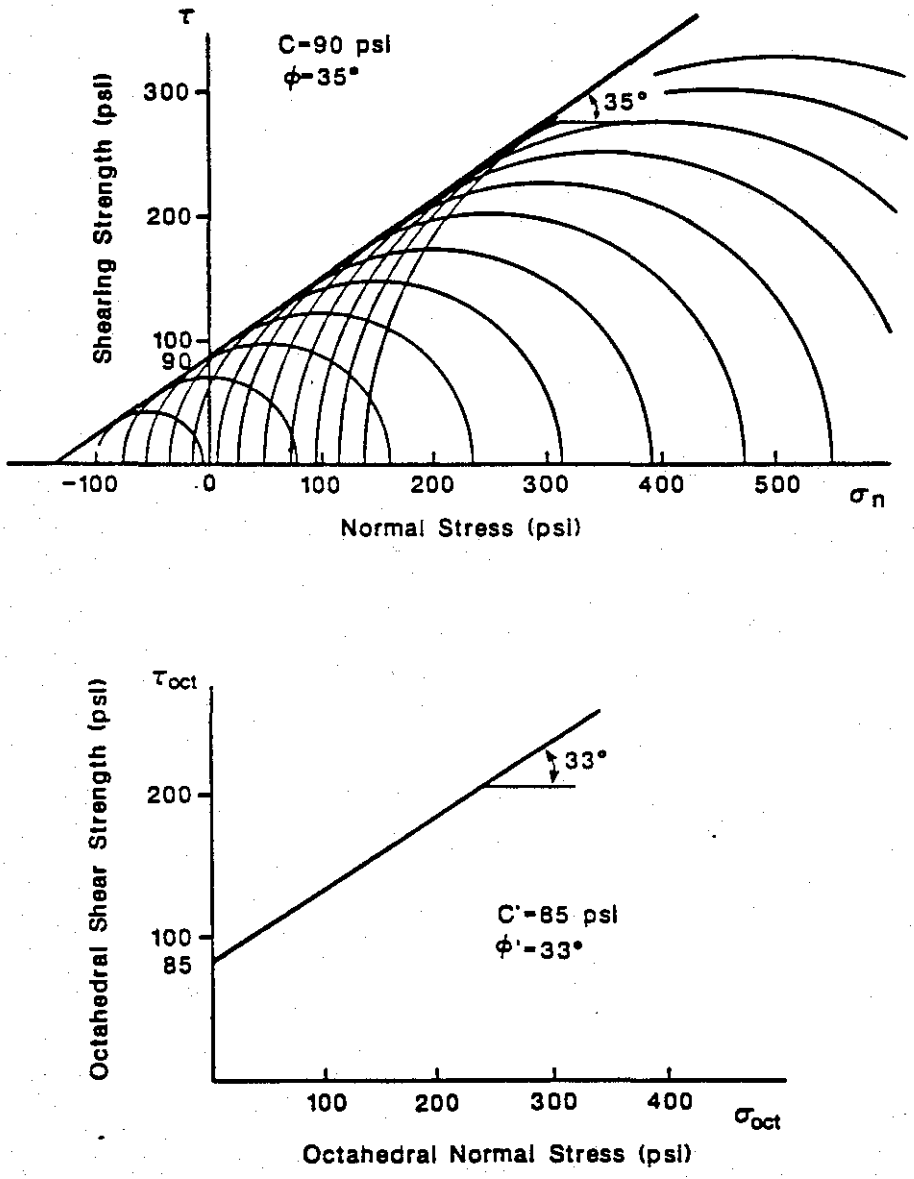

Figure 9.12. Typical octahedral failure envelope developed from Mohr-Coulomb failure envelope.

stress field in which material strength (stability) is sought. Hence, the above procedure provides a direct quantification and comprehensive evaluation of the overlay shearing strength in terms of loading and pavement conditions as well as material properties.

The octahedral shear stress ratio (OSR) is defined as the ratio of critical induced octahedral shear stress in the pavement layer to the octahedral shear stress of the material which causes failure as defined by Equation 9.11.

The sequence of computation of the octahedral shear stress ratio is as follows:

1. From the printout of the finite element ILLIPAVE computer model, determine the critical values of the normal and shear octahedral stresses, σ_{oct} and τ_{oct}, respectively. These stresses become critical (τ_{oct} is maximized) at a position within the ACP overlay that is a function of several pavement structural factors as discussed in Chapters VII and VIII. The level of and position of critical octahedral shear stress ratios are presented in Appendix C.
2. Determine the parameters c and ϕ from triaxial shear testing at the temperature and loading rate that best simulate field conditions (in this state, 104°F and a loading rate of 4-inches per minute). The resilient modulus as a function of temperature must also be determined for each mixture (Appendix D) so that the appropriate τ_{oct} contour curve can be selected from Appendix C.
3. Using the C and ϕ values determined in 2, determine σ_{1f} values concomitant with assumed σ_{3f} values using Equation 9.1.
4. From the values of σ_{1f} and σ_{3f} values in 3 (representing failure conditions) compute $\sigma_{oct(f)} = 1/3\ (\sigma_{1f} + 2\sigma_{3f})$ and $\tau_{oct(f)} = 0.471\ (\sigma_{1f} - \sigma_{3f})$. This yields the octahedral form of the Mohr-Coulomb failure equation, $\tau_{oct} = C' + \sigma_{oct_{(f)}} \tan \phi'$, where ϕ' and C' represent internal friction and cohesion parameters, respectively, commensurate with the octahedral form of the failure equation.
5. Using the octahedral failure equation developed in Step 4 and

the values of σ_{oct} from Step 1, determine the $\tau_{oct(f)}$ (representing failure).

6. The octahedral shear stress ratio (OSR) is thus, $\tau_{oct}/\tau_{oct(f)}$, where τ_{oct} is the maximum octahedral shear stress within the ACP overlay as determined by ILLIPAVE (see for example, Figure 6.3) and $\tau_{oct(f)}$ is the failure octahedral shear stress as computed from Step 5.

Mixture Variables Considered in Mohr-Coulomb Stability Analysis

Table 9.1 presents the mixtures evaluated by triaxial testing in this study. Included in Table 9.1 are air void and VMA's as well as Hveem and Marshall stabilities for the various mixtures which were tested.

A major objective of this study was to evaluate the influence of specific mixture variables on the stability of ACP mixtures placed over PCC bases. Specific attention was given to the following variables:

1. Aggregate grading (dense-graded, gap-graded, fine and coarse graded),
2. Aggregate type (rough-textured, crushed limestone mixtures, and smooth-textured river gravel mixtures),
3. Asphalt grade (AC-5 and AC-20),
4. Asphalt content,
5. Void and VMA content,
6. Use of field sand in lieu of limestone screenings for portions of the #10 sieve to #200 sieve size fraction,
7. The use of hydrated lime as a stabilizer (-#200 sieve size fraction), and
8. Novophalt (polyethylene modified AC-5) as a polymer-modified asphalt used to enhance stability.

Aggregate is the primary load-carrying medium in an asphalt concrete mixture. The proper selection and gradation of the aggregate is crucial in the production of hot-mix asphalt concrete. Therefore, a major improvement in mixtures can be achieved by careful design of aggregate grading.

When studying asphalt paving mixtures, the influence of a large number of factors, such as:

Table 9.1. Matrix of mixtures used in the stability study.

Aggregate	Asphalt Cement AC	Percent Binder P_β	Percent Air Voids A	Voids in Mineral Aggregate (VMA)	Texas Stability (%)	Marshall Stability (%)
Crushed Limestone (Lab-Stand)	AC-5	4	7.7	12.3	48	
		5 (4.6)*	4.0 (4.9)*	10.9	47 (42)	(600)**
		6	2.0	11.0	40	
	AC-20	4	7.3	11.6	52	
		5 (4.6)*	3.8 (4.9)*	11.2	55 (45)	(1300)**
		6	3.7	12.2	40	
Crushed Limestone (TD)	AC-5	4	6.5	10.6	41.	1952
		5	3.9	10.0	42	1975
		6	2.4	10.7	38	2106
	AC-20	4	6.3	10.6	41	2252
		5	3.6	10.0	40	2576
		6	2.4	10.8	36	2577
Crushed Limestone (TC)	AC-5	4	7.8	12.0	47	1950
		5	5.0	11.3	47	1818
		6	1.7	10.8	40	1890
	AC-20	4	6.6	11.2	50	2450
		5	3.7	11.1	45	2429
		6	2.1	11.1	41	2343
Crushed Limestone (GG)	AC-5	4	7.0	11.9	51	1808
		5	3.3	10.6	45	1665
		6	2.0	11.4	26	1344
	AC-20	4	6.3	11.6	52	2380
		5	3.9	11.2	49	2222
		6	2.4	11.4	28	1969

Table 9.1. Continued

Aggregate	Asphalt Cement AC	Percent Binder P_b	Percent Air Voids A_v	Voids in Mineral Aggregate (VMA)	Texas Stability (%)	Marshall Stability (%)
Crushed Limestone + Siliceous River Gravel (TC)	AC-5	4	6.6	12.9	40	1156
		5	3.9	12.3	42	1253
		6	2.2	12.7	37	1423
	AC-20	4	5.8	12.3	40	1163
		5	3.3	11.8	38	1276
		6	1.9	12.5	30	1432
Siliceous River Gravel (TD)	AC-20	4.25*	5.6	12.5	27	616
Siliceous River Gravel (TC)	AC-20	4.85*	4.3	11.4	27	1128
Siliceous River Gravel + 5% Lime (TC)	AC-20	4	5.2	7.6	23	825
		5	2.5	10.1	21	883
		6	2.0	11.6	17	894
		4.85*	2.6	13.4	25	909
Crushed Limestone + 15% FS.	AC-20	5	3.8	10.6	32	1460
Crushed Limestone + 25% FS.	AC-20	5	4.2	11.5	30	1250

Table 9.1. Continued

Aggregate	Asphalt Cement AC	Percent Binder P_b	Percent Air Voids A_v	Voids in Mineral Aggregate (VMA)	Texas Stability (%)	Marshall Stability (%)
Siliceous River Gravel (Lab stand)	AC-5	4	6.1	11.7	43	
		5	4.1	12.2	40	995**
		6	1.6	11.9	35	920**
	AC-20	4	4.4	11.5	47	
		5	3.0	11.0	40	1619**
		6	1.4	10.5	41	1397**
Siliceous River Gravel (Lab stand) with 5% Polyethylene Novophalt by Weight of AC	AC-20	5	4.5	12.5	50	2500**

* Specimens were fabricated at optimum binder content.
** Marshall compaction method 45 blows on each side of specimen.

1. Particle surface texture,
2. Particle size,
3. Particle shape,
4. Binder grade, and
5. Binder content,

does not allow accurate identification of the precise effect of aggregate grading on mixture performance.

The initial objective was to produce a mix that has maximum resistance to deformation, yet provides an adequate level of fatigue resistance. To maximize deformation resistance and at the same time, provide satisfactory voids in mineral aggregate (VMA), a modified version of the Fuller maximum density equation was used. This equation was developed by Cooper et al. (47). The classic Fuller equation could not be used as the range of "n" (slope of the curve) values in the equation results in an unrealistic filler contents as shown in Figure 9.13. The modified equation allows maintenance of the filler content at a predetermined level while enabling the equivalent fines contents to be varied by adjusting the value of "n". The equivalent fines content is defined as the percent passing a sieve having a size equal to 0.03 times the maximum particle size. The following relationship was used to develop the grading curves shown in Figure 9.14 (Texas Type D-TD and Texas Type C-TC):

$$P = \frac{(100 - F)(d^n - 0.075^n)}{D^n - 0.075^n)} + F \qquad (9.14)$$

where: P = percent passing a sieve of size (mm),
D = maximum aggregate size (mm), and
F = percent passing a 0.075 mm sieve.

The aggregate was divided into three fractions for use in the gradation manipulation. These fractions are defined as follows:

1. Coarse (retained on a #4 sieve),
2. Fine (passing a #4 sieve and retained on a #200 sieve), and
3. Filler (passing a #200 sieve).

Two aggregates were used: 1/2-inch (TC) and 3/4-inch (TD). A total of twelve gradations (six with 1/2-inch and six with 3/4-inch top size aggregate) with varying equivalent fines contents were prepared using the

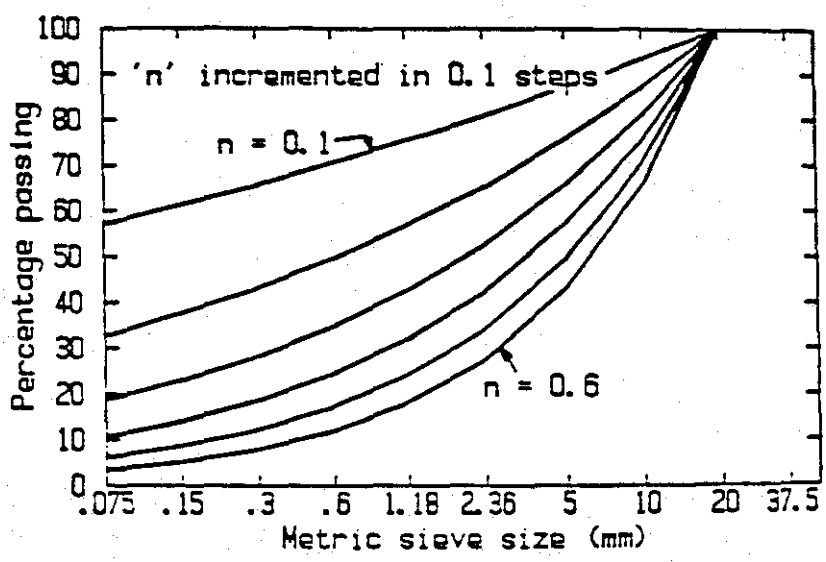

Figure 9.13. Grading curves resulting from the Fuller Relationship, $P = (d/D^n)$.

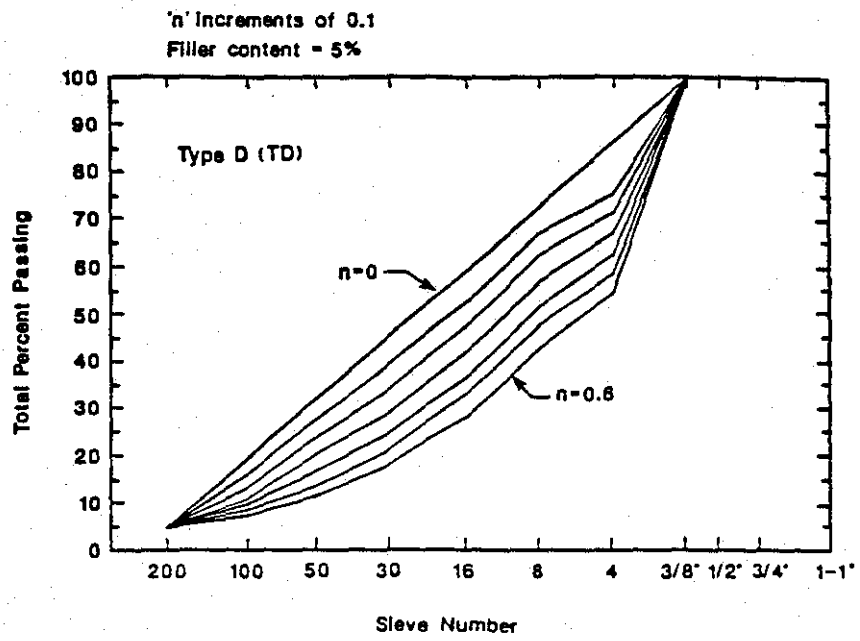

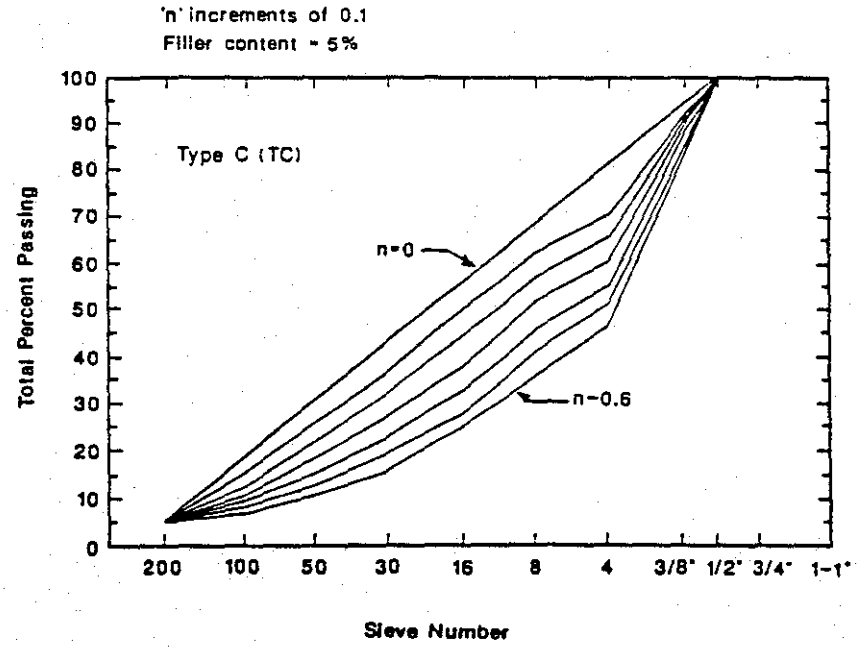

$$P = \frac{(100-F)(d^n-0.075^n)}{(D^n-0.075^n)} + F$$

Figure 9.14. Grading curves resulting from the modified Cooper et al. relationship.

modified Fuller relationship. Each gradation was then compacted without binder in a cylindrical mold mounted on a vibrating table. Volumetric proportions and bulk volumes of aggregate were measured in order to calculate VMA. Bituminous mixes using these twelve aggregate gradations were then compacted using the automatic Marshall drop hammer and the Texas gyratory compactors. Resilient moduli and Marshall and Hveem stabilities were measured on replicate specimens for each gradation. The gradation producing maximum stability and resilient modulus and satisfactory VMA as proposed by the Asphalt Institute was selected as the optimum gradation for further study. From these analyses, two aggregate gradings designated as TD and TC were selected as optimum. In addition to the grading curves discussed above, a standard laboratory grading curve (SD) (Figure 9.15a), which conforms to the Texas gradation specifications, was selected for further investigation as was a gap gradation curve designated as GG. Figure 9.16 summarizes the grading curves used in this study.

Results of Octahedral Shear Stress Ratio Analysis

Of course, an octahedral shear stress ratio (OSR) of one means failure or at least that the mixture is on the verge of failure. However, many questions arise as to the validity of assuming failure at OSR = 1.0. First of all, we have assumed a rate of loading and test temperature for the triaxial testing. These may not accurately mimic true field conditions. Second, an accumulation of permanent deformation may actually occur at OSR's less than, and perhaps substantially less than, 1.0. However, as to what the magnitude of the critical ratio is, at this point, we are not sure.

Thus, the OSR, at present, can only serve as a ratio to guide the user as to the relative criticality of the mixture in a certain structural condition. For example, when considering a selected mixture, the highest OSR for an array of structural conditions identifies the critical situation. On the other hand, for a selected pavement structural category, various mixtures can be compared as to adequacy based on the OSR.

Using the method for predicting the OSR as established in the section entitled, "Determination of Octahedral Shear Stress Ration" OSR's were developed for selected mixtures from Tables 9.1 and 9.2.

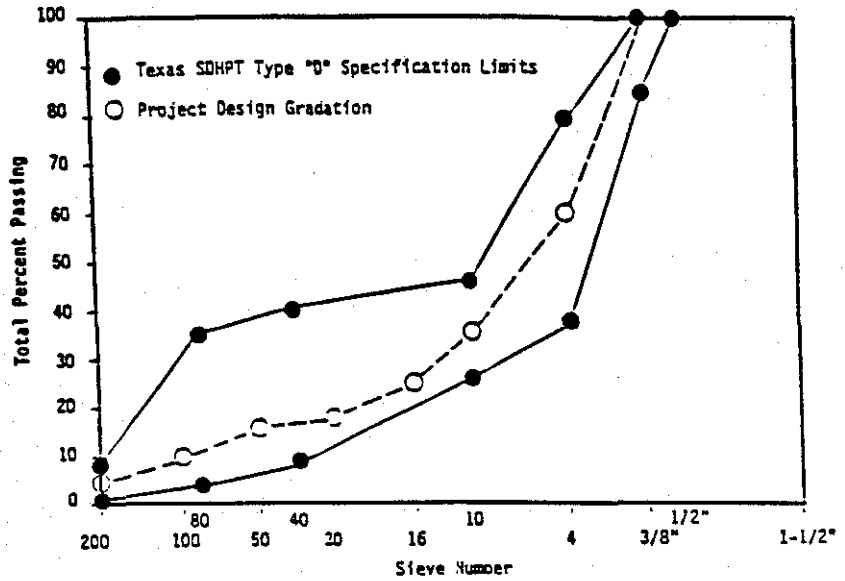

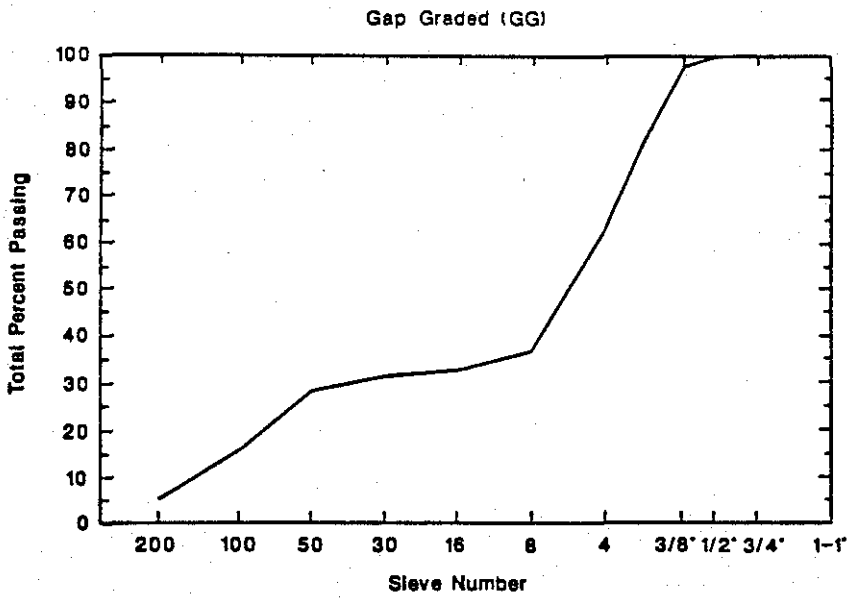

Figure 9.15. Texas SDHPT gradation band (a) and a typical gap grading curve (b).

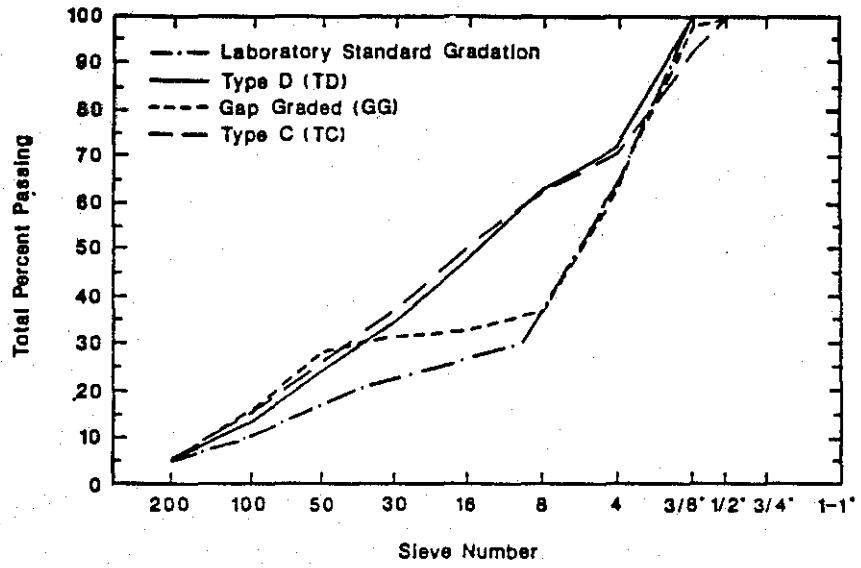

Figure 9.16. Project gradation curves.

Table 9.2 Mohr-Coulomb failure parameters, ϕ and C.

Aggregate	Asphalt Cement AC	Percent Binder P_b	Percent Air Voids A_v	Void In Mineral Aggregate (VMA)	Cohesion PSI (C)	Angle of Internal Friction ϕ
Crushed Limestone (TD)	AC-5	5	9.8	16.0	50	38.0
	AC-20	4	10.8	14.8	75	39.0
		5	8.4	14.6	70	31.5
		6	5.8	14.0	95	27.5
	AC-5	5	9.6	15.7	70	26.0
Crushed Limestone (TC)	AC-20	4	10.0	15.3	100	42.0
		5	10.5	17.2	80	34.0
		6	8.5	16.5	98	31.5
Crushed Limestone (Lab Stand)		4	5.9	10.0	90	26.0
		5	6.4	11.1	100	22.0
		6	4.9	11.3	95	23.5
Crushed Limestone (GG)	AC-5	4.75*	6.9	14.5	48	32.5
	AC-20	5.15	7.5	13.4	105	23.4
Crushed Limestone + 15% Field Sand (TC)	AC-20	5	5.9	12.2	85	28.4

Table 9.2. Continued

Aggregate	Asphalt Cement AC	Percent Binder P_b	Percent Air Voids A_v	Void In Mineral Aggregate (VMA)	Cohesion PSI (C)	Angle of Internal Friction ϕ
Crushed Limestone + River Gravel (TC)	AC-20	5.5*	1.8	12.8	75	27.0
River Gravel (TC)	AC-20	4.85*	5.3	10.5	45	32.0
River Gravel (TD)	AC-20	4.25*	6.3	11.5	55	25.0
River Gravel (TC) + 5% Lime	AC-20	4.85*	5.5	14.1	40	34.0
Siliceous River Gravel (Lab stand) with 5% Polyethylene Novophalt by Weight of AC	AC-5	5.0	4.5	12.5	110	40.0
Lab Stand. River Gravel	AC-5	6.0	1.6	11.9	35	25.0

Because many of the mixtures presented in Tables 9.1 and 9.2 are similar in terms of ϕ and C and resilient modulus properties, only eight mixtures were analyzed in this OSR analysis. These mixtures are:

1. Type D river gravel (AC-20, 4.25%, air voids = 6.3%, ϕ = 25°, C = 55 psi).
2. Lab standard crushed limestone (AC-20, 5%, air voids = 6.4%, ϕ = 22°, C = 100 psi).
3. Type C crushed limestone (AC-20, 4%, air voids = 10%, ϕ = 42°, C = 100 psi).
4. Type C crushed limestone (AC-20, 5%, air voids = 5.9%, ϕ = 28.4°, C = 85 psi).
5. Type D crushed limestone (AC-20, 5%, air voids = 8.4%, ϕ = 31.5°, C = 70 psi).
6. Type C crushed limestone (AC-20, 5%, air voids = 10.5%, ϕ = 34°, C = 80 psi).
7. Novophalt modified lab standard crushed limestone (AC-5, 5%, air voids = 5.0%, ϕ = 40°, C = 110 psi).
8. Type C crushed limestone with 25% field sand (AC-20, 5%, air voids = 4.2%, ϕ = 22°, C = 70 psi).
9. Lab standard river gravel (AC-20, 6%, air voids = 1.6%, ϕ = 25°, C = 35 psi).

Table 9.3 through 9.11 presents the OSR relationships for these mixtures when the ACP is supported both on rigid and flexible bases.

A review of the results summarized in Tables 9.3 through 9.11 reveal the following interpretations:

1. The OSR is an excellent tool for evaluating the relative potential of asphalt mixtures to deform due to the development of shear stresses when the ACP is supported by a rigid PCC base ($E_1/E_2 < 1.0$). This is because the ACP stress conditions (τ_{oct} are always compressive and thus, the OSR works in a predictable manner as a function of ACP thickness as discussed in Chapters VII and VIII.
2. Due to the negative stresses, parameters (τ_{oct} and υ_{oct}) that can be developed when $E_2 \ll E_1$, as is the case in ACP over flexible granular bases, the trend in OSR as a function of

Table 9.3. Octahedral shear stress ratios for the type D river gravel mixture (mixture no. 1)

ACP Thickness in.	Slip Condition		Full Bond	
	No Surface Shear	Surface Shear	No Surface Shear	Surface Shear
Rigid PCC Base				
2	0.55	0.79	0.30	0.45
4	0.64	1.10	0.34	0.61
6	0.63	0.81	0.40	0.71
8	0.49	0.76	0.39	0.71
Flexible Base				
2	0.97	1.43	0.45	0.53
4	3.14	3.10	0.46	0.81
6	1.44	2.38	0.51	0.58
8	1.06	1.50	0.36	0.58

Table 9.4. Octahedral shear stress ratios for the crushed limestone lab standard mixture (mixture no. 2)

ACP Thickness in.	Slip Condition		Full Bond	
	No Surface Shear	Surface Shear	No Surface Shear	Surface Shear
Rigid PCC Base				
2	0.37	0.54	0.18	.028
4	0.43	0.73	0.21	0.39
6	0.42	0.53	0.25	0.45
8	0.32	0.48	0.26	0.45
Flexible Base				
2	0.65	0.94	0.31	0.37
4	2.18	2.08	0.30	0.56
6	0.97	1.01	0.25	0.40
8	1.06	1.50	0.36	0.38

Table 9.5. Octahedral shear stress ratios for the type C crushed limestone mixture (mixture no. 3)

ACP Thickness in.	Slip Condition		Full Bond	
	No Surface Shear	Surface Shear	No Surface Shear	Surface Shear
Rigid PCC Base				
2	1.35	0.50	0.17	0.25
4	0.42	0.69	0.20	0.36
6	0.41	0.50	0.24	0.42
8	0.30	0.45	0.25	0.42
Flexible Base				
2	0.63	0.84	0.28	0.32
4	4.70	2.50	0.30	0.51
6	1.13	2.04	0.34	0.36
8	0.80	1.20	0.23	0.35

Table 9.6. Octahedral shear stress ratios for the type C crushed limestone mixture (mixture no. 4)

ACP Thickness in.	Slip Condition		Full Bond	
	No Surface Shear	Surface Shear	No Surface Shear	Surface Shear
Rigid PCC Base				
2	0.41	0.63	0.20	0.32
4	0.48	0.64	0.24	0.46
6	0.47	0.61	0.28	0.52
8	0.36	0.55	0.30	0.52
Flexible Base				
2	0.71	1.07	0.34	0.43
4	1.96	2.13	0.34	0.62
6	1.00	1.62	0.34	0.46
8	0.74	1.03	0.27	0.46

Table 9.7. Octahedral shear stress ratios for the type D crushed limestone mixture (mixture no. 5).

ACP Thickness in.	Slip Condition		Full Bond	
	No Surface Shear	Surface Shear	No Surface Shear	Surface Shear
Rigid PCC Base				
2	0.46	0.66	0.22	0.34
4	0.55	0.92	0.27	0.48
6	0.55	0.66	0.31	0.56
8	0.41	0.60	0.33	0.56
Flexible Base				
2	0.63	0.94	0.41	0.58
4	0.71	0.94	0.38	0.62
6	0.62	0.78	0.40	0.60
8	0.51	0.61	0.32	0.59

Table 9.8. Octahedral shear stress ratios for the type C crushed limestone mixture (mixture no. 6)

ACP Thickness in.	Slip Condition		Full Bond	
	No Surface Shear	Surface Shear	No Surface Shear	Surface Shear
Rigid PCC Base				
2	0.42	0.62	0.20	0.30
4	0.50	0.90	0.22	0.40
6	0.50	0.60	0.29	0.50
8	0.40	0.52	0.30	0.50
Flexible Base				
2	1.50	3.10	0.40	0.30
4	3.50	7.00	0.70	1.28
6	2.70	8.20	0.80	0.25
8	1.50	0.80	0.65	0.20

Table 9.9. Octahedral shear stress ratios for the Novophalt modified lab standard crushed limestone mixture - AC-5 (mixture no. 7)

ACP Thickness in.	Slip Condition		Full Bond	
	No Surface Shear	Surface Shear	No Surface Shear	Surface Shear
Rigid PCC Base				
2	0.19	0.31	0.11	0.18
4	0.22	0.40	0.11	0.24
6	0.20	0.30	0.14	0.27
8	0.16	0.29	0.14	0.26
Flexible Base				
2	0.30	0.84	0.15	0.21
4	0.55	0.76	0.14	0.27
6	0.36	0.39		0.22
8	0.27	0.26	0.12	0.22

Table 9.10. Octahedral shear stress ratios for the type C crushed limestone with 25 percent field sand (mixture no. 8)

ACP Thickness in.	Slip Condition		Full Bond	
	No Surface Shear	Surface Shear	No Surface Shear	Surface Shear
Rigid PCC Base				
2	0.48	0.77	0.27	0.44
4	0.56	1.02	0.31	0.60
6	0.53	0.76	0.35	0.67
8	0.42	0.72	0.35	0.66
Flexible Base				
2	0.80	1.26	0.40	0.51
4	1.75	2.19	0.38	0.71
6	0.71	1.63	0.37	0.55
8	0.54	1.06	0.31	0.54

Table 9.11. Octahedral shear stress ratios for laboratory standard (low void - 1.6%) river gravel mixture (mixture no. 9).

ACP Thickness in.	Slip Condition		Full Bond	
	No Surface Shear	Surface Shear	No Surface Shear	Surface Shear
Rigid PCC Base				
2	0.71	0.83	0.39	0.46
4	0.87	1.33	0.42	0.64
6	0.90	0.93	0.51	0.78
8	0.66	0.92	0.52	0.78
Flexible Base				
2	1.53	1.60	0.59	0.57
4	----	38.0	0.66	1.09
6	8.79	----	0.70	0.65
8	5.30	22.5	0.51	0.64

overlay thickness is not as predictable as in the case of a PCC (rigid) base. This will be discussed later.

3. In the case of ACP over a rigid PCC base, the mixtures representing the greatest resistance to deformation are ranked in order of greater resistance to deformation as follows:

Mix I.D.	Mixture Type
7	Novophalt modified lab standard limestone (AC-5, 5%, 5% air voids, ϕ = 40°, C = 110 psi).
3	Type C (AC-20, 4%, 10% air voids, ϕ = 42°, C = 100 psi).
2	Lab standard limestone (AC-20, 5%, 6.4% air voids, ϕ = 22°, C = 100 psi).
6	Type C limestone (AC-20, 5%, 10.5% air voids, ϕ = 34°, C = 80 psi).
4	Type C limestone (AC-20, 5%, 5.9% air voids, ϕ = 28.4°, C = 85 psi).
5	Type D limestone (AC-20, 5%, 8.4% air voids, ϕ = 31.5°, C = 70 psi).
8	Type C limestone with 25% field sand (AC-20, 5%, 4.2% air voids, ϕ = 22°, C = 70 psi).
1	Type D river gravel (AC-20, 4.25%, 6.3% air voids, ϕ = 25°, C = 55 psi).
9	Lab standard river gravel (AC-20, 6%, 1.6% air voids, ϕ = 25°, C = 35 psi).

These results indicate that the most important factors influencing resistance to shearing-induced deformation at the stress levels induced in ACP over PCC are a relatively high cohesive intercept. The angle of internal friction is of significant importance only when C is relatively low as is the case for the over-compacted (very low air void) river gravel mixture (mixture No. 9).

4. For ACP overlays over granular bases, the same relative order of mixtures relative to deformation resistance is only slightly different. However, the influence of pavement thickness, with respect to the octahedral stress distributions discussed in Chapter VII, is complicated greatly by the tensile octahedral stress states which may occur when $E_1/E_2 >> 1$ for the granular base cases but not for the PCC base cases.

The relative ordering of mixtures in descending order of deformation resistance is:

a. Mixture No. 7,
b. Mixture No. 6,
c. Mixture No. 3,
d. Mixture No. 2,
e. Mixture No. 4,
f. Mixture No. 8,
g. Mixture No. 1,
h. Mixture No. 5, and
i. Mixture No. 9.

Important Supplementary Considerations

The OSR is an excellent tool by which to evaluate the permanent deformation potential in ACP overlays over PCC (rigid) bases. In fact, the procedure can be employed, in general, whenever the ratio of stiffnesses of the ACP overlay and the supporting layer does not exceed 1.0 ($E_1/E_2 \leq 1.0$).

The OSR can thus be effectively used to determine critical conditions leading to potential cases of shear deformation in ACP over PCC, old ACP and bituminous-stabilized as well as (potentially) portland cement and lime-flyash-stabilized bases. The procedure may also be used to evaluate the deformation potential of various mixtures to be used in specific structural pavement types.

When using the OSR procedure for ACP over unbound, granular bases, the procedure is not as clear-cut because of the tensile octahedral stress states that may exist in the granular layers. Evaluation as to the extent to which these conditions may actually occur in granular bases, which cannot withstand tensile stresses without undergoing substantial reorientation, requires more detailed analytical and in situ evaluation.

For now, this procedure should be limited to ACP deformation evaluation when the pavement stiffness ratios between ACP surface and supporting bases (E_1/E_2) do not exceed or only slightly exceed 1.0 (less than 1.25).

In the case of ACP over PCC base, the general trend revealed by the OSR values in Tables 9.3 through 9.11 are that:

1. When full frictional bonding is developed between ACP surface and PCC base, the thicker overlays are more susceptible to rutting regardless of the mixture type up to a thickness of about 6 inches. At this point, the trend appears to reverse to lower OSR with thickness (greater than 8 inches).
2. When slippage between surface and base occurs, the critical thickness is (as discussed in Chapter VII) about 4 inches.
3. Although there is an interaction between C and ϕ which affects the stability of the mixture, the cohesion parameter is the most important. Based on the testing procedure adopted here, good mixtures have C-values greater than about 70 psi.
4. The critical value of OSR must certainly be less than 1.0 in order for rutting to be of no concern. However, at this point, the value is unknown as can only be determined by extensive field and laboratory investigation and testing. Presently, the OSR magnitude can only be compared in order to evaluate relative performance potential.
5. Although this procedure cannot be used to predict the magnitude of long-term rutting as can the modified ILLIPAVE model, the Shell model or the mechano-lattice model, the use of octahedral shear stress failure theory is reasonable and offers a viable supplementary approach.

CHAPTER X

GRADUAL ACCUMULATION OF PERMANENT DEFORMATION VIA CREEP TESTING AND CYCLIC PERMANENT DEFORMATION TESTING

Background

Every physical body subjected to the action of external loading will, in addition to translation and/or rotation, undergo a deformation. Such a geometric change, which is due to either a change in volume and/or particle orientation, continues indefinitely under the influence of a constant external load or stress. This continuous, time-dependent deformation under constant stress is called creep (48). The amount of deformation that any particular material will undergo is a function of three parameters:

1. Stress level,
2. Time of loading, and
3. Temperature.

During the past decade, researchers (28,49,50,51) have approximated asphalt concrete behavior under sustained loading as if it behaves linearly viscoelastically. The static creep test is considered to be a major tool for material characterization of asphalt concrete and the study the time-dependent, viscous and plastic characteristics of asphaltic concrete mixtures.

At high temperatures and/or long durations of loading, the viscous component of stiffness is predominant. This is the irreversible component that results in permanent deformation. At low temperatures and/or rapid loading rates, the elastic component of stiffness predominates. The elastic component is immediately recoverable upon the load removal. The viscoelastic component deforms with time and its recovery is complete, but is time-dependent. Thus, only the viscous portion is irrecoverable, and leads to permanent deformation. A plastic and viscoplastic component may also be identified. Plastic deformation is also irrecoverable and generally relates to an immediate collapse in the void structure. Viscoplastic deformation is a viscosity-dependent densification. This

fact can be used with respect to creep test data to predict the magnitude of permanent deformation expected for various mixtures. The irreversible deformation can be determined by subtracting the reversible deformation (recovered strain measured upon the load release) from the total deformation measured during the loading time. This procedure is permissible since the reversible deformation is approximately independent of the total cumulative strains preceding the loading time (48).

Permanent Deformation Prediction

Methods of predicting the gradual accumulation of permanent deformation of the asphalt paving mixtures range from the simplified procedure developed by Shell researchers (52,53,54,55) to the complex mechano-lattice computer model developed by Yandell (56,57,58,59,60). However, in this study, the modified ILLIPAVE method and the modified Shell methods were used to predict gradual accumulation of permanent deformation, while considering the variations in traffic and temperature together with variations in material properties. These methods provide a logical prediction of rut-depth for any locality within the state of Texas as discussed in previous sections of this report.

Specific Mixture Variables

One of the objectives of this investigation is to study the influence of mixture-specific variables (i.e., asphalt content, air voids, VMA, etc.) on the long-term deformation characteristics of hot-mix asphalt concrete (ACP) produced from crushed limestone and well-rounded, siliceous, gravel materials.

Specific consideration was given to the following:

1. Aggregate grading,
2. Aggregate type,
3. Asphalt grade,
4. Asphalt content,
5. Field sand as a substitute for crushed fines,
6. Fillers (hydrated lime), and
7. Air voids, and
8. Modifiers.

The first step in developing a mix design is to select aggregates that can be combined to meet the specification limits. Gradation bands, as discussed in Chapter VIII, were used as a guide as to where to start in the aggregate selection process. It is important to properly select the aggregate grading to ensure adequate mixture stability under design loads. Generally, the objective is to produce a blend of aggregate so proportioned that it will compact to form a dense, interlocked structure.

Results of Cumulative Deformation Analysis

Plots of data from repeated load and cyclic permanent deformation testing performed in accordance with the VESYS Manual (26) are presented in Appendix D. Also in Appendix D are plots of data from static creep tests performed in accordance with the modified Shell procedure (48). The modified Shell procedure provides a prediction of viscoplastic strain, ϵv_p, as a function of time. Viscoplastic strain is defined as total strain less the recoverable strain (viscoelastic strain and elastic). The values of viscoplastic strain are determined from a static creep and recovery test. Also, a part of Appendix D is plots of resilient modulus versus temperature for the mixtures analyzed.

Table 10.1 lists the important properties of the mixtures tested in this study including:

1. Asphalt grade,
2. Asphalt content,
3. Aggregate type,
4. Aggregate gradation and top size characteristics,
5. VMA,
6. Air void content,
7. C and ϕ parameters,
8. Creep test parameters (slope, ϵ_{vp} at 10^4 sec),
9. Cyclic deformation parameters (slope, ϵ_{vp} at 10^4 load applications),
10. Permanent deformation from the ILLIPAVE program after 100,000 loading cycles for the traffic and environmental conditions explained in Table 10.2.

Table 10.1. Summary of cumulative deformation analysis for selected mixtures.

Mixture Description	Percent Air Voids	Percent VMA	C and ϕ Parameters psi &	Creep Slope	Test Parameters ϵ_{vp} @ 10^4 sec	Cyclic Slope	Test Parameters ϵ_{vp} @ 10^4 sec	Permanent Deformation (in.) from ILLI-PAVE @ 100,000 cycles	
								Rigid Base	Flexible Base
Crushed limestone (TD) AC-20 w/5% binder	8.4	14.6	70 & 31.5	.09	350	.17	483	.145	.34
Crushed limestone (TC) AC-20 w/5% binder	10.5	17.2	80 & 34	.10	826.41	.16	772	.152	.34
Crushed limestone (TD) AC-5 w/5% binder	9.8	16.0	50 & 38	.05 .02	223 766	--- ---	--- ---	.160	.36
Crushed limestone (TC) AC-5 w/5% binder	9.6	15.7	70 & 26	.04	810	---	---	.160	.36
Crushed limestone (GG) AC-20 w/5-15% binder	7.5	13.4	108 & 34	.19	266	.11	1450	.150	.34
Crushed limestone (TC) +15% FS AC-20 w/5% binder	5.9	12.2	85 & 28.5	.13	510	.25	910	.150	.35
Siliceous river gravel (TD) AC-20 w/5% binder	5.5	14.1	40 & 34	.23	1100	.31	621	.160	.34

Table 10.2. Temperature regions used to simulate the climatic region associated with Dallas, Texas. (Associated with the temperature regions for the 180 hottest days is the distrubtion of traffic within this period.)

Seasonal Change	Temperature °F	Percent Traffic	Percent Time	Length of Time, Months
1	70	15.4	20.7	1.2
2	80	13.3	14.5	0.9
3	90	16.6	15.0	0.9
4	100	23.5	20.0	1.3
5	110	26.3	25.1	1.5
6	120	4.9	3.7	0.2

An analysis of the results of Table 10.1 yields the following conclusions:

1. Gap-graded mixtures deform at a relatively faster rate than other mixtures studied of the same aggregate type. The slope of the gap-graded permanent deformation curve (both cyclic and static) is significantly steeper than for other mixtures with similar aggregate types. This was verified by the triaxial analysis where the gap-graded mixture exhibited a lower shear strength.
2. Mixtures made with crushed limestone aggregates are generally less susceptible to permanent deformation than are similar mixtures made with siliceous river gravel aggregate. This was verified in the triaxial analysis as discussed in Chapter IX. The static creep tests demonstrated that the rate of deformation of all river gravel mixtures (the slope of the creep versus time curve) are significantly higher than for all limestone mixtures).
3. Mixtures were tested for creep and cyclic deformation properties at 104°F and 77°F and at an applied shear stress level of 14.5 psi as directed by the Shell procedure (48). River gravel mixtures could not be tested at 104°F due to their instability; all river gravel mixture testing was performed at 77°F.
4. Replacement of the siliceous mineral filler in the river gravel mixture with crushed limestone fines did not result in detectable differences based on creep and cyclic load deformation testing. However, the triaxial test results demonstrated both a higher cohesion and a higher frictional component when the crushed limestone fines were substituted for the siliceous filler.
5. When a Type C crushed limestone was altered by replacement of the #4 sieve to #200 sieve fraction with siliceous river gravel, the triaxial stability decreased dramatically as did the potential to resist deformation. Creep testing of these mixtures could not be performed above 77°F due to instability. This trend was verified by triaxial testing where C and ϕ parameters were substantially reduced by the replacement in Type

C limestone mixtures. Part of this could be due to the low air void content in the limestone plus river gravel mixtures induced due to the lower resistance of this mixture to densification.

6. When crushed limestone (Type C) mixtures were altered by replacing part of the pure limestone aggregate with 15% field sand, the triaxial stability of the mixtures was substantially reduced. Cyclic deformation testing and creep testing demonstrated an increased rate of deformation for the mixtures with field sand as compared to the pure limestone mixtures. However, although the deformation rates from cyclic deformation testing and static creep testing were greater for the Type C limestone mixture with field sand, a lower initial plastic deformation was recorded for this mixture. This can be attributed to lower air voids in the field sand mixture (air void content of 5.9 percent and VMA of 12 percent). Identical mixtures of Type C crushed limestone without the field sand possessed air void content of 10.5 percent and VMA of 17 percent.
7. Cyclic or repeated load creep testing predicted similar deformation levels in the mixtures tested.
8. Static creep and recovery testing is sensitive to the air void content of the mixture. The initial level of deformation is directly related to the initial void content whereas the slope of the relationship is more highly sensitive to aggregate surface texture, type of mineral filler and angularity of the fine aggregate (aggregate between #4 sieve and #200 sieve) fraction.
9. Low and high air voids mixtures were also included in the experimental matrix. In general, the presence of air voids in the asphalt concrete reduces the effective cross-section of the stressed area. Voids also act as a stress riser which has an adverse influence on the mixture strength. The magnitude of the induced stress is dependent upon the size and the shape of the void (60). With respect to rutting, post construction studies (61) on a number of job sites have shown that all paving mixtures with essentially 4 percent air voids have performed satisfactorily and mixtures with air voids content of about 2

percent or less demonstrated inadequate stability. A limited study by the Army Corp of Engineers (62) also indicates that as long as the amount of air voids in the asphalt mixture is 7 percent or less, the asphalt mixture is essentially waterproof. Therefore, it can be concluded that in asphalt paving mixtures, a minimum air voids content (about 2 to 3 percent) is necessary to maintain desirable stability, while a high air voids content, leading to permeable mixtures (about 7 percent air voids), may result in durability problems.

10. Examination of creep/recovery plots show that high air void mixtures essentially deform at a faster rate and are more susceptible to rutting than are low air void mixtures. The initial deformation is less in the low air void mixtures. Hveem and Marshall stability of the mixtures with higher air voids (8.5 to 13.7 percent) are shown in Table 9.1. Triaxial test results showed no substantial changes in the mixture properties with regard to the air voids content.
11. Mixtures with low VMA will exhibit greater resistance to deformation than mixtures with high VMA. Also lower air voids content mixtures do not experience as much initial consolidation under load as mixtures with higher air voids contents. This is the reason for the better initial performance displayed under load by the mixture containing 15 percent field sand.
12. Polymer modification of asphalt has demonstrated the ability to provide deformation resistant mixtures. For an example, see the results of the triaxial testing of the Novophalt-modified river gravel mixture (Tables 9.1-9.2). Repeated load permanent deformation testing on a lab standard river gravel mixture modified with Novophalt presented a marked improvement in deformation resistance.

Prediction of Permanent Deformation

For a selected mixture composition, the three parameters ρ, β, and ϵ_o were determined. The modified ILLIPAVE was utilized to estimate the rut depth for the ACP overlay placed on PCC base as well as stress sensitive granular base material in different localities within the State of Texas.

The traffic and temperature profile tables used in the analysis are presented in Table 10.2. Actually, temperature profiles from all of the four climatic regions of Texas were evaluated. The results showed no significant differences among them. Thus, the Dallas profile (Table 10.2) was the only profile selected for this analysis. These profiles were obtained from report 2452-1 (23).

Table 10.1 is a summary of the predicted rutting from ILLIPAVE. Although the ϕ, C, and creep properties were substantially different for the mixtures evaluated, the predicted rutting was not substantially different following 100,000, 18,000-pound, single axle load applications. The authors were disappointed in the sensitivity of the modified ILLIPAVE model to these substantially different materials. However, the authors were delighted with the potential demonstrated by the OSR concept to evaluate mixtures susceptible to deformation.

CHAPTER XI

SUPPORTING RESEARCH

Additional Testing for Deformation Potential

It has been well-established that the surface texture and angularity of the sand-size fraction, smaller than #10 sieve size, has a significant influence on the resistance to deformation of an asphalt concrete mixture. To test the influence of this sand-size fraction, three mixtures were evaluated. The gradation of each mixture met Type D (Item 340) specifications, and the coarse aggregate (larger than #10 sieve size) was composed of crushed limestone aggregate. The fine fraction (smaller then #10 sieve) was composed of either:

1. Natural field sand (100%),
2. Manufactured (crushed) sand (100%), or
3. 50-50 blend of natural sand and manufactured sand.

Asphalt concrete samples were prepared with these aggregates using AC-20 Texaco asphalt (5.5% percent by weight). Mixtures were prepared at low (3-5 percent) and high (5-7 percent) air voids. Two replicates for each test were prepared.

Four tests will be performed on these asphalt mixtures: indirect tensile tests, long-term static creep, long-term dynamic or cyclic permanent deformation testing, and unconfined compression tests. The long-term static and dynamic tests were selected because the results of relatively short-term creep and cyclic permanent deformation testing in this study were not deemed satisfactory in terms of their ability to distinguish among the deformation potential of the various mixtures evaluated. On the other hand, the triaxial testing quite satisfactorily distinguished among the deformation potentials of the various mixtures.

Indirect tension and unconfined compression testing of the six mixtures will be performed in order to determine if these quick and relatively simple tests can be used to establish the Mohr-Coulomb failure envelopes in lieu of more complex confined triaxial testing. These data will also supplement research Project 1170, "Verification of Improved Asphalt Concrete Mixture Design Procedure."

At the time of this report, only long-term static creep testing had been completed. The results of further testing will be reported in interim and final reports for Project 1121, "Investigation of Rutting and Asphalt Concrete Pavements."

Figures 11.1 and 11.2 present the results of long-term static creep testing at an applied pressure of 60 psi on the six mixtures (three different blends x two void levels per blend). These figures illustrate the dramatic difference in deformation potential among the various mixtures.

The authors believe that a long-term static creep or long-term dynamic test may be necessary to differentiate among the rutting potential of various mixtures. In addition, it is believed that these tests should be performed at various stress levels in lieu of only one.

The constant stress level applied to the mixtures on long-term creep testing was 60 psi. This is approximately four times higher than the stress level allowed in VESYS or the Shell method deformation testing. However, the objective of these tests were that they be run until failure and not to predict a level of deformation as a function of applied traffic. The same tests will be performed under lower stress levels as prescribed by VESYS and Shell methodologies.

At the high stress level (60 psi, which is far outside the linear viscoelastic region) used to obtain the data presented in Figures 11.1 and 11.2, it is not possible to predict deformation in actual pavement conditions. However, the results provide substantial insight into the deformation potential of the mixtures tested:

1. Void content has a great influence, especially on the most stable mixture (100 percent crushed sand).
2. The larger percentage of crushed, angular fines produces a substantially more stable mixture.
3. The results of the complete 1121 study will yield considerable insight into the most suitable tests to evaluate deformation potential. Specifically, the study will evaluate long-term creep and long-term cyclic deformation tests as well as the ability of indirect tensile strength and unconfined compression tests to predict Mohr-Coulomb failure envelopes, which appear to

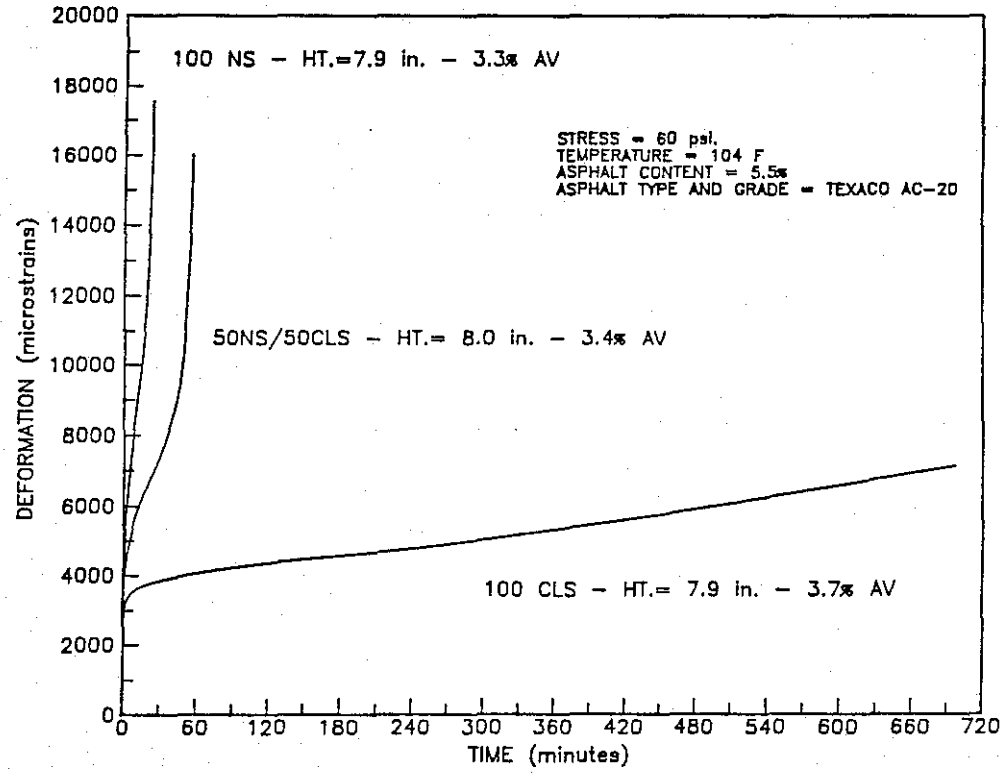

Figure 11.1. Long-term static creep testing (low air void content) for selected mixtures.

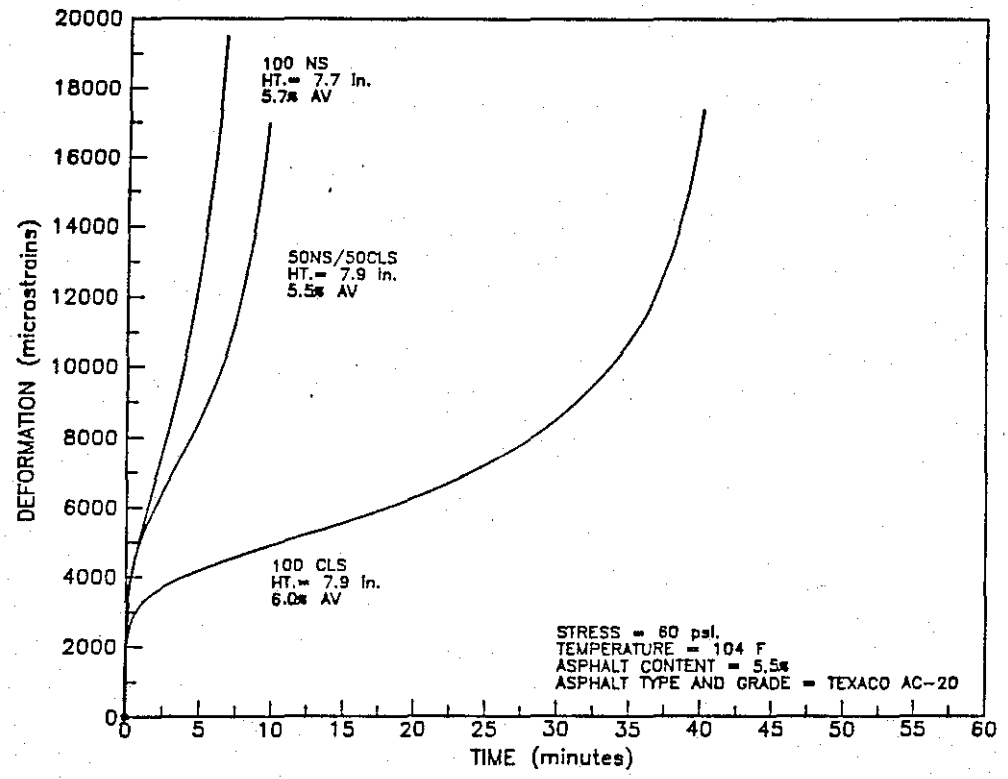

Figure 11.2. Long-term static creep testing (high air void content) for selected mixtures.

be a satisfactory means by which to evaluate deformation potential.

Field Verification

Close coordination between Research Project 2452 and Project 1121, "Investigation of Rutting om Asphalt Concrete Pavements," has provided the ability to evaluate the rutting potential of four in situ ACP over PCC pavements. Tables 11.1 through 11.4 present a detailed summary of the pavements evaluated and the cores retrieved from these pavements (recovered asphalt properties, mixture properties, and aggregate properties).

From the data in Tables 11.1 through 11.4, an approximation of the OSR was made using the following procedures:

1. τ_{oct} (maximum induced) was calculated from the octahedral shear stress contours from Appendix C for the structural and M_R vs. temperature conditions most closely matching the data for the respective mixtures presented in Tables 11.1 and 11.4.
2. The ϕ' and C′ parameters were approximated based on the testing results in Chapter IX and the mixture, asphalt, and aggregate properties discussed in Tables 11.1 through 11.4.
3. The τ_{oct} strength was estimated as discussed in Chapter IX.
4. The OSR was established as:

$$OSR = \frac{\tau_{oct} \text{ (max. induced)}}{\tau_{oct} \text{ (strength)}}$$

Since the field pavements evaluated were significantly rutted, the computed OSR is a link between field performance and the ability to predict rutting potential from the OSR value.

The OSR value for the pavements evaluated are as follows:

Pavement	OSR Value	Measured Rut Depth, in.
US-59 - Lufkin	0.61	0.75
IH-20 - Tyler	0.60	0.73
IH-45 - Centerville	0.60	0.55
IH-45 - Fairfield	0.53	0.52

Table 11.1. Data for asphalts extracted from pavement cores.

General Information	Location					
	Sweetwater	Fairfield	Centerville	Tyler	Lufkin	Dumas
District No.	8	17	17	10	11	4
County	Nolan	Freestone	Freestone	Gregg	Angelina	Sherman
Highway No.	IH-20	IH-45	IH-45	IH-20	US-59	US-287
Control-Section No.	6-3-84	675-2-18		495-6	176-3-81	---
No. Lanes each Direction	2	2	2	2	2	---
Description of Pavment						
Existing Pavement						
Layer 1	1.5″ Ty D	0.75″ Ty D	3.75″ Ty D	1.5″ Ty D	2″ Ty B	3″ Ty D
Layer 2	1″ Ty D	3.75″ Ty C	4.50″ Ty C*	2″ Ty B	Surf. trt.	---
Layer 3	8 1/2″ Recycle	Asph. Rub.	Asph. Rub.	Asph. Rub.	Fabric	Conc. Pvt.
Layer 4	Lime Trt. Base	8″ CRCP	8″ CRCP	8″ CRCP	8″ CRCP	---
Date of Last Constr.	Sept. '84	Sept. '85	Oct. '85	July '81	Nov. '85	July '85
Date Cored	Mar. '87	April '87	April '87	Sept. '87	Dec. '87	Nov. '86
Rut Depth, in. (Site 1)	0.72	0.22	0.55	0.73	0.75	0.41
Rut Depth, in. (Site 2)	0.21	0.52	0.16	----	----	----

Table 11.2. Data for asphalts extracted from pavement cores.

Location:	Sweetwater		Fairfield		Centerville		Tyler		Lufkin	Dumas
Site No.:	1	2	1	2	1	2	Base[1]	Surface[1]	1	1
Rut Depth[2], in.	0.72	0.21	0.22	0.52	0.55	0.16	--	0.73	0.75	0.41
Penetration										
77°F,100 gm,5 sec.	37	36	27	44	27	36	32	72	56	65
39.2°F,200 gm,60 sec.	10	11	13	15	5	3	--	--	21	19
Viscosity, poise										
140°	2230	2330	10,710	5170	6150	4210	4700	2520	4170	1800
275°	3.20	3.30	5.63	3.61	5.05	4.26	5.19	--	4.90	5.39
Asphalt Content, %	5.3	4.6	5.3	4.7	5.6	5.0	5.0	8.7	9.5	7.0
Des. A.C.									8.5	

[1] Mixtures from same location: Type B base and Type D surface mixes.

[2] Average of about 10 measurements where cores were drilled.

Table 11.3 Summary of mixture properties of asphalt surface layers used over PCC pavements.

Pavement Location	ACP Layer Description	% Asphalt (Source)	% Air Voids	% VMA	Rut Depth
Lufkin	3″ Type D mix	8.5	3.45	16.0*	0.75
Fairfield	3.75″ Type C mix (Base)				
Site 1 (unrutted)		5.3 } AC-20 Wright	8.40	18.9	0.22
Site 2 (rutted)		4.7 } AC-20 Wright	4.80	15.2	0.52
		$\bar{x}$ = 5%			
Centerville	4.5″ Type C mix (Base)				
Site 1 (unrutted)		5.6 } Exxon AC-20	2.2	16.07	0.55
Site 2 (rutted)		5.0 } Exxon AC-20	1.0	14.54	0.16
		$\bar{x}$ = 5.3%			
Tyler					
Surface	1.5″ Type D mix	8.7 } McMillan AC-20 Exxon AC-20	3.10	22.1	0.72
Base	2″ Type D mix	5.0 } Exxon AC-20 Port Neches	2.60	17.5	----

* Average of three values.

Table 11.4. Aggregate properties and resilient modulus versus temperature data for mixtures evaluated.

Pavement Location	Resilient Modulus (ksi)/temp			Aggregate Type	Aggregate Blend
Lufkin	- 13°F = 1490 32°F = 858 68°F = 228 77°F = 166 104°F = 23			• Lightweight Aggregate 62% • O&I sand (coarse) 27% • Elliot Sand	71% - 3/8" - # 4 24% - # 4 - # 10 13% - # 10 - # 40 68% - # 40 - # 80 70% - # 40 - # 80 17% - # 80 - # 200 10% - Minus 200
		Site 1	Site 2		
Fairfield	- 13°F	2112	1941	• "C" Rock - 30% DP Frost	17%-5/8", 67%-3/8", 14%-#4
	32°F	1535	1325		
	68°F	927	783	• Processed gravel - 30% Gifford Hill Waco	53% - # 4, 44% - # 10
	77°F	913	749		
	104°F	253	231	• Screenings - 30% DP Frost	42% - #40, 25% - # 80 19% - # 200
				• Field sand - 10% Bohler Field	69% # 80, 26% - # 200
Centerville	- 13°F	2076	1879	• Grade "3" rock - 25%	87.2% - 5/8" - 3/8" 10.9% - 3/8" - #4
	32°F	1647	1645		
	68°F	804	880	• Type "D" Rock - 40%	52% - 3/8" - #4 33% - #4 = #10
	77°F	557	678		
	104°F	84	138	• Screenings - 21% East Texas Stone Co.	28% - #10 - # 40 42% - #40 - #80 20% - #80 - #200
				• Harris field sand - 14%	46% - #40 - #80 33% - #80 - #200 13% Minus 200

The OSR's predicted for the field pavements are realistic as they logically correspond to the level of rutting measured in the field, i.e., the larger OSR's correspond to the larger levels of measured rutting.

Although actual τ_{oct} shear strengths could not be directly calculated from ϕ' and C' parameters as field cores were too small for triaxial testing; the τ_{oct} shear strength was approximated as discussed in Chapter IX. Parameters ϕ' and C' were approximated by matching data in Chapter IX.

Based on this analysis, OSR values greater than or equal to 0.60 appear to signify severe rutting while OSR values greater than or equal to 0.45 signify moderate to severe rutting in ACP over PCC pavements. The reader is cautioned that these are only approximate ratios. More extensive field verification is required to establish critical (statistically valid) octahedral shear stress ratios.

CHAPTER XII

CONCLUSIONS AND RECOMMENDATIONS

Conclusions

Octahedral shear stress theory can be effectively used to evaluate the potential of asphalt concrete pavements over both rigid and flexible bases to deform permanently or rut under the action of traffic. The theory is compatible with permanent deformation analysis in that it is an energy theory which is readily linked to Mohr-Coulomb theory, which is widely-accepted for the strength evaluation of particulate materials.

The finite element program ILLIPAVE is capable of modeling the pavement structural conditions of layer thickness, tire contact stress, horizontal shearing stress, interface level of frictional bonding and material stiffnesses, and consequently, simulating pavement conditions which influence the level of octahedral shear development. Octahedral stress contours for over 300 conditions of surface shear, interface bonding, layer thicknesses, etc., were developed and provide an excellent source by which to evaluate the influence of structural factors or permanent deformation.

The triaxial shear strength test can be effectively used to characterize the shear strength of asphalt concrete mixtures. For the critical stress state induced in a specific pavement, the octahedral shear strength can be calculated from triaxial strength parameters (ϕ' and C'). The ratio of the octahedral shear stress induced in the asphalt concrete pavement to the octahedral shear strength of the mixture coinciding with the stress state detected in the pavement is a logical and reliable tool by which to evaluate the permanent deformation potential of a mixture. This procedure is especially well-suited for asphalt concrete layers placed over portland cement concrete (PCC) bases.

Based on this study, the octahedral shear stress ratio is a more reliable and sensitive procedure by which to evaluate deformation potential in asphaltic concrete overlays than is the more traditional creep test or repeated load permanent deformation testing coupled with computer

analyses using models such as those incorporated in ILLIPAVE and the mechano-lattice method.

This research has demonstrated the important influences of the structural and loading factors of interface bonding, surface shearing stresses and asphalt concrete layer thickness as well as the effects of base type and shear strength and stiffness of the asphalt concrete layer.

Although the interactions of structural and material properties are complex and general rules should be cautiously offered, Tables 9.3 through 9.11 in the test of this report offer an effective summary of the deformation potential of the mixtures studied for various pavement structural conditions based on the octahedral shear stress ratio concept.

Recommendations

More research is required to establish the critical octahedral stress ratio which leads to unacceptable levels of rutting in asphalt concrete pavements over both flexible, unbound bases and over rigid, PCC bases. This research must be based on the field evaluation in the performance of asphalt concrete overlays as is discussed in Chapter XI of this report.

Additional research is required in order to more confidently define the proper temperature and stroke rate for triaxial shear strength testing of asphalt concrete materials. Perhaps a range of such testing conditions should be identified.

Additional research is required in order to identify the level of interface bonding occurring between the asphalt concrete surface and the base layer, whether the base layer is a flexible, granular layer or a rigid, PCC layer.

The long-term status creep test performed at a relatively high level of stress, as discussed in Chapter XI, should be evaluated more completely in Studies 1123 and 1170 as a more reliable technique by which to evaluate long-term deformation potential. Perhaps a combination of the long-term creep test and the octahedral shear stress ratio analysis as discussed in this report should be used to identify permanent deformation potential.

REFERENCES

1. Finn, F.N. and Monismith, C.L., Asphalt Overlay Design Procedures, NCHRP 116, TRB, Washington, D.C., December 1983, p. 3.

2. Asphalt Overlay for Highway and Street Rehabilitation, Manual Series No. 17 (MS-17), The Asphalt Institute, College Park, Maryland, 1983.

3. Yoder, E.J. and Witczack, M.W., Principles of Pavement Design, John Wiley and Sons, 2nd Edition, 1975.

4. Treybig et al., Overlay Design and Reflection Cracking Analysis for Rigid Pavements, Vol. 1 and 2, FHWA Report No. FHWA-RD-77-67, Washington, D.C., 1977.

5. Smith, R.E., Pulmieri, R.O., Darter, M.I. and Lytton, R.L., Pavement Overlay Design Procedures and Assumptions, Vol. I, Analysis of Existing Procedures, Final Report, FHWA-RD-85-006, Federal Highway Administration, Washington, D.C., October 1984.

6. Seeds, S.B., et al., Arkansas Reflection Cracking Analysis and Overlay Design Procedures, Report No. VA-3/1, ARE, Inc., Engineering Consultants, February 1982.

7. Diaz, A.M. and McCullough, B.F., Design Charts for the Design of HMAC Overlays on PCC Pavements to Prevent Reflection Cracking, Research Report 249-6, Center for Transportation Research, University of Texas at Austin, November 198?.

8. Lukanen, E.O. and Skok, E.L., Structural Evaluation of Crack and Sent Overlay Pavements, Proceedings of The Association of Asphalt Paving Technologist, Vol. 56, pp. 720-731, 1987.

9. Carpenter, S.H. and Freeman, T.J., Characterizing Permanent Deformation in Asphalt Concrete Placed over Portland Cement Concrete Pavements, Transportation Research Record 1070, Washington, D.C., 1986.

10. Yandell, W.O. and Lytton, R.L., The Effect of Residual Stress and Strain Buildup In a Flexible Pavement by Repeated Rolling of a Tire, Interim Report, Texas Transportation Institute, College Station, Texas, October 1979.

11. McLeod, N.W., Rational Design of Bituminous Paving Mixtures with Curved Mohr Envelopes, Proceeding of Association of Asphalt Technologists, Vol. 21, January 28-30, 1952.

12. Department of the Army, Bituminous Pavement Standard Practice, T15-822-8, Washington, D.C., 1971.

13. State of California, Department of Transportation, Texas Methods No. 304, 305, 317, 308, 366, 367. Materials Manual, Vol. 2, Sacramento, California, 1974.

14. Little, D.N., Button, J.W., White, R.M., Ensley, E.K. Kim, Y., and Ahmed, S.J., Investigation of Asphalt Additives, Report No. DTFH-61-84-C-00066, Texas Transportation Institute, November 1986.

15. Goetz and Chen, Vacuum Triaxial Technique Applied to Bituminous Aggregate Mixtures, Proceedings of Association of Asphalt Technologist, Vol. 19, February 1950.

16. Kennedy, T.W., A Characterization of Asphalt Pavement Materials Using the Indirect Tensile Test, Proceedings of Association of Asphalt Technologists, Vol. 46, February 1977, pp. 132-150.

17. Tseng, K.H and Lytton, R.L., Prediction of Permanent Deformation in Flexible Pavement Materials, Presented at ASTM Symposium on Implication of Aggregate in The Design, Construction and Performance of Flexible Pavements, New Orleans, Louisiana, December 1986.

18. Mahboub, K., Rutting Characterization in an Improve Asphalt Concrete Mix Design Procedure for the State of Texas, Ph.D. Dissertation, Texas A&M University, College Station, Texas, August, 1988.

19. Duncan, J.M., Monismith, C.L., and Wilson, E.L., Finite Element Analysis of Pavements. Highway Research Record 228, 1968, pp. 18-33.

20. Raad, L. and Figueroa, J.L., Load Response of Transportation Systems, Transportation Engineering Journal, ASCE, Vol. 106, No. 1 TEI, 1980, pp. 111-128.

21. Roberts, F.L., Tielking, J.T., Middleton, D., Lytton, R.L. and Tseng, K.H., Effects of Tire Pressure on Flexible Pavements, Report No. 372-1F, Texas Transportation Institute, August 1986, pp. 223-235.

22. Li, J., Use of Climatic Data for the Prediction of Permanent Deformation in Flexible Pavements, Masters of Engineering Report, Texas A&M University, College Station, Texas, June 1987.

23. Kelly, H.F. and Thompson, M.R., Mechanistic Design Concepts for Heavy Weight F.15 Aircraft on Flexible Pavement, Journal of Transportation Engineering, ASCE, Vol. 114, No. 3, May 1988, pp. 323-340.

24. Yandell, W.O., Prediction of the Behavior of Elastoplastic Road During Repeated Rolling Using the Mechano-Lattice Analogy, Highway Research Record 374, HRB, Washington, D.C., 1971, pp. 29-41.

25. Yandell, W.O., Measurement and Prediction of Forward Movement and Rutting in Pavements Under Repetitive Wheel Loads. Transportation Research Record 888, TRB, National Research Council, Washington, D.C., 1982, pp. 77-84.

26. Kenis, W.J., Predictive Design Procedures, VESYS User's Manual, FHWA Report 77-154, 1978.

27. Perl, M., Uzan, J., and Sides, A., Visco-Elasto-Plastic Constitutive Law for Bituminous Mixtures Under Repeated Loading, Transportation Research Record 911, Washington, D.C., 1984, pp. 20-27.

28. Lai, J.S. and Anderson, D.A., Irrecoverable and Recoverable Nonlinear Viscoelastic Properties of Asphalt concrete, Highway Research Record 468, pp. 73-88, 1973.

29. Helwig, J.T., Council, K.A., and Reinhardt, P.S., SAS User's Guide, SAS Institute, Inc., 1979.

30. Tielking, J.T. and Roberts, F.L., Tire Contact Pressure and Its Effect on Pavement Strain, Journal of Transportation Engineering, Vol. 113, January 1987, pp. 56-70.

31. Weather Bureau Climatologist, Environmental Science Services Administration, Austin, Texas.

32. AASHTO Guide for Design of Pavement Structures, American Association of State Highway and Transportation Officials, Washington, D.C., 1986, p. 11-22.

33. Middleton, D.R., Roberts, F.L. and Chavala, T.C., Measurement and Analysis of Truck Tire Pressures on Texas Highway, Transportation Research Record 1070, Washington, D.C., 1986, pp. 1-8.

34. Sargious, M., Pavements and Surfacings for Highways and Air Ports, John Wiley & Sons, New York, Toronto, 1975, pp. 457-475.

35. Chen, H.H., Marshek, K.M. and Saraf, C.L., Effects of Truck Tire Contact Pressure Distribution on the Design of Flexible Pavements: A Three Dimensional Finite Element Approach, Transportation Research Record 1095, Washington, D.C., 1986, pp. 72-78.

36. Roberts, F.L. and Rosson, B.J., Establishing Material Properties for Thin Asphalt Concrete Surface on Granular Bases, Report No. 3451, Texas Transportation Institute, November 1985.

37. Krauthammer, T., and Khanlarzadeh, H., Numerical Assessment of Pavement Test Sections, Transportation Research Record 1117, Washington, D.C., 1987, pp. 66-75.

38. Uzan, J. and Smith, R.E., TFPS Technical Report, Texas Transportation Institute, Texas A&M University, College Station, Texas, August, 1988.

39. Highler, W.H. and Harr, M.E., Application of Energy Concepts to the Performance of Airfield Pavements, Technical Report No. AFWL-TR-72-225, June 1973.

40. Uzan, J., Livneh, M., and Eshed, Y., Investigation of Adhesion Properties Between Asphaltic Concrete Layers, Proceedings of Association of Asphalt Paving Technologists, Vol. 47, 1978, pp. 495-521.

41. Shahin, M.Y., Kirchner, K., Blackmon, W., and Tomita, H., Effect of Layer Slippage on Performance of Asphalt-Concrete Pavements, Transportation Research Record 1095, Washington, D.C., 1986, pp. 79-85.

42. Smith, R.E., Palmier, R.P., Carter, M.I., and Lytton, R.L., Pavement Overlay Design Procedures and Assumptions, Vol. III: Guide for Designing an Overlay, Final Report, August, 1986.

43. Monismith, C.L., Epps, J.A. and Finn, F.N., Improved Asphalt Mix Design, Proceedings Association of the Asphalt Paving Technologists, San Antonio, Texas, February 11-13, 1985, Vol. 54, pp. 347-391.

44. Monismith, C.L., Department and Institution and City Notes Prepared for ITTE Short Course on Asphalt Paving Mixtures, 1961 and 1962.

45. McLaughlin, J.F. and Goetz, W.H., Comparison of Unconfined and Marshall Tests Results, Proceedings of the Association of Asphalt Paving Technologists, Vol. 21, January 28-30, 1952.

46. McLeod, N.W., The Rational Design of Bituminous Paving Mixtures, Highway Research Board, HRB, Vol. 29, 1949.

47. Cooper, K.E., Brown, S.F. and Pooley, G.R., The Design of Aggregate Gradings for Asphalt Base Courses, Proceedings Association of Asphalt Paving Technologists (AAPT), February 11-13, 1985, pp. 324-347.

48. Bolk, I.H.J., The Creep Test, SCW Record 5, Study Center for Road Construction, 14A Janshuitensigel, 6811 AB Arnhem, The Netherlands, 1981, pp. 1-96.

49. Finn, F.N., Sarat, C., Kulkami, R., Nair, K., Smith, W., and Abdullah, A., The Use of Distress Prediction Subsystem for the Design of Pavement Structures, Proceedings, Fourth International Conference on the Structural Design of Asphalt Pavements, Vol. 1, University of Michigan, Ann Arbor, August 1977, pp. 3-38.

50. Monismith, C.L. and Finn, F.N., Flexible Pavement Design: The State-of-the-Art, ASCE Journal of Transportation, January 1977.

51. Finn, F.N., Monismith, C.L. and Markevich, N.J., Pavement Performance and Asphalt Concrete Mix Design, Proceedings, Association of Asphalt Paving Technologists, Vol. 52, 1983, pp. 121-150.

52. Hills, J.F., Brien, D. and Van de Loo, P.J., The Correlation of Rutting and Creep Tests on Asphalt Mixes, Institute of Petroleum, Paper IPT4-001, January, 1974.

53. Van de Loo, P.J., A Practical Approach to Predictions of Rutting in Asphalt Pavements: The Shell Method, Transportation Research Record, TRR No. 616, Washington, D.C., 1983.

54. Van de Loo, P.J., The Creep Test: A Key Tool in Asphalt Mix Design and in the Prediction of Pavement Rutting, Association of Asphalt Paving Technologists, Vol. 47, 1978.

55. Van de Loo, P.J., Creep Testing, A Simple Tool to Judge Asphalt Mix Stability, Association of Asphalt Paving Technologists, Vol. 43, 1974, pp. 253-284.

56. Yandell, W.O., New Method of Simulating Layered Systems of Unbound Granular Material, Transportation Research Record 1022, Washington, D.C., 1985.

57. Yandell, W.O., The Use of the Mechano Lattice Analysis to Investigate Relative Plastic Behavior, Proceedings International Conference on Constitutive Laws for Engineering Materials, University of Anzom, Tucson, Arizona, January, 1983,

58. Yandell, W.O., Residual Stresses and Strains and Fatigue Cracking, Journal of Transportation Engineering, ASCE, Vol. 108, No. TE1, January 1982, pp. 103-110.

59. Yandell, W.O. and Lytton, R.L., Residual Stress Due to Traveling Loads and Reflection Cracking, FHWA-TX-79-207-6, Texas Transportation Institute and Tests State Department of Highway and Public Transportation, College Station, Texas, June 1979.

60. Egons, T. and Krokosky, E.M., Tensile Properties of Dense Graded Bituminous Concrete, Proceedings, Association of Asphalt Paving Technologists, Vol. 32, 1963, pp. 497-528.

61. Huber, G.A., Effect of Asphalt Concrete Parameters on Rutting Performance: A Field Investigation, Association of Asphalt Paving Technologists, Reno, Nevada, February 1987.

62. Brown, E.R., Experiences of Corps of Engineers in Compaction of Hot Asphalt Mixtures, Placement and Compaction of Asphalt, ASTM, STP 829, American Society of Testing and Materials, 1984, pp. 67-79.

63. Monismith, C.L., Permanent Deformation (Rutting) Considerations in Asphalt Concrete Pavement Sections, Paper Offered for Consideration for the Annual Meeting of the AAPT, Williamsburg, Virginia, February 29-March 2, 1988.

64. Vallerga, B.A. and Lovering, W.R., Evaluation of the Hveem Stabilimeter Method of Designing Asphalt Paving Mixtures, Association of Asphalt Paving Technologists, Vol. 54, pp. 243-265, 1985.

65. Allen, D.L. and Deen, R.C., A Computerized Analysis of Rutting Behavior of Flexible Pavement, Transportation Research Record No. 1095, Washington, D.C., 1986.

66. Tseng, K.H., The Finite Element Method to the Performance Analysis of Flexible Pavement, Ph.D. Dissertation, Texas A&M University, College Station, Texas, August 1988.

APPENDIX A

Discussion of Failure Criteria

APPENDIX A

DISCUSSION OF FAILURE CRITERIA

Introduction

To design a structural part or system to perform a given function, the designer must have a clear understanding of the possible ways or modes in which the part or system may fail to perform its intended function. Once the mode of failure is determined, the designer must then define suitable failure criteria that accurately predict the conditions under which failure will occur. The response of a structural system and hence its failure depend strongly on the material used, which in turn, depends on the type and history of the applied loading. Accordingly, suitable failure criteria must include effects of different material, different loading procedures as well as other potential factors that influence the stress distribution in the member (such as support and cracks).

A tension test of an axially loaded member is easy to conduct and the tensile properties for many types of materials so determined are well known. When such a member fails, the failure occurs at a specific principal (axial) stress, a definite axial strain, a maximum shearing stress of one-half the axial stress, and a specific amount of strain energy per unit volume known as toughness. Since all of these limits are reached simultaneously for an axial load, it makes no difference which criterion (stress, strain, or energy) is used for predicting failure in another axially loaded member of the same material. For an element subjected to biaxial or triaxial loading, however, the situation is more complicated because the limits of normal stress, normal strain, shearing stress, and strain energy existing at failure for an axial load are not all reached simultaneously. In other words, the cause of failure, in general, is unknown. In such cases, it becomes important to determine the best criterion for predicting failure, because test results are difficult to obtain and the combinations of loads are endless.

Modes of Failure

When a structural member is subjected to loads, its response depends not only on the type of material from which it is made, but also on the environmental conditions and the manner of loading. Depending on how the member is loaded, it may fail by excessive deformation, which results in the member being unable to perform its design function; it may fail by plastic deformation (yielding), which may cause a permanent, undesirable change in shape; it may fail due to fracture (breaking). In the latter case, the nature of the fracture may be of a ductile type preceded by appreciable plastic deformation or of a brittle type with little or no prior plastic deformation. Another manner in which a structural member may fail is that of elastic or plastic instability. Several theories have been proposed for predicting failure for various types of material subjected to many combinations of loads. Unfortunately, none of the theories agree with test data for all types of materials and combinations of loads. Several of the more common theories of failure are presented and briefly explained in the subsequent sections of this appendix.

Maximum Normal Stress Theory

The Maximum Normal Stress Theory (often called Rankine's Theory) predicts failure of a specimen subjected to any combination of loads when the maximum normal stress at any point reaches the axial failure stress as determined by an axial tensile or compressive test. In other words, inelastic action (failure) at any point in a member begins when the principal stress reaches the tensile elastic strength of the material, regardless of the normal or shearing stresses that occur on other planes through the point. Thus, according to this theory, if a block of material reaches its yield stress when subjected to a stress $_1$, the yield stress will still be $_1$, even if the block is subjected to the stress $_2$ in addition to $_1$. Furthermore, if this theory is to hold for all kinds of loading, the shearing yield stress of the material must be equal to the tensile yield stress. But for ductile metals, the shearing yield stress, as obtained from a torsion test, is much less than the tensile yield stress as found from the tension test. It is evident, therefore, that for ductile materials, the maximum principle stress criterion of failure is limited. For brittle materials that do not fail by yielding but fail by

brittle fracture, the maximum principle stress criterion may be satisfactory.

Maximum Shearing Stress Theory

The maximum shearing stress theory, sometimes called Tresca's criterion, Coulomb's criterion, or Guest's Law, predicts failure of a specimen subjected to any combination of loads when the maximum shearing stress at any point reaches the failure stress that is equal to one-half failure stress, ($_f/2$), as determined by an axial tensile or compressive test of the same material. Thus, inelastic action at any point in a member at which any state of stress exists begins when the maximum shearing stress at the point reaches a value equal to the maximum shearing stress in a tension specimen when yielding starts. This means that the shearing stress must be no more than one-half the tensile yield stress, since the maximum shearing stress in a tension specimen (on a 45° oblique plane) is one-half the maximum tensile stress. According to this criterion, it is assumed that maximum shearing stress alone produces inelastic action and that the equal tensile stresses have no influence on yield initiation. However, if the state of stress consists of triaxial tensile stresses of nearly equal magnitude, shearing stresses are very small and failure will probably occur by brittle fracture rather than by yielding. The maximum shearing stress criterion seems to be fairly well justified for ductile material in which relatively large shearing stresses are developed. For ductile materials, the shearing elastic limit, as determined from a torsion test (pure shear), is greater than one-half the tensile elastic limit (with an average value of $_f$ of about 0.577 $_f$). Hence, for such a state of stress, the maximum shearing stress criterion errs (on the safe side) by approximately 15 percent, that is, it predicts yielding of loads less than those that actually cause yielding.

Maximum Normal Strain Theory

The maximum normal strain theory, often called St. Venant's criterion, predicts failure of a specimen subjected to any combination of loads when the normal strain at any point reaches the failure strain $\varepsilon_f = \sigma_f/E$ at the proportional limit, as determined by an axial tensile or compressive test of the same material. Therefore, according to this theory,

inelastic action at a point in a member at which any state of stress exists begins when the maximum strain at the point reaches a value that occurs simultaneously with the attainment of the tensile yield stress of the material (in a uniaxial tension test). The limitation of this theory may be best explained if one considers a block of material subjected to tensile stress $_1$. Inelastic action in the block begins when $_1$ becomes equal to yield stress $_y$ and thereby, $\hat{u}_y = {}_y/E$. But, if the block is subjected to a compressive stress $_2$ in addition to $_1$, then $\hat{u} = ({}_1/E + {}_2/E)$. Hence, inelastic action is predicted for a value of $_1$ less than yield stress, since the strain in the direction of $_1$ is increased by the amount ($_2/E$). Therefore, with this theory, $_1$ is somewhat smaller than yield stress at yielding, if the second normal stress $_2$ is a compressive stress. However, if on the other hand, $_2$ is a tensile stress, the maximum value of $_1$ that can be applied without causing yielding is somewhat larger than the tensile yield stress.

Maximum Strain Energy Theory:

This theory proposed by Beltrami and by Haigh also predicts failure of a specimen subjected to any combination of loads when the strain energy per unit volume of any portion of the stressed member reaches the failure value of the strain energy per unit volume as determined by an axial tensile or compressive test of the same material. According to this theory, the resilience of a material is the measured amount of energy that can be absorbed under elastic loading conditions and no material can exceed this energy ($^2_y/2E$) without yielding. The maximum strain energy theory has been largely replaced by the maximum distortion energy theory.

Maximum Distortion Energy Theory

This theory grew out of the analytical work of Huber, von Mises, and Hencky, and out of the result of tests by Bridgman on various materials. The theory differs from the maximum strain energy theory in that the portion of the strain energy producing volume change is considered ineffective in causing failure by yielding. The portion of the strain energy producing change of shape for the element is assumed to be completely responsible for the failure of material by inelastic action. The supporting evidence comes from experiments showing that homogeneous

materials can withstand very high hydrostatic stresses without inelastic action taking place, and that the strain energy density values, are many times greater than those obtained in a simple axial load compression test. Since change of shape involves shearing stresses, this theory is sometimes called (somewhat erroneously), the shear energy criterion. This theory suggests that fracture surfaces in brittle materials under tension are planes that carry the maximum principal stress. Experimental observation has also been obtained as supporting evidence.

Octahedral Shearing Stress Theory

This theory gives the same results as does the maximum energy of distortion theory criterion. According to octahedral shearing stress theory, inelastic action at any point in a member under any combination of stresses begins when the maximum octahedral shear stress $_{oct(max)}$ becomes equal to 0.471 $_{y}$, where $_{y}$ is the tensile yield stress of the material as determined from the standard tension test. This criterion makes it possible to apply the energy of distortion criterion of failure by dealing with stresses instead of dealing with energy directly. Experiments have shown that initiation of yielding in most materials is predicted fairly well by either the maximum shearing stress criterion or the octahedral shearing stress criterion.

The Otto Mohr Theory

This theory states that failure of an isotropic material, either by fracture or by the onset of yielding will occur when (in a three dimensional state of stress) the largest Mohr's circle (having diameter ($_{1}$-$_{3}$)/2 where $_{1}$ $_{2}$ $_{3}$) touches a failure envelope. This criterion may be used to predict the effect of a given state of plane stress on a brittle material when results of various types of tests are available for that material. Mohr's motivation was the simple and spontaneous idea that the region enclosed by Mohr's circle for any possible state of stress not causing failure must be a region safe from failure. Experiments show that the envelope, which is tangent to all the failure circles and which bounds the safe region, is usually curved convex outward. A simple way to approximate the envelope is to draw a pair of straight lines tangent to two Mohr's circles. One circle represents failure under uniaxial tensile

stress $_t$; the other circle represents failure under uniaxial compressive stress whose magnitude is $_c$. Thus failure is predicted when $_1/_t - _3/_c \geq 1$, where unity defines the onset of yielding according to Mohr's criterion. Also, it should be noted that in the above relationship, principal stress $_1$ and $_3$ carry an algebraic sign, as usual.

Discussion

A rational procedure of design requires that a general mode of failure under assumed service conditions be determined or assumed. Also, a quantity such as stress, strain, or energy may be chosen as a critical value to limit the loading that can be applied to the member. Furthermore, suitable tests of the material must be adopted for the determination of the critical value. A theory that works for ductile failure may not work for brittle fracture. Low temperature, high strain rate, and triaxial tension with low shear stress are among other factors that promote brittle behavior. A single theory may not always apply to a given material because the material may behave in a ductile fashion under some conditions and in a brittle fashion under others. Assuming arbitrary state of stress, without a theory of failure, each new state of stress would have to be tested. Because of physical difficulty, and the possibility of unlimited states of stress, not only is it undesirable, but also unacceptable to test every stress state. It would be uneconomical and expensive. In general, we are limited, because of practical considerations to one or two test members to obtain material properties. Thus, a theory of failure provides a means to presume that the action causing failure in static tension for example, will also cause failure in any other static state of stress and thereby avoid examining every possible stress state in the search for a safe design.

REFERENCES

A.1. Boresi, Arthur P, Sidebottom, Omar M., Seely, Fred B., and Smith, James O., Advanced Mechanics of Materials, 3rd. ed., John Wiley & Sons, New York, 1978.

A.2. Higdon, Archie, Ohlsen, Edward H., Stiles, William B., Weese, John A., and Riley, William F., Mechanics of Materials, 3rd ed., John Wiley & Sons, New York, 1976.

A.3. Cook, Robert D., and Young, Warren C., Advanced Mechanics of Materials, Macmillan Publishing Company, New York, 1985.

A.4. Beer, Ferdinand P., and Johnston, E. Russell Jr., Mechanics of Materials, McGraw-Hill Book Company, New York, 1981.

A.5. Hertzberg, Richard W., Deformation and Fracture Mechanics of Engineering Materials, 2nd ed., John Wiley & Sons, New York, 1983.

APPENDIX B

Sample Preparation and Testing Techniques

APPENDIX B

SAMPLE PREPARATION AND TESTING TECHNIQUES

Mixing Method

Aggregate and asphalt were mixed according to Texas SDHPT method TEX-205-F. After proper mixing, the temperature of the asphalt concrete mixture was raised to 250-270°F for compaction.

Creep Specimen Manufacturing

Specimens were compacted in a cylindrical shape of 4 inches in diameter and 8 inches in height.

The compaction effort was delivered by a kneading compactor.

Each specimen was fabricated in three lifts of equal height. To achieve uniform density throughout, a number of test specimens were manufactured at various compactive efforts. These specimens were then carefully sawed at the interface between each lift layer and tested for density and air voids content. The following compaction energy at each layer was obtained to provide the desired uniform density throughout the specimens.

1. First layer: 30 tamps at 250 psi,
2. Second layer: 60 tamps at 250 psi, and
3. Third layer: 140 tamps at 250 psi.

Each specimen was then subjected to a sustained leveling load of 1000 lbs for a period of one minute.

To obtain low air voids content, specimens were subjected to the following energy levels.

1. First layer: 100 tamps at 450 psi,
2. Second layer: 150 tamps at 450 psi, and
3. Third layer: 200 tamps at 450 psi.

The sustaining leveling load for these specimens was 1,500 lbs. for one minute.

Test Procedures

Creep Test

Once the cylindrical specimens of HMAC were manufactured and cured for at least 48 hours, the creep test was conducted according to the following procedure.

Each specimen was preconditioned at a stress level of 14.5 psi for a 10-minute load application, followed by a rest period of 15 seconds. This procedure was repeated three times. Specimens were then allowed to recover for 30 minutes. The creep test procedure calls for a loading frame capable of delivering and maintaining a constant vertical load for a period of one hour. During this period, the vertical displacements were measured at the following intervals: 1, 2, 4, 8, 15, 30 seconds, and 1, 2, 4, 8, 15, 30, 45, and 60 minutes. This data was collected by means of LVDT's and Y-time chart records. A closed loop hydraulic MTS system was used for testing.

The creep load, 14.5 psi at 104°F as suggested by Shell researchers and verified by TTI investigators for nondestructive creep-recovery tests, was maintained for one hour, after which the load was removed instantaneously. During the loading and unloading process, vertical displacements were monitored by two LVDT's on each side of the specimen. Figure B.1 shows schematically the creep-recovery data.

Test Procedure

Different components of vertical displacements or vertical strains may be separated according to the following regression procedures:

$$\epsilon_{creep} = a_1 t^{b1} \qquad (B.1)$$

$$\epsilon_{recovery} = a_2 t^{b2} \qquad (B.2)$$

where: ϵ_{creep} = vertical strain recorded during the creep phase,

$\epsilon_{recovery}$ = vertical stain recorded during the recovery phase, and

a_1, a_2, b_1, b_2 = regression constants.

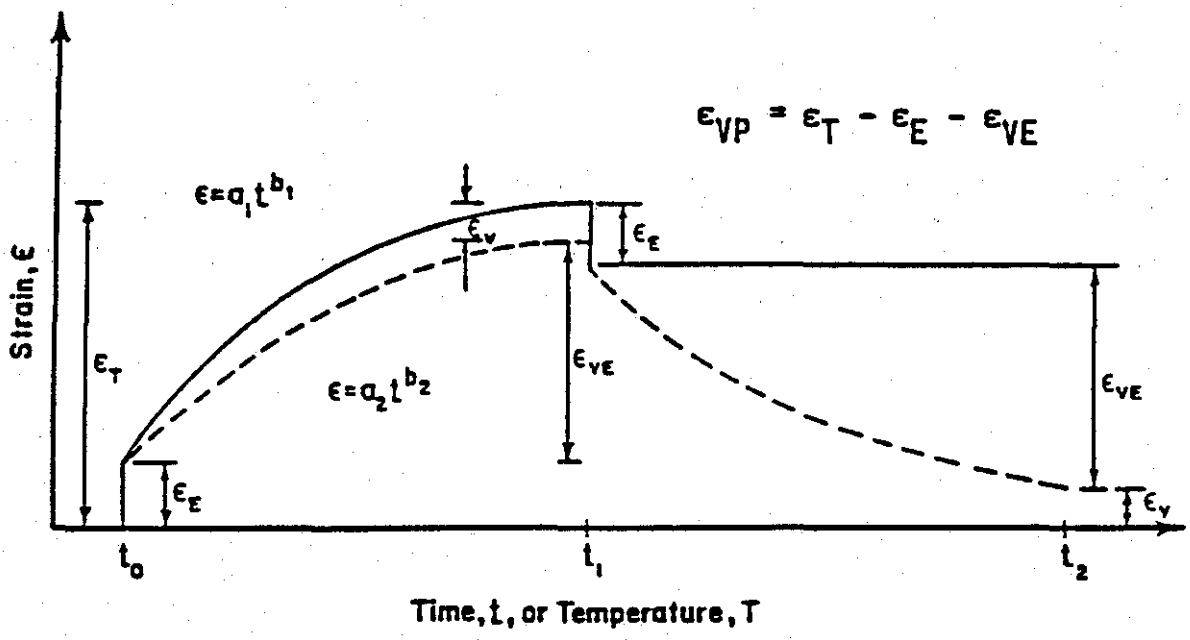

Figure B.1. Displacement recorded in a creep/recovery test.

Cyclic Permanent Deformation Testing

Repeated load compression creep testing was performed in accordance with the procedure outlined in VESYS User's Manual (Reference 26).

Resilient Modulus Testing

Resilient modulus testing was performed in accordance with ASTM D4123 procedures.

APPENDIX C

Octahedral Shear Stress Distribution

for Various Structural and ACP Stiffness Conditions

APPENDIX C

OCTAHEDRAL SHEAR STRESS DISTRIBUTIONS

FOR VARIOUS STRUCTURAL AND ACP STIFFNESS CONDITIONS

Variables considered:

Interface Bonding Condition (B) = 0, 25, 50, 75, and 100%
Surface Shear (S), with shear (WS), without shear (W/O S)
ACP Thickness (T) = 2, 4, 6, 8 inches
ACP Stiffness (E) = 100, 200, 300, 400, and 500 ksi
Supporting Base (SB) = PCC, Flexible (FLX)

Page	Conditions
C.33	B = 0%, S = W/O S, T = 8, E = 300, SB = PCC
C.34	B = 0%, S = W/O S, T = 8, E = 400, SB = PCC
C.35	B = 0%, S = W/O S, T = 8, E = 500, SB = PCC
C.36	B = 0%, S = W/O S, T = 8, E = 100, SB = FLX
C.37	B = 0%, S = W/O S, T = 8, E = 200, SB = FLX
C.38	B = 0%, S = W/O S, T = 8, E = 300, SB = FLX
C.39	B = 0%, S = W/O S, T = 8, E = 400, SB = FLX
C.40	B = 0%, S = W/O S, T = 8, E = 500, SB = FLX
C.41	B = 0%, S = WS, T = 8, E = 100, SB = PCC
C.42	B = 0%, S = WS, T = 8, E = 200, SB = PCC
C.43	B = 0%, S = WS, T = 8, E = 300, SB = PCC
C.44	B = 0%, S = WS, T = 8, E = 400, SB = PCC
C.45	B = 0%, S = WS, T = 8, E = 500, SB = PCC
C.46	B = 0%, S = WS, T = 8, E = 100, SB = FLX
C.47	B = 0%, S = WS, T = 8, E = 200, SB = FLX
C.48	B = 0%, S = WS, T = 8, E = 300, SB = FLX
C.49	B = 0%, S = WS, T = 8, E = 400, SB = FLX
C.50	B = 0%, S = WS, T = 8, E = 500, SB = FLX
C.51	B = 0%, S = WS, T = 6, E = 100, SB = PCC
C.52	B = 0%, S = WS, T = 6, E = 200, SB = PCC
C.53	B = 0%, S = WS, T = 6, E = 300, SB = PCC
C.54	B = 0%, S = WS, T = 6, E = 400, SB = PCC
C.55	B = 0%, S = WS, T = 6, E = 500, SB = PCC
C.56	B = 0%, S = WS, T = 6, E = 100, SB = FLX
C.57	B = 0%, S = WS, T = 6, E = 200, SB = FLX
C.58	B = 0%, S = WS, T = 6, E = 300, SB = FLX
C.59	B = 0%, S = WS, T = 6, E = 400, SB = FLX
C.60	B = 0%, S = WS, T = 6, E = 500, SB = FLX
C.61	B = 0%, S = WS, T = 4, E = 100, SB = PCC
C.62	B = 0%, S = WS, T = 4, E = 200, SB = PCC
C.63	B = 0%, S = WS, T = 4, E = 300, SB = PCC
C.64	B = 0%, S = WS, T = 4, E = 400, SB = PCC
C.65	B = 0%, S = WS, T = 4, E = 500, SB = PCC
C.66	B = 0%, S = WS, T = 4, E = 100, SB = FLX
C.67	B = 0%, S = WS, T = 4, E = 200, SB = FLX
C.68	B = 0%, S = WS, T = 4, E = 300, SB = FLX
C.69	B = 0%, S = WS, T = 4, E = 400, SB = FLX
C.70	B = 0%, S = WS, T = 4, E = 500, SB = FLX
C.71	B = 0%, S = WS, T = 2, E = 100, SB = PCC
C.72	B = 0%, S = WS, T = 2, E = 200, SB = PCC
C.73	B = 0%, S = WS, T = 2, E = 300, SB = PCC
C.74	B = 0%, S = WS, T = 2, E = 400, SB = PCC
C.75	B = 0%, S = WS, T = 2, E = 500, SB = PCC
C.76	B = 0%, S = WS, T = 2, E = 100, SB = FLX
C.77	B = 0%, S = WS, T = 2, E = 200, SB = FLX
C.78	B = 0%, S = WS, T = 2, E = 300, SB = FLX
C.79	B = 0%, S = WS, T = 2, E = 400, SB = FLX
C.80	B = 0%, S = WS, T = 2, E = 500, SB = FLX
C.81	B = 25%, S = WS, T = 2, E = 100, SB = PCC
C.82	B = 25%, S = WS, T = 2, E = 500, SB = PCC
C.83	B = 25%, S = WS, T = 2, E = 100, SB = FLX
C.84	B = 25%, S = WS, T = 2, E = 500, SB = FLX

Page	Conditions
C.85	B = 25%, S = WS, T = 4, E = 100, SB = PCC
C.86	B = 25%, S = WS, T = 4, E = 500, SB = PCC
C.87	B = 25%, S = WS, T = 4, E = 100, SB = FLX
C.88	B = 25%, S = WS, T = 4, E = 500, SB = FLX
C.89	B = 25%, S = WS, T = 6, E = 100, SB = PCC
C.90	B = 25%, S = WS, T = 6, E = 500, SB = PCC
C.91	B = 25%, S = WS, T = 6, E = 100, SB = FLX
C.92	B = 25%, S = WS, T = 6, E = 500, SB = FLX
C.93	B = 25%, S = WS, T = 8, E = 100, SB = PCC
C.94	B = 25%, S = WS, T = 8, E = 500, SB = PCC
C.95	B = 25%, S = WS, T = 8, E = 100, SB = FLX
C.96	B = 25%, S = WS, T = 8, E = 500, SB = FLX
C.97	B = 25%, S = W/O S, T = 8, E = 100, SB = PCC
C.98	B = 25%, S = W/O S, T = 8, E = 500, SB = PCC
C.99	B = 25%, S = W/O S, T = 8, E = 100, SB = FLX
C.100	B = 25%, S = W/O S, T = 8, E = 500, SB = FLX
C.101	B = 25%, S = W/O S, T = 6, E = 100, SB = PCC
C.102	B = 25%, S = W/O S, T = 6, E = 500, SB = PCC
C.103	B = 25%, S = W/O S, T = 6, E = 100, SB = FLX
C.104	B = 25%, S = W/O S, T = 6, E = 500, SB = FLX
C.105	B = 25%, S = W/O S, T = 4, E = 100, SB = PCC
C.106	B = 25%, S = W/O S, T = 4, E = 500, SB = PCC
C.107	B = 25%, S = W/O S, T = 4, E = 100, SB = FLX
C.108	B = 25%, S = W/O S, T = 4, E = 500, SB = FLX
C.109	B = 25%, S = W/O S, T = 2, E = 100, SB = PCC
C.110	B = 25%, S = W/O S, T = 2, E = 500, SB = PCC
C.111	B = 25%, S = W/O S, T = 2, E = 100, SB = FLX
C.112	B = 25%, S = W/O S, T = 2, E = 500, SB = FLX
C.113	B = 50%, S = W/O S, T = 2, E = 100, SB = PCC
C.114	B = 50%, S = W/O S, T = 2, E = 500, SB = PCC
C.115	B = 50%, S = W/O S, T = 2, E = 100, SB = FLX
C.116	B = 50%, S = W/O S, T = 2, E = 500, SB = FLX
C.117	B = 50%, S = W/O S, T = 4, E = 100, SB = PCC
C.118	B = 50%, S = W/O S, T = 4, E = 500, SB = PCC
C.119	B = 50%, S = W/O S, T = 4, E = 100, SB = FLX
C.120	B = 50%, S = W/O S, T = 4, E = 500, SB = FLX
C.121	B = 50%, S = W/O S, T = 6, E = 100, SB = PCC
C.122	B = 50%, S = W/O S, T = 6, E = 500, SB = PCC
C.123	B = 50%, S = W/O S, T = 6, E = 100, SB = FLX
C.124	B = 50%, S = W/O S, T = 6, E = 500, SB = FLX
C.125	B = 50%, S = W/O S, T = 8, E = 100, SB = PCC
C.126	B = 50%, S = W/O S, T = 8, E = 500, SB = PCC
C.127	B = 50%, S = W/O S, T = 8, E = 100, SB = FLX
C.128	B = 50%, S = W/O S, T = 8, E = 500, SB = FLX
C.129	B = 50%, S = WS, T = 8, E = 100, SB = PCC
C.130	B = 50%, S = WS, T = 8, E = 500, SB = PCC
C.131	B = 50%, S = WS, T = 8, E = 100, SB = FLX
C.132	B = 50%, S = WS, T = 8, E = 500, SB = FLX
C.133	B = 50%, S = WS, T = 6, E = 100, SB = PCC
C.134	B = 50%, S = WS, T = 6, E = 500, SB = PCC
C.135	B = 50%, S = WS, T = 6, E = 100, SB = FLX
C.136	B = 50%, S = WS, T = 6, E = 500, SB = FLX

Page	Conditions
C.137	B = 50%, S = WS, T = 4, E = 100, SB = PCC
C.138	B = 50%, S = WS, T = 4, E = 500, SB = PCC
C.139	B = 50%, S = WS, T = 4, E = 100, SB = FLX
C.140	B = 50%, S = WS, T = 4, E = 500, SB = FLX
C.141	B = 50%, S = WS, T = 2, E = 100, SB = PCC
C.142	B = 50%, S = WS, T = 2, E = 500, SB = PCC
C.143	B = 50%, S = WS, T = 2, E = 100, SB = FLX
C.144	B = 50%, S = WS, T = 2, E = 500, SB = FLX
C.145	B = 75%, S = WS, T = 2, E = 100, SB = PCC
C.146	B = 75%, S = WS, T = 2, E = 500, SB = PCC
C.147	B = 75%, S = WS, T = 2, E = 100, SB = FLX
C.148	B = 75%, S = WS, T = 2, E = 500, SB = FLX
C.149	B = 75%, S = WS, T = 4, E = 100, SB = PCC
C.150	B = 75%, S = WS, T = 4, E = 500, SB = PCC
C.151	B = 75%, S = WS, T = 4, E = 100, SB = FLX
C.152	B = 75%, S = WS, T = 4, E = 500, SB = FLX
C.153	B = 75%, S = WS, T = 6, E = 100, SB = PCC
C.154	B = 75%, S = WS, T = 6, E = 500, SB = PCC
C.155	B = 75%, S = WS, T = 6, E = 100, SB = FLX
C.156	B = 75%, S = WS, T = 6, E = 500, SB = FLX
C.157	B = 75%, S = WS, T = 8, E = 100, SB = PCC
C.158	B = 75%, S = WS, T = 8, E = 500, SB = PCC
C.159	B = 75%, S = WS, T = 8, E = 100, SB = FLX
C.160	B = 75%, S = WS, T = 8, E = 500, SB = FLX
C.161	B = 75%, S = W/O S, T = 8, E = 100, SB = PCC
C.162	B = 75%, S = W/O S, T = 8, E = 500, SB = PCC
C.163	B = 75%, S = W/O S, T = 8, E = 100, SB = FLX
C.164	B = 75%, S = W/O S, T = 8, E = 500, SB = FLX
C.165	B = 75%, S = W/O S, T = 6, E = 100, SB = PCC
C.166	B = 75%, S = W/O S, T = 6, E = 500, SB = PCC
C.167	B = 75%, S = W/O S, T = 6, E = 100, SB = FLX
C.168	B = 75%, S = W/O S, T = 6, E = 500, SB = FLX
C.169	B = 75%, S = W/O S, T = 4, E = 100, SB = PCC
C.170	B = 75%, S = W/O S, T = 4, E = 500, SB = PCC
C.171	B = 75%, S = W/O S, T = 4, E = 100, SB = FLX
C.172	B = 75%, S = W/O S, T = 4, E = 500, SB = FLX
C.173	B = 75%, S = W/O S, T = 2, E = 100, SB = PCC
C.174	B = 75%, S = W/O S, T = 2, E = 500, SB = PCC
C.175	B = 75%, S = W/O S, T = 2, E = 100, SB = FLX
C.176	B = 75%, S = W/O S, T = 2, E = 500, SB = FLX
C.177	B = 100%, S = W/O S, T = 2, E = 100, SB = PCC
C.178	B = 100%, S = W/O S, T = 2, E = 200, SB = PCC
C.179	B = 100%, S = W/O S, T = 2, E = 300, SB = PCC
C.180	B = 100%, S = W/O S, T = 2, E = 400, SB = PCC
C.181	B = 100%, S = W/O S, T = 2, E = 500, SB = PCC
C.182	B = 100%, S = W/O S, T = 2, E = 100, SB = PCC
C.183	B = 100%, S = W/O S, T = 2, E = 200, SB = FLX
C.184	B = 100%, S = W/O S, T = 2, E = 300, SB = FLX
C.185	B = 100%, S = W/O S, T = 2, E = 400, SB = FLX
C.186	B = 100%, S = W/O S, T = 2, E = 500, SB = FLX
C.187	B = 100%, S = W/O S, T = 4, E = 100, SB = PCC
C.188	B = 100%, S = W/O S, T = 4, E = 200, SB = PCC

Page	Conditions
C.189	B = 100%, S = W/O S, T = 4, E = 300, SB = PCC
C.190	B = 100%, S = W/O S, T = 4, E = 400, SB = PCC
C.191	B = 100%, S = W/O S, T = 4, E = 500, SB = PCC
C.192	B = 100%, S = W/O S, T = 4, E = 100, SB = FLX
C.193	B = 100%, S = W/O S, T = 4, E = 200, SB = FLX
C.194	B = 100%, S = W/O S, T = 4, E = 300, SB = FLX
C.195	B = 100%, S = W/O S, T = 4, E = 400, SB = FLX
C.196	B = 100%, S = W/O S, T = 4, E = 500, SB = FLX
C.197	B = 100%, S = W/O S, T = 6, E = 100, SB = PCC
C.198	B = 100%, S = W/O S, T = 6, E = 200, SB = PCC
C.199	B = 100%, S = W/O S, T = 6, E = 300, SB = PCC
C.200	B = 100%, S = W/O S, T = 6, E = 400, SB = PCC
C.201	B = 100%, S = W/O S, T = 6, E = 500, SB = PCC
C.202	B = 100%, S = W/O S, T = 6, E = 100, SB = FLX
C.203	B = 100%, S = W/O S, T = 6, E = 200, SB = FLX
C.204	B = 100%, S = W/O S, T = 6, E = 300, SB = FLX
C.205	B = 100%, S = W/O S, T = 6, E = 400, SB = FLX
C.206	B = 100%, S = W/O S, T = 6, E = 500, SB = FLX
C.207	B = 100%, S = W/O S, T = 8, E = 100, SB = PCC
C.208	B = 100%, S = W/O S, T = 8, E = 200, SB = PCC
C.209	B = 100%, S = W/O S, T = 8, E = 300, SB = PCC
C.210	B = 100%, S = W/O S, T = 8, E = 400, SB = PCC
C.211	B = 100%, S = W/O S, T = 8, E = 500, SB = PCC
C.212	B = 100%, S = W/O S, T = 8, E = 100, SB = FLX
C.213	B = 100%, S = W/O S, T = 8, E = 200, SB = FLX
C.214	B = 100%, S = W/O S, T = 8, E = 300, SB = FLX
C.215	B = 100%, S = W/O S, T = 8, E = 400, SB = FLX
C.216	B = 100%, S = W/O S, T = 8, E = 500, SB = FLX
C.217	B = 100%, S = WS, T = 8, E = 100, SB = PCC
C.218	B = 100%, S = WS, T = 8, E = 200, SB = PCC
C.219	B = 100%, S = WS, T = 8, E = 300, SB = PCC
C.220	B = 100%, S = WS, T = 8, E = 400, SB = PCC
C.221	B = 100%, S = WS, T = 8, E = 500, SB = PCC
C.222	B = 100%, S = WS, T = 8, E = 100, SB = FLX
C.223	B = 100%, S = WS, T = 8, E = 200, SB = FLX
C.224	B = 100%, S = WS, T = 8, E = 300, SB = FLX
C.225	B = 100%, S = WS, T = 8, E = 400, SB = FLX
C.226	B = 100%, S = WS, T = 8, E = 500, SB = FLX
C.227	B = 100%, S = WS, T = 6, E = 100, SB = PCC
C.228	B = 100%, S = WS, T = 6, E = 200, SB = PCC
C.229	B = 100%, S = WS, T = 6, E = 300, SB = PCC
C.231	B = 100%, S = WS, T = 6, E = 400, SB = PCC
C.232	B = 100%, S = WS, T = 6, E = 500, SB = PCC
C.233	B = 100%, S = WS, T = 6, E = 100, SB = FLX
C.234	B = 100%, S = WS, T = 6, E = 200, SB = FLX
C.235	B = 100%, S = WS, T = 6, E = 300, SB = FLX
C.236	B = 100%, S = WS, T = 6, E = 400, SB = FLX
C.237	B = 100%, S = WS, T = 6, E = 500, SB = FLX
C.238	B = 100%, S = WS, T = 4, E = 100, SB = PCC
C.239	B = 100%, S = WS, T = 4, E = 200, SB = PCC
C.240	B = 100%, S = WS, T = 4, E = 300, SB = PCC
C.241	B = 100%, S = WS, T = 4, E = 400, SB = PCC

Page	Conditions
C.242	B = 100%, S = WS, T = 4, E = 500, SB = PCC
C.243	B = 100%, S = WS, T = 4, E = 100, SB = FLX
C.244	B = 100%, S = WS, T = 4, E = 200, SB = FLX
C.245	B = 100%, S = WS, T = 4, E = 300, SB = FLX
C.246	B = 100%, S = WS, T = 4, E = 400, SB = FLX
C.247	B = 100%, S = WS, T = 4, E = 500, SB = FLX
C.248	B = 100%, S = WS, T = 2, E = 100, SB = PCC
C.249	B = 100%, S = WS, T = 2, E = 200, SB = PCC
C.250	B = 100%, S = WS, T = 2, E = 300, SB = PCC
C.251	B = 100%, S = WS, T = 2, E = 400, SB = PCC
C.252	B = 100%, S = WS, T = 2, E = 500, SB = FLX
C.253	B = 100%, S = WS, T = 2, E = 100, SB = FLX
C.254	B = 100%, S = WS, T = 2, E = 200, SB = FLX
C.255	B = 100%, S = WS, T = 2, E = 300, SB = FLX
C.256	B = 100%, S = WS, T = 2, E = 400, SB = FLX

APPENDIX D

Test Data from Static Creep, Repeated Load Permanent Deformation and Resilient Modulus Testing of Selected Asphalt Concrete Mixtures

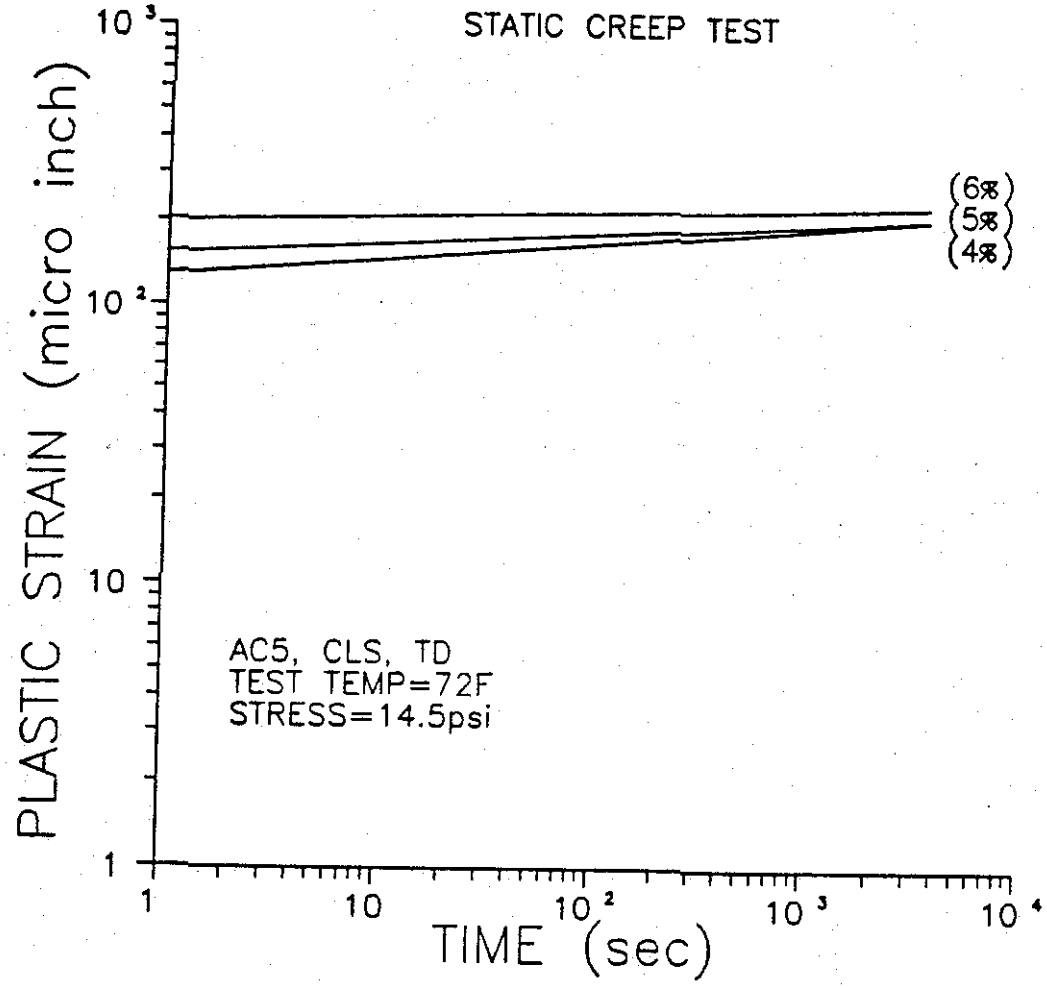

Figure D.1. Permanent deformation trends for AC-5 and crushed limestone mixtures.

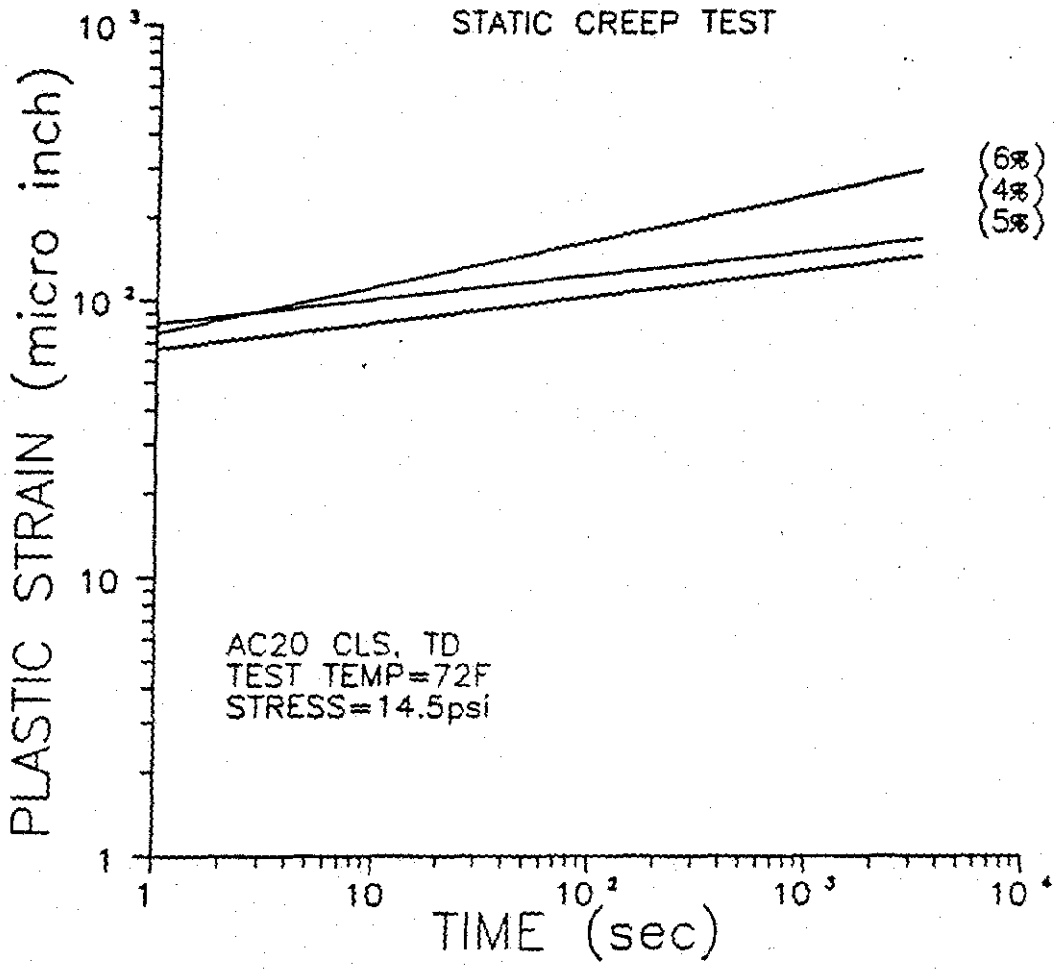

Figure D.2. Permanent deformation trends for AC-20 and crushed limestone mixtures.

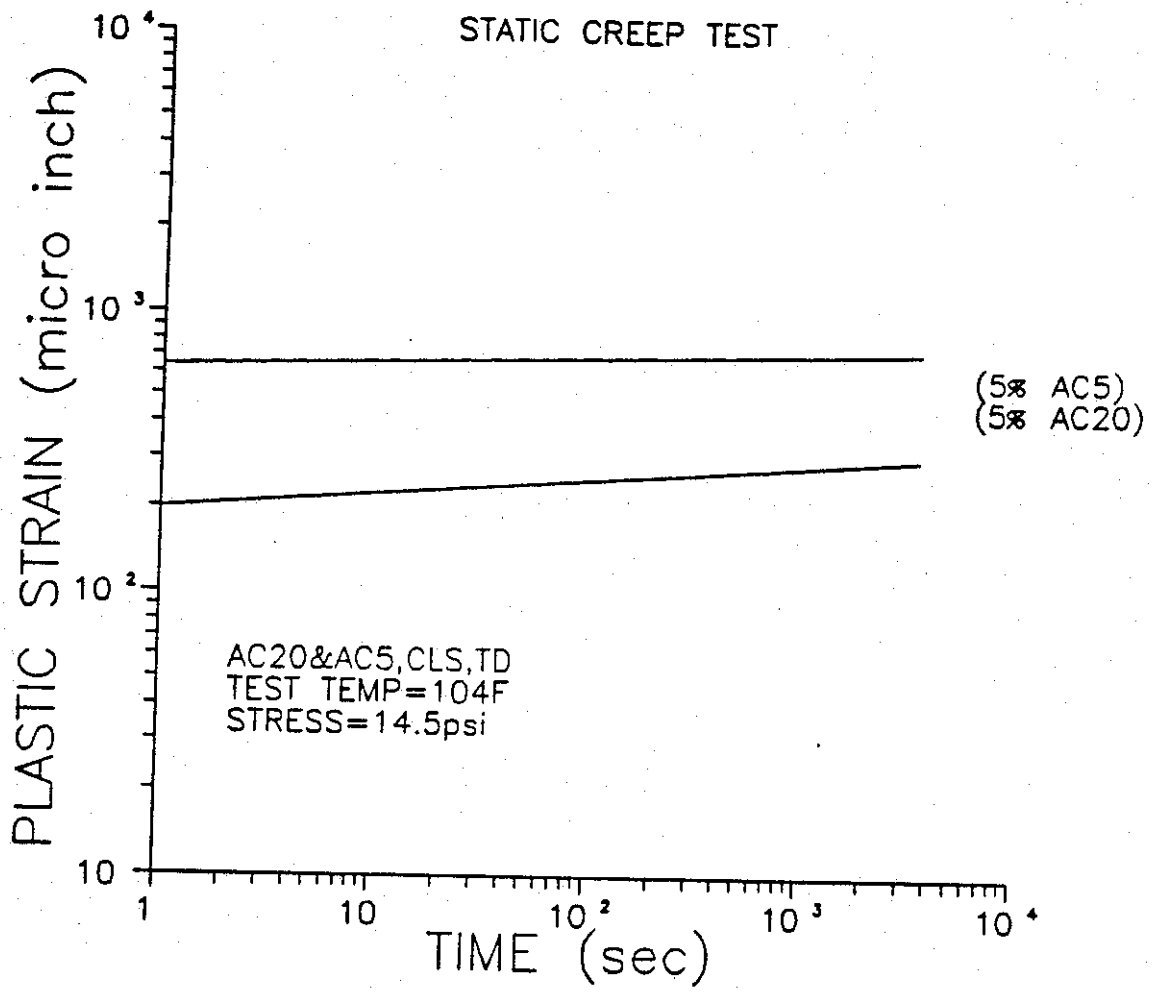

Figure D.3. Permanent deformation trends for AC-5, AC-20, and crushed limestone mixtures.

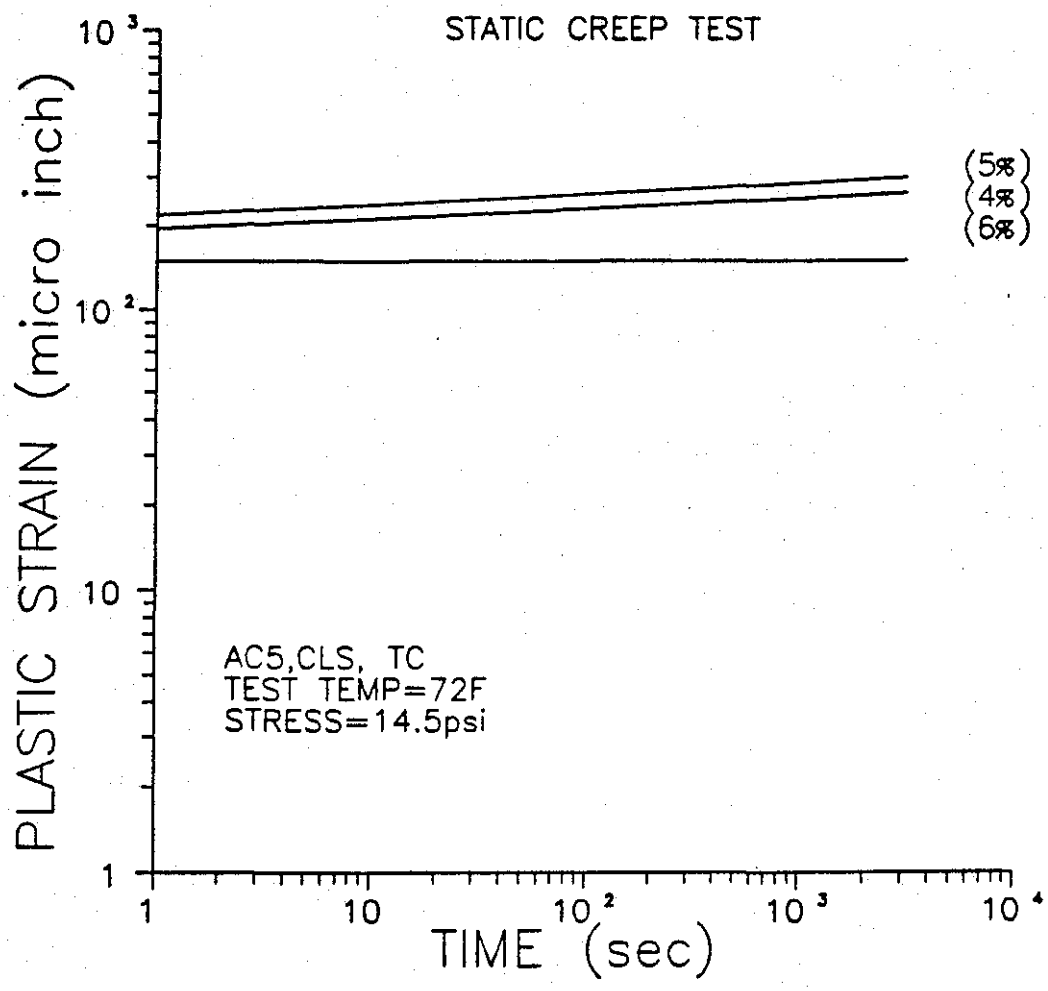

Figure D.4. Permanent deformation trends for AC-5 and crushed limestone mixtures.

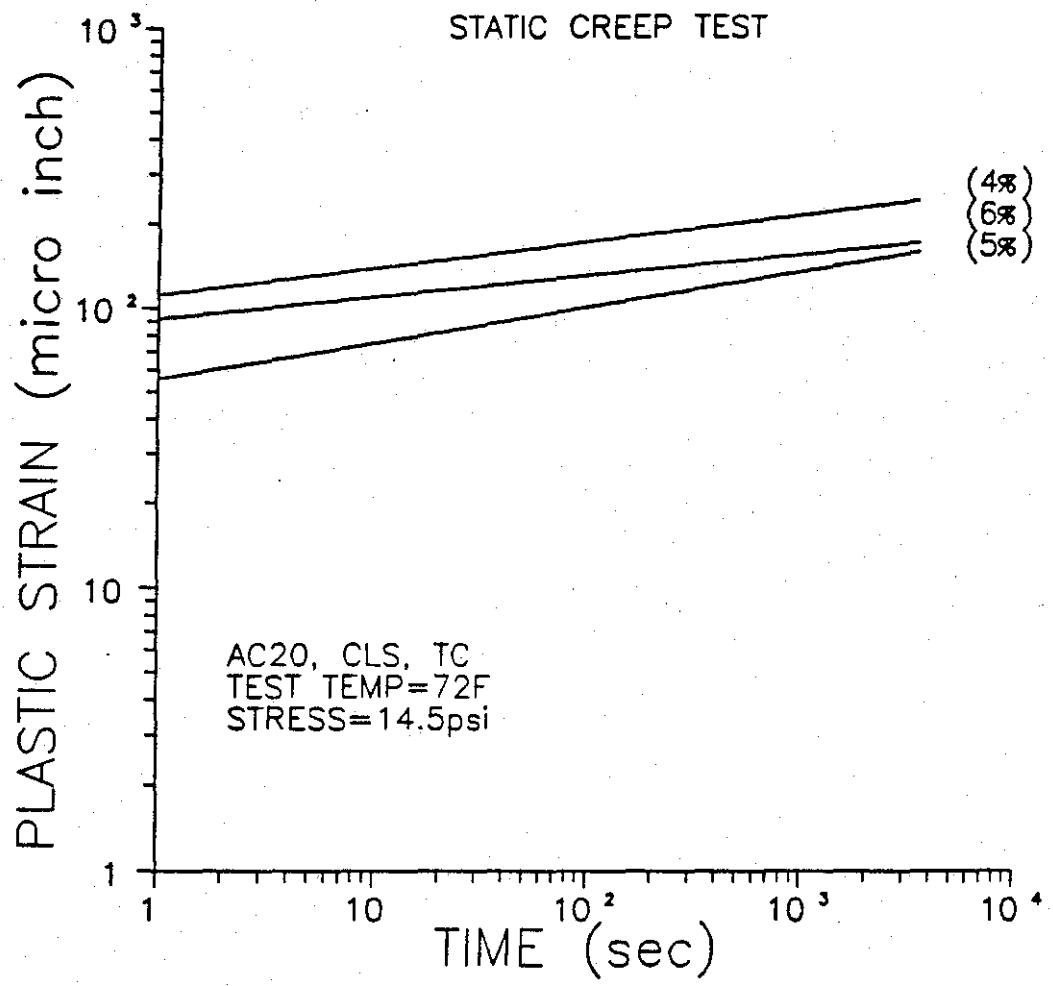

Figure D.5. Permanent deformation trends for AC-20 and crushed limestone mixtures.

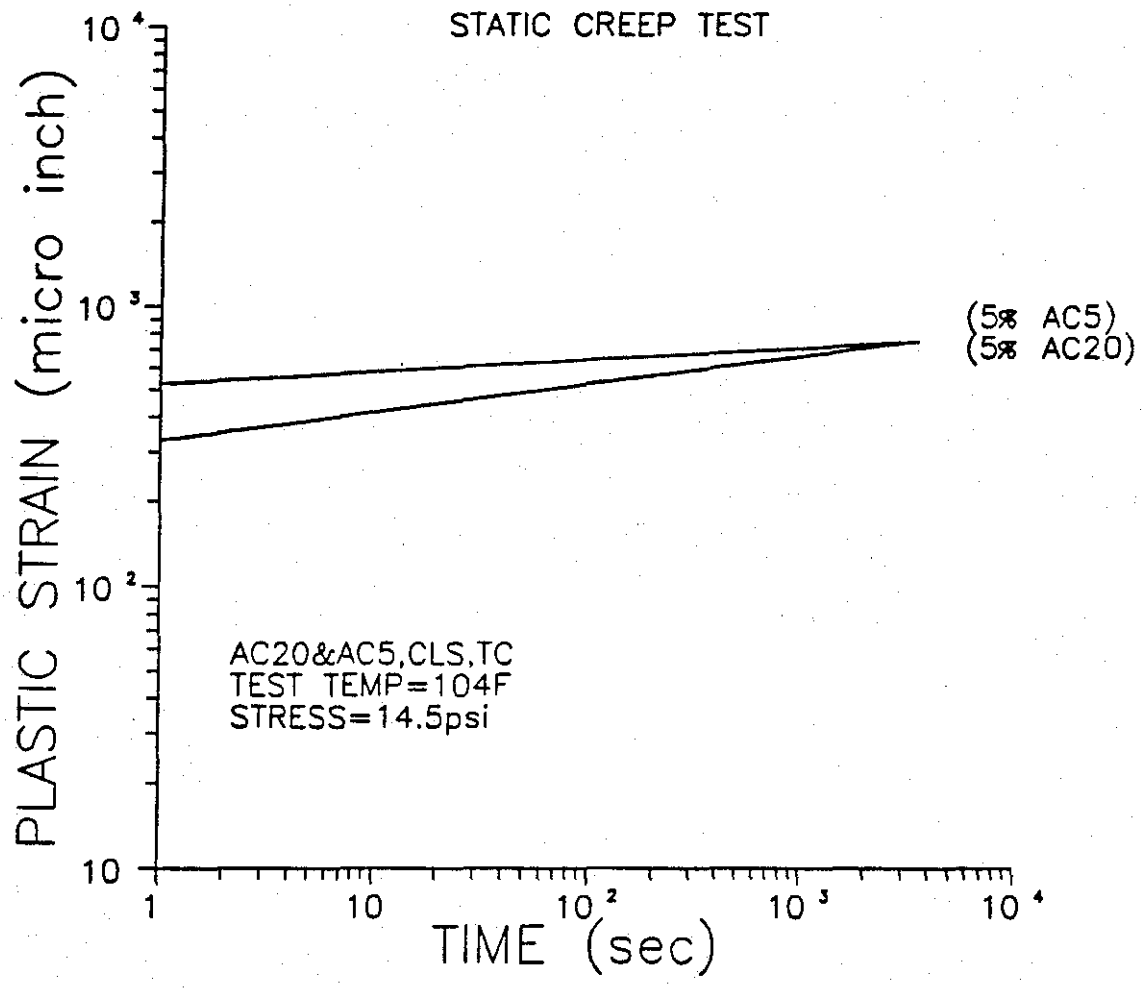

Figure D.6. Permanent deformation trends for AC-5, AC-20, and crushed limestone mixtures.

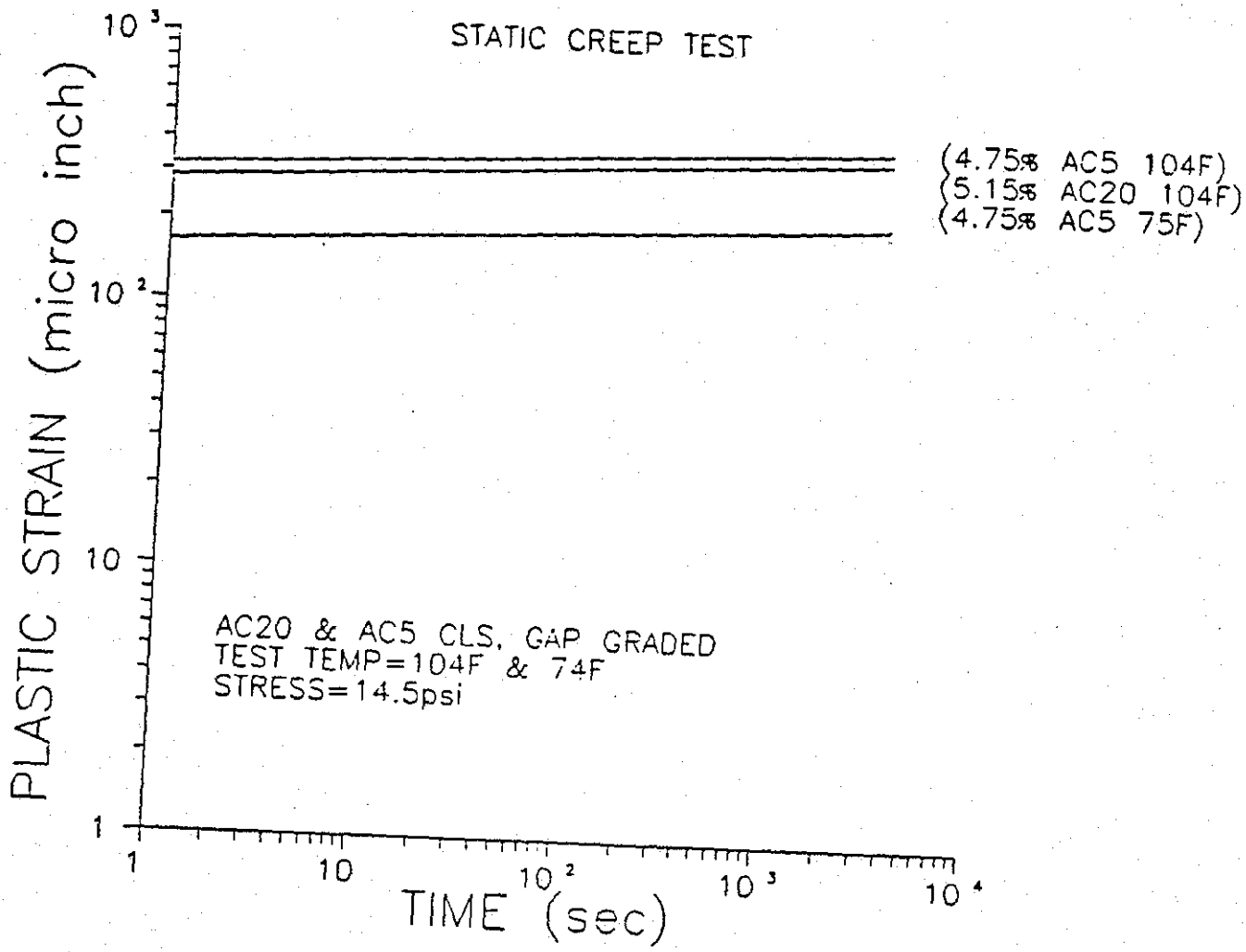

Figure D.7. Permanent deformation trends for AC-5, AC-20, and crushed limestone, gap-graded mixtures.

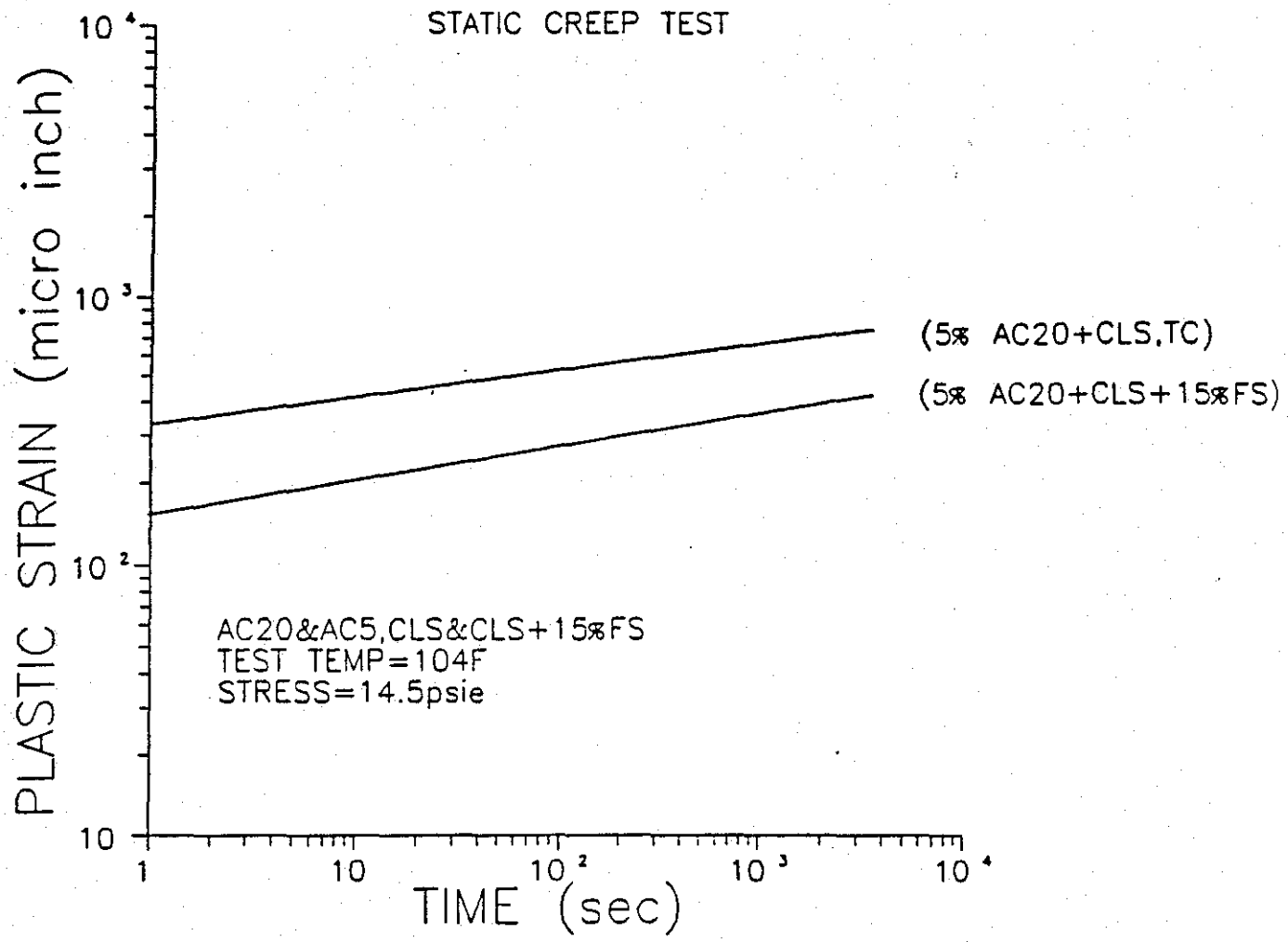

Figure D.8. Permanent deformation trends for AC-20 and crushed limestone mixtures and crushed limestone mixtures with field sand.

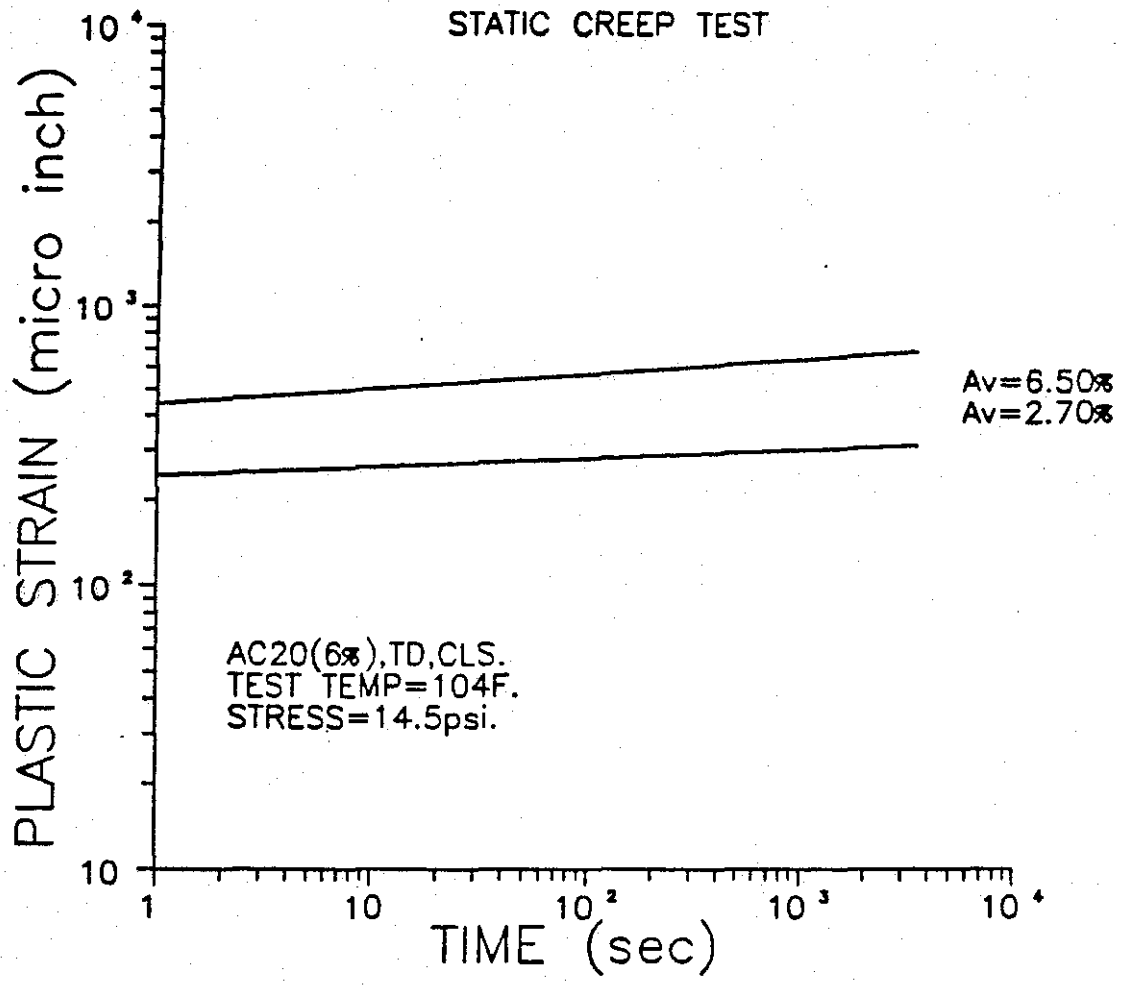

Figure D.9. Permanent deformation trends for AC-20 and crushed limestone mixtures at various levels of air voids content.

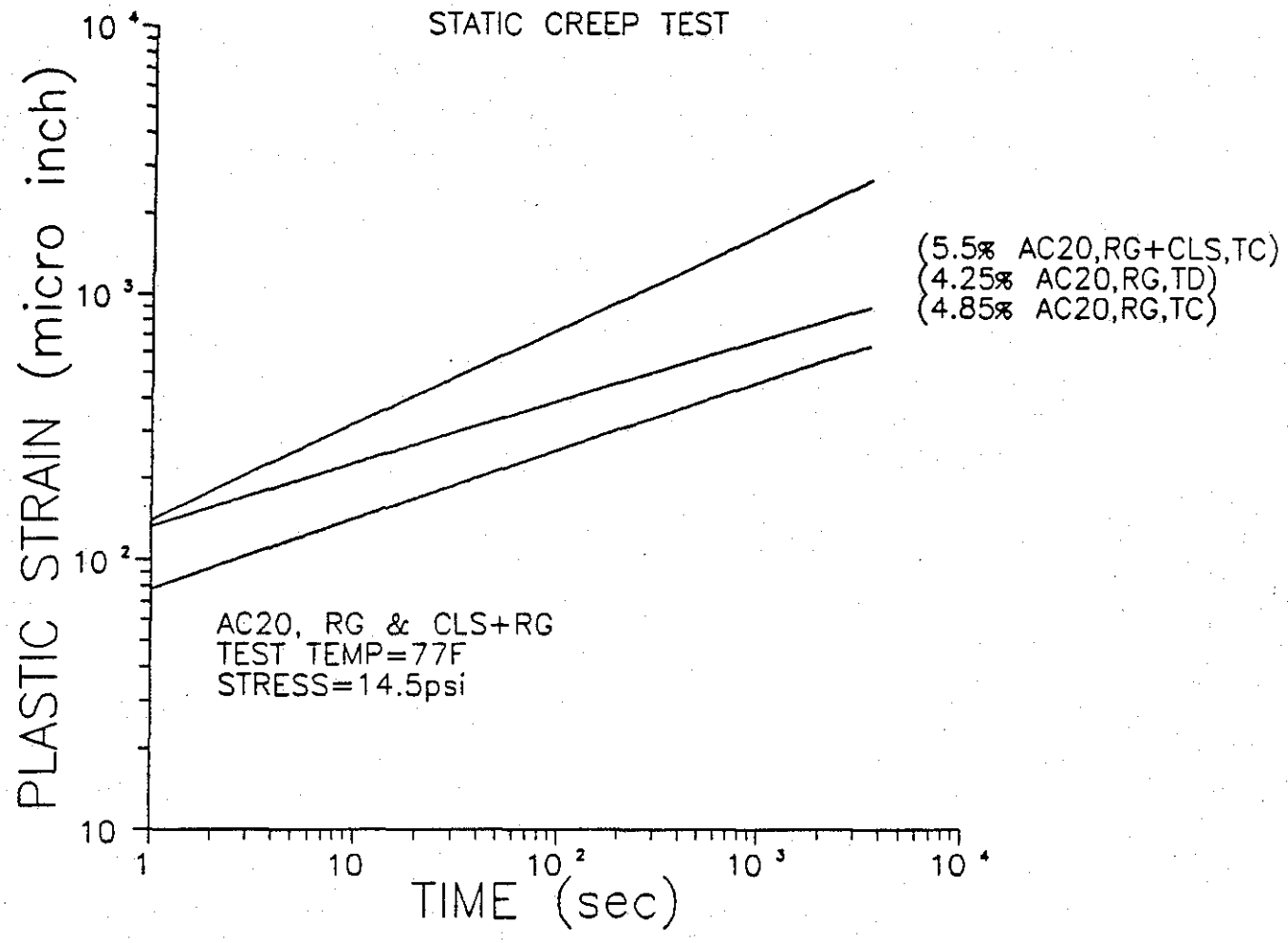

Figure D.10. Permanent deformation trends for AC-20 and both siliceous gravel and siliceous gravel with crushed limestone mixtures.

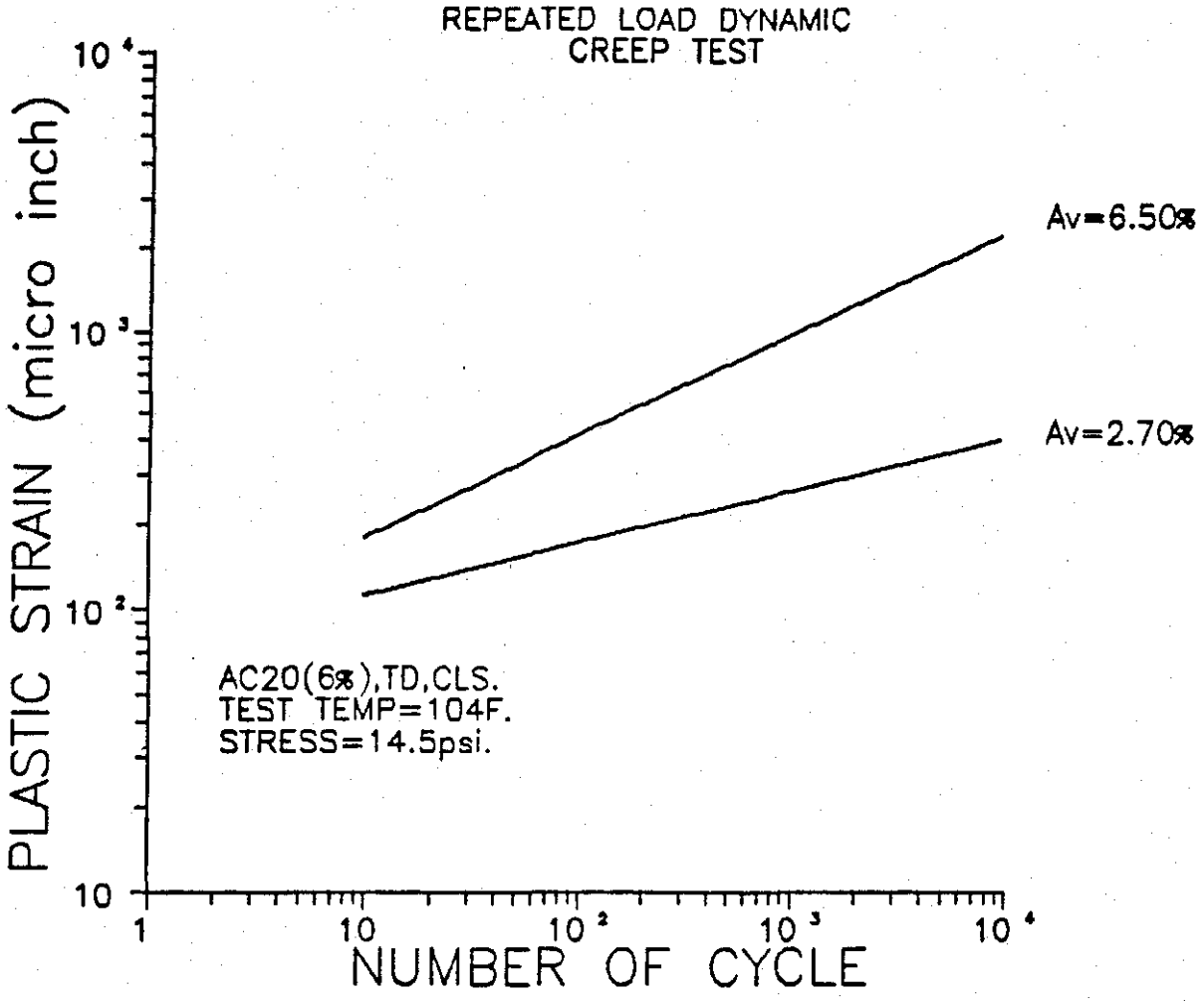

Figure D.11. Permanent deformation trends for AC-20 and crushed limestone mixtures at various levels of air voids content.

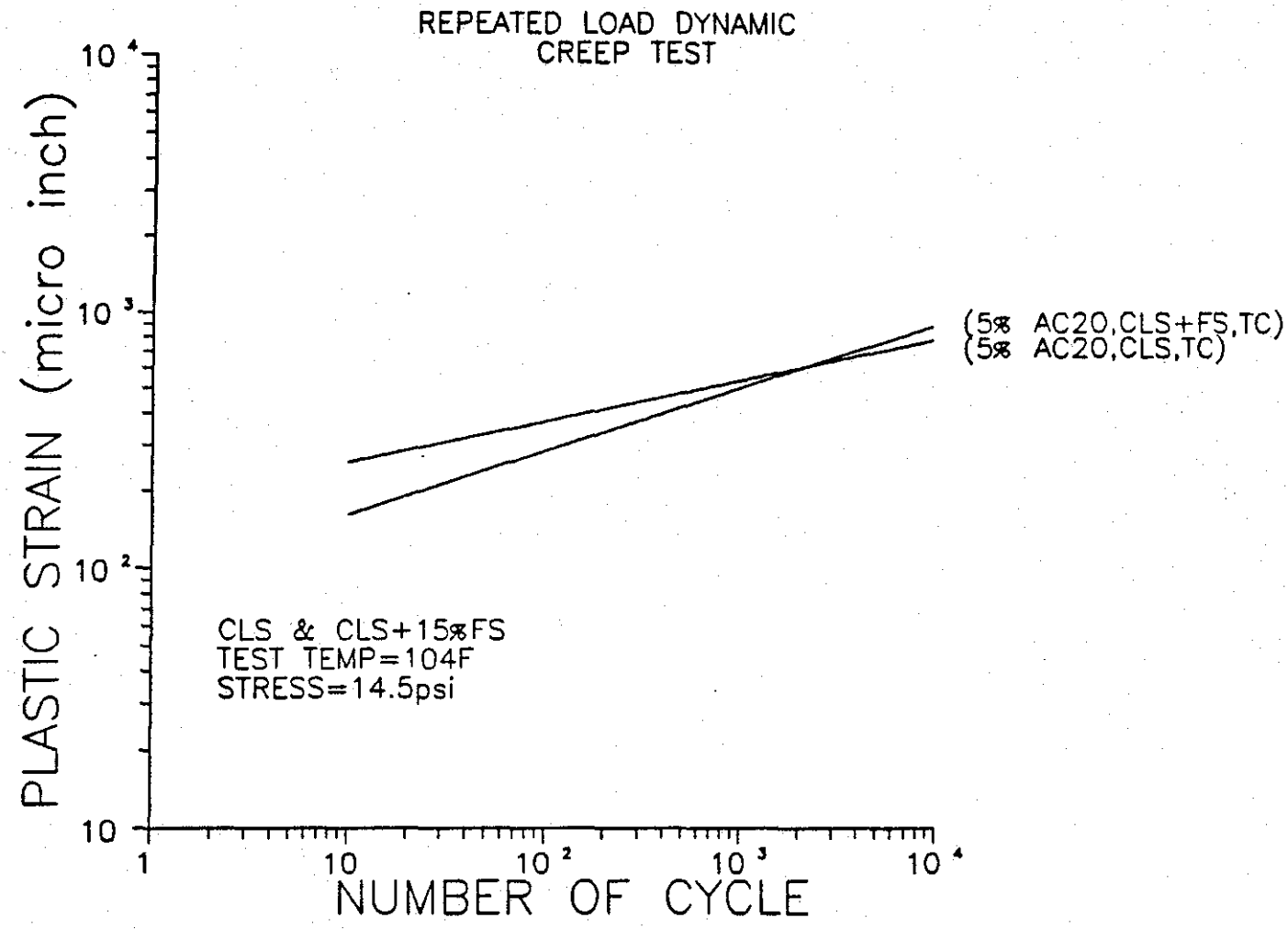

Figure D.12. Permanent deformation trends for AC-20 and crushed limestone mixtures and crushed limestone mixtures with field sand.

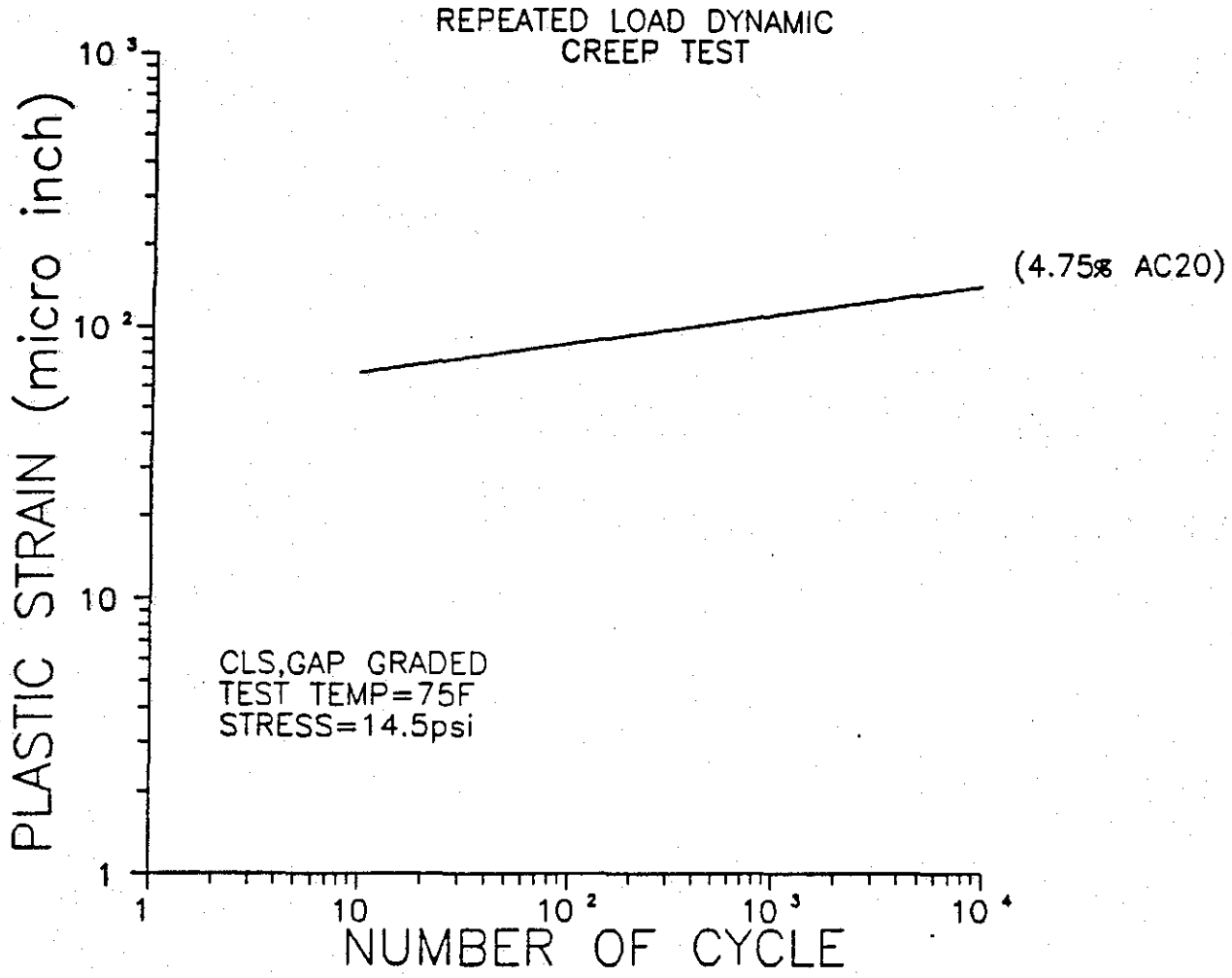

Figure D.13. Permanent deformation trends for AC-20, and gap-graded, crushed limestone mixtures.

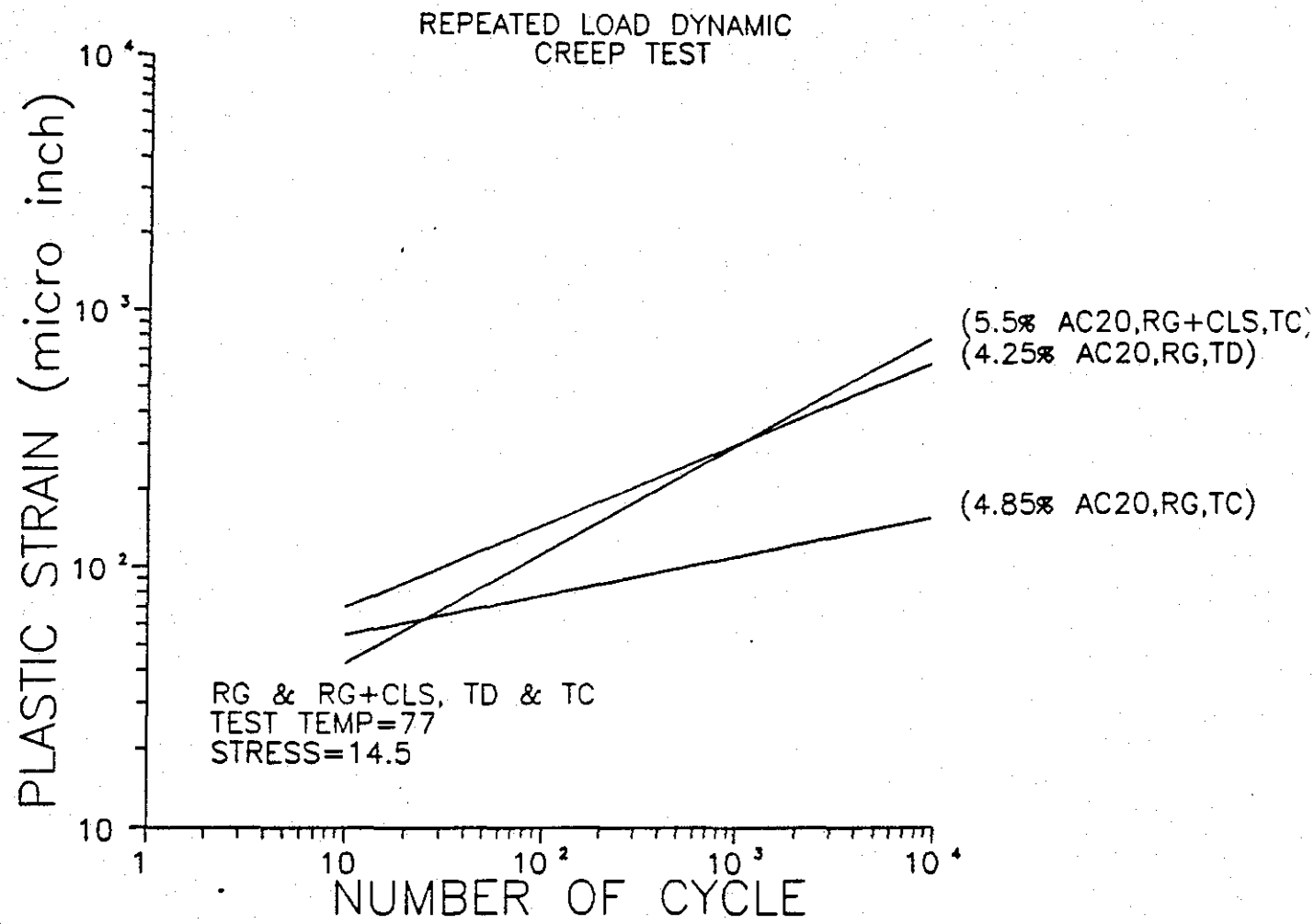

Figure D.14. **Permanent deformation trends for AC-20 and crushed limestone and siliceous river gravel mixtures and AC-20 and siliceous river gravel mixtures.**

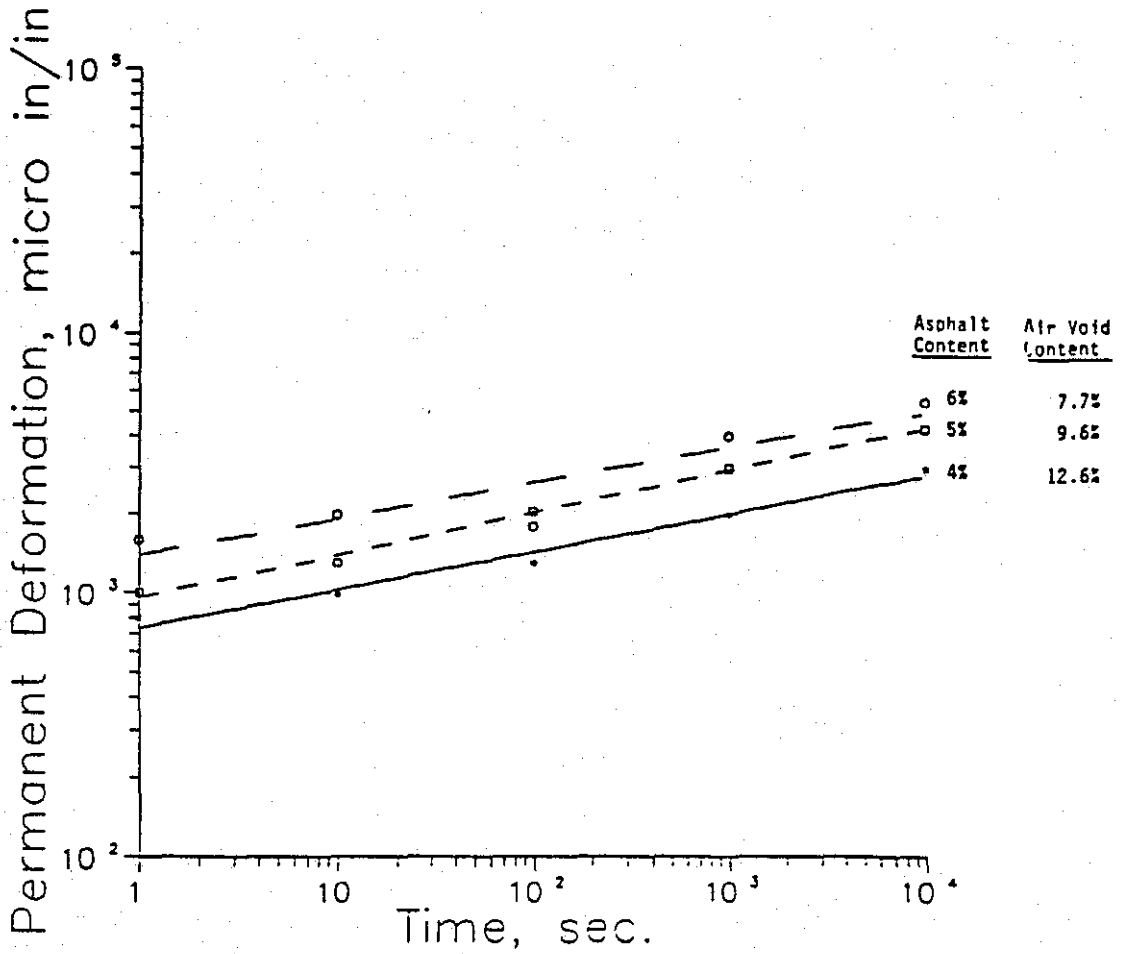

Figure D.15. Permanent deformation trends for AC-5 and crushed limestone mixtures (after Reference 18).

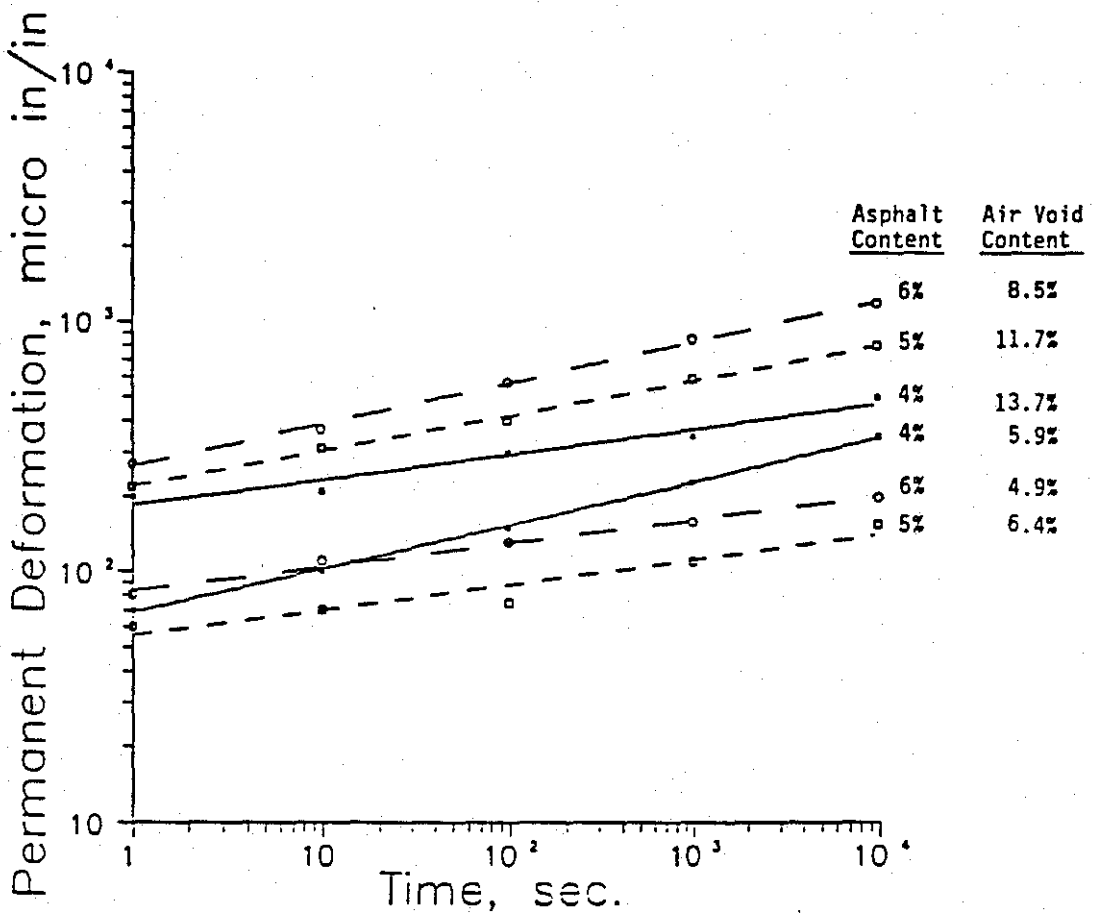

Figure D.16. Permanent deformation trends for AC-20 and crushed limestone mixtures (after Reference 18).

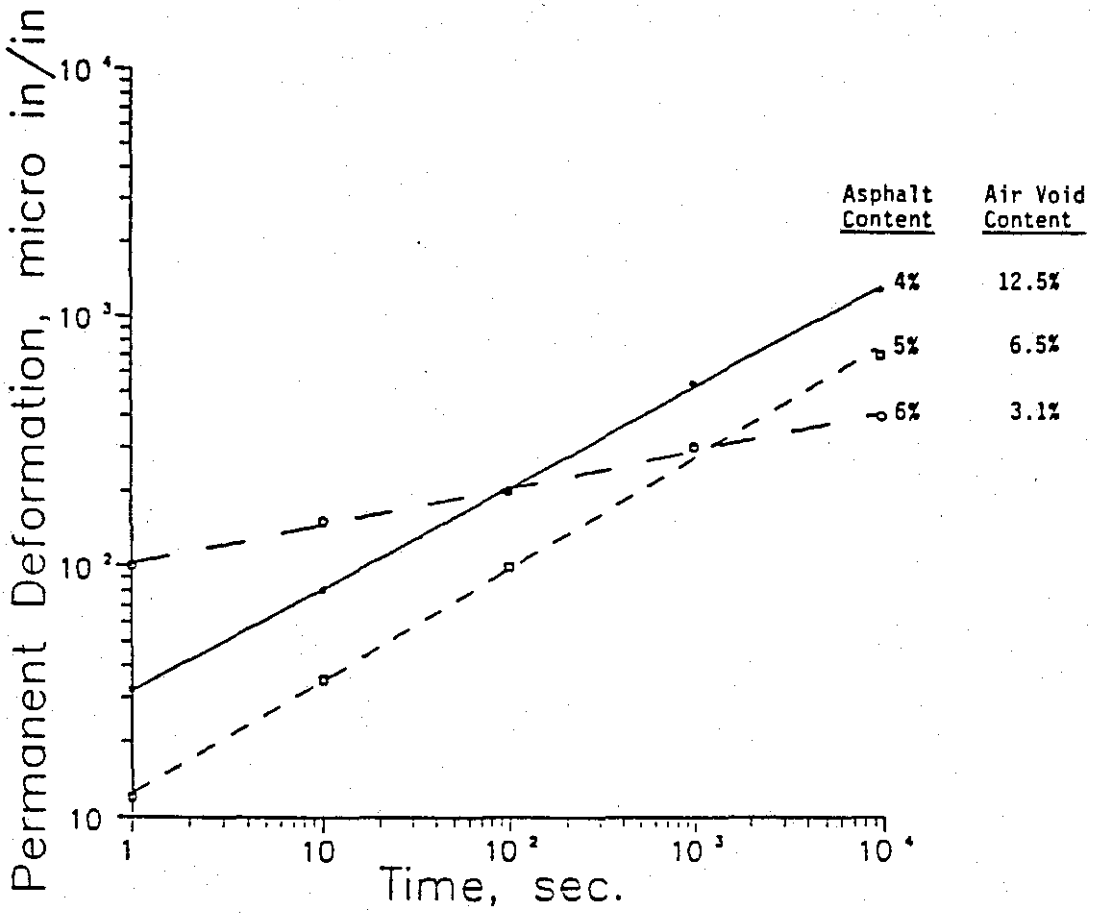

Figure D.17. Permanent deformation trends for AC-5 and siliceous gravel mixtures (after Reference 18).

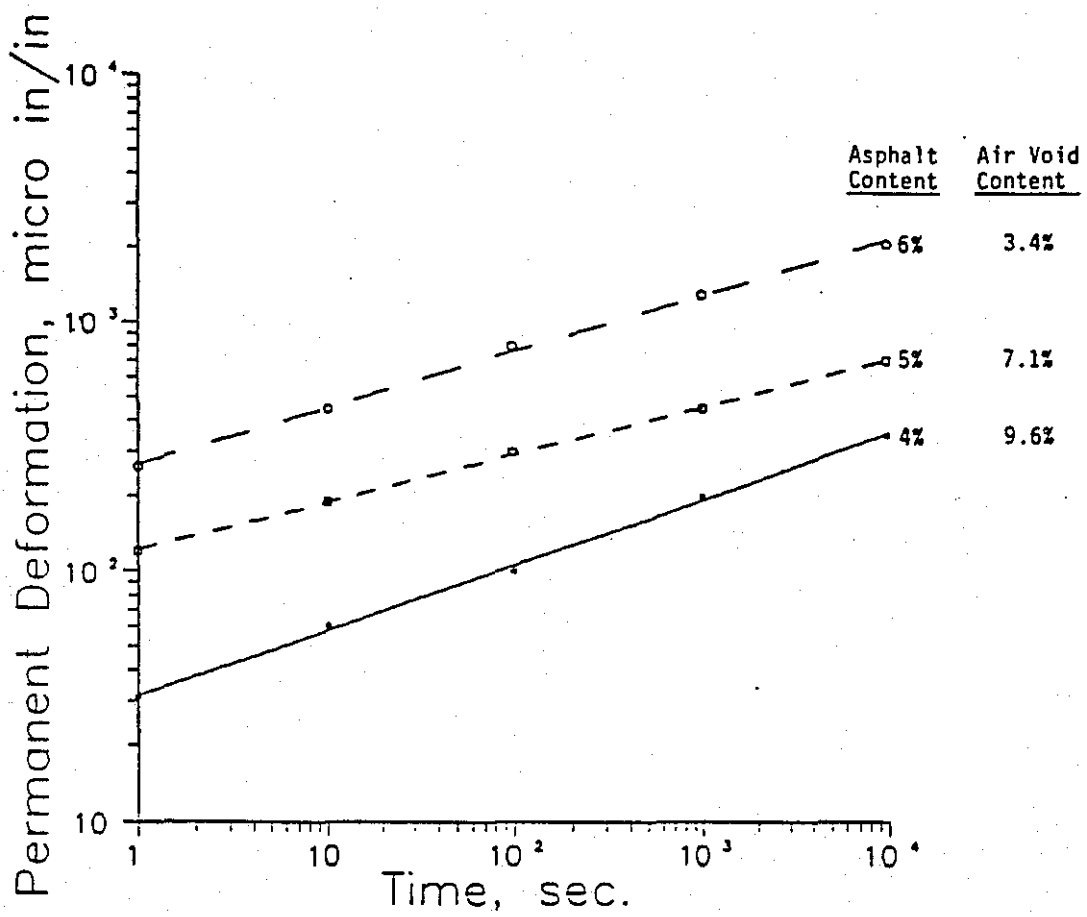

Figure D.18. Permanent deformation trends for AC-10 and siliceous gravel mixtures (after Reference 18).

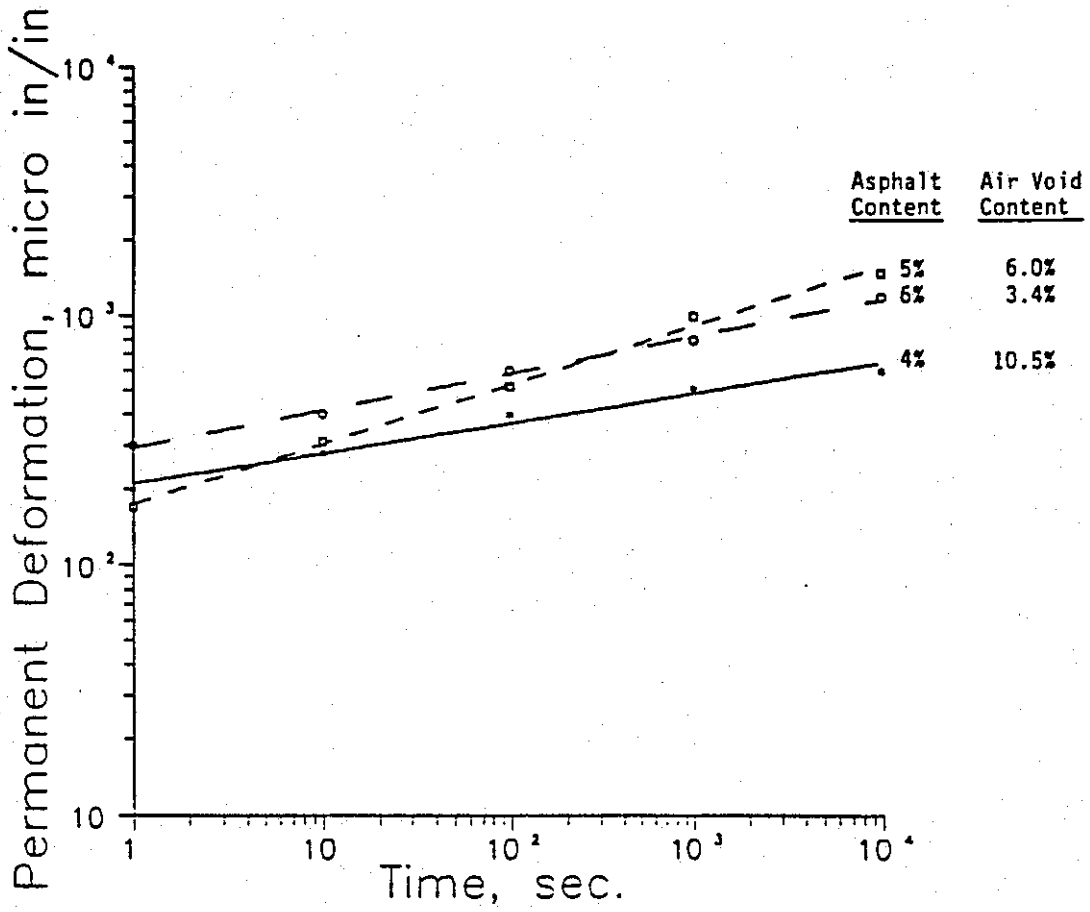

Figure D.19. Permanent deformation trends for AC-20 and siliceous gravel mixtures (after Reference 18).

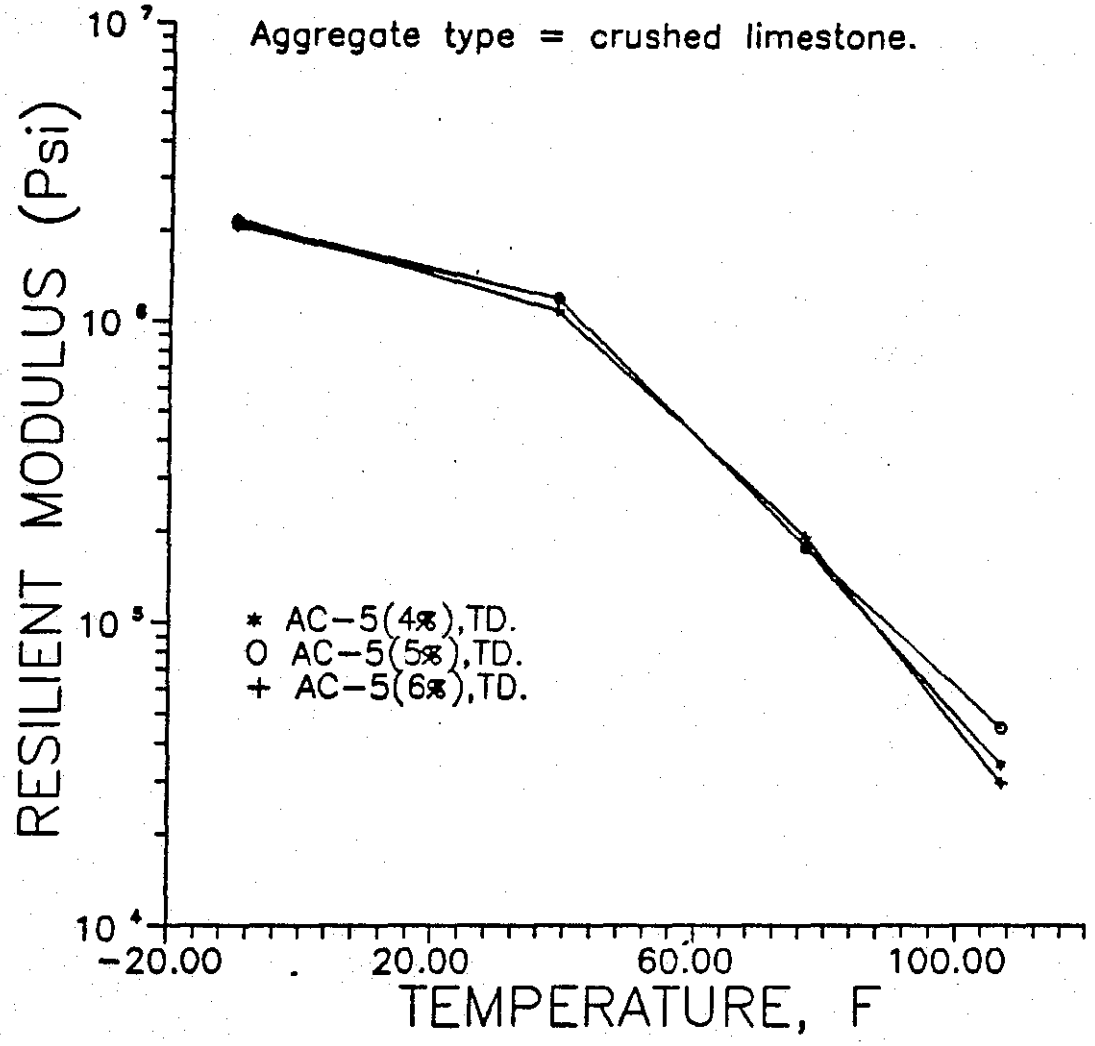

Figure D.20. Variation of resilient modulus with temperature.

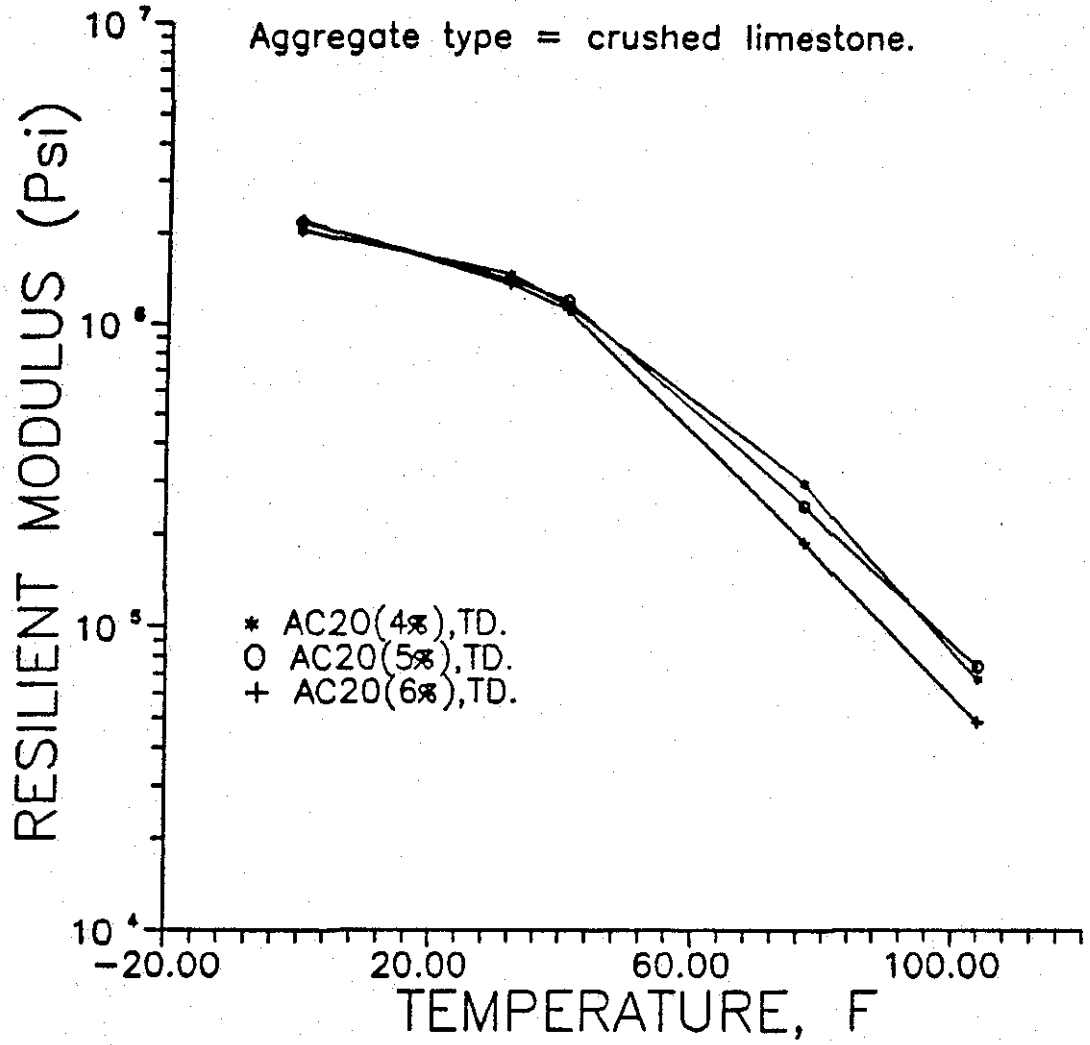

Figure D.21. Variation of resilient modulus with temperature.

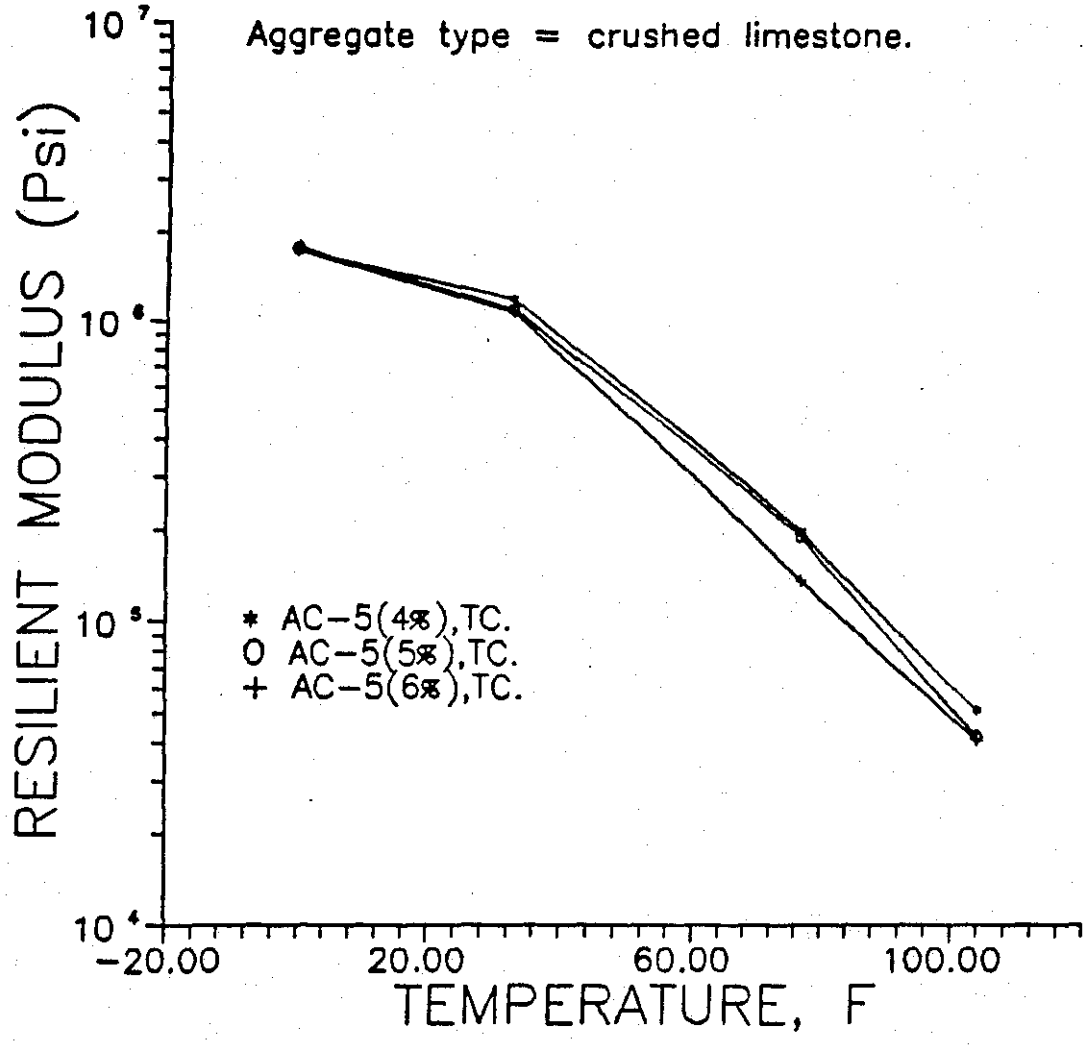

Figure D.22. Variation of resilient modulus with temperature.

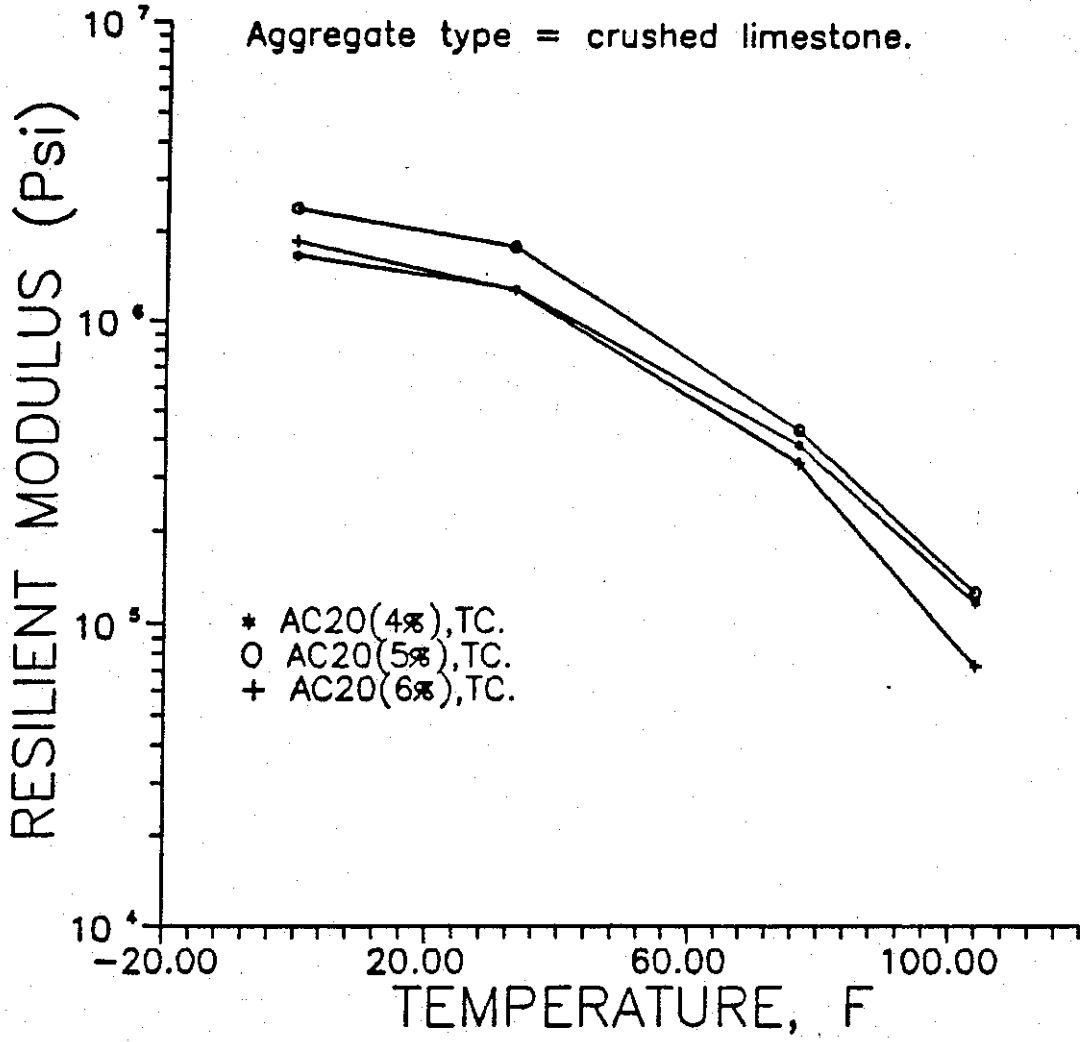

Figure D.23. Variation of resilient modulus with temperature.

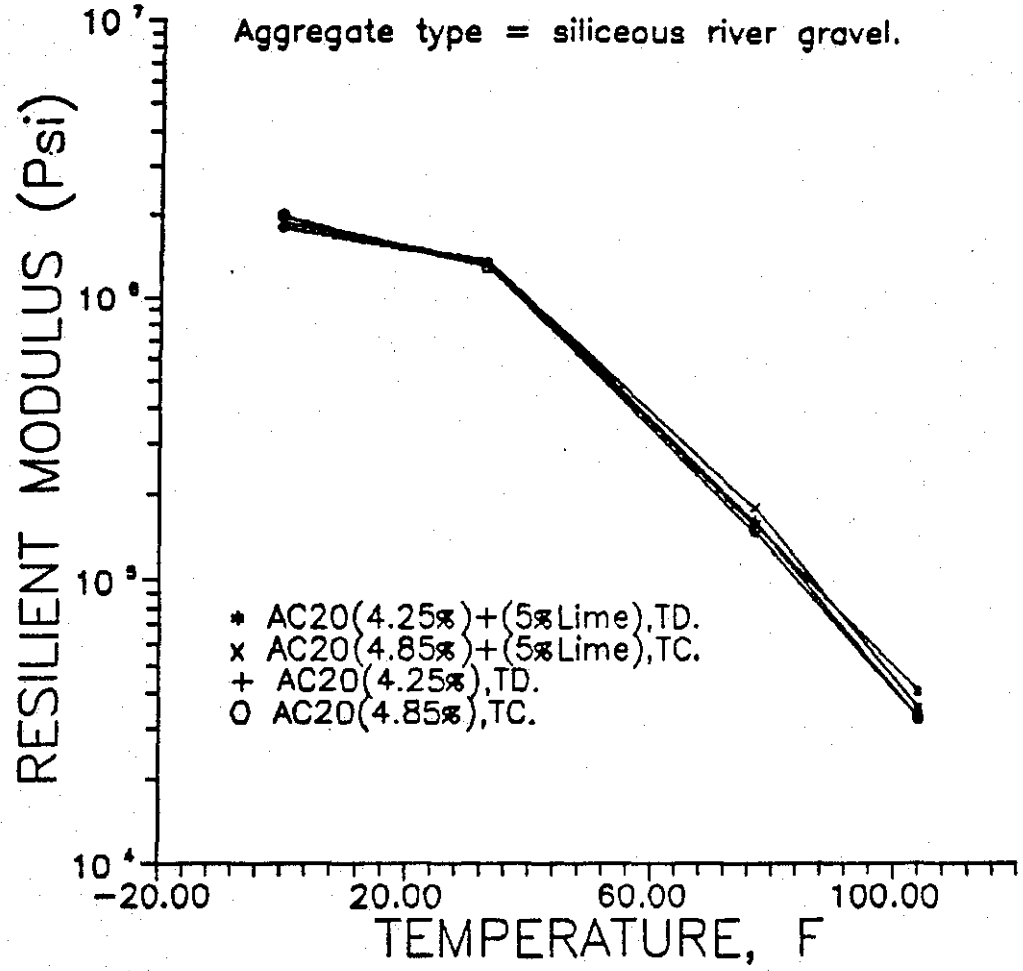

Figure D.24. Variation of resilient modulus with temperature.

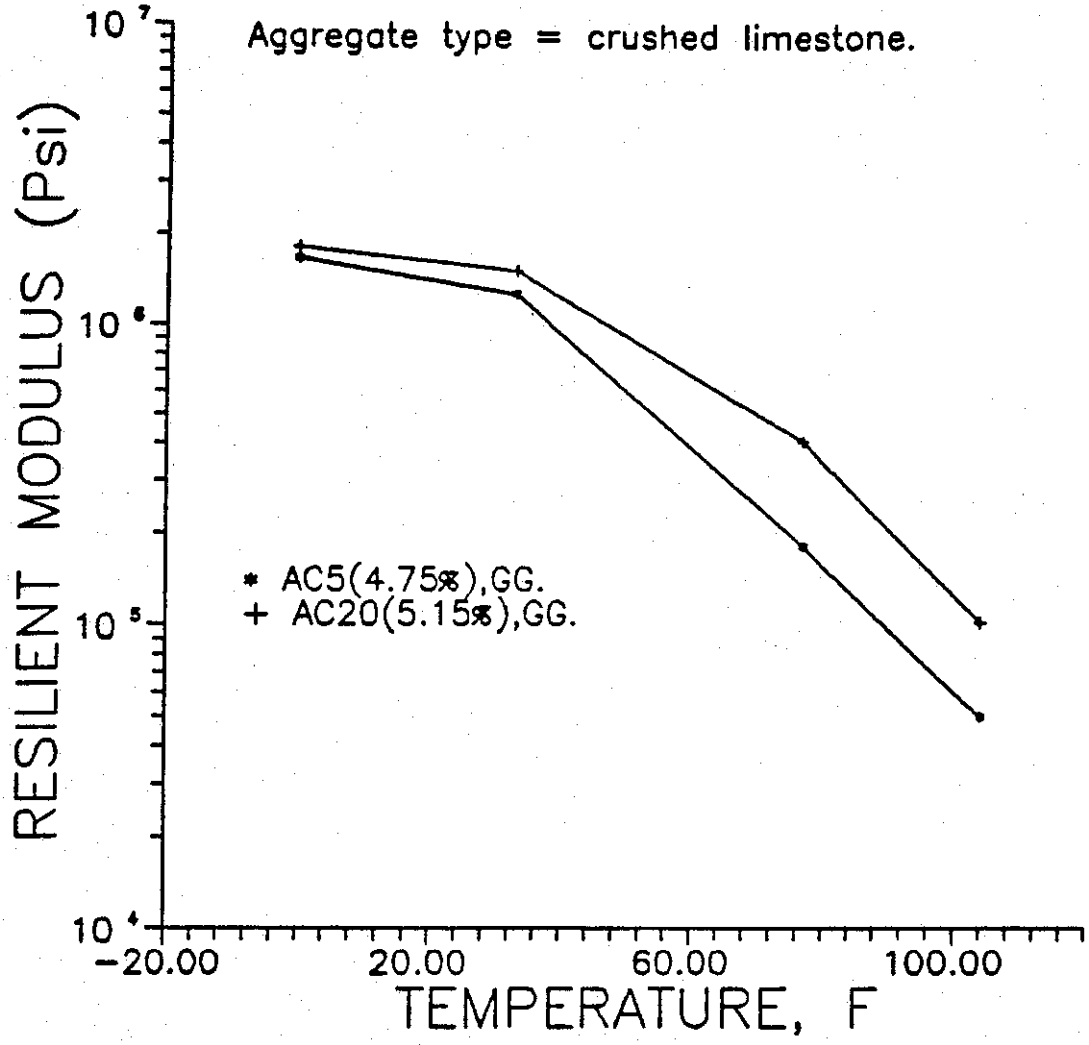

Figure D.25. Variation of resilient modulus with temperature.

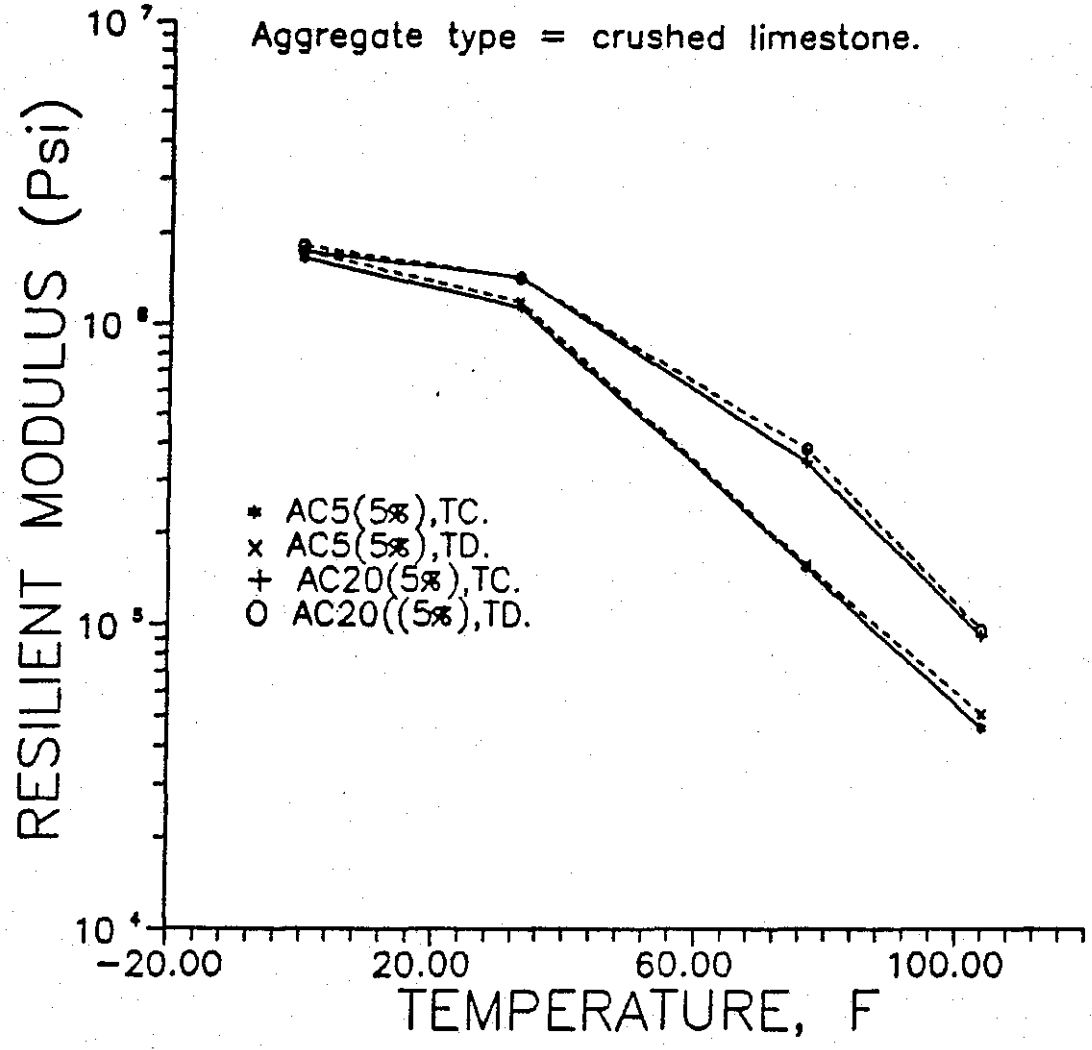

Figure D.26. Variation of resilient modulus with temperature.

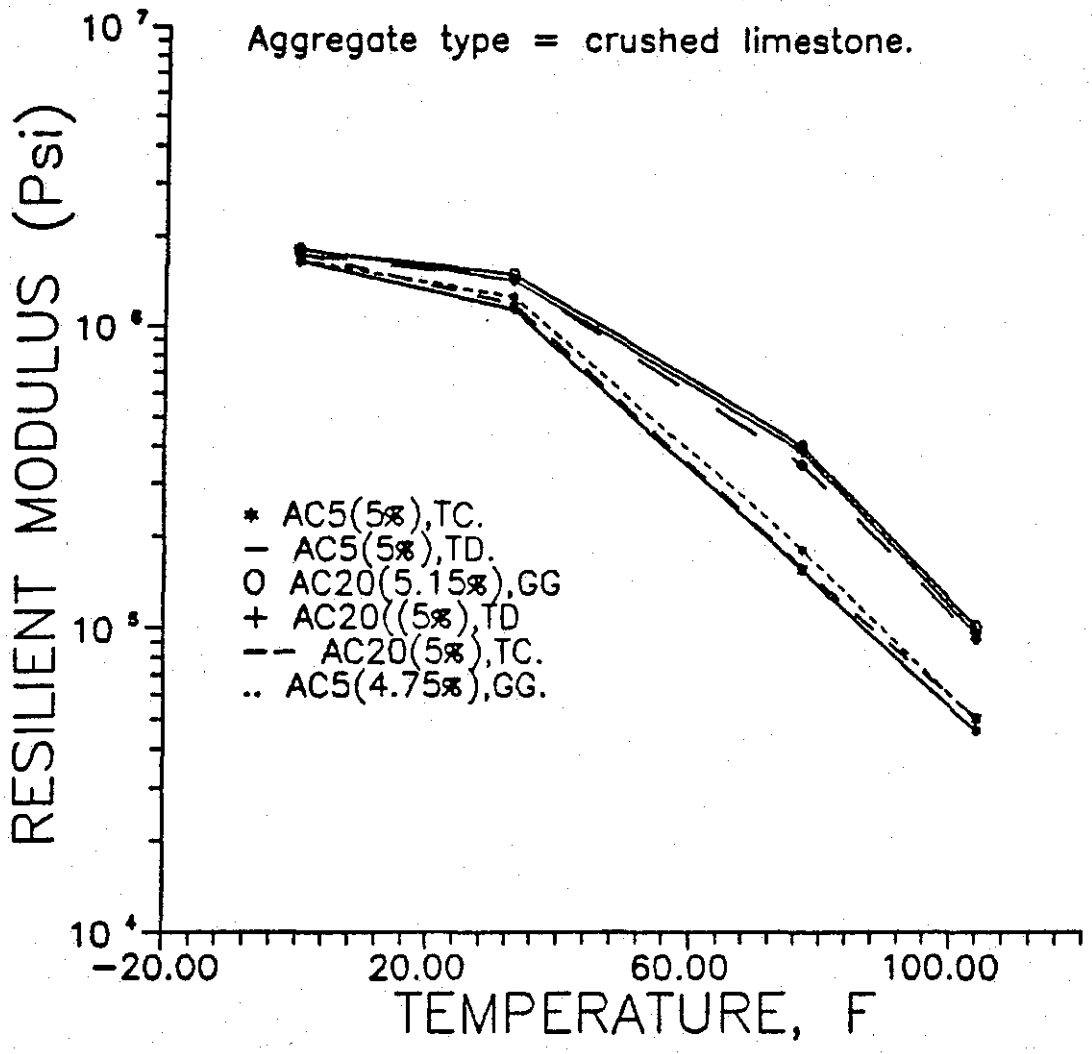

Figure D.27. Variation of resilient modulus with temperature.